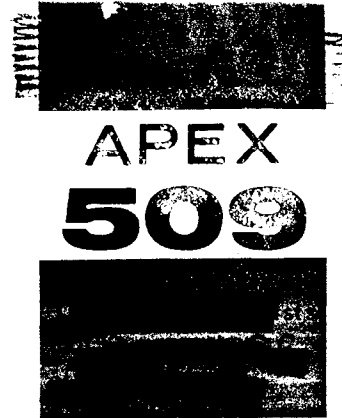


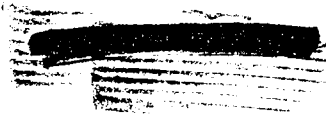
UNCLASSIFIED

00 1030  
00 713

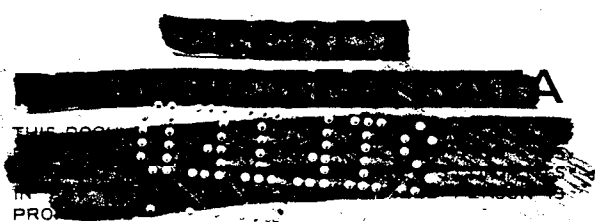


Research and  
Development Report

# SUMMARY REPORT OF HTRE NO. 3 NUCLEAR EXCURSION



GENERAL  ELECTRIC  
ATOMIC PRODUCTS DIVISION  
AIRCRAFT NUCLEAR PROPULSION DEPARTMENT



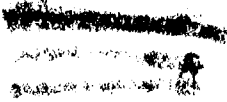
UNCLASSIFIED

UNCLASSIFIED



UNCLASSIFIED

DECLASSIFIED



LEGAL NOTICE

This report was prepared as an account of Government sponsored work. Neither the United States, nor the Commission, nor the Air Force, nor any person acting on behalf of the Commission or the Air Force:

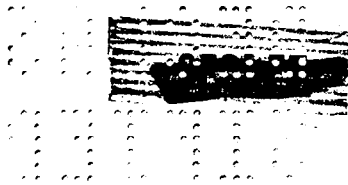
- A. Makes any warranty or representation, express or implied, with respect to the accuracy, completeness, or usefulness of the information contained in this report, or that the use of any information, apparatus, method, or process disclosed in this report may not infringe privately owned rights; or
- B. Assumes any liabilities with respect to the use of, or for damages resulting from the use of any information, apparatus, method, or process disclosed in this report.

As used in the above "person acting on behalf of the Commission or Air Force" includes any employee or contractor of the Commission or Air Force to the extent that such employee or contractor prepares, handles, or distributes, or provides access to, any information pursuant to his employment or contract with the Commission or Air Force.

DECLASSIFIED

UNCLASSIFIED

UNCLASSIFIED



**APEX - 509**

C-84 Reactors - Special Features  
of Aircraft Reactors  
(M-3679, 23rd Ed.)

## SUMMARY REPORT OF HTRE NO.3 NUCLEAR EXCURSION

~~Classification changed to UNCLASSIFIED  
by authority of the U. S. Atomic Energy Commission,  
Per \_\_\_\_\_  
By REPORT LIBRARY \_\_\_\_\_~~

United States Air Force

Contract No. AF 33(600)-38062

United States Atomic Energy Commission

Contract No. AT (11-1)-171

**GENERAL  ELECTRIC**

ATOMIC PRODUCTS DIVISION  
AIRCRAFT NUCLEAR PROPULSION DEPARTMENT  
CINCINNATI 15, OHIO

~~Classification changed to UNCLASSIFIED  
by authority of the U. S. Atomic Energy Commission,~~

Per J. H. Henderson by AEC Reg. Int. # 45X504 *4-18-62*  
By REPORT LIBRARY M. Long *7-9-62*

Published by  
TECHNICAL PUBLICATIONS SUB-SECTION  
August 1959

~~SECRET  
THIS DOCUMENT CONTAINS NEITHER  
RECOMMENDATIONS NOR CONCLUSIONS  
OF THE AEC IN THE ATOMIC ENERGY  
ACTIVITY OF THE DISCLOSURE OF  
WHICH MAY BE TO THE UNLAWFUL  
PROHIBITED.~~

UNCLASSIFIED

UNCLASSIFIED

~~SECRET~~

## DISTRIBUTION

### EXTERNAL

#### STANDARD DISTRIBUTION

- 1 AiResearch Manufacturing Company
- 2-5 Air Force Ballistic Missile Division
- 6-7 AFPR, Boeing, Seattle
- 8 AFPR, Boeing, Wichita
- 9 AFPR, Douglas, Long Beach
- 10-12 AFPR, Douglas, Santa Monica
- 13-14 AFPR, Lockheed, Marietta
- 15 AFPR, North American, Downey
- 16-17 Air Force Special Weapons Center
- 18-19 Air Research and Development Command (RDZN)
- 20 Air Technical Intelligence Center
- 21-23 ANP Project Office, Convair, Fort Worth
- 24 Albuquerque Operations Office
- 25 Argonne National Laboratory
- 26 Armed Forces Special Weapons Project, Washington
- 27-28 Army Ballistic Missile Agency
- 29 Army Rocket and Guided Missile Agency
- 30 Assistant Secretary of the Air Force, R&D.
- 31-36 Atomic Energy Commission, Washington
- 37 Atomics International
- 38 Battelle Memorial Institute
- 39-41 Bettis Plant (WAPD)
- 42 Brookhaven National Laboratory
- 43 Bureau of Aeronautics
- 44 Bureau of Aeronautics General Representative
- 45 BAR, Aerojet-General, Azusa
- 46 BAR, Chance Vought, Dallas
- 47 BAR, Convair, San Diego
- 48 BAR, Grumman Aircraft, Bethpage
- 49 BAR, Martin, Baltimore
- 50 Bureau of Yards and Docks
- 51-52 Chicago Operations Office
- 53 Chicago Patent Group
- 54 Director of Naval Intelligence
- 55 duPont Company, Aiken
- 56 Engineer Research and Development Laboratories
- 57-59 General Electric Company, Richland
- 60 General Nuclear Engineering Corporation
- 61 Hartford Aircraft Reactors Area Office

UNCLASSIFIED

~~SECRET~~

**SECRET**

**UNCLASSIFIED**

- 62 Idaho Test Division (LAPCO)
- 63-64 Knolls Atomic Power Laboratory
- 65 Lockland Aircraft Reactors Operations Office
- 66 Los Alamos Scientific Laboratory
- 67 Marquardt Aircraft Company
- 68 Martin Company
- 69 National Aeronautics and Space Administration, Cleveland
- 70 National Aeronautics and Space Administration, Washington
- 71 National Bureau of Standards
- 72 Naval Air Development Center
- 73 Naval Air Material Center
- 74 Naval Air Turbine Test Station
- 75 Naval Research Laboratory
- 76 New York Operations Office
- 77 Nuclear Metals, Inc.
- 78 Oak Ridge Operations Office
- 79 Office of Naval Research
- 80 Office of the Chief of Naval Operations
- 81 Patent Branch, Washington
- 82-83 Phillips Petroleum Company (NRTS)
- 84-87 Pratt and Whitney Aircraft Division
- 88 Sandia Corporation
- 89-90 School of Aviation Medicine
- 91 Sylvania-Corning Nuclear Corporation
- 92 Technical Research Group
- 93 Thompson Products, Inc.
- 94-101 Union Carbide Nuclear Company (ORNL)
- 102 USAF Headquarters
- 103 USAF Project RAND
- 104 U. S. Naval Postgraduate School
- 105 U. S. Naval Radiological Defense Laboratory
- 106-107 University of California, Livermore
- 108-119 Wright Air Development Center
- 120-144 Technical Information Service Extension
- 145 C. K. Beck - Atomic Energy Commission, Washington, D. C.
- 146 W. H. Jordan - Oak Ridge National Laboratory, Oak Ridge, Tennessee
- 147 M. M. Mann - Atomic Energy Commission, Washington, D. C.
- 148 C. R. McCullough - Advisory Committee Reactor Safety, Washington, D. C.
- 149 H. W. Newson - Advisory Committee Reactor Safety, Washington, D. C. (USAEC)

**INTERNAL**

**GENERAL ELECTRIC COMPANY - VENDORS - SUBCONTRACTORS**

- 150 R. K. Andersen - APED, San Jose, California
- 151 K. Cohen - APED, San Jose, California
- 152 J. F. Flagg - Research Laboratory, Schenectady, New York
- 153 O. H. Greager - HAPO, Richland, Washington
- 154 J. W. Healy - HAPO, Richland, Washington

**UNCLASSIFIED**

**SECRET**

UNCLASSIFIED

~~SECRET~~

- 155 H. Hurwitz - Research Laboratory, Schenectady, New York
- 156 W. R. Kanne - APED, San Jose, California
- 157 ANPD - Reports Library
- 158 R. Plunkett - General Engineering Laboratory, Schenectady, New York
- 159 R. W. Porter - Engineering Services, New York City, New York
- 160 R. B. Richards - APED, San Jose, California
- 161 E. J. Schmidt - Atomic Products Division, Palo Alto, California
- 162 T. M. Snyder - Vallecitos Atomic Laboratory, Pleasanton, California
- 163 G. B. Warren - Turbine Division, Schenectady, New York
- 164 W. K. Woods - Vallecitos Atomic Laboratory, Pleasanton, California

ANP DEPARTMENT

- 165 E. R. Barker
- 166 B. Blumberg
- 167 J. W. Conley
- 168 C. H. Crandall
- 169 A. R. Crocker
- 170 J. W. Darley
- 171 T. DeRosier
- 172 A. E. Focke
- 173 D. L. Francis
- 174 C. C. Gamertsfelder
- 175 C. R. Gray
- 176 A. S. Hintze
- 177 C. S. Lankton
- 178 M. C. Leverett
- 179 S. J. Levine
- 180 F. C. Linn
- 181 W. H. Long
- 182 P. E. Lowe
- 183 H. F. Matthiesen
- 184 F. W. Mezger
- 185 H. Miller
- 186 S. H. Minnich
- 187 J. W. Morfitt
- 188 G. W. Newton
- 189 A. G. Orillion
- 190 W. G. Root
- 191 T. W. Schoenberger
- 192 R. E. Scott
- 193 D. R. Shoults
- 194 C. L. Storrs
- 195 F. G. Tabb
- 196 G. Thornton
- 197 L. M. Tupman
- 198 L. F. Yost
- 199-202 Reports Library (Idaho)
- 203-214 Reports Library (Evendale)

UNCLASSIFIED

4  
~~SECRET~~

**SECRET**

**UNCLASSIFIED**

## **CONTENTS**

1. Introduction and Summary.....	7
2. Description of HTRE No. 3 D102A Test Assembly .....	17
3. Account of the Event.....	51
4. Theoretical Analysis of Data .....	79
4.1 Interpretation of Period and Flux Records.....	79
4.2 Analytical Verification .....	84
4.3 Analysis of Circuit Performance .....	101
5. Postoperation Studies.....	113
5.1 Disassembly Inspection .....	113
5.2 Hydrogen Migration.....	136
5.3 Oxidation Analysis and Fuel Loss .....	142
5.4 Radiation Survey.....	146

**UNCLASSIFIED**

5  
**SECRET**

~~SECRET~~

UNCLASSIFIED

## 1. INTRODUCTION AND SUMMARY

The HTRE No. 3 prototype aircraft power plant, designed and built by the Aircraft Nuclear Propulsion Department and assembled at the Department's Idaho Test Station, was delivered to the Initial Engine Test (IET) facility on October 20, 1958. A series of low-power experiments was planned, to be followed by a number of full-power runs. Prior to the series of experiments extensive testing was performed on the reactor core at the Low Power Test Facility.

During operations on November 18, 1958, a power excursion and fuel element meltdown occurred. The following points summarize the incident:

1. The cause of the power excursion was the addition of reactivity brought about by the control system withdrawing dynamic and shim rods in normal sequence. This action occurred in response to a false demand caused by a less-than-actual indication of reactor power. The false indication of the linear ion chamber circuit is attributed to its installed condition as opposed to any inherent fault in design.
2. Two safety actions did not occur, either of which, in theory, could have stopped the excursion. The first was a power-level limit, which existed on two linear ion chamber channels, neither of which could indicate the correct level because of the condition of their installation. Although the period safeties operated by the log flux channels were retained in operation because of the low level, the period indication was incorrect. Saturation of the period circuits prevented any period signal that could initiate the safety actions associated with the period indication.
3. The excursion involved no inherent instabilities of the reactor and no additions of reactivity that cannot be explained by normal control rod motion. There appears to be no factor contributing to the incident that cannot be eliminated by minor changes in operating procedure and circuitry installation.
4. The mechanism of reactor shutdown was partly self-initiated. It appears that a scram due to fuel element temperature indication (or due to melting of thermocouple lead wires) and a reactivity loss of about 2 percent caused by melting and collapse of fuel rings occurred within a very short time interval and that both contributed to reactor shutdown. Even had the safety system not scrammed, the reactor would probably have shut itself down because of this local redistribution of fuel due to collapse of rings around the midplane of the reactor, which is the highest power region. This redistribution of fuel locally is contrasted with loss of reactivity due to ejection of fuel or due to redistribution longitudinally within the fuel tube. In this sense, the shutdown represented a fail-safe mechanism inherent in the reactor. The shutdown occurred soon enough that all of the reactor components will be reusable with the exception of the fuel cartridges and some moderator components. The tube sheets, reflector, and all of the shield and ducting remained intact and usable.
5. Examination of the reactor indicates that all of the fuel cartridges experienced melting in the middle stages. The amount of heat required to produce such melting

7  
~~SECRET~~

UNCLASSIFIED



is consistent with the total energy release of 770 megawatt-seconds as measured by an indium foil attached to the reactor.

The following pages contain a comprehensive summary of the event and diagnosis of the causes. Following this are separate sections dealing with detailed explanation of or justification for the statements made in the summary.

#### Description of the HTRE No. 3 Power Plant

The HTRE No. 3 power plant assembly consists of a hydrided zirconium moderator reactor, nickel-chromium fuel elements, primary and removable auxiliary shielding, engine-reactor ducting, a chemical combustor, power plant and test accessories, and turbojet engines.

The reactor core has a nominal diameter of 51 inches, active core length of 30.7 inches, and an over-all length of 43.5 inches. The core is composed of a hexagonal array of 151 moderator cells surrounded by a beryllium reflector. Each cell has as its components a moderator of hydrided zirconium (a hexagonal bar 4 inches across flats with a 3-inch-diameter hole through its center), metallic fuel elements of 80 Ni - 20 Cr and uranium oxide, an insulation liner, and a structural tube. Each fuel element consists of 19 stages, each 1-1/2 inches in length. These stages are composed of 12 concentric rings. The fuel inventory consists of fully enriched uranium in the form of the oxide with an equivalent total U<sup>235</sup> investment of 390 pounds. The total amount of 80 Ni - 20 Cr associated with the fuel is approximately 1478 pounds. The uranium oxide is embedded in the 80 Ni - 20 Cr matrix and is clad with 80 Ni - 20 Cr. The core components are air-cooled by proper division of the primary airflow.

The primary shield is approximately 20 inches thick and consists of an Inconel X - stainless steel shell containing water for neutron shielding and lead slabs for gamma shielding. An auxiliary shield composed of a stainless steel shell filled with water surrounds the primary shield. The upper half of this auxiliary shield was not installed for this test.

The reactor is controlled by insertion or removal of control rods containing europium oxide as a neutron absorber. These rods extend 20 inches into the active core from the inlet end. There are three dynamic rods used only in automatic servo control, 30 shim rods grouped in frames, and 15 safety rods.

Control of the reactor involves three modes, depending upon the power. In the source range, neutrons from the source or photoneutrons from the reflector are detected by three fission chambers with associated circuits and instruments which display the logarithm of the count rate. Control of the reactor is manual in this range. In the intermediate range, which extends from 0.0001 percent to 10 percent of full power, the flux is measured by three compensated ion chambers, which display the logarithm of the flux and the period. The logarithm of the flux and the period is recorded from one of these channels. In the power range, which extends from 10 percent to 100 percent of full power, the flux is detected by three uncompensated ion chambers, from one of which the power is recorded. The uncompensated ion chamber channel that records the reactor power also provides the reference signal to the power-range servo control system. Full power in this sense is an arbitrary number depending on the location of the ion chambers. Control in the intermediate and power ranges may be either automatic or manual. Although one of each type channel is recorded or used as a control signal, any of the channels initiates safety action. The safety system was designed to use coincident (two out of three) type circuits; however, the absence of a signal or circuit placed that particular circuit in the safety mode. This was the case with the power-range circuitry, since one ion chamber had been replaced by a heat-rate sensor.

Safety signals of three kinds are provided at three levels: interlock, which prevents further power demand increase; override, which provides a gradual decrease in power demand; and scram, which provides a sudden, emergency shutdown. The signals that initiate these safety responses originate with any of the following conditions: short period, high power, high temperatures on fuel elements or discharge air. The safety rods are fail-safe on electrical power failure.

A scram action is entirely independent of the control system. It normally is initiated only after the lesser safety actions, interlock and override, which respectively prevent shim rods from withdrawing and reduce power demand, have failed to correct a safety violation. A scram signal releases the latching current of all safety rods, which are spring-loaded, and allows them to drive in. To insure shutdown at a maximum rate, a followup action fully inserts the dynamic rods and drives all shim rods in at their maximum speed.

#### Description of the Event

On Tuesday, November 18, 1958, at 2022, a power excursion occurred at the IET with the HTR No. 3 reactor. This power excursion caused fuel element overtemperature and melting and resulted in a release of radioactive material.

At the time of the event the reactor was on automatic servo control and on a power demand setting that was expected to bring the reactor to a power of 0.12 megawatt or 80 percent of fuel range. A few hours earlier a successful run had been made at a power of 0.06 megawatt. The later run was expected to be similar in all respects to the previous run except that the power was to be doubled. This was to be the highest power for the reactor to date.

The power-range servo and instrumentation systems were usable at these low levels because the ion chambers were inserted to their deepest position within the shield, so that currents of the same magnitude as those designed for full power were produced at this lower power level.

The airflow for this experiment was provided by two electrically driven blowers supplying approximately 3 pounds of air per second, passing the air through the reactor and out the No. 2 jet engine turbine. The jet engine motored at approximately 600 rpm, and this indication was evident to the operator at the main console at all times. The airflow was adequate for this condition. There was no manipulation of any duct valves throughout the operation.

The experiments being conducted were designed to yield data concerning the rate of heat addition (rate of temperature increase) in the moderator, control rods, and shield. For these tests, three shim rods and one safety rod were removed and replaced with heat-rate sensors. One fission chamber and one uncompensated ion chamber were also removed and replaced with heat-rate sensors. In addition to these heat-rate sensors, an indium foil was placed under the reactor between the primary and secondary shields to calibrate the reactor power. This configuration was the same as for the previous run at 0.06 megawatt.

The safety trips in the power range were set at the circuit trip levels corresponding to the following power indications: interlock, 105 percent; override, 110 percent; and scram, 120 percent. Either of the two chambers would actuate the safety circuits, although only one chamber recorded on the Brown recorder and supplied the signal to the servo control. Although, by design, the period safety is eliminated in the power range, the circuit that accomplishes this had been bypassed to retain period safety protection. The period trips were set to give interlock at 10 seconds, override at 7 seconds, and scram at

~~SECRET~~

5 seconds. Fuel element temperature scrams were at 1600° to 1900°F. The signals were taken from the last stage of the fuel cartridges.

The normal pre-operational checks of instrumentation and controls were conducted, and all controls and instruments were determined to be in the anticipated operating condition. The run was started shortly after 2000 hours and the reactor power was brought up through the intermediate range and into the power range.

At the time of transfer to the power range, all appeared normal and the rod configuration was as expected. That is, all of the frames were in midposition except for frame A, which was fully withdrawn, and frame F (which contained five rods), which was withdrawing. The servo power demand, which calls for a linear increase in power to the demanded level, was on its slowest rate setting. This rate setting called for a linear rate of demand equal to that required for increasing the power from 10 to 100 percent in 40 seconds. The demanded steady-state level was 80 percent full scale.

The power of the reactor increased in a manner that appeared normal. A composite of the various traces is presented in Section 4.1, Figure 49. Shortly before the indicated power reached the expected level, the power indication dropped sharply as observed on the linear-flux instrumentation. This drop was accompanied by an indicated increasing period. Shortly after this, the reactor scrammed and the indicated power went back up rapidly with the actual power decreasing. Following the indicated increase in power the indicated power fell in a manner similar to that following a scram. The time interval from initiation of power increase in the power range until the power trace returned to its initial value was about 140 seconds. It was observed that the following safety lights were on: (1) all three levels (interlock, override, scram) of fuel element temperature, (2) all three levels of intermediate-range period on all three channels, and (3) all three levels of source-range period on both channels. From these indications it was impossible to infer whether the scram occurred because of the fuel element temperature or because of the intermediate range period. However, the people present in the control room observed that the fuel element temperature scram light was the first to give an indication. The operator also scrammed the reactor manually, but his action was preceded by perhaps 3 seconds by the automatic scram. Following the event, fuel element temperature indications of full scale or 3000°F were visible from the operator's position and moderator temperature indications of the order of 1000°F were visible.

Activity was released from the exhaust stack, and a narrow band of fallout occurred that was contained fully within the boundaries of the National Reactor Testing Station. The maximum dose rate observed in the Assembly and Maintenance area and approximately 3000 feet from the cloud centerline was 0.04 milliroentgen per hour. At a distance of 3 to 5 miles from the IET, the measured fallout was 1.25 microcuries per square meter for I<sup>135</sup>. The ratio of I<sup>131</sup> to I<sup>135</sup>, obtained from vegetation, was 0.0089. The maximum fallout observed, at about 4 hours after the incident, measured 0.8 to 2 milliroentgens per hour at contact roughly 1-1/2 miles from the IET.

Throughout the test all control circuits (with the exception of the flux indications), all safety settings, and the control rod actuators behaved in a normal and expected manner. Immediately following the test, checks again indicated that these components were behaving as expected with the exception of three rods that could not be withdrawn.

From the time of the test run until Saturday, November 22, the reactor and power plant assembly were purposely left in the condition that existed after the occurrence so that no evidence might be destroyed that could lead to an explanation of the event. Except for checks of the control rods, which involved moving each rod, and the removal

~~SECRET~~

of some electrical leads to check instrumentation circuitry, nothing was done to alter the assembly. On November 23 a critical experiment was performed to determine whether any change in the reactivity had occurred. It was found that the reactor had sustained a loss of 2.13 percent in reactivity.

Analysis of Incident and Determination of Probable Cause

One of the important numbers needed for analysis of the observed event was the total energy released during the excursion. The most reliable indication of integrated power was an indium foil that was placed under the reactor between the primary and secondary shield. An analysis of all the previous runs with indium foils calibrated with the critical experiment work at the Low Power Test Facility (LPTF) gave an indicated power of 770 megawatt-seconds during this excursion.

Calculations have been made which assume that the 770 megawatt-seconds indicated by the indium foil is the correct total energy release for the excursion. On this basis if heat is assumed to be distributed among the fuel sheets according to the theoretical power distribution in the reactor, and if no cooling is assumed, enough heat is delivered to the rings in the longitudinal central region of the reactor to raise the temperature well above the melting point, which is 2500°F. Examination of typical fuel cartridges showed that stage 3 is intact but that stage 4 is partially melted. The total energy required to produce this effect has been calculated to be about 650 megawatt-seconds.

These data show clearly that the nuclear instrumentation was not indicating the true power of the reactor to the operator. The data further indicate that high fuel temperature did cause a scram, but since all the control thermocouples were installed on stage 19, the temperatures in the central region of the reactor fuel had already reached the melting point. Scram could occur by the melting of the thermocouple leads, which traverse the cartridge. A possible conclusion is that the thermocouple leads melted through in the middle-stage region and formed new couples, which sensed the high temperatures existing in that region or else gave upscale readings because of grounding of the leads. This is the only logical explanation for the upscale readings (3000°F) reported by the persons present. Since the critical experiment showed the reactor had sustained a 2.13 percent reactivity loss, it appears that the shutdown mechanism could have been in part a redistribution of the fuel by melting.

An intensive examination of all the nuclear instrumentation revealed that the source of the event was indeed in the nuclear instrumentation systems. The initiating cause of the rapid increase in power was the inability of the linear-flux-chamber circuitry to supply a current proportional to flux above a certain flux level. This was caused by a resistance in the chamber supply voltage line, part of a voltage-smoothing filter, which limited the maximum current that could be drawn from the chamber. The current in this chamber circuit provides a signal to the control system and recorders. The servo sees the same signal as the recorder. The power supply was set to deliver 800 volts. Therefore, the maximum current, limited by the 1-megohm resistor in the filter, that can be passed by the circuit (if it is assumed that the ion chamber has no resistance whatsoever) is about 0.8 milliamperes. The signal required to actuate the high power level scram trip at 120 percent full scale is 0.96 milliamperes. While the current corresponding to the demanded power signal (80 percent full scale) is only 0.64 milliamperes, the presence of the high resistance causes abnormally high fluxes to be required at the chamber to pass this current. Because of the current limitation imposed by the power-supply circuitry, the signal to the control system and the recorders did not continue to increase as flux and power level increased, nor did the indicated flux ever satisfy the demanded power. This deviation of flux indication resulted in continued demand to the automatic control system for withdrawal of rods, since the indicated power continued

~~SECRET~~

below the demanded power. Actual power, therefore, must have increased on a decreasing period until the reactor shut down. Following the scram the actual flux fell to the point at which the chamber current was again proportional to flux, whereupon the circuits recovered and the indications tended toward normal.

A further anomaly in the power traces, the decrease followed by an increase, has also been explained. This phenomenon is a result of the situation and did not contribute to its initiation. This decrease was caused by the continued buildup of the gamma ionization in the chambers after the neutron current reached its maximum value. In the uncompensated chamber this results in a decreasing resistance between the high-voltage electrode and the case, which is grounded. This effectively shorts out the indicating circuit. The current (limited by the high-resistance filter) divides, part flowing to ground, and the signal to the recorder, thus, decreases.

The use of such a filter in the power-range flux-sensing circuitry was a standard practice for HTRE No. 1 and HTRE No. 2 operations. This filter was introduced to reduce noise in the circuitry early in the HTRE No. 1 testing sequence and was retained through the testing of HTRE No. 1 and HTRE No. 2. Because of this, the filter became identified with the power supply as opposed to being identified with the HTRE No. 2 circuitry. Although the same power supplies were to be used for HTRE No. 3 operation, the use of this filter was not contemplated in the design of the HTRE No. 3 power-range circuitry. Nevertheless, it was used for certain initial checkouts at low levels in which the flux signal was amplified. Although the amplifiers had been removed from the circuit, the filters had not. This condition existed on both of the linear-flux-sensing channels that were in use. Although only one of these circuits fed the control system, both circuits had interlock, override, and scram settings intended to provide duplication of safety circuitry.

The HTRE No. 2 control system used compensated ion chambers, the currents from which were considerably lower than the currents contemplated for HTRE No. 3. Thus, the current limitation imposed by the filter did not adversely affect HTRE No. 2 control.

If reasonable combinations of shim and dynamic rod motion are assumed, the power trace can be reconstructed as a function of time. Such reconstruction shows that it is possible to account for shutdown in approximately the correct timing to place the peak power at the same point as the bottom of the dip in the linear-flux trace (which is consistent with the theory of saturation and short-circuiting of the chamber due to gamma ionization). The time required for the power to decay to the point at which the circuit can again detect faithfully appears to be also consistent. Such calculations also reproduce a total energy in the neighborhood of 770 megawatt-seconds. These calculations place the peak instantaneous power between 100 and 500 megawatts. Because the exact interrelationship of the scram and fuel-element-collapse shutdown mechanism is not known, nor is the exact sequence of rod motions known, a number of calculations have been tried to obtain the best fit.

The log-flux (intermediate-range) circuitry exhibited a behavior similar to that of the power-range circuitry. However, the behavior of the log-flux circuits has been explained as a result of the high power produced rather than any circuit or instrument malfunction. The log-flux traces show that, although the signals were above the top reading of the recorder during the early part of the excursion, the indication dips sharply at approximately the same time that the dip occurs in the linear flux channel. The period trace, which is derived from the log-flux indication, shows an analogous behavior that is consistent with the derivative of the log-flux trace. That is, the indicated period becomes longer, going negative as the log-flux trace moves downscale, becomes suddenly positive as the log-flux trace moves rapidly back upscale, and becomes negative again

~~SECRET~~

as the log-flux trace moves back downscale, corresponding to the true falloff of power in the reactor. The behavior of the period circuits has been shown to be a result of circuit saturation, which limited the current to that corresponding to the 200 percent full range. (The log-flux chambers were inserted in the shield at such a depth that the range of indication matched that of the linear-flux chambers.) Therefore, the period circuits saw a steady-state signal, even though the power was continually rising. Reconstruction of the incident shows that the periods were, in general, longer than the scram trip setting, which was 5 seconds. Had the log-flux circuit not saturated, it is conceivable that the other safety actions, interlock or override, might have been initiated. The interesting point is, however, that the power level rose to the point at which the circuit saturated before any of the short-period safety actions were initiated.

The condition that caused the log flux to drive downscale was similar to that affecting the linear-flux circuits. That is, both the neutron and gamma sides of the compensated chamber circuits saturated (due to the intentional presence of an electrical noise filter), their signals becoming equal so that their subtraction produced zero input to the log-flux circuitry. This behavior is explained in more detail in section 4.1.

The postulated behavior of both the linear-flux and log-flux circuits has been verified by intensive examination of circuit constants in addition to actual circuit checkout in the MTR.

#### Inspection

The radiation levels around the power plant were such that manual maintenance was possible. The power plant was moved to the hot shop, the reactor-shield assembly was removed, and the rear plug was removed for inspection of the rear face of the core, shown in section 5.1, Figure 72. Inspection revealed that the damage appeared to be confined to the fuel cartridges; the rear stages of all fuel cartridges were intact, although 35 showed signs of severe overtemperature. Since manual attempts to remove the cartridges were unsuccessful, it was necessary to disassemble the reactor. The disassembly was accomplished routinely. The reactor core was separated from the front plug; the moderator cell latches were released by hand from the front of the reactor and the moderator cells individually removed. Fuel cartridges were then removed from the separated moderator cells. In many cases it was possible to remove the insulation sleeve - cartridge combination through the exertion of sufficient pull. In other cases it was necessary to remove the moderator support tube by cutting the front casting, thus removing fuel cartridge, insulation sleeve, and support tube as a unit, but preserving the moderator block. The condition of typical fuel cartridges is shown in section 5.1, Figures 76 and 88. Every fuel cartridge in the reactor had experienced melting in the central stages (as would be expected because the reactor was power flattened). The collapse of the stages in the center of the reactor produced the loss in reactivity observed after the incident.

Many of the hydrided zirconium hexagonal moderator blocks were intact and will be reusable. In a few isolated cases molten slag had burned through the moderator block and welded the moderator block to the adjacent control rod guide tubes. A typical moderator block with melt-through is shown in section 5.1, Figure 101. It has been determined that 74 moderator blocks will be reusable. The control rod guide tubes, in general, will be reusable after replating.

In summary, the damage was limited principally to the fuel cartridges with some auxiliary damage to moderator and control rod guide tubes. Every other component of the power plant remained in operable and reusable condition. This may be regarded as a natural result of the configuration of the reactor. The power is generated in a fuel

UNCLASSIFIED

SECRET

element which has, relatively, much less heat capacity than the rest of the system. Therefore, the fuel element temperatures rise at a rapid rate before any heat can be transferred to the remainder of the system; this produces an action somewhat like that of a fuse to shut down the reactor.

#### Conclusion

Examination of the events of November 18, 1958, and of the reactor has revealed that the reactor, power plant components, and the control and safety system components all functioned as designed and the excursion was caused solely by the addition of a filter in the ion chamber power-supply circuitry, which caused an incorrect signal. During the run there was no indication of any reactor instability nor was there any indication that the positive moderator temperature coefficient played any part in the event. In fact, moderator temperature peaks were not reached until some minutes following the scram.

A reactivity loss of approximately 2.13 percent was measured. Measurements of the effluent show that less than 2 percent of the fuel and fission products escaped, an indication that the loss in reactivity was not caused by loss of fuel but by local changes in geometry. The geometry changes are attributed to melting of the fuel in place as opposed to ejection of fuel from the reactor or to redistribution longitudinally. This local change in geometry causes a loss in reactivity through the mechanism of increased self-shielding and increased streaming losses.

Aside from this local redistribution of fuel, there was no shifting or relocation of parts of the reactor.

The damage to the power plant was restricted to the fuel and minor damage to the moderator. These items can be readily replaced.

It can be concluded that the primary cause of the incident was that the linear-flux circuitry was unable to indicate true reactor power because of the presence of electrical noise filters in the circuitry. In addition the power supply was set at 800 volts. The recommended setting for these power supplies when the circuitry was designed was 1500 volts. Had the power supply been set at 1500 volts the flux level at which saturation occurred would have been increased. For this particular run this increase might have been sufficient to permit the indicated flux signal to satisfy the demand. Thus it is seen that the physical cause of the incident was the presence of two conditions, the removal of either of which might have prevented the incident. These two conditions can be attributed to human factors and not to basic design of the reactor or of the instrumentation.

The human elements involved appear to have been twofold. The presence of the electrical noise filters was a common situation at the IET, since these filters were in routine use during the operation of the HTRE No. 1 and the HTRE No. 2 reactors. The power supplies and filters for HTRE No. 1 and HTRE No. 2 were permanently mounted in separate panels in the facility and interconnected by coaxial cables. While the HTRE No. 3 circuits called for the use of these same power supplies, the drawings did not show the filter interconnection, but showed connection of the chamber leads directly to the power supplies. Out of habit, however, the chamber leads were connected to the filter terminal and the filter leads were then connected to the power supply.

The fact that the voltage setting of the power supply was 800 rather than 1500 volts was another human error. The checkout procedure called for a setting of 800 volts. However, this checkout procedure was in error, the recommended voltage settings of the power-range, uncompensated ion chamber circuits having been interchanged with recommended voltage settings for the intermediate-range compensated ion chamber circuit. The correct settings were 800 volts on the intermediate-range circuits and

UNCLASSIFIED

SECRET

~~SECRET~~  
UNCLASSIFIED

15

1500 volts on the power-range circuits. Subsequent examination of the circuitry confirmed the fact that these two settings had been reversed.

It should be noted that the voltage setting for the operation of these circuits is relatively arbitrary. The linear-flux uncompensated ion chamber circuits would have operated quite well with 800 volts. It is only the presence of the high-resistance electrical noise filter that makes the voltage setting crucial.

~~SECRET~~  
UNCLASSIFIED



UNCLASSIFIED

## 2. DESCRIPTION OF HTRE NO.3 D102A TEST ASSEMBLY

HTRE No. 3 was planned to provide the data required to determine the reactor's power extraction characteristics. Tests of the HTRE No. 3 power plant were made at the Idaho Test Station in the Initial Engine Test facility (IET).

The D102A assembly, shown in Figure 1, consists of a reactor, primary shield, external auxiliary shielding, engine-reactor ducting, a single chemical combustor with surrounding auxiliary shield, accessories, and two modified J47 turbojet engines. The reactor uses the direct cycle, and all components are air-cooled. The moderator is hydrided zirconium, fuel elements are 80 Ni - 20 Cr concentric ribbon, the reflector is beryllium, and the reactor is controlled by europium oxide air-cooled rods.

The shield consists of water, lead, steel, and boral and is designed for a 1000-hour life at 175-megawatt operation. The complete assembly is shown in Figure 2. The primary shield has as its principal objective the simulation of a flight-type shield structure; therefore, its radiation shielding characteristics are correspondingly low.

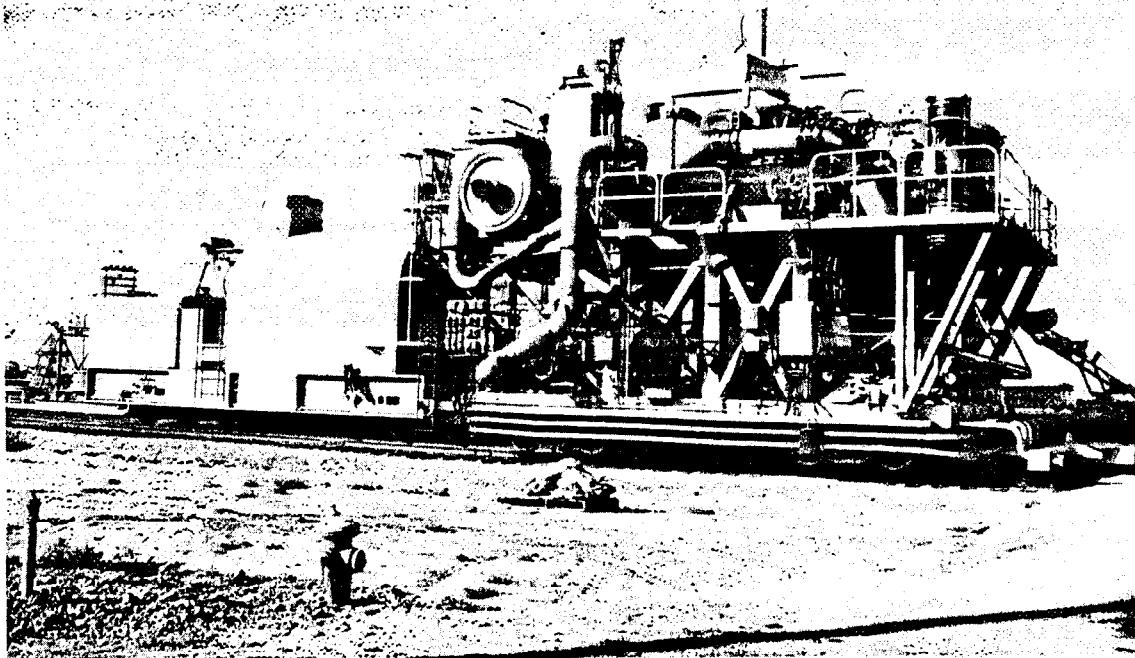


Fig. 1 - D102A test assembly with shielded locomotive

SECRET

UNCLASSIFIED

UNCLASSIFIED

SECRET

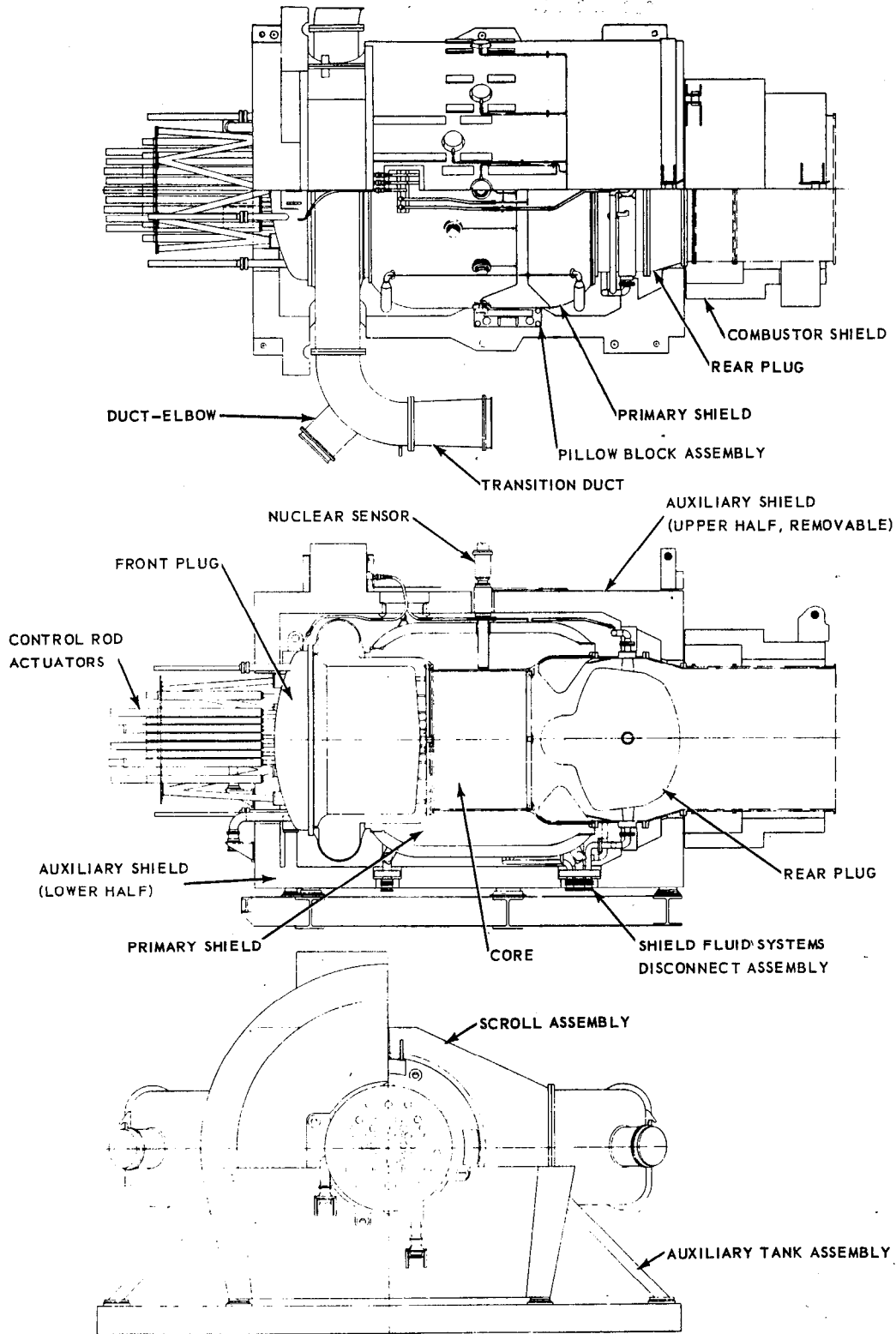


Fig. 2 - Reactor-shield assembly

UNCLASSIFIED

SECRET



However, in conjunction with the external auxiliary shield, the radiation levels are expected to fall within the limits of  $10^4$  rep per hour for fast neutrons and  $10^5$  roentgens per hour for operating gammas.

An airflow cycle of this assembly is shown in Figure 3. The air enters the turbojet engine and passes through the cold ducting to the forward transition scroll, where it is distributed radially through the front plug and into the core through the front tube sheet. Some of this air is used to cool the beryllium reflector and the control rods; the remainder (97 percent of total) is passed through the active core. The air is heated to approximately  $1300^\circ\text{F}$  and is exhausted into a plenum from which it passes through the combustor and aft header and back down through the engine turbine. The air is then exhausted to the atmosphere via the exhaust-handling system. Station designations are shown in Figure 4. When the system is operating on chemical fuel, the compressor air is passed through the cold reactor, since no reactor bypass ducting is provided. Single-engine operation may be obtained by closing the compressor and turbine shutoff valves in the external ducting of the inactive engine.

The power plant is started on chemical fuel along with compressor air passing through the cold reactor. Then, with the engine speed and turbine inlet temperature controls set at a predetermined level, the reactor is started and the power is increased. When the nuclear heat added to the air is detected by the engine temperature control

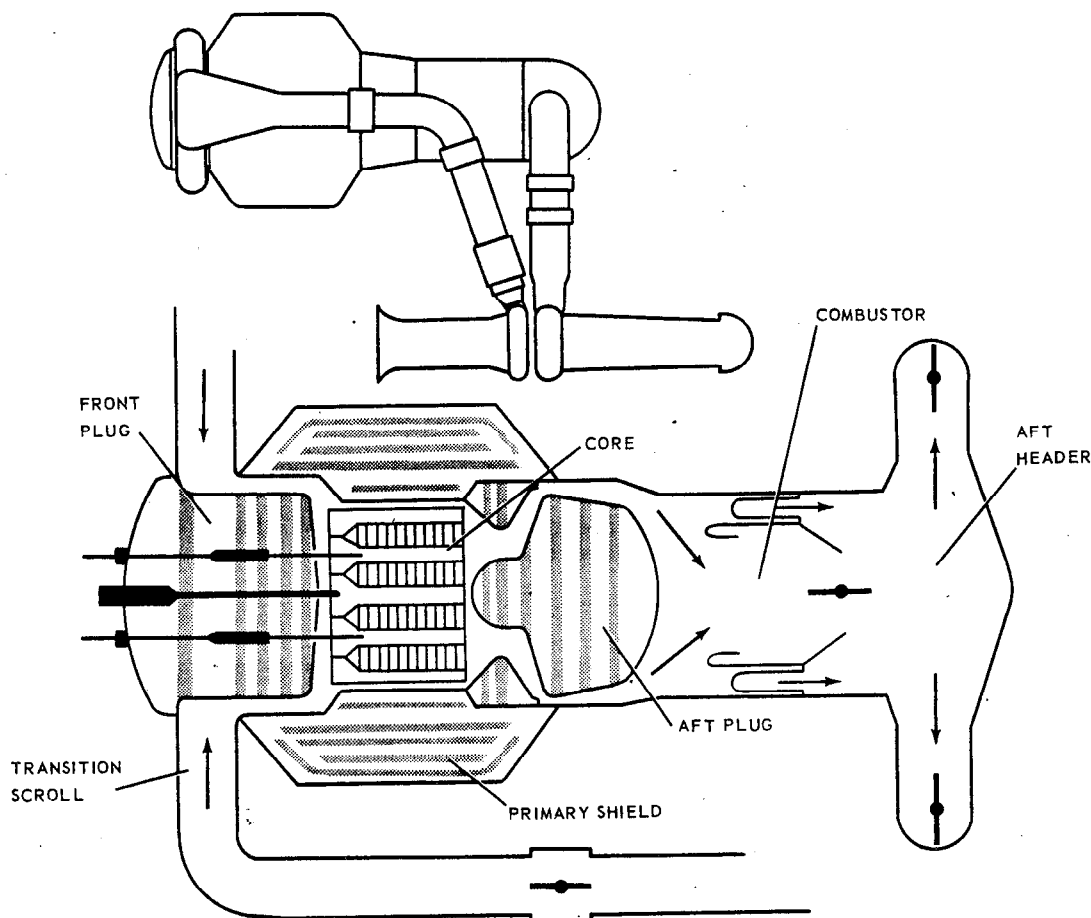


Fig. 3 - D102A air flow cycle

UNCLASSIFIED

SECRET

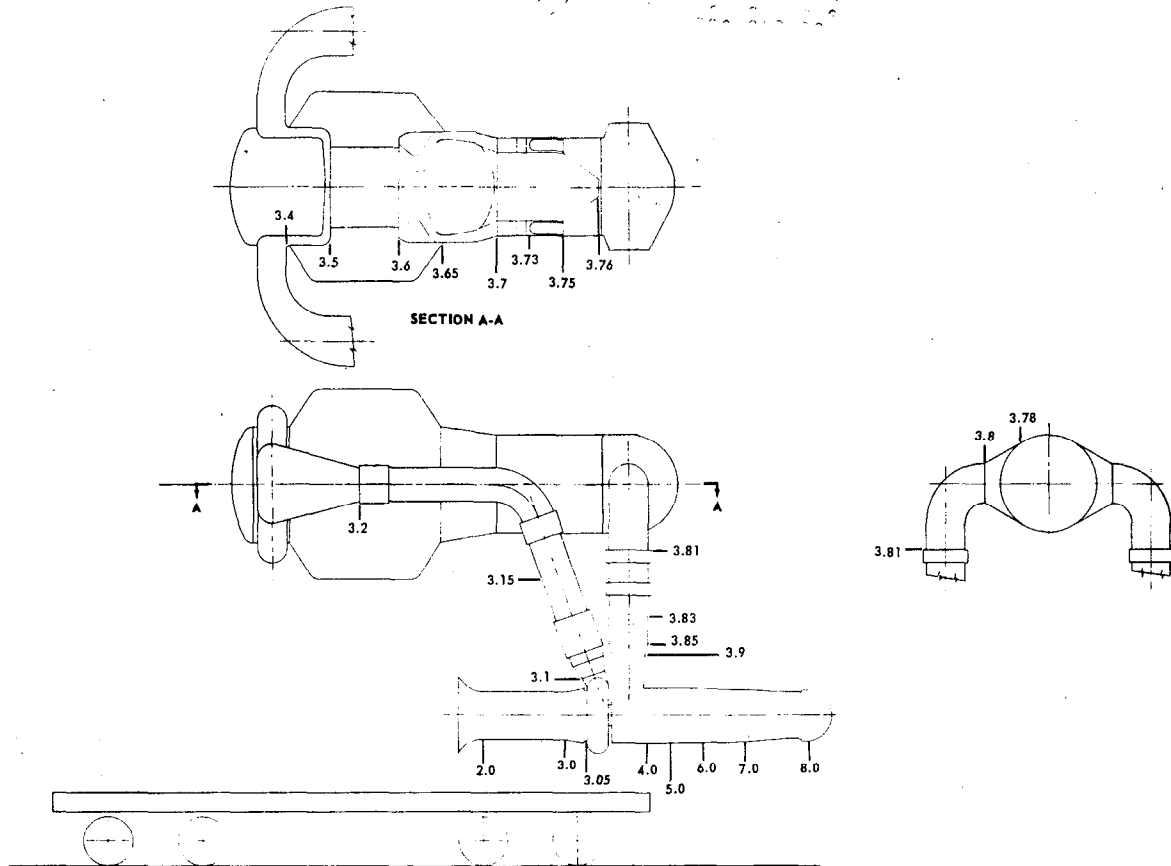


Fig. 4 - Station designations, D102A assembly

thermocouple, the chemical fuel valve starts to close to maintain the exhaust temperature at the predetermined level. As reactor power increases, the fuel valve closes completely, with engine speed held constant throughout the transfer cycle.

Each engine is independently and automatically controlled during either chemical or nuclear operation by automatic speed control systems. The turbine inlet temperature of the engine ( $T_4$ ) is automatically controlled at any point between 800° and 1600°F with an accuracy of ± 1 percent with chemical operation. The speed of the engine is independently and automatically controlled at any point between 5500 and 7950 rpm with an accuracy of ± 0.5 percent. Manual electrical methods of controlling jet nozzle area and fuel flow are also provided.

Reactor power is controlled by insertion and withdrawal of poison rods. The present control system utilizes flux level as a measure of reactor power. Later, reactor exit air temperature measurement will be integrated into the over-all control. The flux system automatically controls reactor power from 10<sup>-4</sup> percent to 100 percent full power, with the 10 to 100 percent full-power range controlled to ± 1 percent full power. The temperature system automatically controls  $T_4$  from 1000° to 1600°F, ± 10°F.

D102A SPECIFICATIONS AND DESIGN DATA

The following is a list of general physical, nuclear, and thermodynamic characteristics of D102A with the X39-5 engine.

UNCLASSIFIED

SECRET

PHYSICAL CHARACTERISTICS

Primary Shield

Structural type	Flight prototype
Structural material	Inconel X
	Stainless steel
Shielding material	Lead (gamma)
	Boral
	Water (neutron)
Required heat removal	2% reactor power
Cooling water flow	612 gpm
Maximum cooling capacity	2.5% (175-mw operation)
Augmentation	Mercury
Outside diameter	97.5 in.
Inside diameter	58.0 in.

Engines

Type	X39-5
Quantity	2
Compression ratio	4.95
SLS airflow	75 lb/sec
Maximum turbine inlet temperature	1600°F
Combustor	Common

Moderator

Material	Hydrided zirconium
Clad	None
Volume fraction	0.358
Distance across flats	3.923 in.

	<u>Depth</u>	<u>Width</u>
Cooling slots, cells X10-X65		
Corner slots	0.320 in.	0.147 ± 0.005 in.
Middle slots	0.215 in.	0.194 ± 0.005 in.
Cooling slots, cells X72-X75		
Corner slots	0.320 in.	0.161 ± 0.005 in.
Middle slots	0.229 in.	0.207 ± 0.005 in.
Element spacing		0.030 in. nominal
Length of hydrided zirconium		35.69 in.
NH Specifications	<u>Number of Cells</u>	
	27	2.9 ± 0.05
	24	3.0 ± 0.05
	9	3.1 ± 0.05
	30	3.25 ± 0.05
	36	3.45 ± 0.05
	24	3.95 ± 0.05

Insulation liner - fuel-annulus hydraulic diameter 0.18 in.

~~UNCLASSIFIED~~~~SECRET~~Reflector

Material Beryllium  
 Outside diameter 57.0 in.  
 Configuration Hexagonal shapes  
 Cooling configuration 7 holes per segment

Fuel Elements

Material 80 Ni - 20 Cr  
 Number of identical stages per cartridge 19  
 Distance from leading edge of stage 1 to  
 leading edge of stage 19 29.250 ± 0.020 in.  
 Nominal spacing between successive stages 0.134 in.  
 Number of rings per stage 12

Inter-ring gap spacing, in.

Ring	Type A	Type B	Ring	Type A	Type B
1-2	0.054	0.054	7-8	0.084	0.088
2-3	0.072	0.067	8-9	0.083	0.088
3-4	0.077	0.072	9-10	0.083	0.090
4-5	0.083	0.076	10-11	0.084	0.090
5-6	0.085	0.081	11-12	0.085	0.087
6-7	0.085	0.087			

Ring-spacing tolerance - outside of rings 1,  
 2, 3, 4

±0.004 in.

- all others

±0.005 in.

Active cartridge length

30.741 in.

Meat width of rings

1.450 ± 0.030 in.

Dead-edge width

0.0205 ± 0.1445 in.

Over-all width of rings

1.491 ± 0.059 in.

Ring thickness tolerance

±0.001 in. maximum per ring

±0.0005 in. weighted average

Cut length tolerance

±0.010 in.

Cladding thickness

0.004 ± 0.0006 in.

Linear density tolerance

±3.5%

Area density tolerance (reference)

±6.0%

Weight percentage uranium in UO<sub>2</sub>

87.5 ± 0.5%

Weight percentage U<sup>235</sup> in uranium (enrichment)

93.2 ± 0.5%

U<sup>235</sup> weight per core (reference)

390 lb

Total UO<sub>2</sub> weight per stage

Type A	Type B
0.1697 ± 0.005 lb	0.1700 ± 0.005 lb
3.224 ± 0.060 lb	3.230 ± 0.060 lb
13.114 ± 0.430 lb	13.057 ± 0.430 lb

Total UO<sub>2</sub> weight per cartridge

Total weight of assembled cartridge

Nominal 80 Ni - 20 Cr weights

Cladding plus dead edge

80 Ni - 20 Cr mixture in core

Inner structure (combs, spacers, etc.)

Rails

Wire seals

Grams Per Stage	
Type A	Type B
97.5	95.8
106.5	106.6
21.7	21.7
8.8	8.8
2.1	2.2

Inside diameter of insulation liner

2.961 in. (cold)

~~UNCLASSIFIED~~~~SECRET~~

Center-to-center distance of cells 3.953 in.  
 Fuel and air frontal area 963 in.<sup>2</sup>  
 Heat transfer area 3200 ft<sup>2</sup>  
 Moderator-cooling-air frontal area 87 in.<sup>2</sup>

Control Rods

Material Europium oxide  
 Type and quantity - dynamic 3  
                                   - shim 30  
                                   - safety 15  
 Location of rods - center 23  
                                   - outer 25  
 Clad, 310 stainless steel 0.040 in. thick  
 Diameter 0.70 in.  
 Active length 20.0 in.

Core General

Structural material INCONEL X  
 Over-all length 43.5 in.  
 Active length 30.7 in.  
 Nominal diameter 51.0 in.

Materials of active core (excluding tube sheets, reflector, and control rods)

	<u>Volume Fraction</u>	<u>Weight, lb</u>
UO <sub>2</sub>	0.020	483.16
80 Ni - 20 Cr	0.078	1478
Type 310 stainless steel	0.032	540
Hydrided zirconium	0.348	4620
INCONEL X	0.002	80
MgO	0.038	
Void	0.482	

<u>Component Weights, lb</u>	<u>Dry</u>	<u>Water Added</u>	<u>Mercury Added</u>
Dolly	87,009	-----	-----
Superstructure (includes platforms and supports)	35,250	-----	-----
Auxiliary shield, lower half	35,242	44,717	-----
Front plug	21,167	25,388	-----
Pressure vessel	1,760	-----	-----
Side shield	51,435	58,795	107,645
Reactor	14,615	-----	-----
Aft plug	20,897	23,751	-----
Scroll assembly (20-inch ducts)	6,652	-----	-----
Auxiliary shield, upper half	39,068	52,392	-----
Chemical fuel combustor	1,700	-----	-----
Combustor shield	28,089	30,267	-----
Engine ducting and supports (cold)	5,000	-----	-----
Engine ducting and supports (hot)	8,000	-----	-----
X39-5 engines (2)	10,640	-----	-----

UNCLASSIFIED

<u>Component Weights, lb</u>	<u>Dry</u>	<u>Water Added</u>	<u>Mercury Added</u>
Shield-liquid system	13,411	17,500	18,500
Fuel system	200	-----	-----
Lubrication system	600	-----	-----
Shield-liquid vent system	500	-----	-----
Aftercooling system	27,000	-----	-----
Fire extinguisher	750	-----	-----
Electrical system (includes instrumentation)	8,000	-----	-----
Walkways	2,000	-----	-----
Hydraulic powerpack	400	-----	-----

THERMODYNAMIC CHARACTERISTICS

Compressor discharge temperature	385 <sup>o</sup> F
Compressor discharge pressure	53.3 psia
Reactor airflow	122.2 lb/sec
Compressor airflow (both engines)	126 lb/sec
Reactor power design point	31.8 mw
Reactor discharge temperature	1330 <sup>o</sup> F
Turbine inlet pressure	43.3 psia
Core inlet air pressure	49.4 psia
Core airflow	120.7 lb/sec
Fuel element exit air temperature (including outer annulus)	1415 <sup>o</sup> F
Moderator-cooling-slot discharge temperature	1000 <sup>o</sup> F
Fuel element airflow	106.1 lb/sec
Moderator-cooling-slot airflow	14.6 lb/sec
Pressure ratio across core	0.91
Pressure ratio, compressor to turbine	0.81
Fuel-element maximum design temperature	1850 <sup>o</sup> F
Moderator maximum temperature (highest N <sub>H</sub> region)	1200 <sup>o</sup> F
Pressure drop across fuel stage	0.2-0.3 psi
Maximum dynamic head within fuel elements	0.8 psi

NUCLEAR CHARACTERISTICS

Reactivity Summary Based on Initial Criticality Measurements

<u>Cold, Clean Reactivity Measurement</u>	<u>%Δk/k</u>
Reactivity held by shims	3.048
Dynamic rods worth (1/2 insertion)	0.152
Reactivity of 21 poison liners	0.442
Addition of rear plug	0.750
Cold, clean, excess reactivity	4.392

Cold, Startup Reactivity Measurement

Reactivity held by shims and dynamics	1.46
Addition of rear plug	0.75
Cold, excess with 84 liners	2.21

UNCLASSIFIED



<u>Reactivity During Operation</u>	<u>%Δk/k</u>
Cold, excess with liners	2.21
Temperature increase 68°F to 1000°F	+0.57
Hot clean excess	2.78
Equilibrium xenon at 38 mw	-1.30
Hot, dirty excess	1.48

<u>Reactivity with H<sub>2</sub>O Removal</u>	
(four individual measurements)	
Drain front plug	+0.25
Drain side shield	+1.50
Drain rear plug	+0.78
Drain all shield compartments	+2.99

#### Active Core Average Fluxes

Fast	5.44 x 10 <sup>6</sup> n/cm <sup>2</sup> -sec-watt
Thermal	0.12 x 10 <sup>6</sup> n/cm <sup>2</sup> -sec-watt

#### Calculated Radial Fluxes,\* n/cm<sup>2</sup>-sec-watt

<u>Region</u>	<u>N<sub>H</sub></u>	<u>Fast</u>	<u>Thermal</u>	<u>Nominal Outer Radius, cm</u>
central cell	--	7.1 x 10 <sup>6</sup>	0.070 x 10 <sup>6</sup>	5
1	2.8	6.9 x 10 <sup>6</sup>	0.095 x 10 <sup>6</sup>	32.1
2	2.5	6.1 x 10 <sup>6</sup>	0.090 x 10 <sup>6</sup>	41.2
3	3.0	5.4 x 10 <sup>6</sup>	0.11 x 10 <sup>6</sup>	50.3
4	3.3	4.4 x 10 <sup>6</sup>	0.13 x 10 <sup>6</sup>	59.4
5	3.95	3.5 x 10 <sup>6</sup>	0.20 x 10 <sup>6</sup>	64.8
Beryllium		1.5 x 10 <sup>6</sup>	0.30 x 10 <sup>6</sup>	72
Pressure shell		0.9 x 10 <sup>6</sup>	0.21 x 10 <sup>6</sup>	74
At inner surface of first lead shield		~0.1 x 10 <sup>6</sup>	~0.07 x 10 <sup>6</sup>	84

#### Calculated Longitudinal Fluxes,† n/cm<sup>2</sup>-sec-watt

<u>Region</u>	<u>Fast</u>	<u>Thermal</u>	<u>Distance from front of forward tube sheet, cm</u>
Front plenum (average)	~0.1 x 10 <sup>6</sup>	~0.0005 x 10 <sup>6</sup>	---
Front of forward tube sheet	0.4 x 10 <sup>6</sup>	0.002 x 10 <sup>6</sup>	0
Rear of forward tube sheet	1.3 x 10 <sup>6</sup>	0.1 x 10 <sup>6</sup>	6
Front reflector (average)	2.2 x 10 <sup>6</sup>	0.25 x 10 <sup>6</sup>	8-18.8
Front of active core	3.9 x 10 <sup>6</sup>	0.24 x 10 <sup>6</sup>	18.8
3 inches from front of core	4.5 x 10 <sup>6</sup>	0.1 x 10 <sup>6</sup>	26.4
Core midplane	7.2 x 10 <sup>6</sup>	0.16 x 10 <sup>6</sup>	57
Rear of core	2.1 x 10 <sup>6</sup>	0.054 x 10 <sup>6</sup>	97
Front of rear tube sheet	1.6 x 10 <sup>6</sup>	0.022 x 10 <sup>6</sup>	101
Rear of rear tube sheet	0.6 x 10 <sup>6</sup>	0.002 x 10 <sup>6</sup>	107.3
Rear plenum (average)	~0.1 x 10 <sup>6</sup>	0.0005 x 10 <sup>6</sup>	----

\*These are average neutron fluxes in the moderator of the active core and in external radial regions. They are averaged over the 30-inch active length. To obtain midplane fluxes (peak), multiply above values by 1.30.

†These are average neutron fluxes in the moderator of the active core in external longitudinal regions. The values correspond roughly to a longitudinal traverse made in core region No. 3 (N<sub>H</sub> = 3.0), which is close to the radial average.

~~UNCLASSIFIED~~~~SECRET~~

Longitudinal power distribution	Values shown in Table 1
Gross radial power distribution	Flat within 8% peak
Fine radial power distribution	Values shown in Table 1
Cell power	Values shown in Table 2
Excess reactivity:	
Cold	2.21% $\Delta$ k/k
Hot	2.78% $\Delta$ k/k
Reactivity versus total core $N_H$	Values shown in Figure 5
Reactivity versus fuel loading	Values shown in Figure 6
Reactivity loss	Values shown in Figure 7
Xenon buildup following shutdown	Values shown in Figure 8
Excess reactivity versus reactor period	Values shown in Figure 9
Afterheat	Values shown in Figure 10

#### Control Rod Values, $\Delta$ k/k (Total)

Shim rods	6.67 (unshadowed)	5.28 (shadowed)
Safety rods	2.30 (unshadowed)	2.21 (shadowed)
Dynamic rods	0.490 (unshadowed)	0.480 (shadowed)

#### Nuclear Heating (% of total power)

Moderator	6.8
Fuel elements	1.6
5 inches ZrH <sub>x</sub>	0.4
Front tube sheet	0.1
Rear tube sheet	0.1
Radial shield	0.8
Front plug	0.3
Rear plug	0.3

#### Rod Locations and Worths

Frame	Number of Rods	Positions	% $\Delta$ k/k Per Frame	
			Unshadowed	Shadowed
<b>Shims</b>				
A	3	221, 110, 410	0.73	0.54
B	6	320, 220, 321, 121, 510, 610	1.40	1.07
C	6	232, 231, 420, 421, 120, 621	1.36	1.06
D	6	330, 230, 332, 131, 520, 620	1.30	1.05
E	3	331, 132, 521	0.67	0.53
F	6	243, 241, 130, 631, 432, 430	1.21	1.03
Dynamics	3	352, 153, 542	0.49 $\pm$ 0.05	0.48 $\pm$ 0.05
Safeties	15	351, 265, 263, 261, 154, 152, 150, 653, 651, 543, 541, 454, 452, 450, 353	2.30 $\pm$ 0.20	2.21 $\pm$ 0.20
			} 5.28 $\pm$ 0.60 Total	

~~UNCLASSIFIED~~~~SECRET~~



Composition of Active Core (excluding tube sheets, reflector, and control rods)

	<u>Volume Fraction</u>	<u>Weight, lb</u>
UO <sub>2</sub>	0.020	483.16
80 Ni - 20 Cr	0.078	1478
Type 310 stainless steel	0.032	540
Hydrided zirconium	0.348	4620
INCONEL X	0.002	80
MgO	0.038	
Void	0.482	

Composition of Fuel Elements

Weight percentage uranium in UO <sub>2</sub>	87.5 ± 0.5%
Weight percentage U-235 in uranium (enrichment)	93.2 ± 0.5%
Total UO <sub>2</sub> weight per stage, lb	0.1674 ± 0.005
Total UO <sub>2</sub> weight per cartridge, lb	3.180 ± 0.030
Total weight of assembled stage, lb	0.6734 ± 0.0150
U-235 weight per core (reference), lb	389.5 ± 6.0
Number of fuel cartridges per core	150
Number of identical stages per cartridge	19
Nominal 80 Ni - 20 Cr weight:	<u>Grams per stage</u>
Cladding plus dead edge	99.07
80 Ni - 20 Cr mixture in core	105.05
Inner structure (combs, spacers, etc.)	23.4
Rails	11.1
Wire seals	1.99
	<u>240.61</u>
Total	240.61

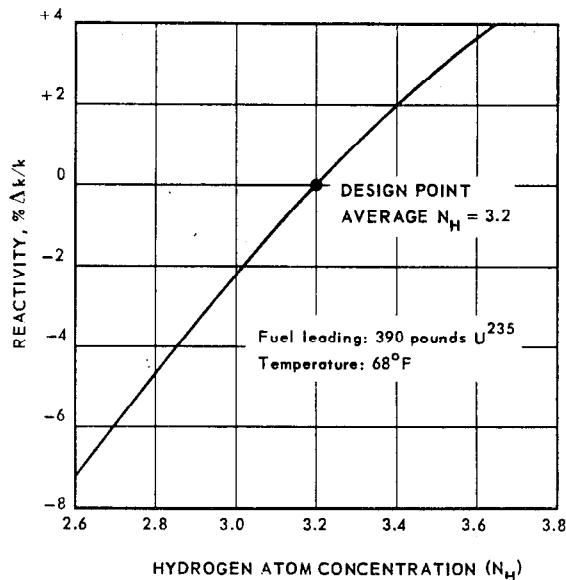


Fig. 5 - Reactivity versus total N<sub>H</sub> in core

UNCLASSIFIED

Corrected by D102A nuclear  
 element criticality data  
 19-Stage fuel element  
 No xenon

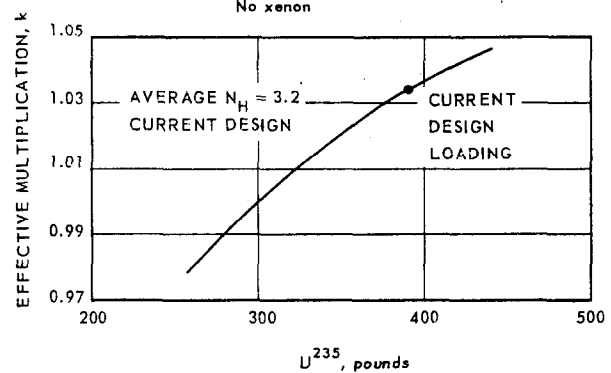


Fig. 6 - Core loading versus reactivity

TABLE 1  
 FINE RADIAL AND LONGITUDINAL POWER DISTRIBUTION FACTORS

Ring "i"	Ring Heat Flux Factor						
	A-10 <sup>a</sup>	A-2X	A-3X A-4X	B-3X B-4X	B-5X	B-6X	B-7X
1	0.61	0.61	0.56	0.53	0.54	0.49	0.54
2	0.70	0.69	0.65	0.62	0.62	0.58	0.61
3	0.81	0.80	0.76	0.73	0.72	0.69	0.71
4	0.88	0.86	0.83	0.81	0.78	0.76	0.78
5	0.96	0.93	0.91	0.89	0.84	0.85	0.86
6	0.99	0.98	0.96	0.99	0.93	0.95	0.97
7	0.98	0.98	0.96	1.00	0.95	0.98	0.98
8	0.97	0.99	0.97	1.01	1.01	1.01	1.00
9	0.98	1.01	1.00	1.04	1.07	1.07	1.04
10	1.00	1.04	1.04	1.10	1.14	1.12	1.11
11	0.96	1.00	1.02	1.02	1.05	1.02	1.02
12	1.23	1.24	1.30	1.18	1.20	1.24	1.22

Stage "n"	Longitudinal Factor			
	0 Rods	1 Rod	2 Rods	3 Rods
1	0.72	0.65	0.56	0.46
2	0.82	0.75	0.66	0.59
3	0.92	0.85	0.76	0.71
4	1.00	0.95	0.87	0.84
5	1.08	1.05	1.01	0.99
6	1.15	1.13	1.12	1.10
7	1.20	1.19	1.21	1.21
8	1.23	1.23	1.25	1.29
9	1.25	1.27	1.30	1.33
10	1.25	1.28	1.31	1.35
11	1.23	1.28	1.30	1.34
12	1.20	1.24	1.27	1.32
13	1.14	1.18	1.19	1.21
14	1.07	1.10	1.13	1.15
15	0.98	1.01	1.05	1.07
16	0.88	0.91	0.95	0.98
17	0.75	0.78	0.84	0.87
18	0.62	0.65	0.71	0.75
19	0.48	0.51	0.59	0.63

<sup>a</sup>Column headings designate cartridge location: e. g., A-10 denotes all cartridges of type A having cell numbers ending in 10; A-2X denotes all cartridges of type A in which the second digit is 2. Figure 27 shows cartridge types and cell numbers.

UNCLASSIFIED

TABLE 2

## CELL POWER

Cell Number <sup>a</sup>	Heat Flux (Cell/Core Avg)	Adjacent Rods	Type Element
X10 <sup>b</sup>	1.066	2	A
X20	0.959	3	A
121, 321, 521	0.915	3	A
221, 421, 621	0.918	3	A
X30	0.996	2	A
131, 132, 331, 332, 531, 532	1.031	2	B
231, 232, 431, 432, 631, 632	0.991	2	A
X40	1.098		B
141, 143, 341, 343, 541, 543	1.044		B
241, 243, 441, 443, 641, 643	1.009	1	A
142, 342, 542	1.058	1	B
242, 442, 642	1.069		B
X50	0.952		B
151, 154, 351, 354, 551, 554	0.999		B
251, 254, 451, 454, 651, 654	1.012		B
152, 153, 352, 353, 552, 553	0.962	1	B
252, 253, 452, 453, 652, 653	1.001		B
X60	1.015		B
161, 165, 361, 365, 561, 565	1.013		B
261, 265, 461, 465, 661, 665	1.015		B
162, 164, 362, 364, 562, 564	1.013		B
262, 264, 462, 464, 662, 664	1.037		B
163, 363, 563	1.045		B
263, 463, 663	1.000		B
172, 175, 372, 375, 572, 575	0.931		B
173, 174, 373, 374, 573, 574	0.960		B
272, 275, 472, 475, 672, 675	0.931		B
273, 274, 473, 474, 673, 674	0.960		B

To find local to core average heat flux for ring "i" at stage "n," multiply the relative cell heat flux by the tabulated ring and longitudinal factors for the appropriate rod and fuel element condition.

<sup>a</sup>Cartridge types and cell numbers are shown in Figure 27.

<sup>b</sup>X designations indicate first digit of cell number: e. g., X10 denotes all cell numbers ending in 10.

### REACTOR ASSEMBLY

The D102A reactor is air-cooled, has metallic fuel elements, hydrided zirconium moderator, and a beryllium reflector. The reactor is operated in the horizontal position and its components are supported at each end by Inconel X tube sheets. The reflector is divided into six equal segments that form a circular container for the active core.

The active core contains 150 cells, each of which includes an individual moderator section and a fuel cartridge. The moderator sections are circular inside and hexagonal outside. The fuel cartridges fit inside the moderator sections and are supported along their full length. Each component is free to seek full thermal expansion as the temperature varies. The moderator sections and fuel cartridges are attached to the forward tube sheet by remotely operable disconnects and are freely supported at the rear tube sheet. Both tube sheets are supported by splines that extend from the pressure shell and are free to expand within the pressure shell. The core assembly is illustrated in Figure 11.

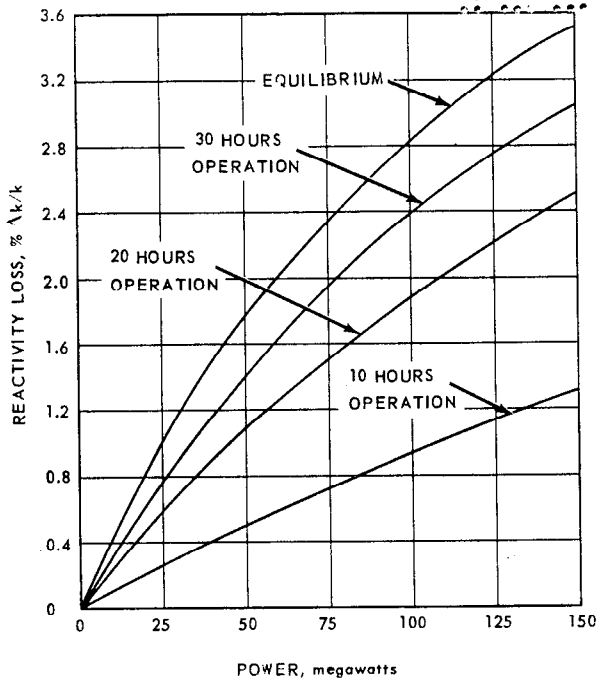


Fig. 7 - Reactivity loss due to xenon buildup versus power level

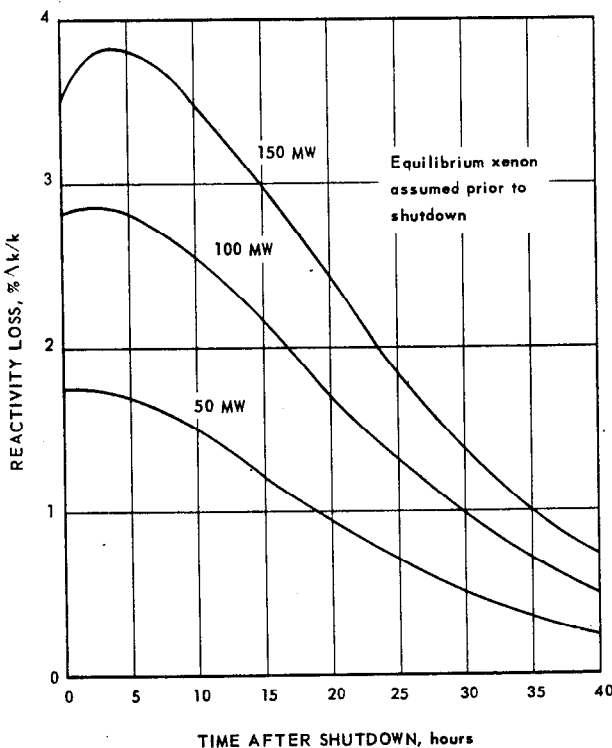


Fig. 8 - Reactivity loss due to xenon buildup following reactor shutdown

Reflector

The beryllium reflector is made in six 60-degree segments that form a circular container for the active core. The reflector support structure is Inconel X and consists of a circular plate that is welded to flange headers at each end. The headers bolt to the tube sheets at each end to complete the core structure.

Hexagonal blocks of beryllium with round cooling holes are held in place by the forward end flange and three equally spaced bulkheads. An insulation sandwich separates the beryllium from the active core.

The minimum margin of safety for the reflector structure is 0.68, based on 80 percent of stress rupture values at temperatures of 1000°F and pressures of 200 psi. Thermal shock tests on beryllium blocks have shown that thermal gradients in excess of 150°F will not crack the blocks, and a 50°F gradient was chosen as the maximum design point. The maximum temperature expected in the reflector is 1000°F.

Moderator

The moderator is a hollow hydrided zirconium tube having a cross section that is hexagonal on the outside and circular on the inside for the full length. The inside diameters are arranged in four steps within the tube: from the forward end, for about 3/4 inch, the diameter is 3.1445 inches; from that point to about the ninth stage location, the diameter is 3.089 inches; from the ninth-stage location to about 1-1/2 inches from the rear, the diameter is 3.104 inches; and for the remaining distance, the diameter is 3.149 inches.

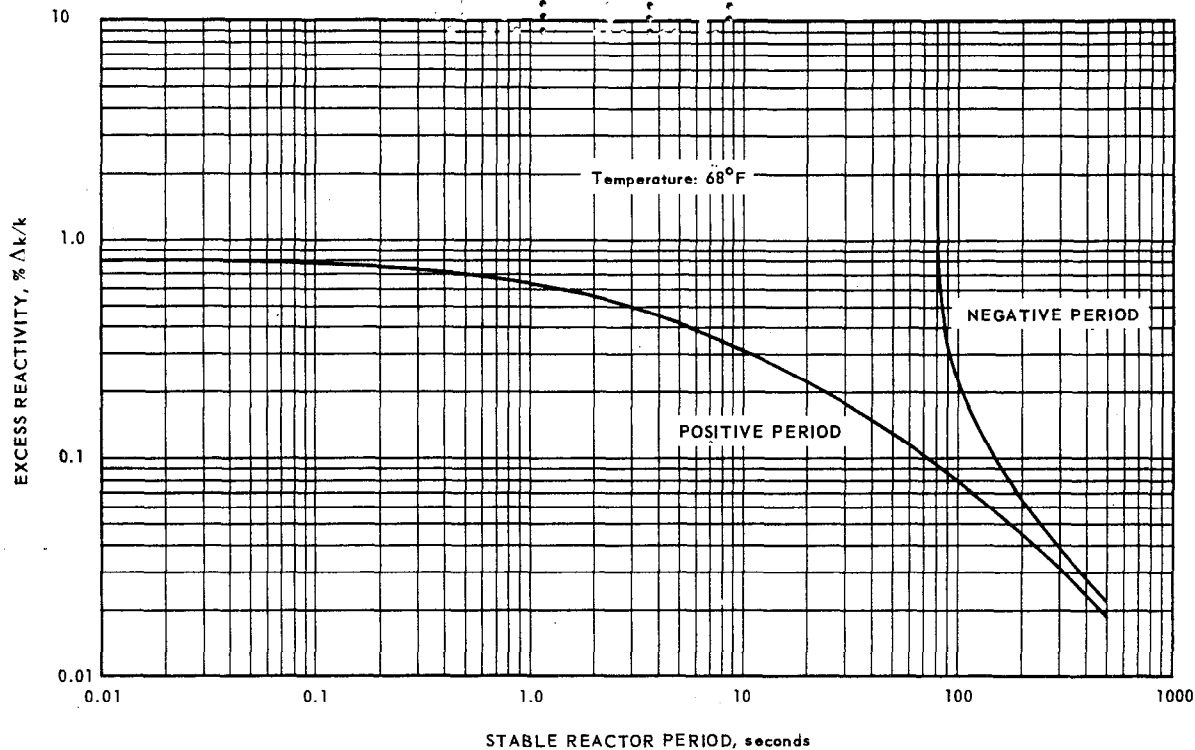


Fig. 9 - Excess reactivity versus reactor period

The distance across the outside hexagon flats is 3.923 inches. The zirconium tube is supported on a 0.025-inch-thick 310 stainless steel tube and held at the two ends by 310 stainless steel end-connectors.

The moderator has cooling slots cut radially out from the inside diameter. A cooling inlet is provided by matching slots 1 inch long through the support tube at the forward end. Exhausting is provided through holes in the aft connector.

The moderator is held to the forward tube sheet by a remotely operated fastener that clips into grooves in the tube sheet. The clips are held in position by the fuel cartridge during operation and cannot be removed until the cartridge is removed.

A universal joint between the fastener and the moderator sections prevents deflections of the tube sheet from introducing excessive stresses in the moderator sections.

Hydrogen loss characteristics have been determined from the unclad  $ZrH_x$  bar operating for 100 hours in a temperature gradient similar to that expected in the reactor. Results are shown in Figure 12. The integrated hydrogen loss was 1.2 percent, and oxidation was not excessive. Combustion tests have indicated  $ZrH_x$  will not sustain combustion at temperatures up to 3000°F.

#### Control Rod Guide Tube

The core contains 48 Inconel X control rod guide tubes. The tubes are 0.841 inch inside diameter with 0.060-inch walls and have a 0.002-inch chromium plate inside to improve the sliding friction characteristics. The tube is supported by a flange and retained at the forward tube sheet. The moderator sections are recessed along their length at the guide tube position to form a circular cavity for the tubes.

The support is designed to withstand a forward load of 800 pounds at 1000°F.



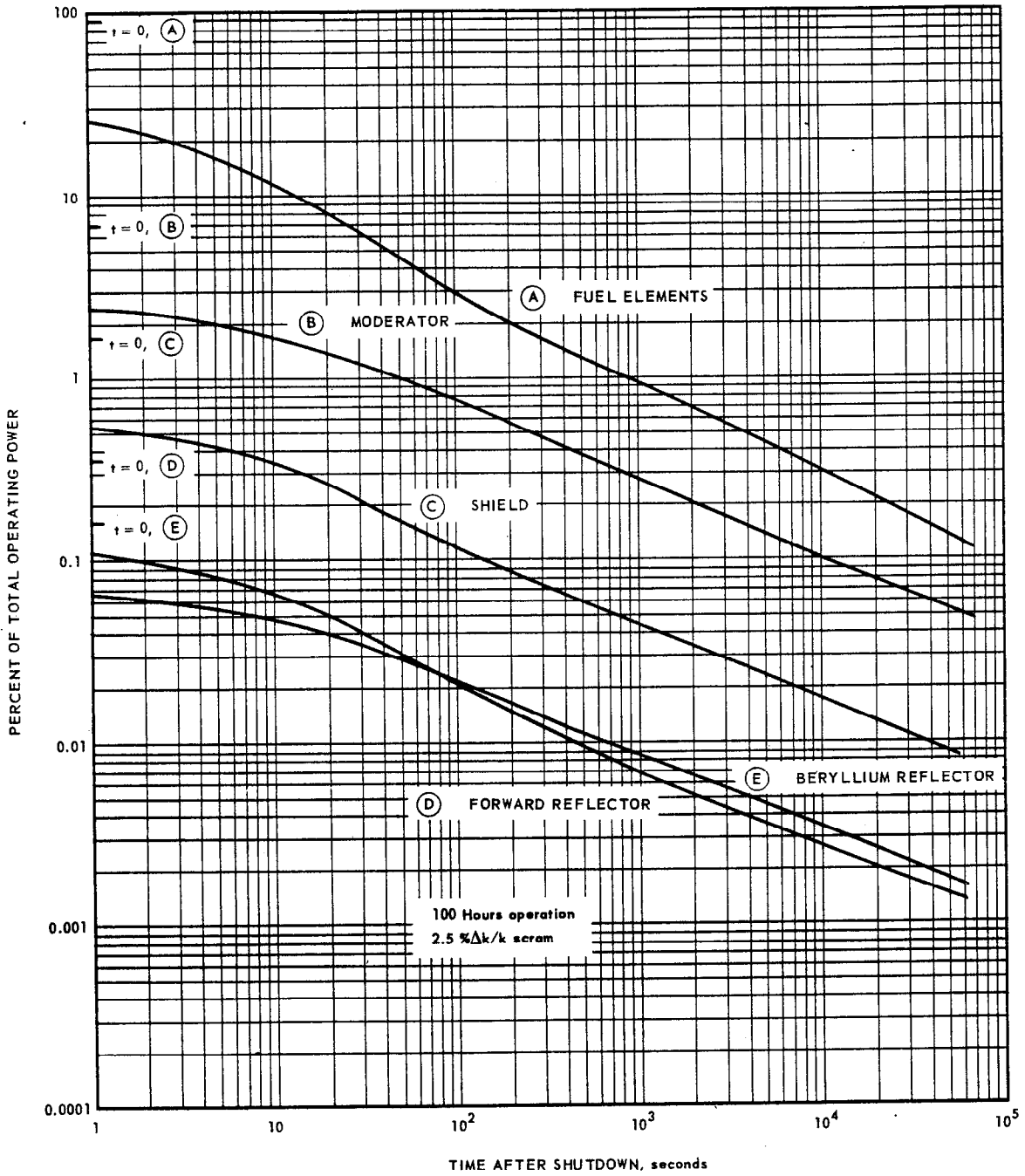


Fig. 10 - Nuclear afterheat

UNCLASSIFIED

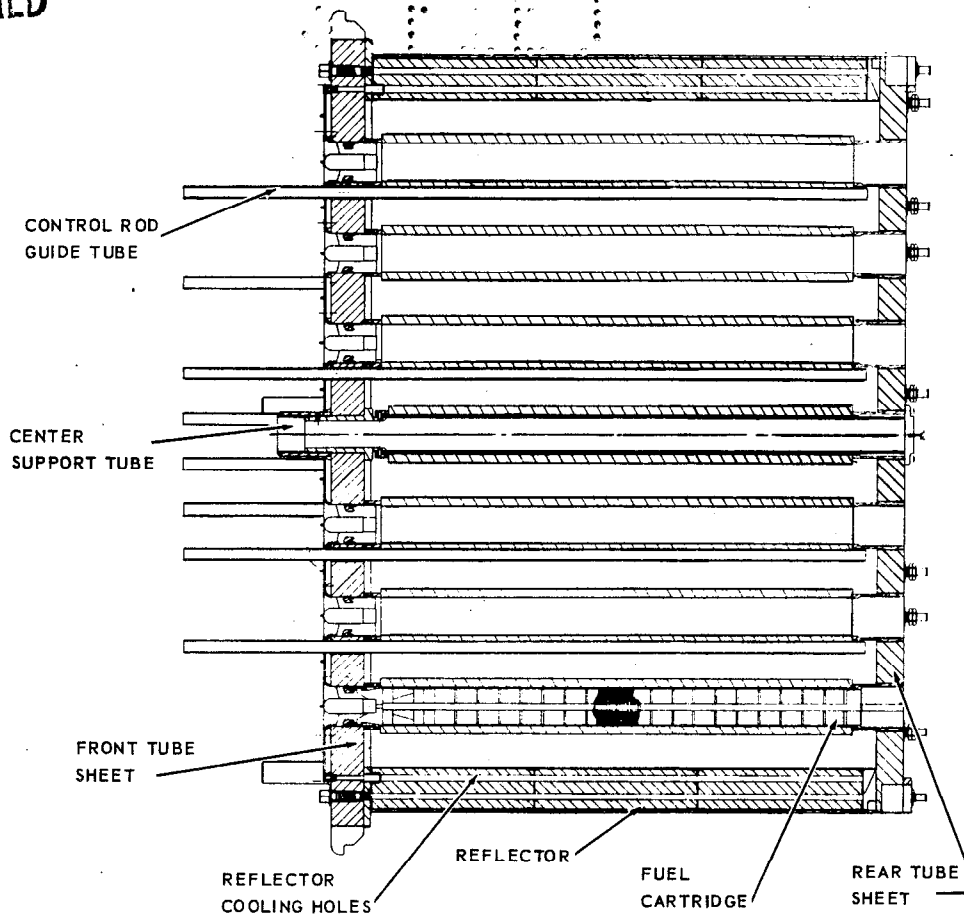


Fig. 11 - D102A core assembly

### Control Rods

The control rods are made up of short segments strapped together to allow deflection and to prevent binding during operation of the reactor. The control rod configuration is shown in Figure 13. These segments are composed of 42 percent  $\text{Eu}_2\text{O}_3$  dispersed within a matrix of 80 Ni - 20 Cr and clad with 310 stainless steel. The straps link the poison segments together and provide two point bearings for each segment.

These rods have been operated at temperatures up to 1600°F in passages offset from the actuator axis by 0.180 inch. The travel rate for the dynamic rods is 5 feet per second, and the length of the rod stroke is 20 inches. The rod was cycled 34,000 times under varying conditions without a failure or malfunction.

### Tube Sheets - Core

The material used for the tube sheets, both forward and aft, is Inconel X. This material has been fully age-hardened for maximum strength properties for use at about 1100°F.

The allowable stress values used in the design of the tube sheets are based on 80 percent of 1000-hour stress-rupture properties for 1200°F for the forward tube sheet and 1400°F for the aft tube sheet.

### Fuel Cartridge

The HTRE No. 3 fuel cartridge, shown in Figure 14, consists of 19 fuel stages; a nose assembly of 310 stainless steel, which contains the thermocouple connection

UNCLASSIFIED

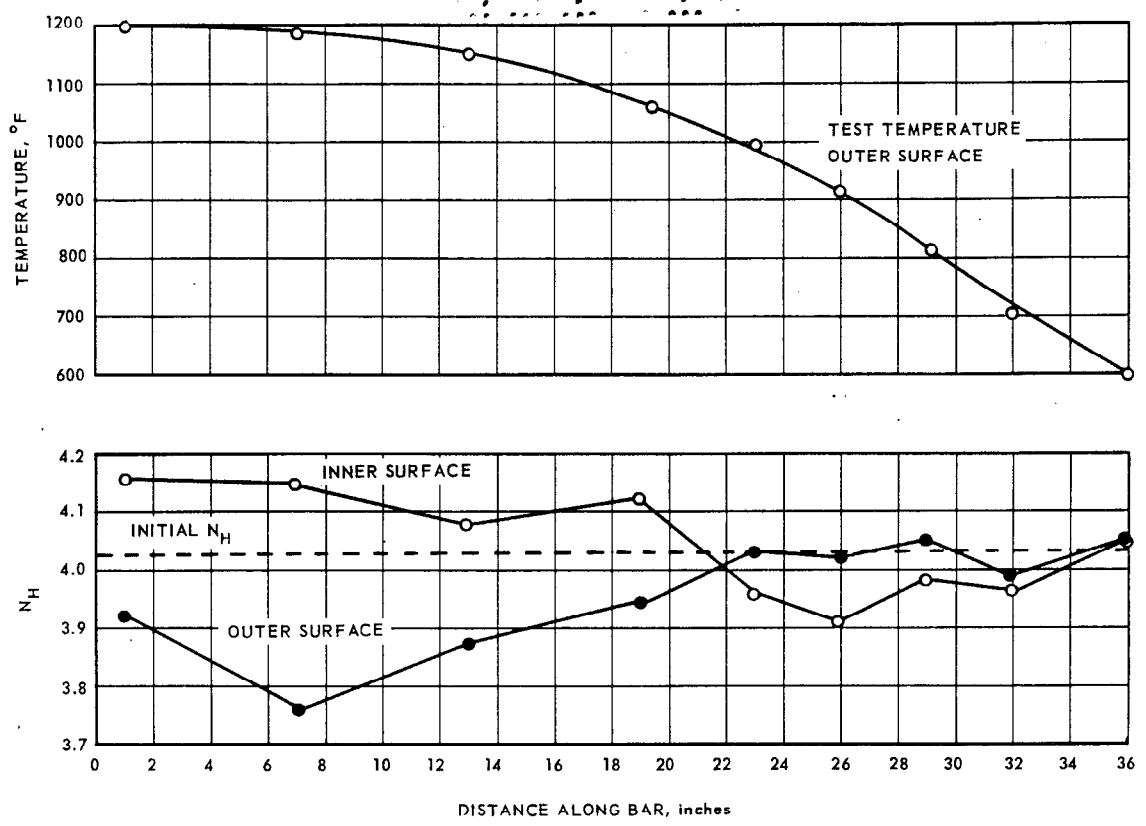


Fig. 12 - Temperature and hydrogen-loss characteristics of unclad ZrH<sub>x</sub> bar after 100 hours

and latching mechanism; and a tail assembly, also of 310 stainless steel, which functions mainly to provide a means of remotely handling the cartridge. The cartridge components are connected by four 80 Ni - 20 Cr rails, which are spot-welded to tabs on the fuel elements and spot-welded to the nose and tail assemblies. Theoretical stress analysis of all structural components of the fuel cartridge (exclusive of the fuel elements) indicates a minimum margin of safety of + 1.03 for a dynamic head of 6 psi and plate temperature of 1850°F.

The fuel elements consist of 12 concentric rings of varying thicknesses connected at their leading edges by 16 comb-ribs, the rings being brazed into slots in the ribs. There is no supporting structure in the rear of the fuel elements. The fuel material is UC<sub>2</sub> in a matrix of 80 Ni - 20 Cr. Cladding and structural comb-ribs are niobium-stabilized 80 Ni - 20 Cr. The fuel elements are essentially the same elements as those used in HTRE No. 1.

SHIELD ASSEMBLY

The shielding for the D102A assembly is composed of a primary and an auxiliary shield. The primary shield simulates a flight-type shield structure without flight-type shielding materials. The auxiliary shield was incorporated so that radiation levels outside the assembly would be consistent with test requirements.

The primary shield, shown in Figure 15, consists of a radial shield, front plug, and rear plug. The assembly of these components forms the inlet and exit air passages

and the container for the core. The primary shielding materials in these components are alternate layers of lead and water. An outer tank, which will contain water during operation, is provided on the radial shield. Upon shutdown this water will be replaced with mercury. Boral plates are located on the surfaces of the rear plug to reduce the radiation streaming through this passage. A drain is provided in the lower half of the scroll on the front plug to prevent water from accumulating in the core in the event of a leak. This drain is closed during operation and is opened upon shutdown.

The primary shield is cooled by circulation of the water to a heat exchanger on the dolly. A control system maintains the temperature of this water to the designated level. The shield water distribution to each component is controlled, but the total flow rate of the shield water is a constant and its temperature is regulated by controlling the amount of raw cooling water to the heat exchanger. The water in the outer tank of the radial shield is not circulated. Convection and conduction to the circulated water is sufficient to maintain this water below the boiling point at reactor powers up to 175 megawatts.

The main structure for the radial shield is the Inconel X inner pressure vessel. This vessel has been tested at pressures up to 240 psi without failure. The maximum pressure anticipated for this operation is 60 psi. This inner pressure vessel has four splines that locate and support the core at the front and rear tube sheets. All of the primary shield components are welded tank assemblies. There are no gaskets or flanges that would permit leakage into the core.

The auxiliary shield consists of a large annular tank completely covering the primary shield assembly and a smaller annular tank around the combustor. These shielding components are shown in Figures 16 and 17. The shielding materials in these tanks are lead and water. The water in the tank around the primary shield is borated to reduce the thermal flux. This borated water is not circulated; the combustor shield water is circulated with the primary shield water. Radiation

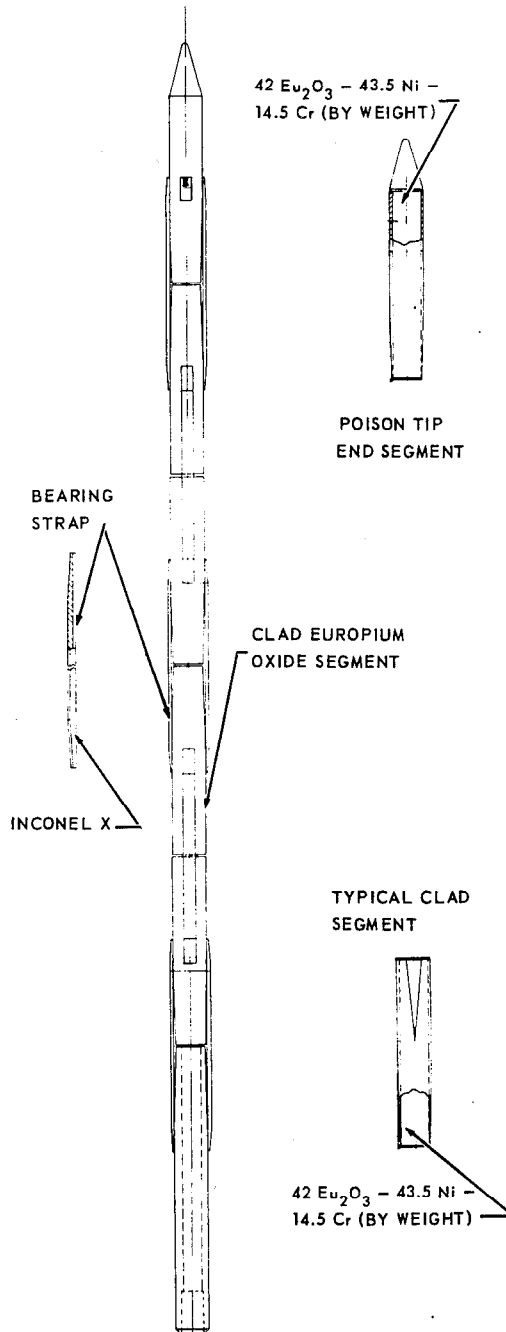


Fig. 13 - D102A control rod configuration

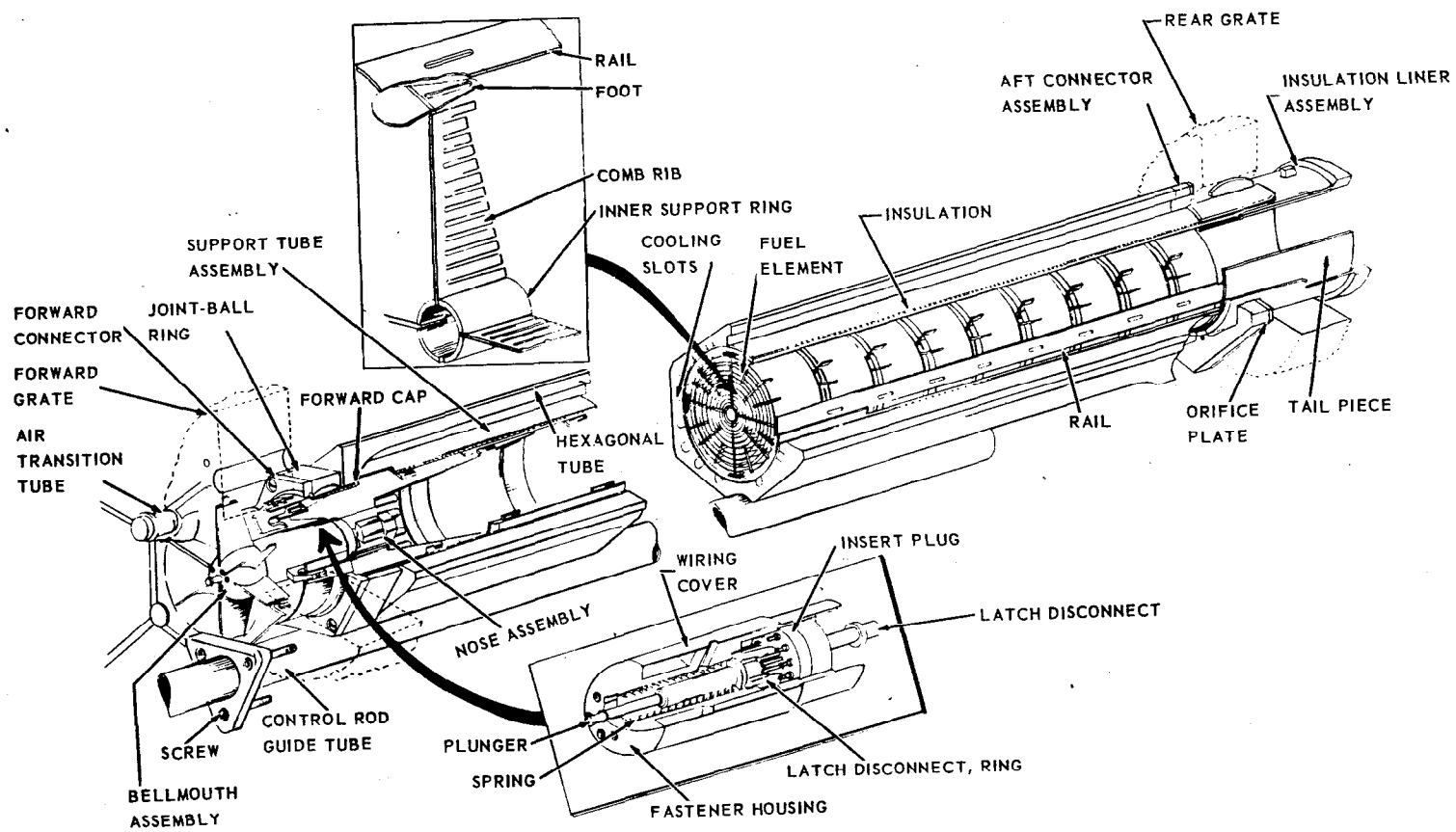


Fig. 14 - D102A fuel cartridge assembly

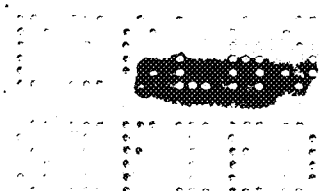


TABLE 3

CALCULATED DOSE RATES AT SURFACE OF D102A SHIELD  
(Direct plus Duct-Scattered)

Pos. No. <sup>a</sup>	Fast Neutrons, rep/hr <sup>b</sup>	Thermal Neutrons, n/cm <sup>2</sup> -sec <sup>b</sup>	Operating Gammas, r/hr <sup>b</sup>	Shutdown Gammas, r/hr <sup>c</sup>
1	2.8 x 10 <sup>3</sup>	9.8 x 10 <sup>8</sup>	8.48 x 10 <sup>2</sup>	1.65
2	2.94 x 10 <sup>3</sup>	1.03 x 10 <sup>9</sup>	8.40 x 10 <sup>2</sup>	1.65
3	4.13 x 10 <sup>3</sup>	9.52 x 10 <sup>7</sup>	5.71 x 10 <sup>1</sup>	1.93 x 10 <sup>-2</sup>
4	8.54 x 10 <sup>2</sup>	1.53 x 10 <sup>7</sup>	2.79 x 10 <sup>2</sup>	2.01 x 10 <sup>-2</sup>
5	8.22 x 10 <sup>2</sup>	1.45 x 10 <sup>7</sup>	3.80 x 10 <sup>1</sup>	2.00 x 10 <sup>-2</sup>
6	9.34 x 10 <sup>2</sup>	1.77 x 10 <sup>7</sup>	2.47 x 10 <sup>1</sup>	1.98 x 10 <sup>-2</sup>
7	2.41 x 10 <sup>2</sup>	2.14 x 10 <sup>6</sup>	1.24 x 10 <sup>2</sup>	1.63 x 10 <sup>-4</sup>
8	2.46 x 10 <sup>3</sup>	2.63 x 10 <sup>7</sup>	1.84 x 10 <sup>3</sup>	6.79 x 10 <sup>-3</sup>
9	2.99 x 10 <sup>3</sup>	1.05 x 10 <sup>9</sup>	6.42 x 10 <sup>2</sup>	0.248
10	2.27 x 10 <sup>3</sup>	2.59 x 10 <sup>7</sup>	1.68 x 10 <sup>3</sup>	6.03 x 10 <sup>-3</sup>
11	1.76 x 10 <sup>2</sup>	4.22 x 10 <sup>6</sup>	8.18 x 10 <sup>1</sup>	1.58 x 10 <sup>-4</sup>
12	1.16 x 10 <sup>4</sup>	9.15 x 10 <sup>7</sup>	8.04 x 10 <sup>4</sup>	4.41 x 10 <sup>-1</sup>
13	1.06 x 10 <sup>4</sup>	8.44 x 10 <sup>7</sup>	8.91 x 10 <sup>4</sup>	3.05 x 10 <sup>-1</sup>
14	1.02 x 10 <sup>4</sup>	2.45 x 10 <sup>10</sup>	7.09 x 10 <sup>2</sup>	3.29 x 10 <sup>-1</sup>
15	7.97 x 10 <sup>4</sup>	3.29 x 10 <sup>11</sup>	1.22 x 10 <sup>4</sup>	12.0
16	1.20 x 10 <sup>4</sup>	9.00 x 10 <sup>9</sup>	1.86 x 10 <sup>3</sup>	1.83
17	3.95 x 10 <sup>4</sup>	1.40 x 10 <sup>11</sup>	2.66 x 10 <sup>2</sup>	5.33 x 10 <sup>-1</sup>

<sup>a</sup>Positions are shown in Figure 18

<sup>b</sup>Operation at 175 megawatts

<sup>c</sup>18 hours after shutdown after 100 hours operation at 175 megawatts

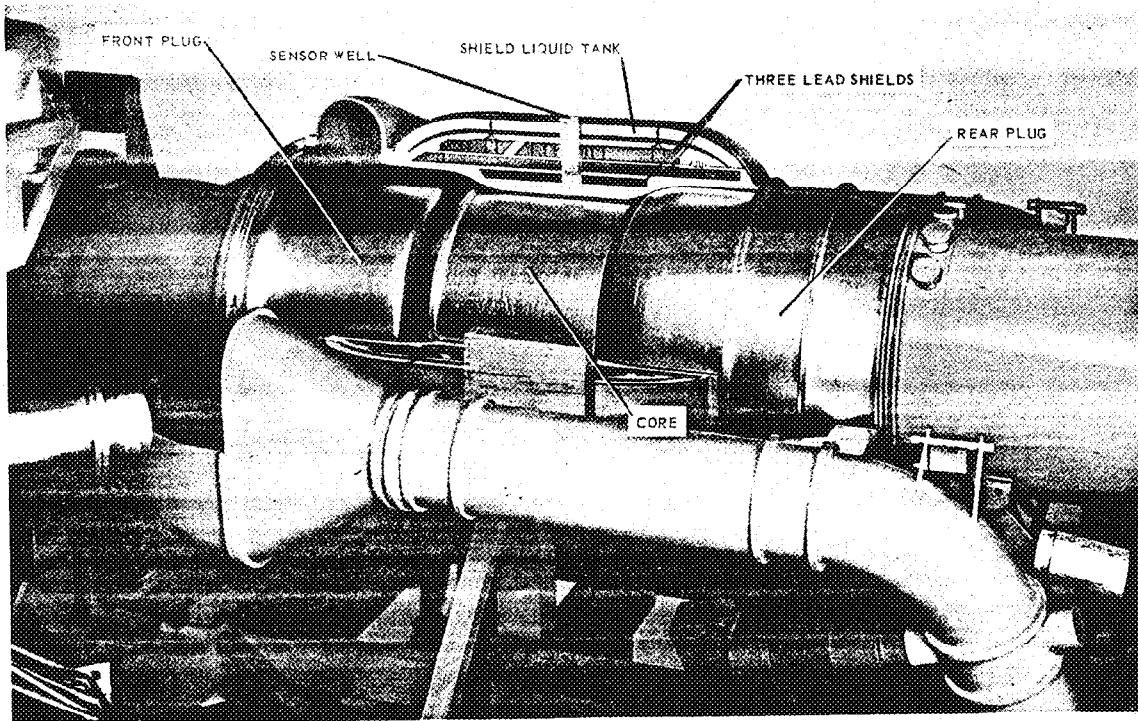
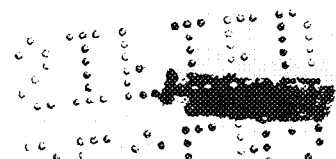


Fig. 15 - Primary shielding, D102A assembly



and convection are sufficient to maintain the boric acid water below the boiling point with the operating powers up to 175 megawatts. The maximum power expected in this operation is 35 megawatts.

Table 3 lists the calculated dose rates at the points indicated in Figure 18. Figure 19 shows the calculated shutdown dose rates near the combustor and combustor shield resulting from direct radiation from the active core, duct-scattered radiation, and combustor activation.

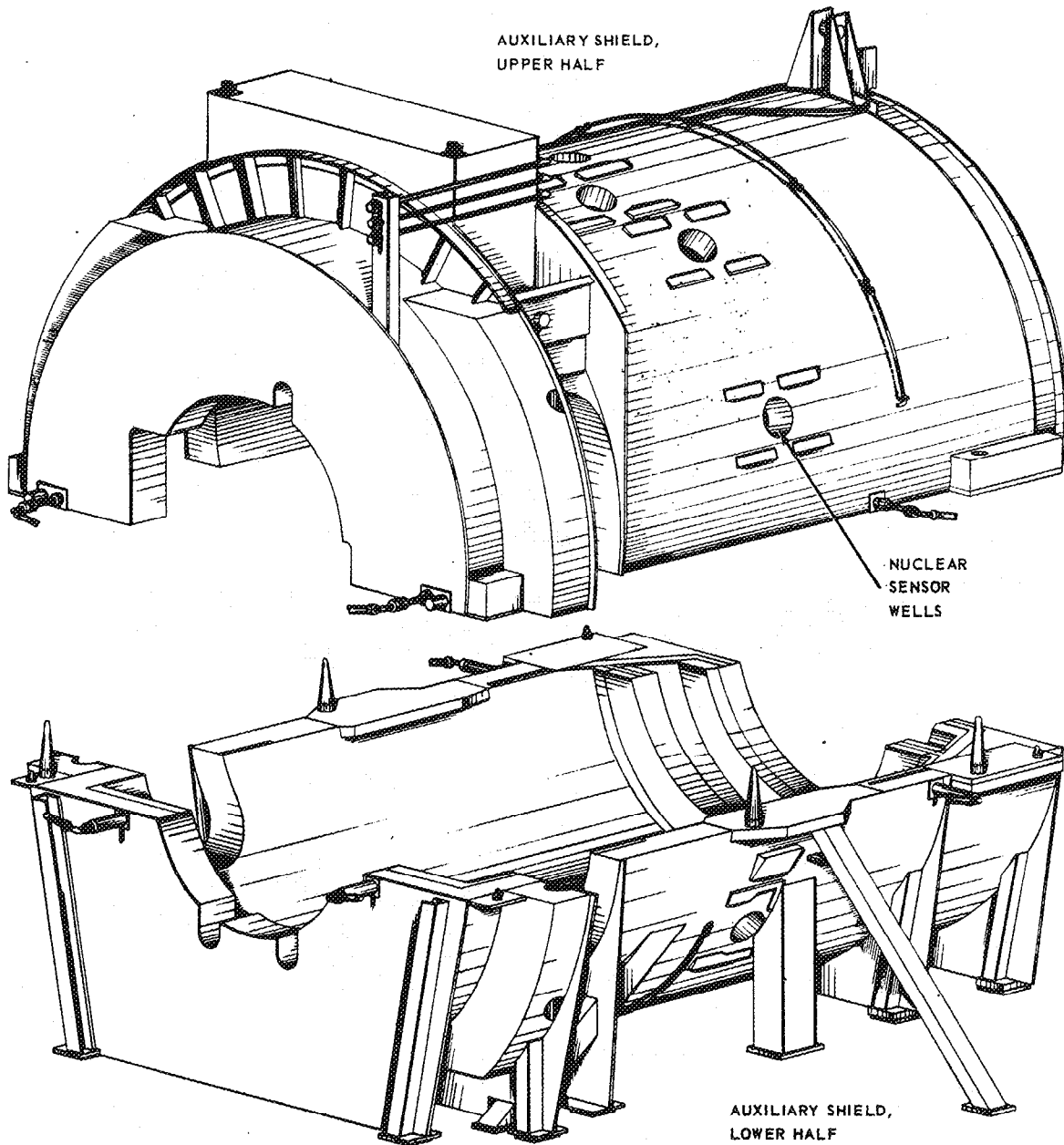
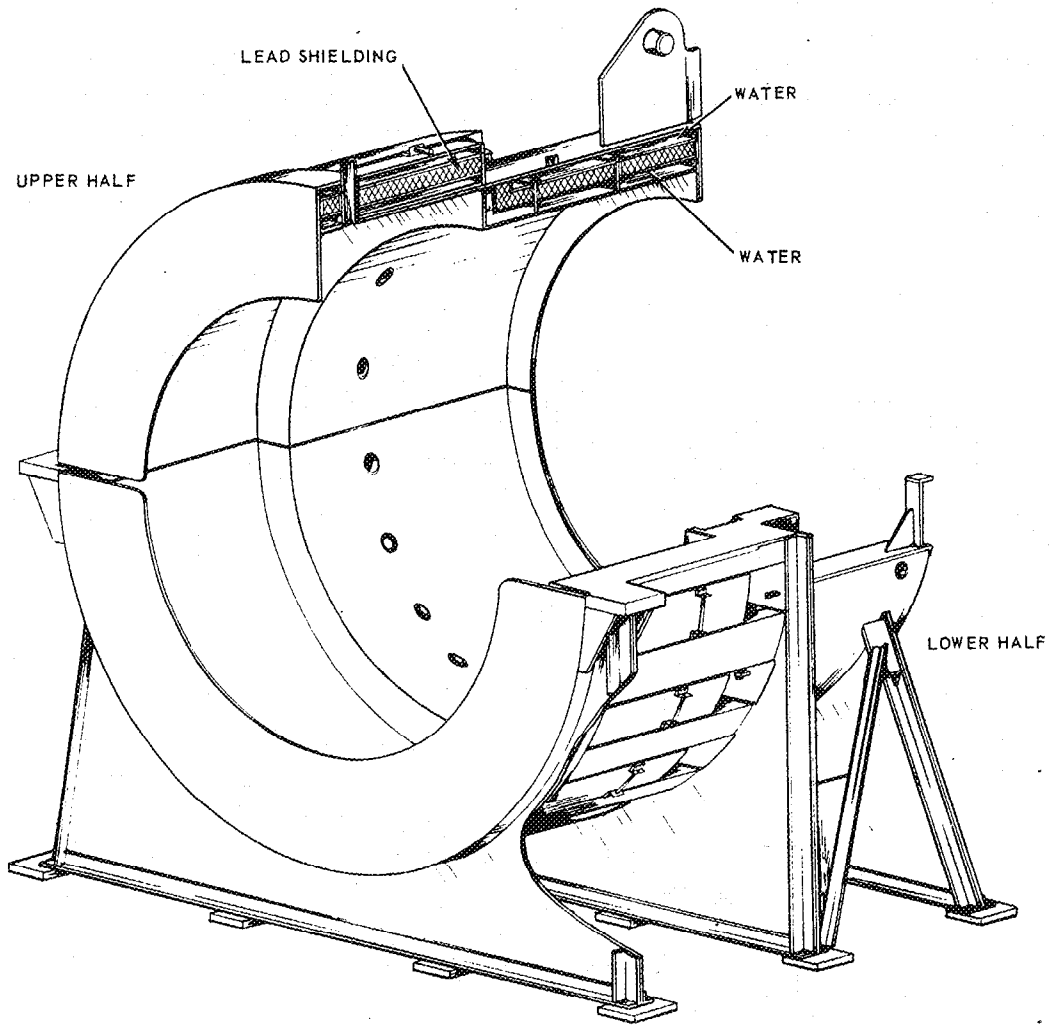
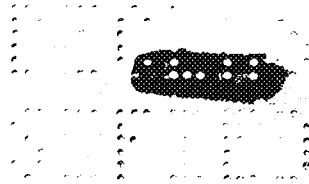


Fig. 16 - External auxiliary shield



SLIDING DOOR CONSTRUCTION

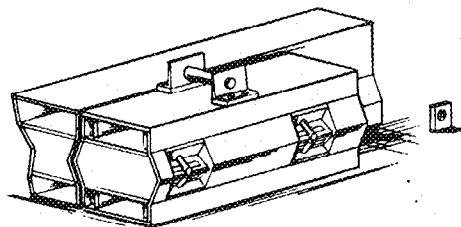
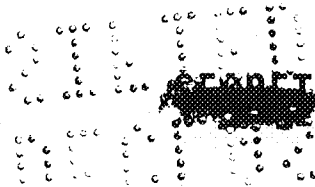


Fig. 17 - Combustor shield





UNCLASSIFIED

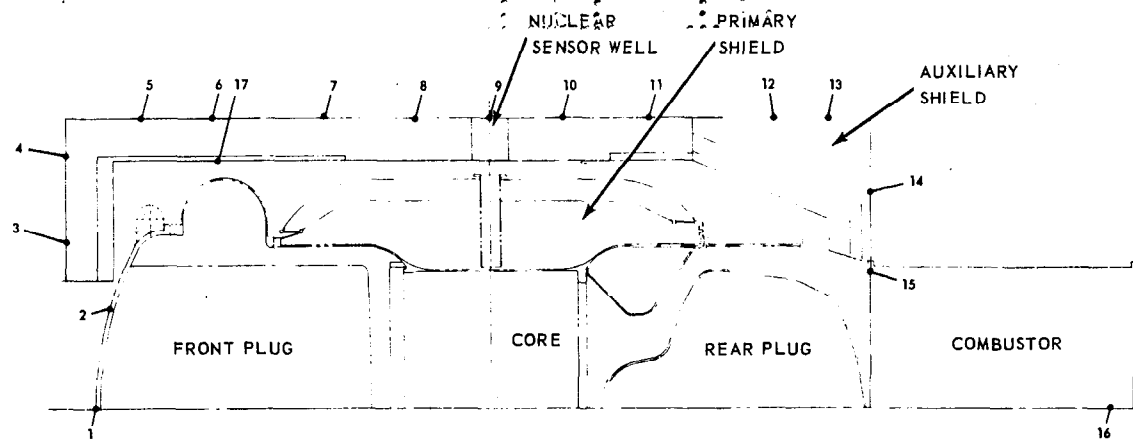


Fig. 18 - Reference points for calculation of shield dose rates (see Table 3)

CONTROL SYSTEM

Actuators and Control Rods

The control of the D102A reactor is accomplished through the use of 48 control rod actuators consisting of three types: 3 dynamics, 30 shims, and 15 safeties.

The safety actuator, shown in Figure 20, is withdrawn and latched pneumatically. It is scrammed by a 200-pound spring. The withdraw controls are fed through a selector switch, which prevents the removal of more than one rod at a time. A safety actuator limits the rate of withdrawal to 2 seconds for the full stroke. The scram rate is 2 inches in 0.05 second and the full stroke in 0.5 second.

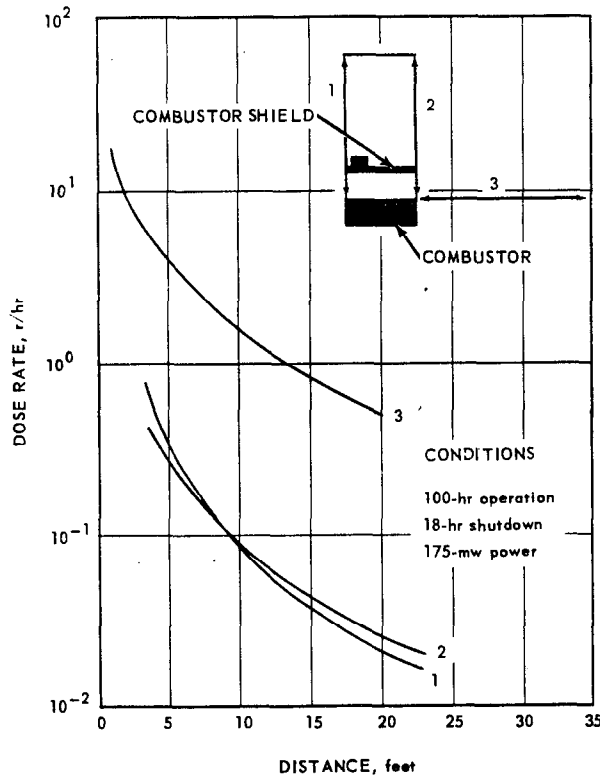


Fig. 19 - Calculated shutdown gamma-ray dose rate due to combustor activation and duct leakage in vicinity of combustor and combustor shield

The shim actuator, shown in Figure 21, is an electromechanical device accomplishing rod motion through a synchronous motor, gear train, and ball lead screw. The shim actuator will move a rod at a rate of 1 foot per minute in either direction. When not in motion, the rod is held in the set position by dynamic braking. This braking holds the rod fixed against forces that may be exerted by reactor air pressure and by vibration. In case of an electrical power failure, a mechanical brake is actuated which holds the rod fixed against these forces.

The 30 shim rod actuators are grouped into four frames of six actuators and two frames of three actuators. The actuators in each

UNCLASSIFIED

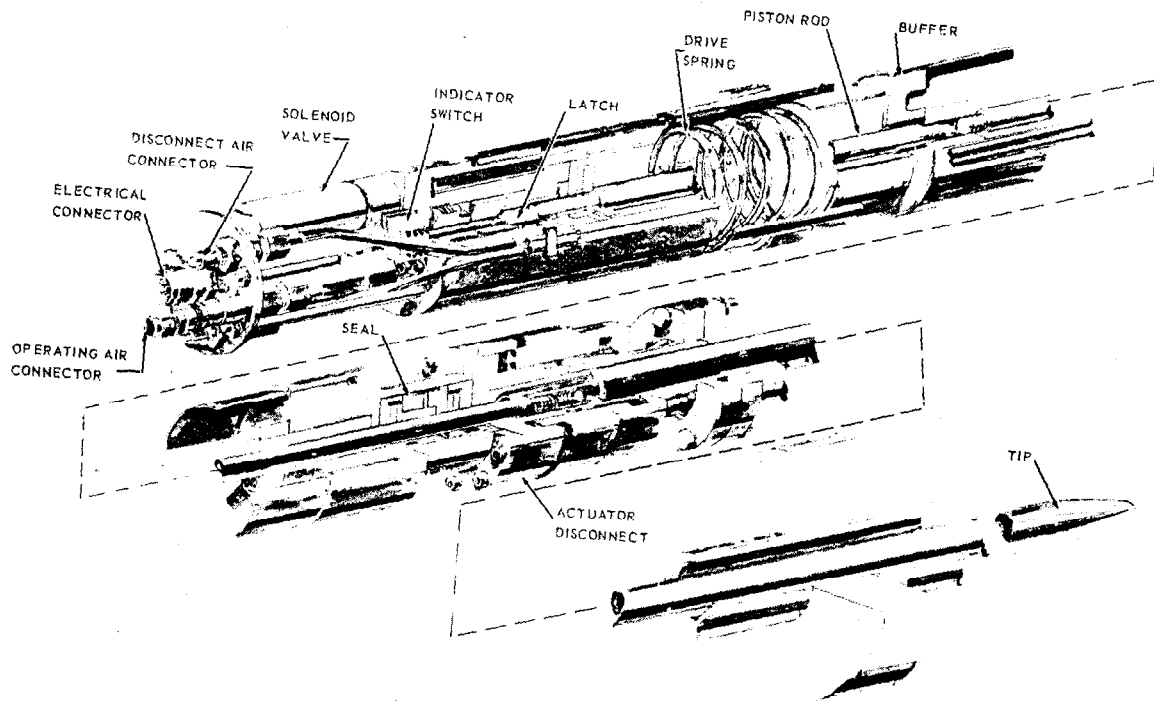


Fig. 20 - Safety actuator

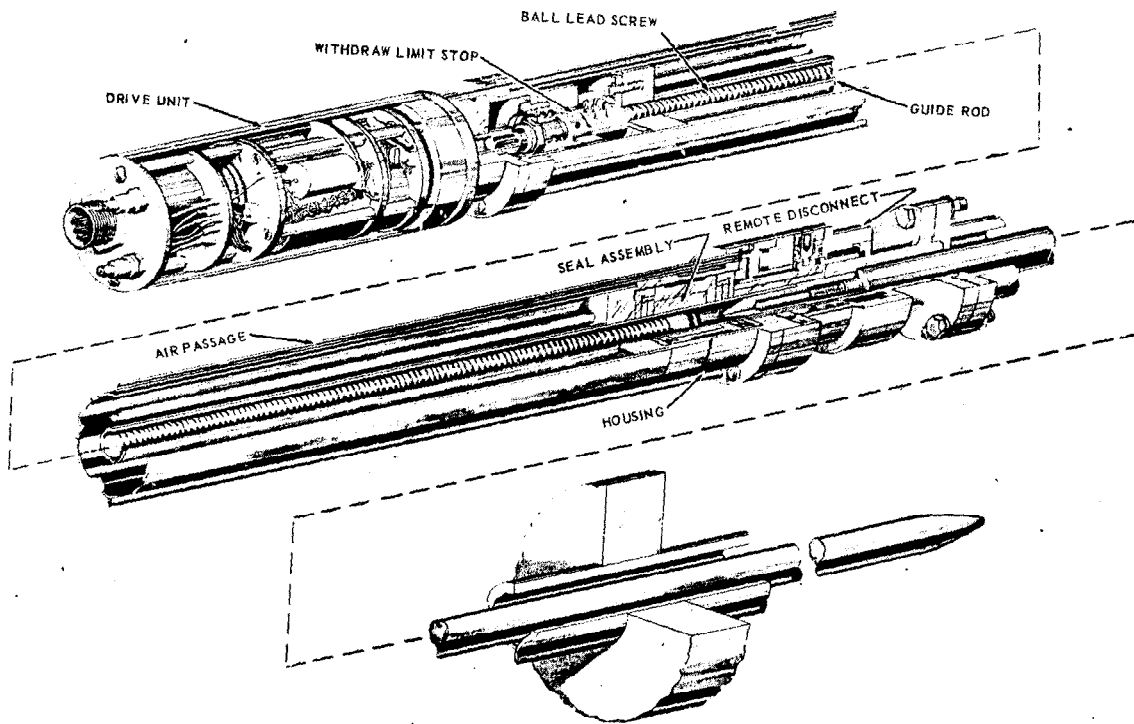


Fig. 21 - Shim actuator

UNCLASSIFIED

SECRET

frame move in synchronism, accomplished by the use of the synchronous motor drives. Prototype testing has shown that this is an acceptable method of keeping the rods in unison. Through a system of selector switches and relays, the shim rods can be moved individually or by frames. With manual control, the frames can be moved in sequence or at random. In either case, the system of relays and switches prevents the movement outward of more than one frame at a time. For safety reasons all shim rods can be inserted at the same time regardless of whether they have been moved out by individual or by frame control. Under automatic control the frames are controlled in sequence only. The shim rod drives are electrically interlocked so that no shim rods can be withdrawn until all safety rods are out and latched ready for scram.

The dynamic actuator, shown in Figure 22, is actuated by hydraulic power and can accomplish a full stroke in approximately 0.33 second.

The source is attached to one of the shim rods, which can be moved individually during the startup procedure. After criticality is reached, at the operator's discretion, the rod can be regrouped with the frame and operated as a control rod or it can be left isolated and remain withdrawn.

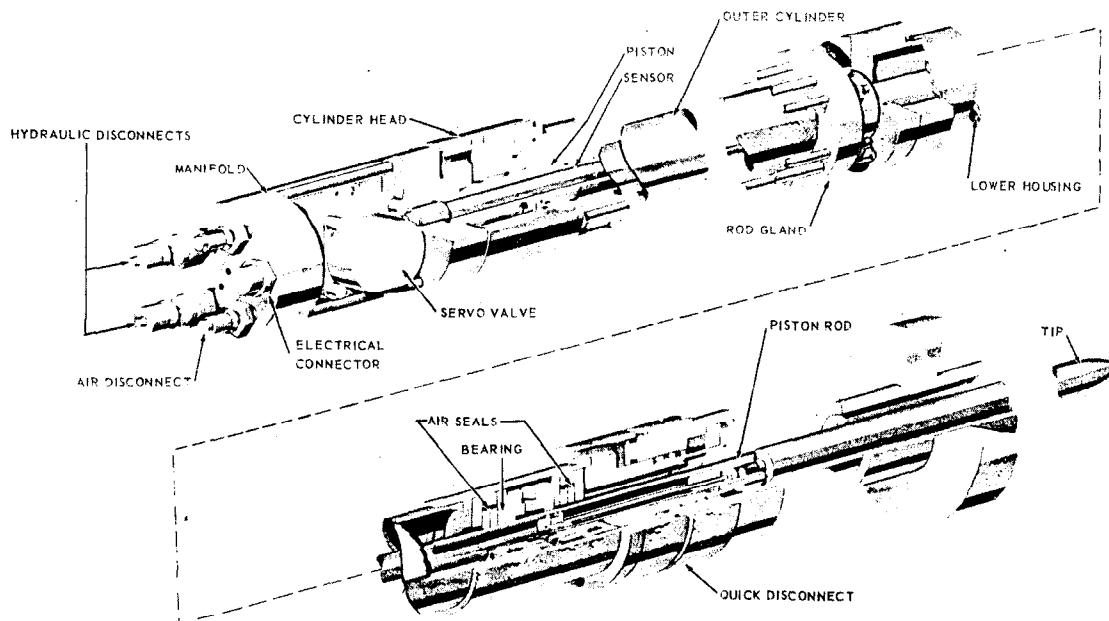


Fig. 22 - Dynamic actuator

### System Operation

The D102A automatic control is designed to operate through six decades of reactor flux density, beginning at  $10^{-6}$  full power. Below  $10^{-6}$  FP is considered the source range and is controlled manually.

Before shim rods can be withdrawn, all safety rods must be withdrawn and latched and the log-count-rate meters must be reading on scale. This reading is from the source rod in the clean reactor. The reactor parameters indicated during source range operation are log count rate, period, and shim rod position. Other safety parameters must be energized and are monitoring operations but are not necessarily reading on

scale. They are outlet air temperature, fuel element temperature, and engine speed. In addition, essential mechanical conditions must be met prior to source-range operation (115-volt, 400-cycle electrical power; 28-volt d-c hydraulic power).

The operator may change the reactor flux to whatever level he desires. However, he is limited in the rate of change of flux level to a minimum period of 15 seconds. This limiting action is imposed by a three-level safety feature, which will be discussed later.

Intermediate-range servo control can be initiated anywhere between  $10^{-6}$  FP and  $10^{-1}$  FP, but operation above  $10^{-6}$  FP requires a minimum pressure drop across the core of 1 psi to assure adequate coolant flow. After the transfer to servo control has been made, flux level is regulated automatically. Changes in flux level are accomplished by a rate-limited demand servo. The operator may schedule the rate at which the power change will be effected by selecting a period between 10 and 25 seconds.

In the power range the feedback is directly proportional to the flux level. Changes in power level are demanded with a linear potentiometer and linear feedback in contrast with the logarithmic demand feedback and linear demand potentiometer in the intermediate range. The linear demand causes power increases to be accomplished at slower rates near the end of the transient. Thermal shock and stresses should be minimized through this mode of operation.

Analog studies have been made of the adequacy of the design of D102A control to meet performance specifications. These requirements and the results of simulation tests are shown in Figures 23 through 26.

#### Safety Features

A three-level safety plan was adopted for HTRE No. 3 in an attempt to regulate the reactor so as to reduce the number of scram responses to a minimum. The levels are interlock, override, and scram.

Interlock was designed to prevent further increases in reactor power level. Violation of any interlock parameter initiates the following safety actions:

1. The demand servomotor circuit is opened, preventing any change in power-demand setting.
2. The shim-rod withdrawal signal is opened, preventing further rod withdrawal.
3. The dynamic loops regulate power at the level demanded when the interlock occurred. When the safety parameters producing the interlock have cleared, the control reverts to normal servo operation.

The override was designed to reduce reactor power at a fixed rate until the override condition has been corrected. Power reduction is effected in the following manner:

1. The demand-servo output is reduced at a fixed rate. The dynamic rods are free to follow the error signal; that is, if demand is greater than actual they will withdraw, and if less than actual, will insert.
2. All partially or fully withdrawn shim rods are driven into the core at normal speeds (approximately 1 percent  $\Delta k$  per minute per frame). When the override condition has been corrected, the demand-servomotor circuit is opened and power is regulated at the reduced level. (If the shim-rod insertion reduces power faster than the demand is being reduced, the dynamic rods can withdraw in an attempt to match the true power with the demand.)
3. When all safety parameter conditions producing override have been satisfied, the control can be returned to normal servo operation by operator reset action.

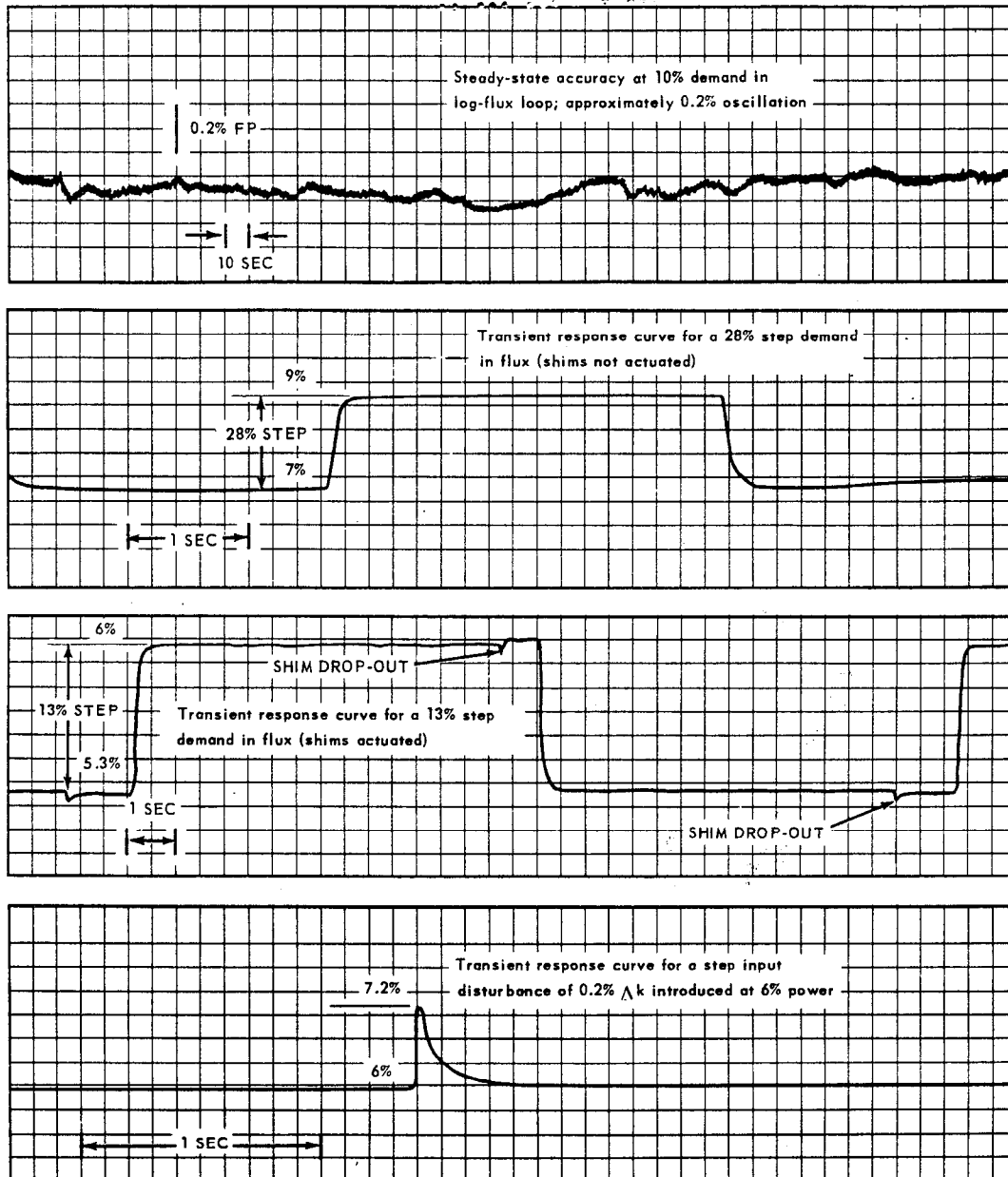


Fig. 23 - Log-flux loop, range  $10^{-6}$  to  $10^{-1}$  percent full power

The scram action is independent of the automatic level control system and is initiated only after interlock and override have failed to correct a safety violation. A scram signal releases the latching current of all safety rods, allowing them to scram. To insure shutdown at a maximum rate, a followup action fully inserts the dynamic rods and initiates override and interlock. These secondary actions drive all shim rods in.

Multiple control channels are provided in all three control ranges (source, intermediate, power) for increased reliability. The operator can observe the loop error in any control channel and select the channel he chooses to use. Also, in the interest of reliability and continuity of operation, coincident safety signals are required to

UNCLASSIFIED

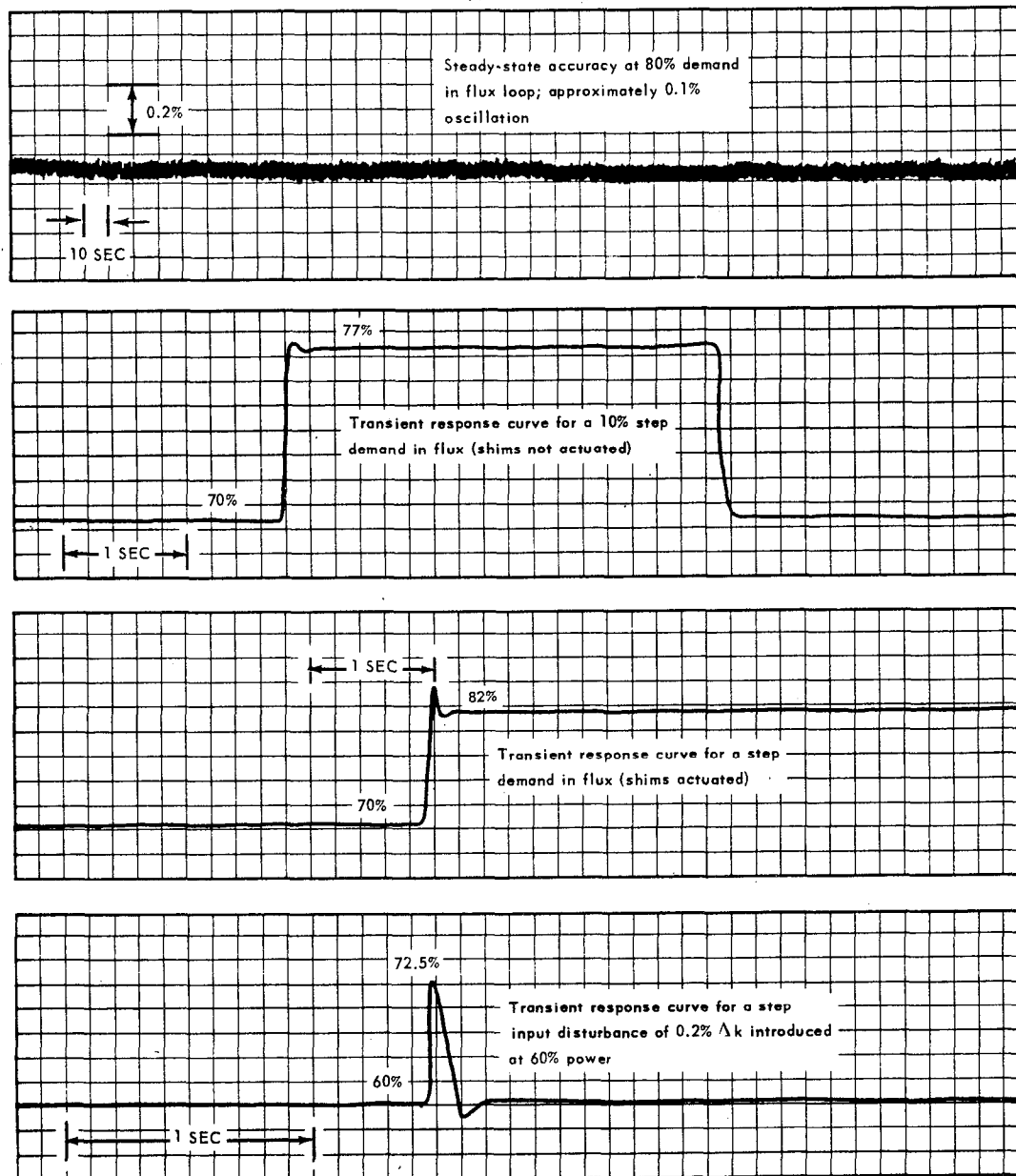


Fig. 24 - Log-flux loop, range  $10^{-1}$  to 100 percent full power

initiate a safety action for the period and flux parameters. It is permissible to operate with only two channels in any of the ranges of control, but when this is done only one signal is required for safety action.

So far as possible, control circuit design has followed the fail-safe philosophy so that any circuit or component failure will initiate a safety action.

Reactor safety parameters are listed in Table 4 with their associated trip levels for the three safety response actions. Distribution of control rods, fuel cartridges, and moderator  $N_H$  regions is shown in Figure 27.

UNCLASSIFIED

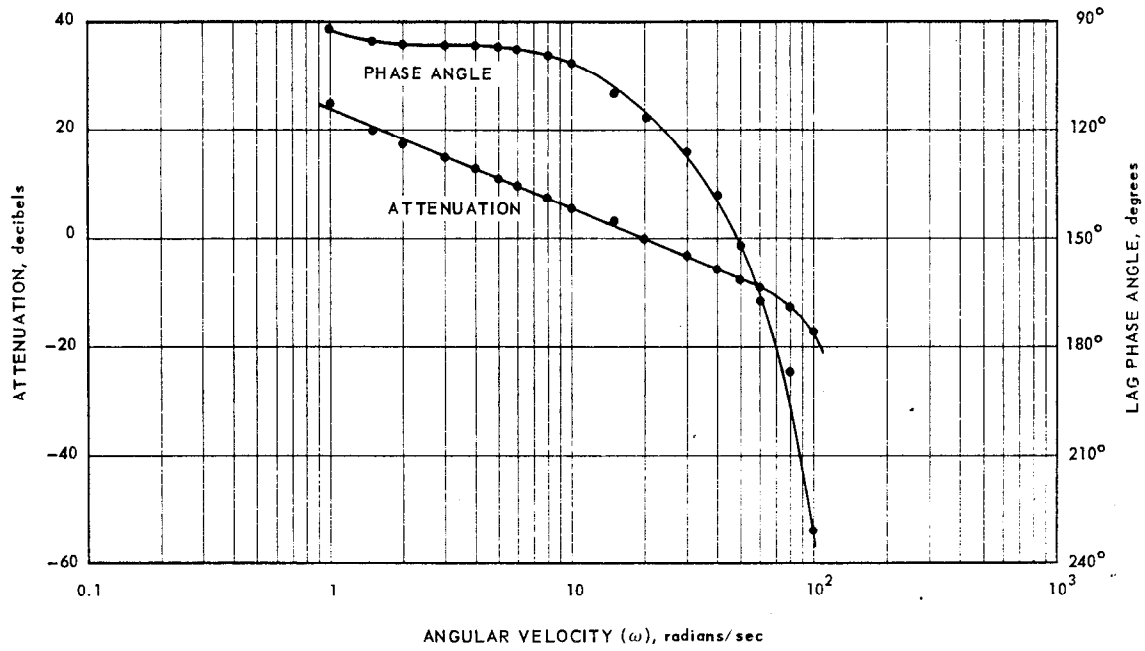


Fig. 25 - Open loop frequency response of the flux loop

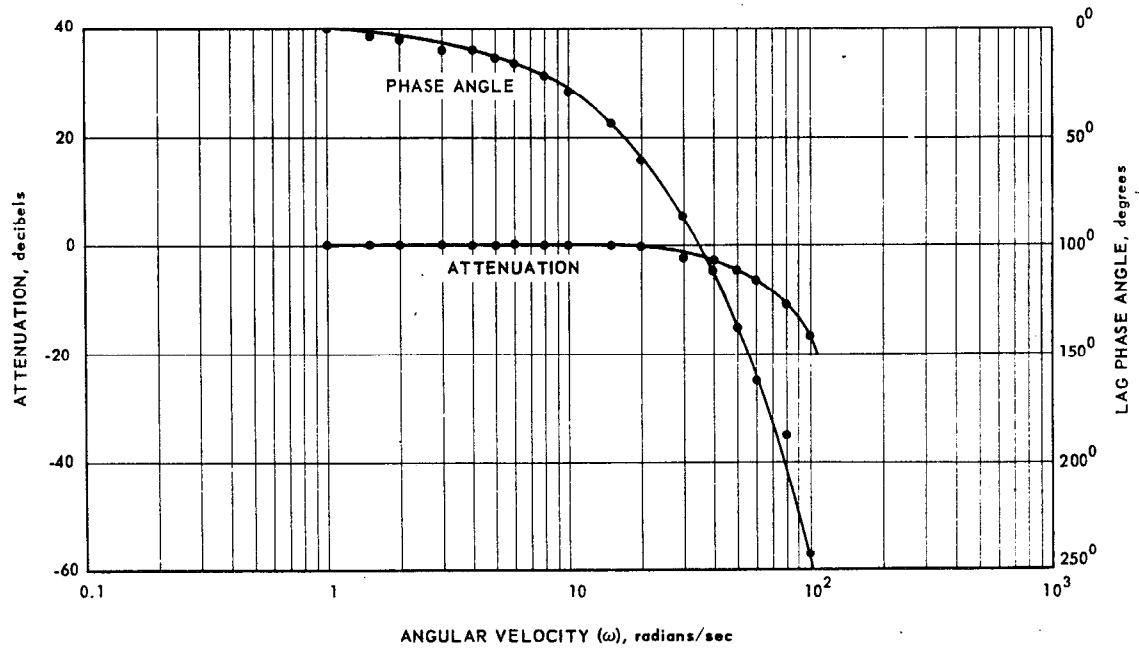
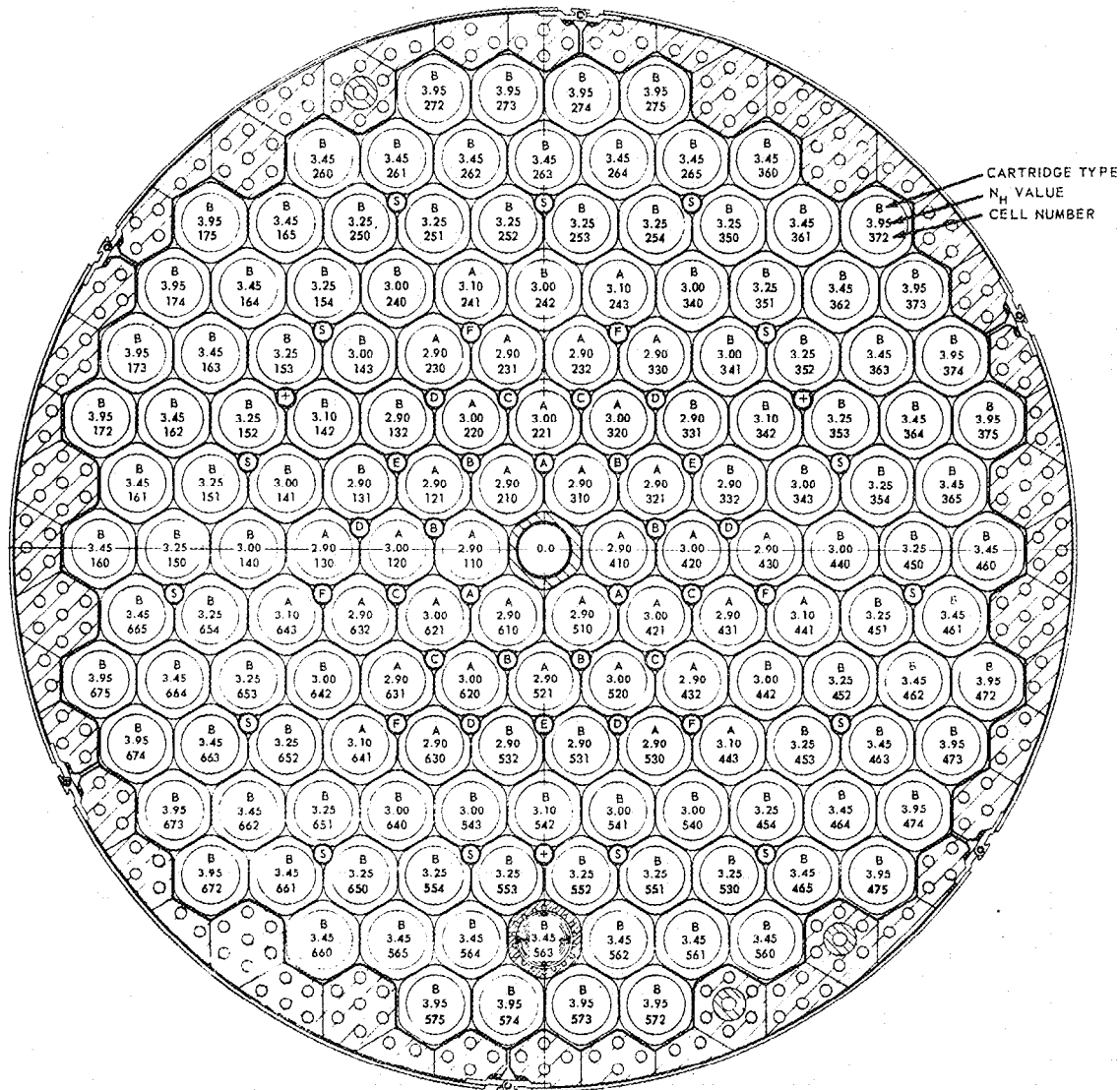


Fig. 26 - Closed loop frequency response of the flux loop



CONTROL RODS			MODERATOR CELLS		
FRAME	TYPE	NUMBER OF RODS	NUMBER OF CELLS	$N_p$	CARTRIDGE TYPE
A	SHIM	3	24	3.95	B
B	SHIM	6	36	3.45	B
C	SHIM	6	30	3.25	B
D	SHIM	6	9	3.10	A
E	SHIM	3	24	3.00	A
F	SHIM	6	27	2.90	A
-	DYNAMIC	3	1	0	-
S	SAFETY	15			

Fig. 27 - Distribution of control rods, fuel elements, and  $N_p$  regions



UNCLASSIFIED

TABLE 4

## REACTOR SAFETY PARAMETERS, HTRE NO. 3

	Response		
	Interlock	Override	Scram
Source-range period	15 sec	10 sec	5 sec
$10^{-6}$ to $10^{-1}$ period	10 sec	7 sec	5 sec
Power-range flux	105%	110%	120%
Average air temperature	1550°F	1600°F	1650°F
Fuel element temperatures above 1950°F	1	3	5
Engine speed		7950 rpm	8200 rpm
Minimum airflow (above $10^{-6}$ FP)	---	1000 rpm	---
115-volt, 400-cycle power	---	---	95 volts
28-volt, d-c power	---	---	20 volts
Hydraulic oil pressure	---	1000 psi <sup>a</sup>	---
Safety rod latching	---	unlatched	---
Log-count-rate meter	---	off-scale	Low
Dynamics turned off	---	3 off	---
Operator action	yes	yes	yes

<sup>a</sup>On automatic operation only

UNCLASSIFIED

UNCLASSIFIED

### 3. ACCOUNT OF THE EVENT

#### DETAILED DESCRIPTION OF TEST CONFIGURATION

A special configuration of the power plant was used on November 18 for the purpose of performing the heat-rate-sensor test. Departures from the expected full-power operating condition of the power plant are described in the following list of significant differences from the power operating condition.

1. The top half of the auxiliary shield had been removed for isodose measurements around the power plant.
2. The devices for nuclear instrumentation, uncompensated ion chambers in the linear-flux circuit and compensated ion chambers for the log-flux circuit, were at the bottom of their wells. One linear-flux chamber had been removed and replaced with a heat-rate sensor.
3. The control of the reactor, although at a low power level, was accomplished by the power-range system. The intermediate-range period signal was retained.
4. Heat-rate sensors had been installed within the core in four control rod positions. One safety rod and the three shim rods normal for these positions had been removed.
5. One fission chamber had been removed and replaced with a heat-rate sensor.
6. The fuel element temperature scrams were set slightly lower than they would have been for power operation.
7. Flux-measuring foils were in position around the shield.
8. Cooling of the reactor was to be accomplished with aftercooling blowers, capacity 3 pounds per second, because of the expected low power levels.

#### Installation of Nuclear Instrumentation

The nuclear instruments, consisting of uncompensated ion chambers for the linear-flux power-range circuits and compensated ion chambers for the log-flux intermediate-range circuits, were overdesigned to insure that sufficient signal would be available even if the predicted radiation levels at the sensor locations were low. In previous tests it had been determined that currents delivered by these instruments, when in their originally designed positions at the bottom of their wells in the side shield, were a factor of 100 greater than the current required by the design of the sensing circuits. It therefore would be necessary to move the chambers to a position farther out in their wells for power operations. It had been determined that the linear-flux uncompensated chambers should be moved back approximately 11 inches and that the log-flux compensated chambers should be moved back approximately 14 inches.

In other words, the linear-flux circuit and indicating instruments would be at top scale, or 100 percent power, at an actual power level 1/100 of the maximum design power level of the reactor, which is about 40 megawatts (this number varies with ambient conditions and with the speed at which the turbojet engines are operated). Thus, 100 percent on the flux-indicating scales is an arbitrary number depending on position of the instruments and the calibration of the circuits.

UNCLASSIFIED

These flux-indicating circuits had been calibrated by means of indium foil measurements. However, the primary calibration of the circuits was to have been established by a heat balance when suitable power levels were reached.

In the critical experiment phase of operations a power calibration had been established for indium foils placed in selected control rod holes. In previous operations these indium foils in the control rod holes had been cross-calibrated with indium foils placed on the outside of the shield so that for these particular operations a correlation between a given percentage scale reading on the power trace and the absolute power of the reactor had been established. Although the reactor operator was under the impression that this calibration was such that the indicated 100 percent scale reading was 0.5 megawatt, re-examination of the data has shown that the actual 100 percent scale reading was 0.15 megawatt. The true calibration has been used in most of the discussions in this report. For the heat-rate-sensor tests, the exact level of the power plant operation was not important as long as the level was subsequently determined from temperature and heat balance data, since the moderator heat rates were to be measured as a fraction of total reactor power.

The nuclear sensors were left in their positions at the bottom of the wells for this run for two reasons. First, the adapting hardware for firmly positioning the instrumentation in the required withdrawn position was not yet available. Second, the IET facility supervisor wished to operate the reactor on the power-range servo system as a matter of convenience, principally because this system provided rather fine control of the flux level. Although the system was designed so that the intermediate-range instrumentation could be used as input to the servo system (if the chambers were in their power-range positions), this control was not as fine and precise as that available using the linear instrumentation. For previous operation of the reactor (and of HTRE No. 1 and HTRE No. 2) it had been the practice to insert KAPL amplifiers into the linear-flux circuits so that a sufficient signal would be available for the servo system when the reactor was being operated below the intended operating range of the instruments. However, in this circumstance, because of the overdesign of the instrument it was possible to use the power-range instrumentation at reactor power levels well below the power range with disposition of the chambers of their deepest position.

#### Period Trips

The intermediate-range instrumentation provides for display of the logarithm of the flux and of the reactor period. In addition, the reactor period is connected to the safety circuits during operation in the intermediate range. For power operation of the reactor the period signal was not designed as part of the safety system, primarily because in this range the level trip is the most sensitive. The period circuits were designed for automatic disconnection of the period trip at 10 percent power level. However, realizing that he was operating in a range in which period protection would be desirable, the supervisor had eliminated this automatic period bypass for these operations. Therefore, the period signal generated by the compensated ion chamber was connected to the safety circuit as follows: interlock at 10-second period, override at 7-second period, and scram at 5-second period. These period trips were in each case connected through a coincident circuit so that two of the three operating channels must simultaneously give the short period signal to initiate the safety action. These period safety signals were connected and in operation throughout the entire data run.

High-flux safety trips were connected to the power-range channels at levels of 105 percent for interlock, 110 percent for override, and 120 percent for scram. Either of the two power-range channels that were operating would initiate the scram responses.

In addition to these safety responses from the nuclear instrumentation there were scram trips on the control room temperature recorders listed in Table 5.

In addition to these scram responses there were scram signal circuits for failure of either the 115-volt, 400-cycle power or the 28-volt d-c power supply.

TABLE 5

SCRAM TRIPS ON CONTROL ROOM TEMPERATURE RECORDERS						
Brown Recorder No.	Fuel Element Thermocouples,				Scram Setting, <sup>a</sup> °F	
	Cell	stage	radial	circumferential		
1	110	- 19	- 10	- 10	1800	
2	340	- 19	- 10	- 08	1800	
3	410	- 19	- 10	- 02	1800	
4	440	- 10	- 10	- 06	1800	
5	540	- 19	- 10	- 00	1920	
6	542	- 19	- 10	- 02	1620	
7	551	- 19	- 10	- 07	1630	
8	561	- 19	- 11	- 07	1650	
9	260	- 19	- 11	- 00	1600	
10	661	- 19	- 10	- 10	1630	

Bristol Recorders No.	Thermocouple Rings	Settings, °F
1 and 2	T <sub>3.65</sub> (Core Discharge Air)	1100 Interlock 1150 Override 1200 Scram

<sup>a</sup>The fuel element counting circuit requires that five Brown recorders must exceed the scram settings to initiate a scram. Temperature scram would occur if all of the ten thermocouples read open circuits.

Nuclear Instrumentation Installed

As a result of having shielding heat-rate sensors (calorimeters) installed in nuclear instrumentation wells 5 and 6, there remained in the reactor two fission chamber clusters (holes 3 and 8), three compensated ion chambers connected to the log-flux circuitry (holes 2, 4, and 7), and two uncompensated ion chambers connected to the power-range circuitry (holes 1 and 9). All chambers were installed at the bottom of the instrumentation well, which is the design position.

Additional Test Instrumentation

A calibrating indium foil was placed in the foil exposure hole under the reactor near the forward edge of the primary shield.

For the aft-plug shielding measurements a steel cable equipped with copper foils, sulfur pills, gamma film, and chemical dosimeters was pulled through a fuel-nozzle mounting hole (horizontal plane), around the aft plug, and out the adjacent fuel-nozzle mounting hole.

Moderator and control rod heat-rate sensors (calorimeters) were installed in control rod holes as follows:

Control Rod Hole	Type of Rod Originally in Hole	Type of Heat-Rate Sensor
110	Shim Rod	Control Rod
265	Safety Rod	Moderator
520	Shim Rod	Moderator
631	Shim Rod	Moderator

The three dynamic rods in control rod holes 153, 352, and 542, and the remaining safety and shim rods, not listed above, were unchanged from previous reactor operation.

On November 18, 1958, the reactor was being operated for a series of heating-rate tests. These tests involved the use of calorimeters designed in such a way that the rate of temperature increase of a shielding or moderator material could be measured at constant reactor power. The plan was to map the moderator and shielding heating rates in the reactor. Observations were to be conducted at various power levels to provide sets of independent data and also to explore rates of temperature increase, necessary to determine the best power level at which to obtain good data. During the afternoon of November 18 the reactor had been operated at 60.2 kilowatts as part of the heat-rate-sensor test series. That test was made in manual control, and behavior of the reactor and all circuitry appeared normal. It was planned that the heat-rate-sensor test run would be repeated during the second shift that evening at twice the power level of the afternoon test.

### REACTOR CHECKOUT

Prior to the operation on the evening of November 18 the standard reactor checkout procedure was followed. This procedure consists of checking each safety system and verifying that it is correctly connected to the control system. The reactor check list is shown in Figure 28. Test signals are used to simulate the errors in a variety of appropriate ways.

The Reactor Check List is used to assure that the reactor is properly prepared for operation, that all necessary components and safety circuits are functioning properly before operation, and that the reactor is properly secured after shutdown. These items are performed in conjunction with the daily reactor operation. Additional, more detailed checkout of proper reactor control and safety circuitry is made at less frequent intervals, e.g., weekly. The daily Reactor Check List is completed in approximately the order given:

#### Before Operation

1. MG Sets On - Check that the motor-generator sets No. 6 and No. 7 are operating. No. 6 provides 400-cycle, single-phase, 120-volt, a-c power; No. 7 provides 28-volt d-c power for reactor operation and control.  
Caution: MG Set No. 7 also supplies d-c power to the engine, data, and systems circuitry.
2. Circuit Breakers Closed - Check that the designated circuit breakers are closed to provide power for reactor instrumentation and control. These switches are located in circuit-breaker panels labeled A, C, and D. Circuit breaker D-19 is locked during shutdown periods to prevent unauthorized reactor operation. The "C" circuits are 60-cycle, single-phase, 120-volt, a-c power to the various reactor control panels.
3. Power Supplies and Amplifiers On - Reactor control, nuclear instruments, and power supplies shall be checked that they are turned on as follows:
  - A. Log-Count-Rate Circuits
    - 2 - LCR Safety Circuit Power Supplies - Panel WW
    - 3 - LCR Power Supplies - Panel WW
    - 3 - LCR Linear Amplifiers A1C - Panel XX
    - 3 - LCR High Voltage Supply - Panel XX Back

Note: Where voltage indication is provided, check voltage output of power supplies to determine if correct.

### REACTOR CHECK LIST

Date \_\_\_\_\_

#### Before Operation

- 1. MG Sets On: 6 & 7 \_\_\_\_\_
- 2. Circuit Breakers Closed: A1, C4, C7, C9, C10, C11, C13, D19 \_\_\_\_\_
- 3. Power Supplies and Amplifiers On \_\_\_\_\_
- 4. Console Annunciator Lights \_\_\_\_\_
- 5. Calibrate Log Flux Amplifiers \_\_\_\_\_
- 6. Dynamic Pump On \_\_\_\_\_
- 7. Nuclear Circuits & Safeties:
 

	<u>Interlock</u>	<u>Override</u>	<u>Scram</u>
Source Range	_____	_____	_____
Intermediate Range	_____	_____	_____
Power Range	_____	_____	_____
- 8. Dynamic Rods Operation \_\_\_\_\_
- 9. Process Safeties:
 

Outlet Air Temp	_____	3 Dyn Off	_____
Fuel Element Temp	_____	FE Rupture	_____
Low Air Flow 10 <sup>-6</sup>	_____	400 ~ Power	_____
Eng Speed	_____	Manual Interlock	_____
Hyd Oil Press	_____	Manual Override	_____
Low Count Rate	_____	Manual Scram	_____
- 10. Safety Rods Operation \_\_\_\_\_
- 11. Shim Rods Operation \_\_\_\_\_
- 12. Standardize Recorders & Zero Console Meters \_\_\_\_\_
- 13. Switches in Operate Position & Panels Locked \_\_\_\_\_
- 14. Safety Circuits Bypassed \_\_\_\_\_

Operator \_\_\_\_\_

#### After Shutdown

- 1. Shim Rods In \_\_\_\_\_
  - 2. Safety Rods Scrammed \_\_\_\_\_
  - 3. Dynamic Pump Off \_\_\_\_\_
  - 4. Chart Drives Off \_\_\_\_\_
  - 5. D19 Off and Locked \_\_\_\_\_
- Operator \_\_\_\_\_

Fig. 26 - Reactor check list.

**B. Log Flux and Linear Flux**

- 3 - Log-Flux Compensated Ion Chamber High-Voltage Power Supplies, Positive and Negative 1500 Volts - Panel NN
- 3 - Linear-Flux Uncompensated Ion Chamber High-Voltage Power Supplies, Positive Only 800 Volts - Panel NN

**C. Intermediate-Range, Power-Range, and Temperature Control**

- 6 - Rack Power Supplies, Racks 1, 2, and 3, Lambda AC and DC Panels DD, EE, and FF

Note: Check voltage output to determine if normal

4. Console Annunciator Lights - Trouble lights on the control console are checked simultaneously by pressing the Test and Reset switches on the console. The cause for any light remaining on will be determined and corrected. Any burned-out lights will be replaced.
5. Calibrate Log Flux Amplifiers - The daily pre-operational check of the log-flux (intermediate-range) amplifiers consists of the following.  
Check the Ground, Lo Cal, and Hi Cal settings in that order, and adjust as required. This is done for each of the intermediate-range channels in panels DD, EE, and FF. It is necessary to check these in the order given, and to return the selector switches to "operate" when checking is complete.
6. Dynamic Pump On - This pump is turned on at the S-1 panel. It is necessary for dynamic rod control and it must be operating in order to clear Override. (Automatic control only.)
7. Nuclear Circuits and Safeties - Nuclear safeties shall be checked for the log-count-rate, log-flux, and linear-flux circuits. On each of these circuits, Interlock, Override, and Scram results when the safety levels are reached on two out of three circuits. Turning off a safety circuit switch on the log-count-rate circuits or disconnecting a drawer page on the log-flux or linear-flux circuits, supplies a Scram signal from that respective channel.

In the event that a given channel is inoperative, the scram switch or the drawer page for that channel shall be left off or disconnected. For checking all nuclear safeties, it is necessary first to place the Safety Rod override switch in bypass position on the Bypass at panel J. After all nuclear safeties are checked, this switch should be returned to the normal position.

**A. Log Count Rate**

- (1) Turn off the scram switch for channel 1. Switch each of the fission chamber selector switches on the master console to the Low position. Press the scram reset and the light reset switches to clear all annunciator lights. Turn the Pulse Height Selector on No. 2 AIC amplifier down to a low voltage at a fast enough rate to generate spurious period signal on No. 2 Log Count Rate from alphas and noise via the fission chamber. Periods less than 5 seconds should be observed on channel 2, and Interlock, Override, and Scram should be indicated by the annunciator lights on the console. Return the Pulse Height Selector to its original setting.
- (2) Press the scram reset and the light reset switches, and then turn the No. 3 Pulse Height Selector down to a low voltage. Periods less than 5 seconds should be observed on channel 3, and Interlock, Override, and Scram should be indicated on the console. Return the Pulse Height Selector to its original setting.
- (3) Turn the No. 1 scram switch on, and the No. 2 scram switch off. Press the scram reset and light reset switches and turn the No. 1 Pulse Height Selector

down. Periods less than 5 seconds should be observed on channel 1, and Interlock, Override, and Scram should be indicated on the console. Return the Pulse Height Selector to its original setting. Turn the No. 2 scram switch on.

#### B. Log-Flux Channels (Intermediate Range)

##### (1) Ion chamber signal check.

(a) Click the No. 1 log-flux ion chamber, high voltage, negative, coarse voltage control down one or two positions. This should result in a spurious signal from the ion chamber, which should produce a positive period shorter than 5 seconds and an increase of percent power, as indicated on the master console and on panel DD. Click the negative voltage control back to the 1500-volt setting.

Wait a few seconds, then click the positive coarse voltage control up one or two positions. This should also produce short period and increased power indication. Click the voltage control back to the 1500-volt setting.

(b) Repeat the procedure for channels 2 and 3.

##### (2) Period and Power Level Safeties

(a) On No. 1 intermediate-range drawer, rack No. 1, panel DD, switch from Operate to Interlock and adjust the Period Calibrate as required. The Interlock lights on the drawer and on the console should come on at  $10 \pm 1$  second period. Switch to Override and observe the Override lights, which should come on at  $7 \pm 1/2$  second period. Switch to Scram and observe the Scram lights, which should come on at  $5 \pm 1/2$  second period. As the percent power increases, observe that the  $10^{-6}$  and  $10^{-1}$  lights on the drawer and console go out about the set point. Leave the switch on Scram.

(b) Repeat the procedure for channel 2. When the test signal reaches the proper set points the  $10^{-1}$ ,  $10^{-6}$ , Interlock, Override, and Scram lights on the console should indicate safety action because there are now two coincident channels above set point. Return either channel 1 or channel 2 to Operate condition.

(c) Press the Scram Reset and Lights Reset switches. Repeat the procedure for channel 3.

(d) Place all three channels in Operate condition.

#### C. Linear-Flux Channels

There are no provisions for an ion-chamber signal check; however, the linear flux will come on scale before transferring from the intermediate range, and the linear chambers can be checked at this time.

(1) On No. 1 power-range drawer, rack No. 1, panel DD, switch from Ion Chamber to Test; switch to 15V Scale, and slowly increase Test Signal. The  $10^{-1}$  lights on this drawer and on the console should go out at  $9.6 \pm 0.5$  volts. Switch to 150V Scale and continue increasing Test Signal. The Interlock lights on this drawer and on the console should come on at  $105 \pm 1$  volts. The Override lights should come on at  $110 \pm 1$  volts. The Scram lights should come on at  $120 \pm 1$  volts. Leave the No. 1 test signal at high enough voltage to light the Scram light.

(2) Repeat the procedure for channel 2. When the test signal reaches the proper set points the  $10^{-1}$ , Interlock, Override, and Scram lights on the console should indicate safety action because there are now two coincident channels above set point. Return either channel 1 or channel 2 to operate condition by switching to Ion Chamber and removing test signal.

(3) Press the Scram Reset and Lights Reset buttons. Repeat the procedure for channel 3.

(4) Place all three channels in operate condition by switching to Ion Chamber and removing test signal. Switch the Safety Rod override to normal on the Bypass at panel J.



UNCLASSIFIED

SECRET

8. Dynamic Rods Operation - Each dynamic rod is checked separately as follows:
- (a) On No. 1 power-range drawer, rack No. 1, panel DD, switch from A. C. AMP to GND. The No. 1 dynamic rod will go to the midposition as indicated on the Shim Control Amplifier Drawer and on the console. Switch back to A. C. AMP and switch from A. C. AMP to Test. The No. 1 dynamic rod will go to 7.0-8.0 inches inserted. This rod movement will occur if the rod system is working normally, when the dynamic pump is on, regardless of the safety circuit condition (scram, etc.). The valve current meter in the No. 1 Power-Range drawer will indicate the signal current to the No. 1 dynamic valve. Return the switches to A. C. AMP.
  - (b) Repeat the procedure for channels 2 and 3 at panels EE and FF respectively.
9. Process Safeties - For checking all process safeties, it is necessary first to place the Safety Rod override switch in bypass position on the Bypass at panel J. After all process safeties are checked, this switch should be returned to the normal position.
- (a) Outlet Air Temperature - There are two recorders for outlet air temperature. These recorders, mounted in panels TT and UU, each have Interlock, Override, and Scram switches to actuate at the set point temperature. Turn off the recorders and observe that the Interlock, Override, and Scram lights on the console come on at the proper temperatures when each of the recorders is manually driven upscale. Turn both recorders on.
  - (b) Fuel Element Temperature - There are ten recorders for fuel element temperature. These recorders, mounted on panels PP, QQ, RR, and SS each use a single limit switch to actuate at the set point temperature. Turn off one recorder and manually increase it. Observe that the Interlock light comes on at the proper temperature. Turn three recorders up and observe the Override light. Turn five recorders up and observe the Scram light. Turn all ten recorders on. Check the remaining five recorders on alternate days.
  - (c) Low Airflow  $10^{-6}$  - An override safety is established when there is less than 1 psia across the reactor (stations 3.45 to 3.65) when the reactor power is above  $10^{-6}$ . With engines off there will be less than 1 psia. Simulate more than  $10^{-6}$  power by means of the Lo Cal or Hi Cal switches on two of the intermediate-range drawers. Check for Min Air Flow Override lights on the console. Return both Intermediate-Range switches to operate.
  - (d) Engine Overspeed - Centrifugal switches, which are included as part of the engine accessories, actuate at  $7950 \pm 40$  and  $8200 \pm 30$  rpm and provide Override and Scram at these respective engine speeds. Manually trip the engine overspeed relays in panels HH and LL and observe the Override and Scram lights on the console. The centrifugal switches are checked on each engine during its component test on the engine test pad.  
Caution: Do not trip these relays if an engine is operating.
  - (e) Low Hydraulic Oil Pressure - Turn off the dynamic pump and check the Hyd Press override light on the console. Turn the hydraulic pump back on.
  - (f) LCR Downscale - Check that the Min Count Rate scram light comes on when the log-count-rate recorder on the primary panel is driven downscale below the proper set point. This is effective only below  $10^{-6}$ . Turn the LCR recorder on.
  - (g) Three Dynamics Off - Check that the POS Loop Cut Off override light comes on when all three dynamic rod switches on the console are off, with the reactor switch in automatic control. Switch these rods back on.
  - (h) Fuel Element Rupture - The rupture detector system is designed to provide a Warning and a Scram signal when the count rate from the off gas activity reaches predetermined values such as 50 and 800 counts per minute respectively. These values may vary depending upon the normal background for the particular test,

UNCLASSIFIED

SECRET

but the procedure for checkout will remain unchanged. Push the Scram Reset and the Lights Reset switches on the console. On the Rupture Detector, panel CC, place the Setback Range and the Scram Range switches for the No. 1 system in the Trip Adjust position. Turn the Trip Level Adjust screw on the rear of the unit to drive the count-rate meter upscale. When the meter reaches the proper warning level, on the bottom scale of this meter, the Setback light on this unit and the FE Rupture warning light on the console should come on. Continue increasing the level, and when the proper scram level is reached, the Scram light on the unit and the FE Rupture and Scram lights on the console should come on. Return the Trip Level Adjust screw to the normal extreme position, and place the Setback Range and the Scram Range switches in the proper decade for operation. The proper decade setting might vary depending upon the normal background for the particular test. Repeat the procedure for the No. 2 system.

- (i) 400-Cycle Power - Momentarily turn off the 400-cycle power switch on the Safety Relay drawer in panel EE. The 400 and Scram lights on the console should come on. Turn this switch back on.
- (j) Manual Interlock - Clear lights and safeties by pressing the reset switches. Switch to Manual Operation and withdraw one frame about 1 inch, observing the frame position indicator. Check that all shim rods in that frame withdrew by checking each rod on the position indicator. Press the operator's discretion Interlock switch and hold it down. It should not be possible to withdraw the frame, and the interlock light should come on.
- (k) Manual Override - Clear lights and safeties by pressing the reset switches. This test follows the manual Interlock test, and one frame of rods is therefore withdrawn about 1 inch. Press the operator's discretion Override switch and hold it down. The frame should insert and the Override and Interlock lights should come on.
- (l) Manual Scram - Clear lights and safeties by pressing the reset switches. Withdraw one safety rod and latch it. Observe whether lights function normally. Switch to Manual Operation and withdraw another frame about 1 inch, observing the frame position indicator. Check that all shim rods in that frame withdrew by checking each rod on the position indicator. Press the operator's discretion Scram switch momentarily. The safety rod should scram as indicated by the Scram light coming on. The frame should insert, and the Scram, Override, and Interlock lights should come on.

**Caution:** The process safeties are now all checked, and the Safety Rod override bypass switch should now be placed in operate position in the Bypass at panel J.

10. Safety Rods Operation - Clear all safeties by pressing the reset switch. Check the remaining safety rods, one at a time. (One was checked on the Manual Scram test.) Withdraw it, latch it, then scram it with its individual scram switch. Check the Out and Scram lights for each rod to observe proper function. Observe whether the count rate increases as each rod is withdrawn. Record any malfunctioning rod. Leave all individual switches in scram position.
11. Shim Rods Operation - Clear all safeties by pressing the reset switches. Switch to Manual Operation and check the remaining frames of shim rods, one at a time (two frames of shim rods have already been checked during the manual interlock and scram tests). Press the Safety Latch Bypass switch, then withdraw the frame about 1 inch. Check that all shim rods in that frame withdrew by checking the frame position indicator for each rod. Release the Safety Latch Bypass switch until that frame is inserted, then check the next frame of shim rods. Record any malfunctioning rods.

12. Standardize Recorders and Zero Console Meters - A standardizing switch is provided on each recorder. With the recorder turned on, press the switch until the reading stabilizes. All the recorders on the primary and secondary panels should be standardized. There are five vacuum tube voltmeters on the console which should be zeroed by pushing switches and adjusting potentiometers.
13. Switches in Operate Position and Panels Locked - A final check should be made to ascertain that all necessary switches are in the operate position. This includes all switches that were used during previous checkout procedures, e.g., the Ion Chamber - Test switch on the power-range drawers, and also all other switches in the reactor control and safety circuitry. Lock the back of panel XX and the Bypass board at panel J.
14. Safety Circuits Bypassed - A record should be made here of any and all safety circuits that are bypassed. The bypass switches are located in the Bypass board at panel J.

The before-operation portion of the reactor check list is now complete and the operator should sign it to signify his acceptance of these checked items.

#### After Shutdown

The following items are checked to assure that the reactor is satisfactorily secure.

1. All Shim Rods In - All shim rods are inserted as indicated by the frame-insertion lights and the frame-position indicators. This assures that all shim rods are inserted before power is turned off. Record any rod that does not insert.
2. Safety Rods Scrammed - Each scram rod will be checked by flipping its individual scram switch and observing that the Scram light comes on. If the reactor has been scrammed to shut down, it is not necessary to relatch and check rods individually; merely check that all Scram lights are on. Record any rod that does not scram.
3. Dynamic Pump Off - Switch off on panel S-1.
4. Chart Drives Off - Switch off all recorders except those that the Engineer-In-Charge orders left on.
5. D19 Off and Locked - This assures that the reactor cannot be operated by an unauthorized person.

The reactor operator signs to signify that the reactor is properly secured.

Caution: Do not turn off MG Set No. 6 or switches A1, C4, C7, C9, C10, C11, or C13 for this would cause too much disturbance in the reactor amplifiers. Do not turn off the d-c MG Set No. 7 if the engine is operating, or if d-c power is required for data or systems.

#### DESCRIPTION OF THE EVENT

The tests being conducted on the day of the excursion were designed to yield data concerning the rate of temperature increase in the moderator, control rods, and shield. The following account of the event is compiled from data obtained from instrument records and the accounts presented by operating personnel.

On Tuesday afternoon November 18, between the hours of 1530 and 1630, a data run at 0.06 megawatt was successfully accomplished to observe heating rates. This data run was accomplished by operating the reactor on manual controls. The general level of temperature in the reactor during the run was 210°F on fuel elements and 190°F air discharge. After a preliminary analysis of the data, it was determined that a second data run should be accomplished at twice the power level of this run.

On Tuesday evening starting at 2000, the second data run (Run 15-4) was attempted and resulted in the power excursion. At the time of the event, the reactor was on automatic servo control and on a power-demand setting that was expected to bring the reactor to a power level of 0.12 megawatt or 0.4 percent of design power. This power corresponded to a reading of 80 percent on the power-range instrumentation.

The airflow for this experiment was provided by two electrically driven blowers supplying a total flow of approximately 3 pounds of air per second through the reactor and out the No. 2 jet engine turbine. The jet engine motored, because of blower airflow, at approximately 600 rpm; the engine-speed indication was evident to the operator at the main console at all times. During the data run there was no manipulation of any duct valves.

The normal pre-operational checks of instrumentation and controls were conducted, and all controls and instruments were determined to be in the anticipated operating condition. Reactor operations were started shortly after 2000 hours. The photoneutron level from the previous run was high enough that the indications from the intermediate-range chambers at the operator's console were on scale at a reading that permitted immediate automatic servo operation. (See section 4.1 for the reproduction of recorder traces.) After all the safety rods were cocked, the reactor was put on servo control in intermediate range with the power-demand setting at the lowest level ( $10^{-4}$  percent, or an expected power of 0.1 watt). This initiated dynamic rod withdrawal and shim rod sequence withdrawal. To obtain the desired rod pattern (all rods equally withdrawn) each frame was bypassed when it was halfway withdrawn. In this manner all the frames were placed at their midposition. Before this was accomplished, however, the flux level had reached the demanded flux (0.1 watt). The power demand was consequently raised to the highest limit (15 percent), and the servo system continued to withdraw shim rods. The system withdrew all the shim rods halfway and frame A fully. At this point, since further shim rod withdrawal was indicated, frame F was removed from bypass. Frames A and F were then not bypassed and remained in this condition throughout the operation. The servo system was unable to raise the power as rapidly as the programmed power demand because of the slowness of the shim rod withdrawal. The servo continued to withdraw shim rods until the reactor was increasing at a period less than 25 seconds, which is the demanded rate of power increase. As shim rod withdrawal continued, the shortening period resulted in an interlock and override situation. This very quickly restored the balance between the demanded and actual power. As soon as this balance was accomplished, the override was reset and the servo system proceeded to increase the power on a very steady 25-second period.

When the power had reached the 4.5 percent level corresponding to an expected power of 6.8 kilowatts on the linear flux (uncompensated or power-range chambers), the ready-to-transfer light came on, because the 10 percent interlock was bypassed, and the servo control was switched from the intermediate range to the power range. At the time of transfer to the power range, all appeared normal and the rod configuration was as expected. That is, all the frames were in midposition except for frame A, which was fully withdrawn, and frame F (containing five rods), which was withdrawing.

The switching of servo control from the intermediate range to the power range resulted in a transient due to transferring before zeroing the error. The dynamic rods responded by moving fairly rapidly in and out with corresponding changes in period. Twenty seconds later, when this transient situation had died down, the power-range demand was raised to the desired setting of 80 percent. The servo-power-demand rate was set at its slowest setting, which called for a linear increase in power of 2.4 percent of full scale per second. This rate would take the power from 10 percent to 100 percent in 40 seconds, or, in this case, from 10 percent to 80 percent in 32 seconds.

UNCLASSIFIED

The power of the reactor increased in a manner that appeared to be as expected. Shortly before the power reached the demanded 80 percent level, something caused the indicated flux to fall as observed on the linear-flux instrumentation. This drop was accompanied by an indicated increasing period. Shortly after this the indicated power went back up rapidly, the reactor had scrambled, and the fuel element temperatures were observed to be high, with several recorders going off-scale at 3000°F. The indicated flux fell slowly following the scram. After the excursion it was observed that the following safety lights were on: (1) all three levels (interlock, override, scram) of fuel element temperature, (2) all three levels of intermediate-range period on all three channels, and (3) all three levels of source-range period on both channels. With these indications it was impossible to infer whether the scram was caused by the fuel element temperature or by the intermediate-range period. However, persons present in the control room observed that the fuel element temperature scram light was the first to give an indication. (A modification to the safety circuit had permitted the intermediate-range period safeties to be operative even though the power plant was operating in the power range.) The reactor operator also scrambled the reactor manually, but his action was preceded by perhaps 3 seconds by the automatic scram.

Following the event, fuel element temperature indications of full scale or 3000°F and moderator temperatures of the order of 1000°F were reported by persons in the control room. The data-scanning system was turned on approximately 4 minutes after scram and left on for approximately 42 minutes. Temperature data on fuel elements, moderators, and other core components were obtained. One-minute effluent spot samples, an 80-foot-level chilled charcoal trap sample, and radiation levels in and around the IET facility were obtained following the scrambling of the reactor.

Approximately 25 minutes after the event it seemed desirable to increase the cooling air through the reactor, because of the slow rate of cooling of the core components. Consequently, the 100 psi diesel air compressors were started, permitting the motoring of the turbojet engines on their starters. This was continued for approximately 20 minutes, following which all temperatures had reduced to such a low level that the electric blowers were again turned on.

#### TEMPERATURE DATA FOLLOWING SCRAM

Following the scram, the Brown recorders in the data room were turned on and a continuous data scan was initiated. The scan was started approximately 4 minutes following the incident and continued for 42 minutes. The scan cycle was intermittent, since in general the thermocouple signals were erratic, driving the recorders off-scale, or were fluctuating so wildly that it was impossible for the scanner to null out the signal. When a scanner "hung up" on a point, that point was bypassed so that the scan could continue.

Component temperatures recorded following scram are presented in Figures 29 through 41. The highest temperatures recorded for a given component have been selected and are plotted as a function of elapsed time. In addition, circumferential, longitudinal, and radial temperature distributions are presented where data were available. Temperature information on the moderator bars, control rod discharge air, and both the front and rear tube sheets was fairly complete since thermocouple loss was slight; however, loss of instrumentation on the fuel elements was extensive, and few data were obtained. Only the peak temperatures recorded during the scan have been selected for presentation here. Instrumentation on hotter elements probably failed during the power excursion. Thermocouples in the reactor shield and core support structure indicated a temperature of approximately 60° to 100°F 5 minutes following the scram.

UNCLASSIFIED

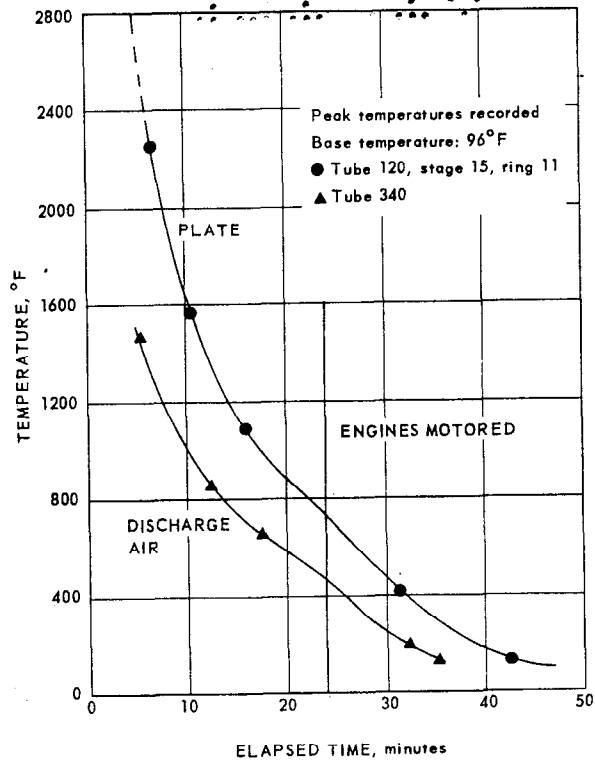


Fig. 29 - Fuel element plate and air temperatures during power falloff from scram

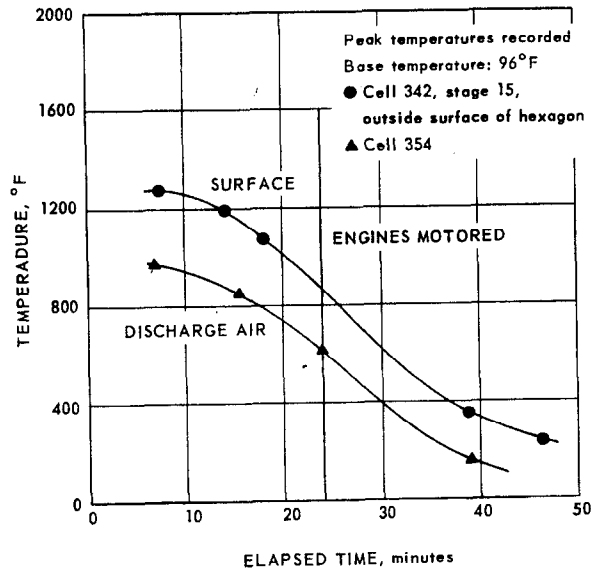


Fig. 30 - Moderator surface and air temperatures during power falloff from scram

~~SECRET~~

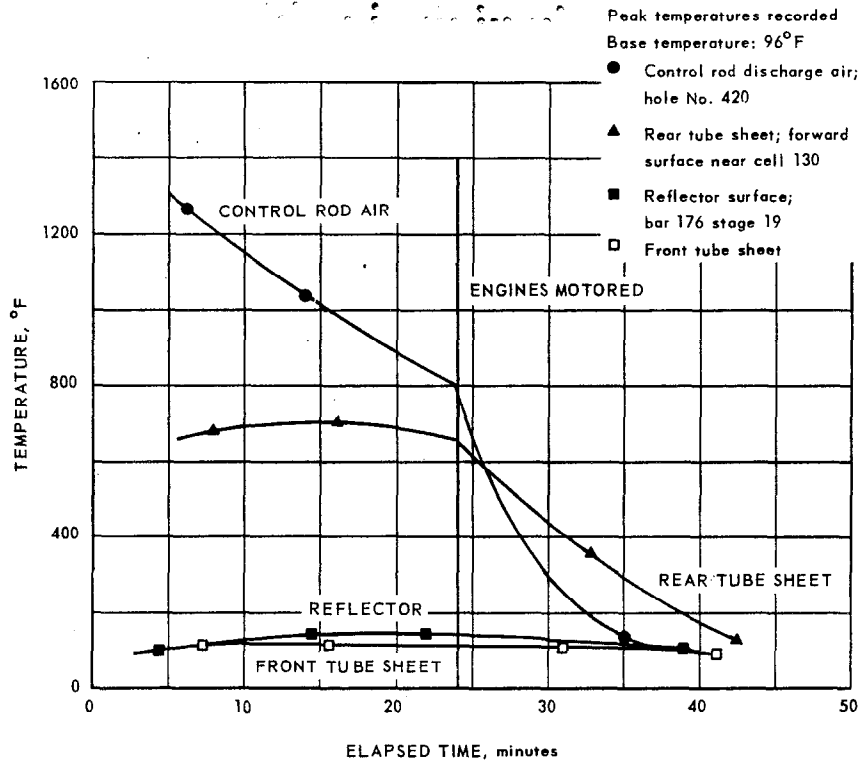


Fig. 31 - Reactor component surface temperatures during power falloff from scram

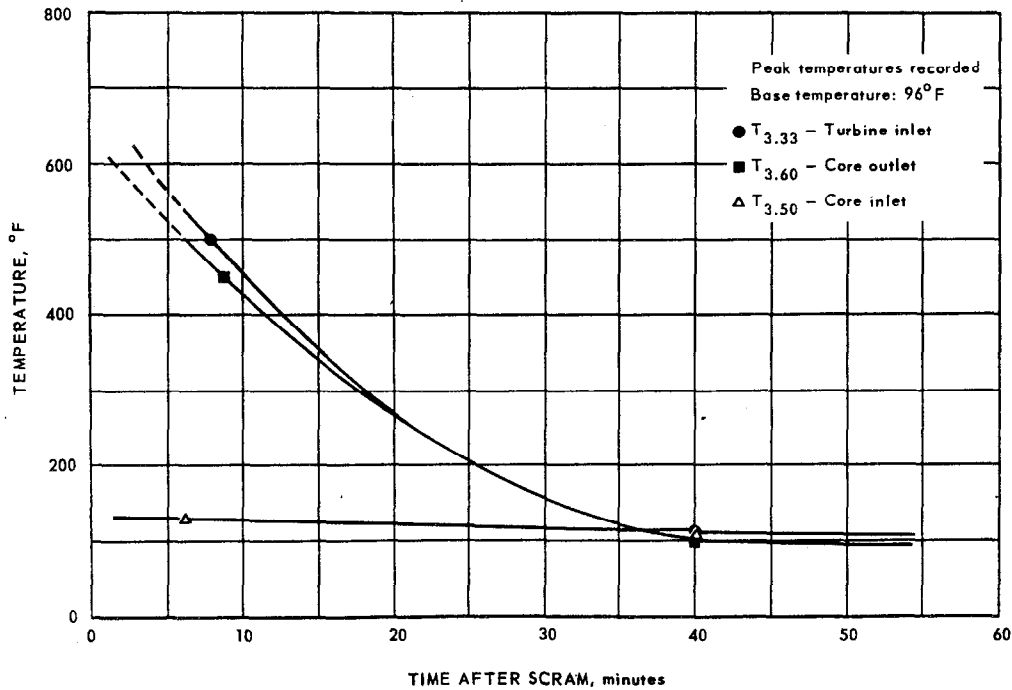


Fig. 32 - System loop temperatures during power falloff from scram

UNCLASSIFIED

~~SECRET~~

UNCLASSIFIED

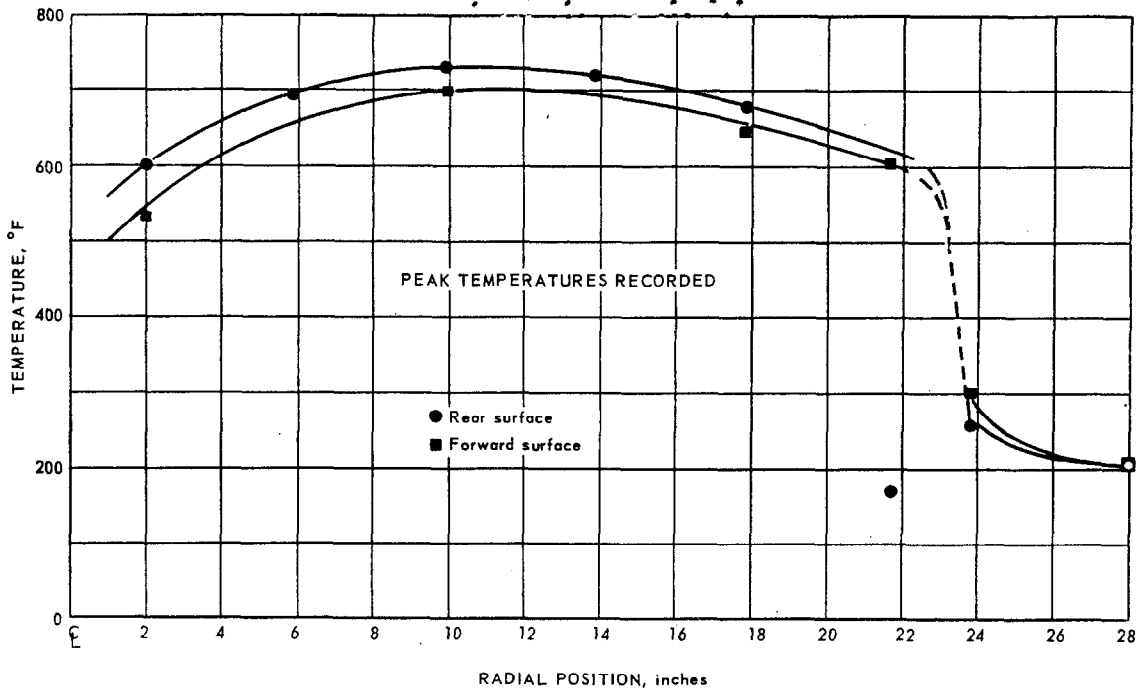


Fig. 33 - Rear tube sheet radial surface temperatures 16 minutes after scram

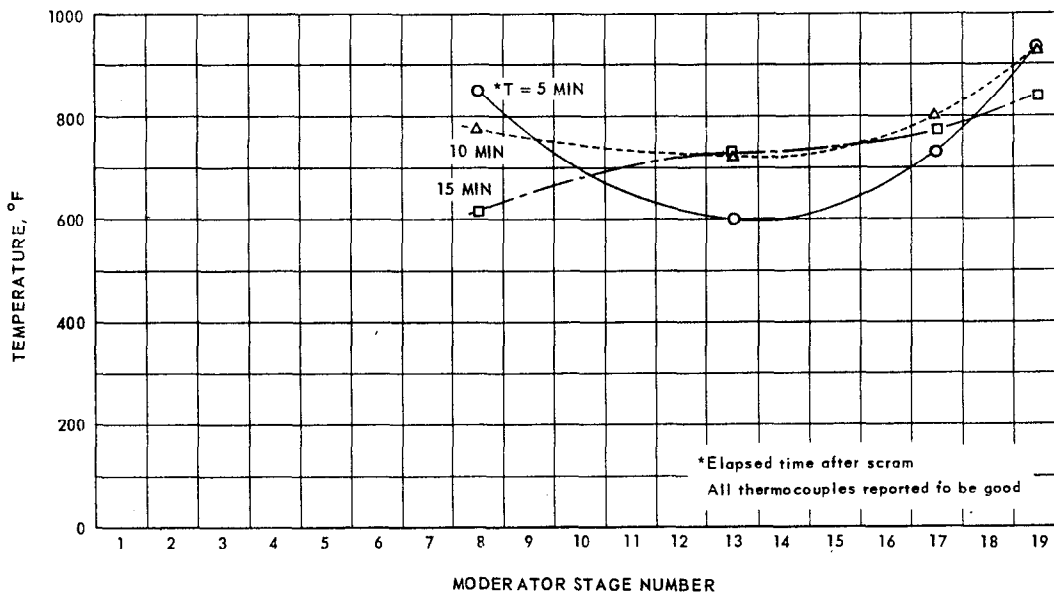


Fig. 34 - Longitudinal moderator temperatures after scram, cell 463

UNCLASSIFIED



UNCLASSIFIED

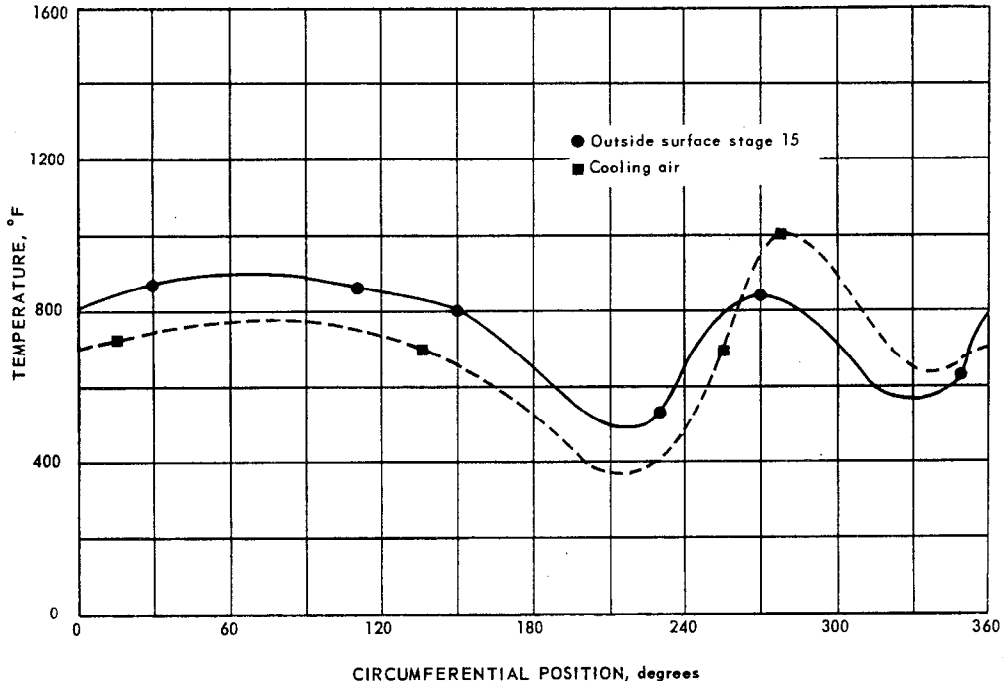
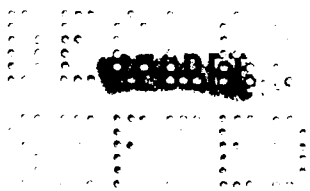


Fig. 35 - Circumferential moderator surface and air temperatures 6 minutes after scram, cell 160

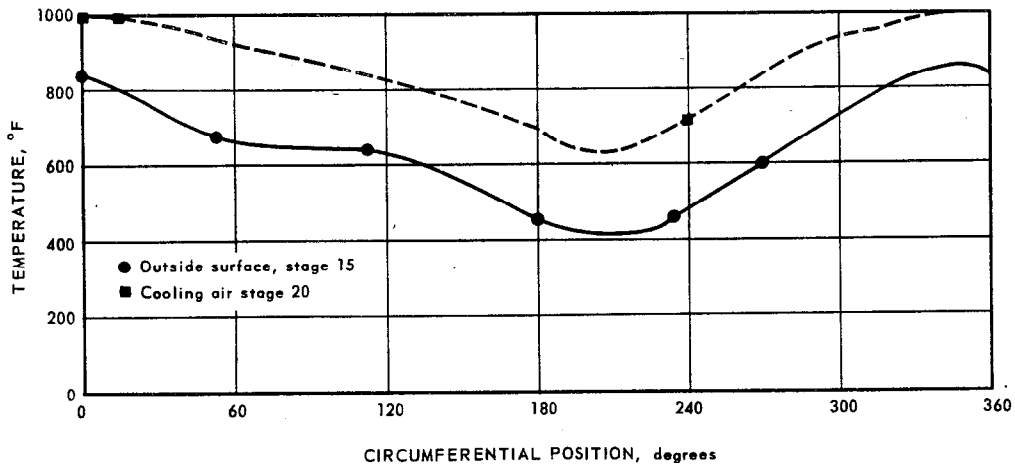
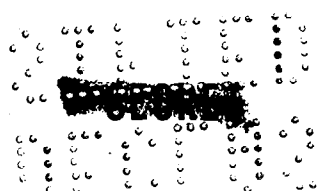


Fig. 36 - Circumferential moderator surface and air temperatures 6 minutes after scram, cell 273

UNCLASSIFIED



UNCLASSIFIED

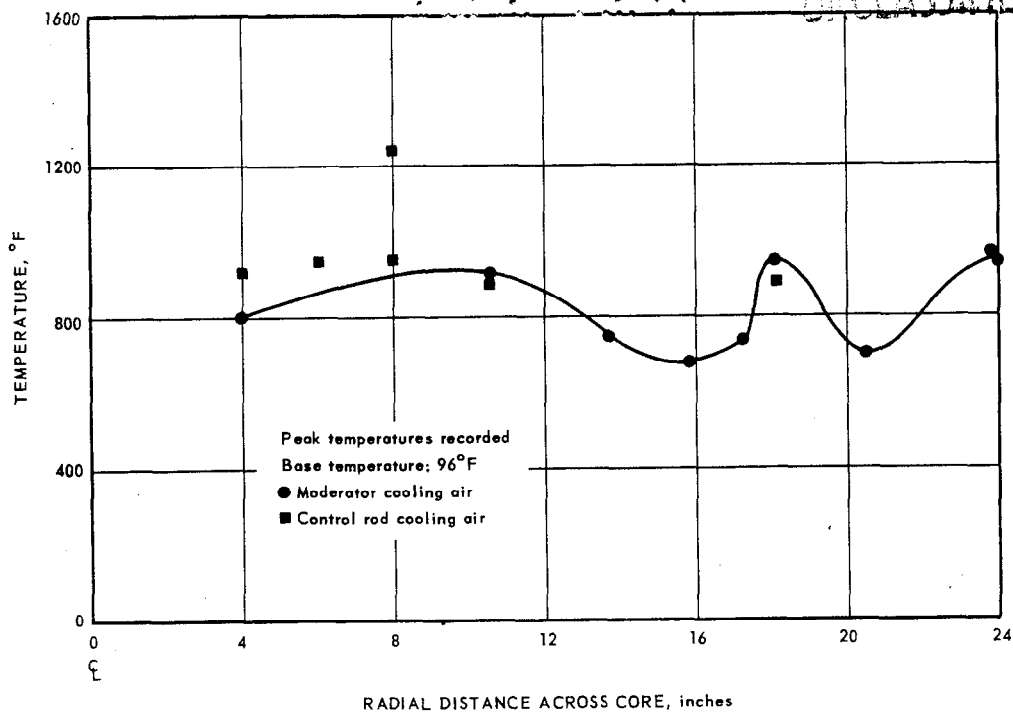


Fig. 37 - Moderator and control rod radial discharge air temperatures approximately 8 minutes after scram

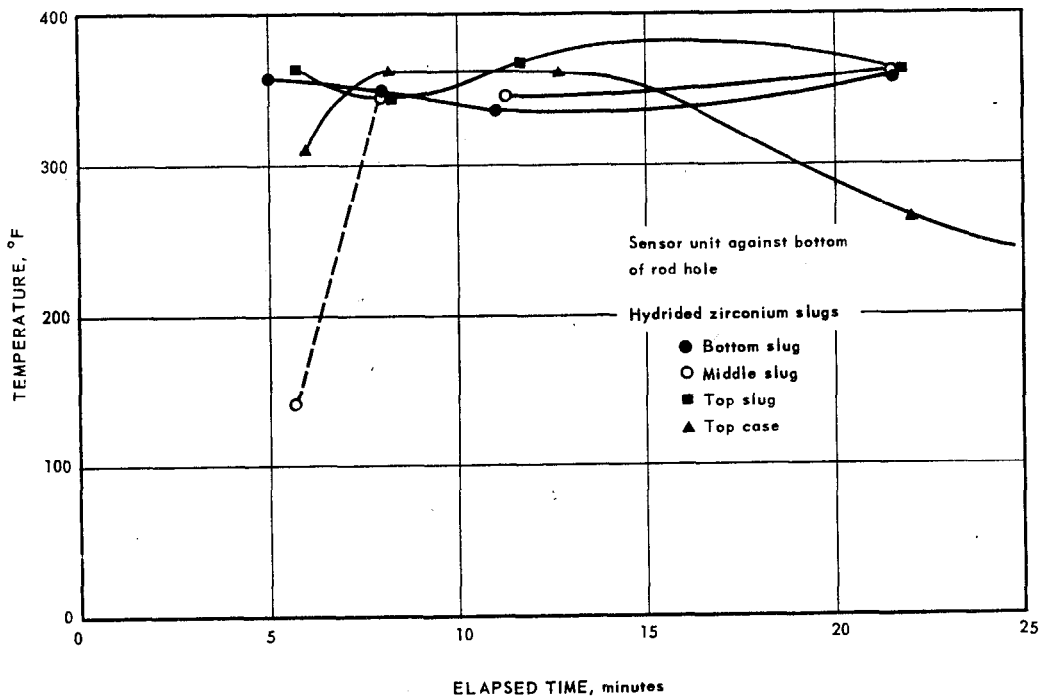


Fig. 38 - Heat-rate-sensor temperatures during power falloff, control rod hole 520

UNCLASSIFIED

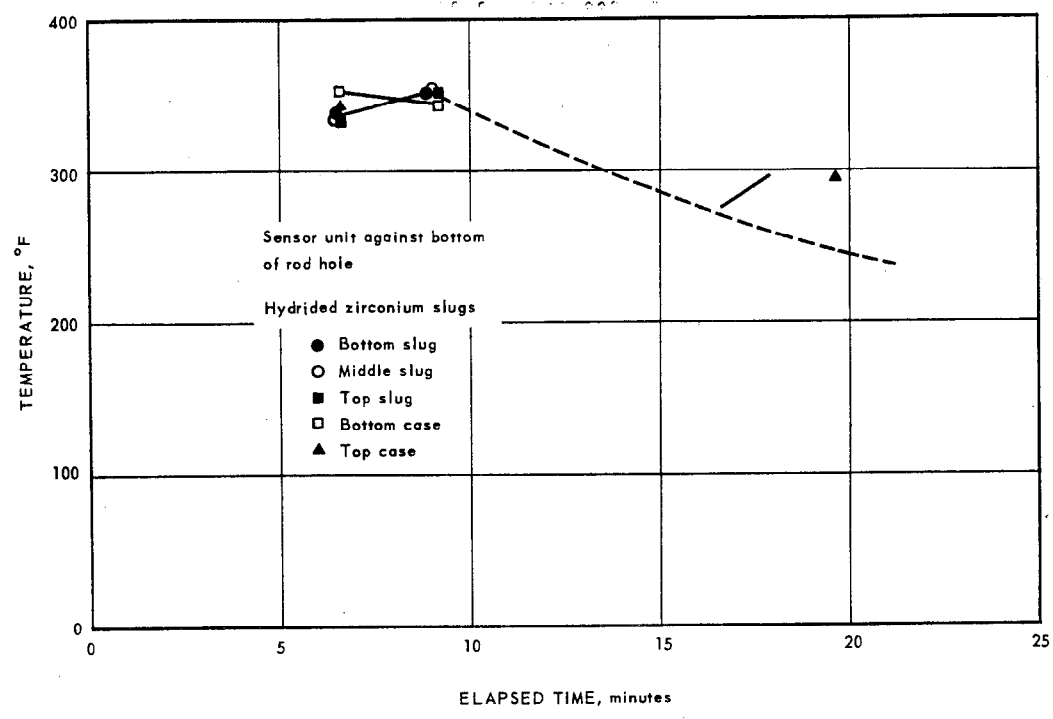


Fig. 39 - Heat-rate-sensor temperatures during power falloff, control rod hole 631

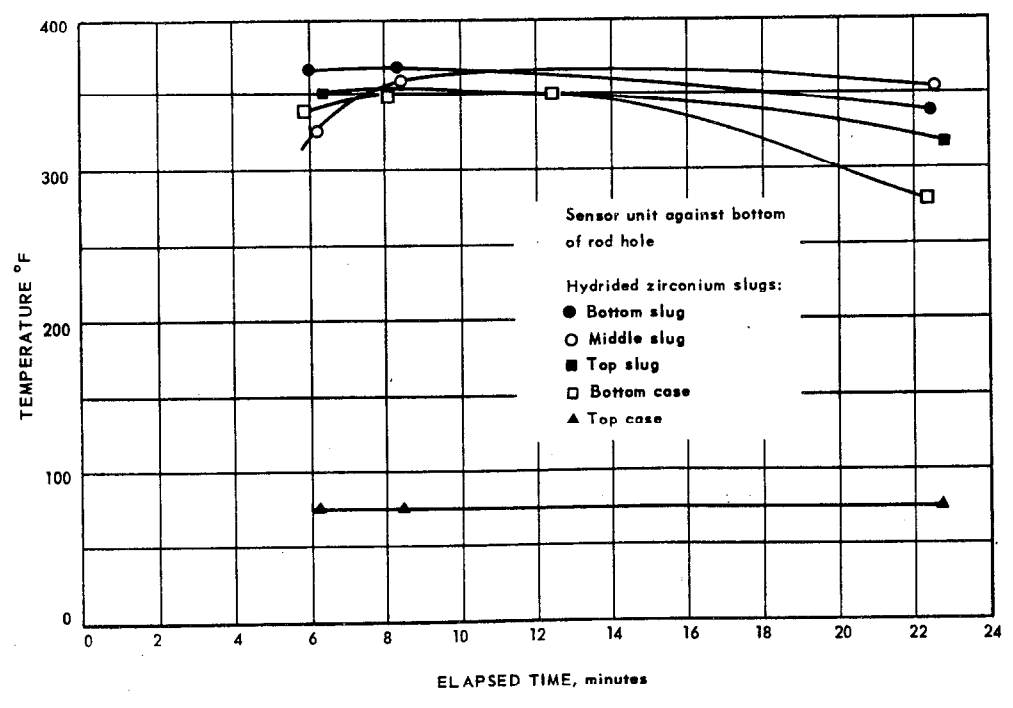


Fig. 40 - Heat-rate-sensor temperatures during power falloff, control rod hole 265

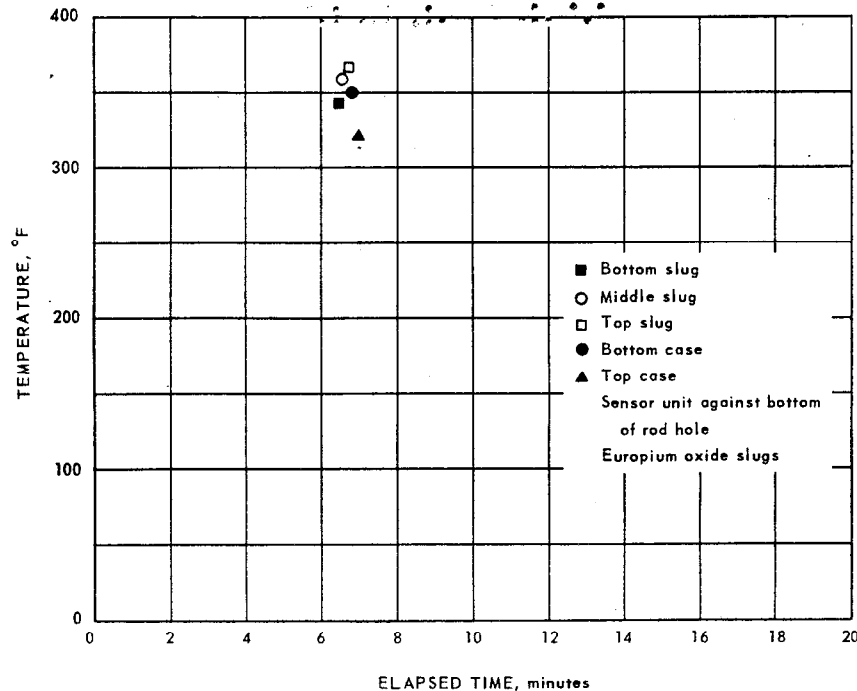


Fig. 41 - Heat-rate-sensor temperatures during power falloff, control rod hole 110

The temperature data for components other than fuel element and moderator, such as shield and tube sheets, have little significance other than that they are low; no previous pattern had been established for comparison.

The fuel element, air, and moderator temperatures are relatively uninterpretable. Because so many thermocouples failed, the remaining readings are suspect and not enough remained to establish a pattern. The data are presented primarily as a matter of record.

Throughout the excursion six calorimeter units were situated inside the reactor. Units were positioned in control rod holes 110, 520, 631, and 265, and in nuclear instrumentation sensor holes 5 and 6. The temperature of the slugs in the calorimeters within the core as a function of elapsed time is plotted in Figures 32 through 35. The slugs ranged in temperature from 330° to 355°F approximately 5 minutes following the scram. During the power excursion, the heat calorimeters located in the primary shield remained essentially at ambient temperature.

#### POSTOPERATION INSTRUMENTATION CHECK

The day after the event an instrumentation check was accomplished with the following results:

Thermocouple Locations	Good Prior to Incident	Good Following Incident	Percent Loss
Fuel element plates	127	18	86
Air thermocouples at end of fuel elements	51	6	88
Moderator surface	34	30	12
Air thermocouples at end of moderator bars	22	22	0

Loss of air thermocouples is explained by the fact that the lead wires run along the fuel cartridges to the front of the core, as do the fuel element thermocouple leads.

UNCLASSIFIED

Thermocouples on the reflector front and rear tube sheet, control rod guide tubes, nuclear heat rate sensors, and all components external to the immediate core area were reported as being good.

Following the incident a resistance check was made on the ten thermocouples that were connected into the scram circuit. The data thus obtained are presented in Table 6 along with the scram settings.

TABLE 6  
POSTEXCURSION CHECK OF SCRAM CIRCUIT THERMOCOUPLES

Thermocouple Location <sup>a</sup>	Condition	Scram Setting, °F	Loop Resistance <sup>b</sup>	Positive to Ground	Negative to Ground
110-19-10-10	Bad	1800	200	200	9
340-19-10-08	Bad	1800	Open	Open	Open
410-19-10-02	Bad	1800	Open	Open	Open
440-19-10-06	Questionable	1800	20	12	7
540-19-10-0	Bad (uncapped)	1920	Open	Open	Open
542-19-10-02	Bad	1620	Open	Open	Open
551-19-10-07	Good	1630	20	Open	Open
561-19-11-07	Questionable	1650	19	Open	8
260-19-11-0	Bad	1600	Open	Open	Open
661-19-10-10	Good	1630	19	Open	Open

<sup>a</sup>Cell - stage - radial position - circumferential position

<sup>b</sup>20Ω is normal loop resistance. Low resistance to ground is basis of questionable rating.

### ENERGY RELEASE CALCULATIONS

Prior to Run 15-4, a 1/4-inch indium foil was positioned in the special test foil hole. The flux at this location was related to that inside the core during previous tests and consequently was correlative to reactor power. Approximately 2 hours following the excursion, the foil was removed from the reactor and counted. The foil count was 3.02 x 10<sup>5</sup> counts per minute after a decay period of 132 minutes. The total energy generated during the excursion was obtained using the following power-to-foil-count relationship:

$$\int P dt_e = K A_s t_e = \frac{c e^{\lambda t_d}}{1 - e^{-\lambda t_e}} = K t_e$$

where:

A<sub>s</sub> = Activity of foil in counts per minute normalized to saturation level

t<sub>e</sub> = Foil exposure time in minutes

t<sub>d</sub> = Foil decay time in minutes

K = Constant relating saturated foil activity in counts per minute to reactor power in kilowatts

$$\text{From Run 11-1: } K = \frac{4.78 \text{ (kw)}}{4.79 \times 10^4 \text{ (cpm)}}$$

∫ P dt = Total energy generated

c = Uncorrected activity counts from foil

λ = Decay constant for indium (0.0128 min<sup>-1</sup>)

UNCLASSIFIED

UNCLASSIFIED

expanding the term  $(1 - e^{-\lambda t_e})$  gives

$$1 - (1 - \lambda t_e + \frac{\lambda t_e^2}{2} + \frac{\lambda t_e^3}{3} + \dots)$$

For a short exposure time, the expanded term reduces to simply  $\lambda t_e$ . Substituting and solving for the original equation gives

$$\begin{aligned} \int P dt_e &= K \left( \frac{c e^{\lambda t_d}}{\lambda t_e} \right) t_e \\ &= 0.998 \times 10^{-4} \left( \frac{3.02 \times 10^5 e^{0.0128 (132)}}{0.0128} \right) \\ &= 12750 \text{ kilowatt-minutes} \\ &= 765 \text{ megawatt-seconds} \end{aligned}$$

#### POSTOPERATION CRITICAL EXPERIMENT

On December 21, 1958, a reactor critical experiment was performed to determine whether a loss in reactivity had occurred during the power excursion and, if so, to what extent as measured in terms of percent  $\Delta k/k$ .

The configuration of the reactor at the start of the test was as follows:

1. All shield compartments were intact and full of water.
2. Four control rods (three shims and one safety) were removed and heat rate calorimeter units were inserted in their locations.
3. Four control rods (three shims and one safety) would not withdraw during the pre-operational checkout; one shim rod was stuck at approximately 2 inches withdrawn.

In this configuration the rods were withdrawn in sequence until all the rods were pulled without criticality being achieved. At this point the water in the shield compartments was drained (which increases reactivity), and each control rod was actuated to determine whether the rod was attached to the actuator. Every rod actuator that could withdraw was confirmed to have a poison tip attached.

The reactor was subsequently made critical and the following rod positions were recorded:

Frame	Position, inches withdrawn *	Excess Reactivity, % $\Delta k/k$
A	10.42	0.100
B	9.77	0.280
C	9.85	0.214
D	5.59	0.502
E	4.81	0.342
F	4.94	0.551
Dynamics	10.00	0.141
		<u>2.130</u>

Previous testing indicated that the total excess reactivity with the shield compartments empty was 4.84 percent  $\Delta k/k$ . If no loss in reactivity had occurred, the excess reactivity

\*This measurement includes only those rods that moved with the particular frame.

UNCLASSIFIED

should have been 4.84 percent  $\Delta k/k$  minus the loss in available reactivity due to rods being fully or partially stuck in the inserted position. The following tabulation presents the fixed rods and the excess reactivity associated with each:

Rod No.	Position, inches withdrawn	Excess Reactivity, $\% \Delta k/k$
510	0	-0.160
621	0	-0.154
231	18	-0.135
Safety	0	-0.125
		<u>-0.574</u>

The loss in excess reactivity was then equal to  $\left[ (4.84 - 0.57) - 2.13 \right]$  or 2.14 percent  $\Delta k/k$ .

#### FACILITY SURVEY, EFFLUENT, AND FIELD DATA

Immediately following the incident, radiation surveys in the facility were started and samples of the effluent were taken. Later field surveys were made to determine the amount of contamination on the ground and vegetation. These data were then used to estimate the magnitude of release of radioactive materials.

##### IET Facility Survey

Within the IET Facility approximately 1/2 hour after the event, gamma dose measurements in the control and data room were observed to be 15 to 20 milliroentgens per hour. The background on the counting equipment in the shielded counting room was increased by a factor of 100. However, air samples drawn from within the facility indicated normal level of air activity.

During the same time interval, isodose plots were obtained in the area surrounding the test cell. These plots indicate that the dose rate on the upper surface of the IET control room roof was between 0.2 and 2 roentgens per hour, depending on location. Since 28 inches of concrete would reduce this dose rate to the 15 milliroentgens per hour noted, and the IET Control and Equipment Building has roughly 14 feet of tamped earth over 2 feet of ordinary concrete, the validity of the measurement is seriously questioned. It is impossible at this point to determine why the reading was so high, but contamination of the measuring instrument is suggested as a possibility. The presence of radioactive samples in the shielded counting room may have been responsible for the increase in background noted.

Outside the facility, in the test cell, a smear survey indicated a contamination level of  $1.2 \times 10^7$  disintegrations per minute per  $100 \text{ cm}^2$ . This contamination did not decay as mixed fission products, but decayed with a half-life of 4 hours. Air samples drawn in the test cell, at the times indicated, yielded the following data:

Date	Time of Sample	Concentration, microcuries per cubic centimeter
11/18/58	2022	Scram from event
	2400	$1.2 \times 10^{-6}$
11/19/58	0220	$10^{-6}$
	0600	$5 \times 10^{-7}$

Portable survey instruments (radium calibrated) were used to obtain gamma dose measurements at various distances and directions from the core at 1-hour intervals from 4.7 hours to 42 hours after the event. Isodose plots for 1 minute, 1 hour, and 62 hours after the event are presented in Figures 42, 43, and 44, respectively.

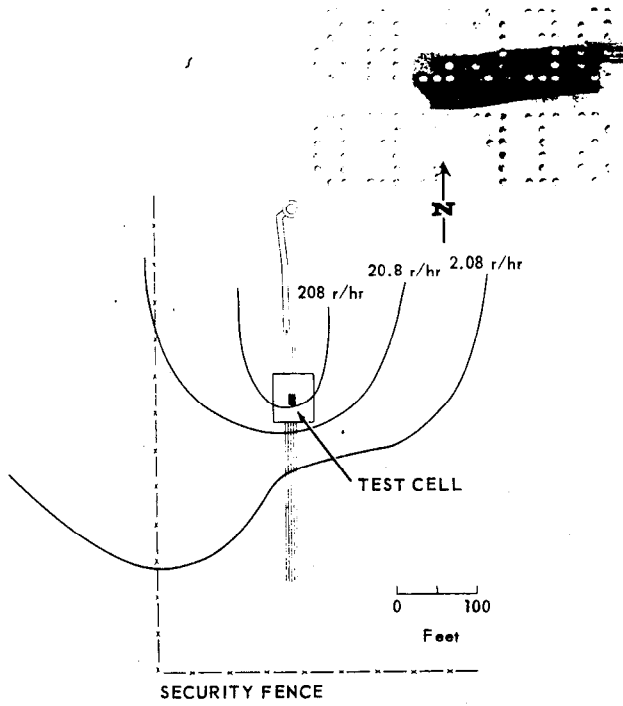


Fig. 42 - Gamma dose rate measurements corrected to 1 minute after scram

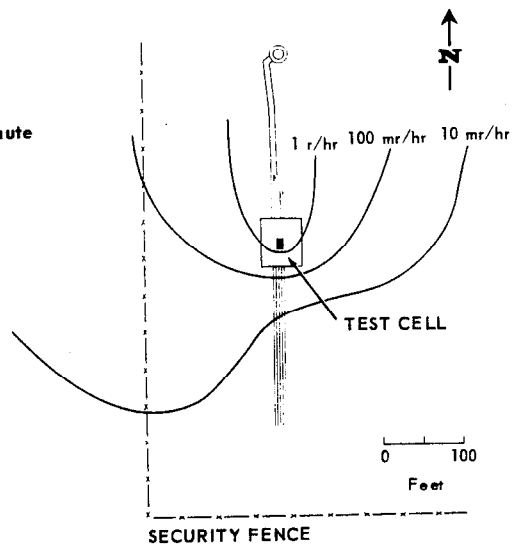


Fig. 43 - Isodose measurements 1 hour after scram

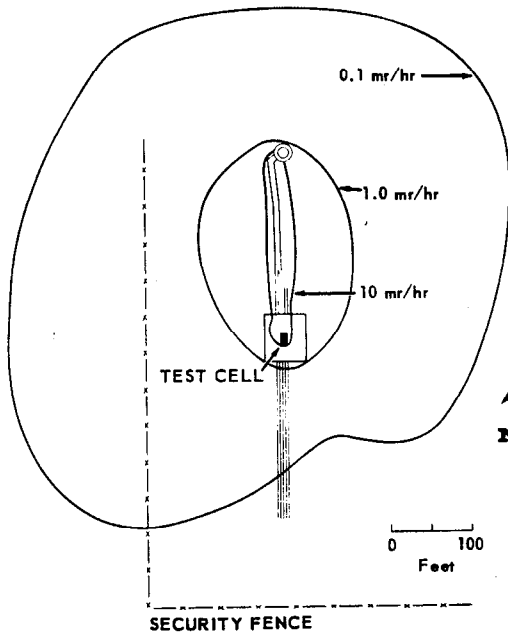


Fig. 44 - Gamma dose rate measurements 62 hours after scram



UNCLASSIFIED

The isodose plot for 1 minute after scraft was constructed by extrapolating the observed decay rates obtained with the portable survey instruments at time 4.7 hours and beyond back to time 1 hour, and then, by following the decay curve as observed by the test cell Jordan ion chamber from time 1 hour to 1 minute. The 62-hour isodose plot was measured directly using Geiger-Mueller and Cutie Pie instruments.

Radiation levels were measured with Cutie Pie meters at various points in and around the test cell including contact readings at several points on the D102A reactor assembly and on the IET large duct (approximately 100 feet from core centerline). Readings were repeated over a period of approximately 24 hours to follow the decay of the radiation levels. The resultant curves are shown in Figure 45. The highest radiation levels indicated are about 5 roentgens per hour, which tend to substantiate the belief that large quantities of fuel did not leave the reactor core and deposit in the dolly ducting or the IET large duct.

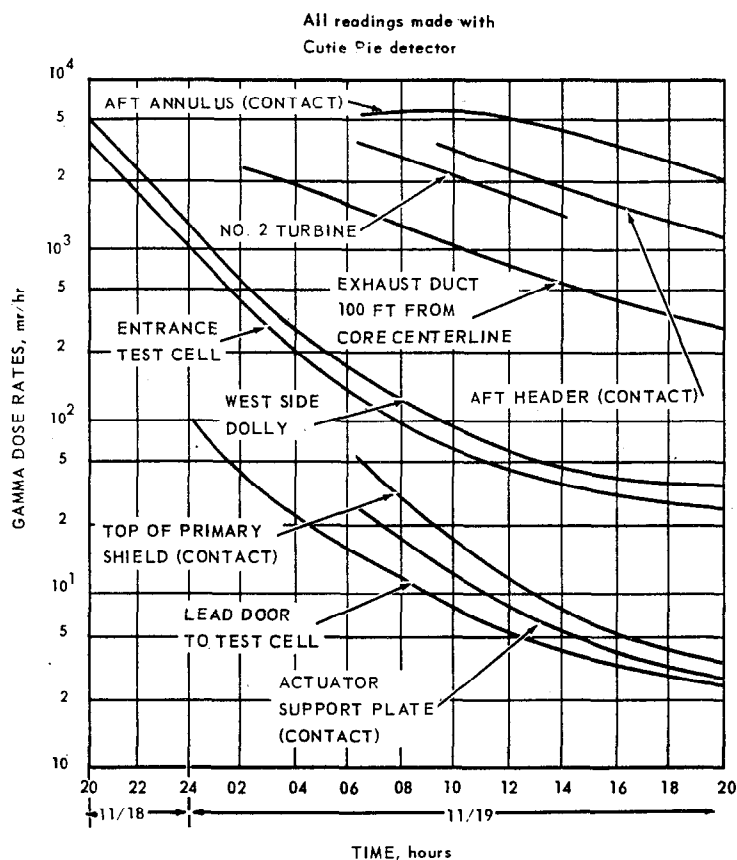


Fig. 45 - Radiation levels in test cell

### Stack Effluent Data

The IET stack monitor samples the stack effluent at the 80-foot level. The sample is collected on a moving filter-paper tape, which passes over a scintillator head and produces a record of the collected activity. The stack monitor ran continuously during operations at the IET and recorded the entire event.

The stack monitor had not been calibrated with the low airflow rates being used for the test in progress. If the air moved uniformly through the duct and stack, it should have taken 4 or 5 minutes for activity to reach the stack monitor. However, it is quite probable

UNCLASSIFIED

UNCLASSIFIED

that the relatively small quantity of hot air produced in the incident flowed in a layer at the top of the duct and hence reached the monitor in a shorter time. This non-uniform flow means that the calculated amounts of activity leaving the stack are subject to considerable error.

Approximately 1 minute after the event the stack monitor began to climb from background, reaching a maximum reading approximately 2 minutes later. Beginning at 2035 a 1-minute spot sample was drawn from the exhaust stream. The first count of this spot sample (at 2145) indicated that the activity of the sample was  $3.25 \times 10^{-4}$  curie (age 83 minutes). If a gross fission product decay scheme is assumed, this would correspond to  $1.93 \times 10^{-3}$  curie at 2035.5 or, by use of the appropriate correction, to a release rate of 3.9 curies per minute of activity in the total effluent. This release rate of 3.9 curies per minute was used to calibrate the stack monitor curve at 2035.5. With this calibration, the peak release rate was  $2.66 \times 10^3$  curies per minute (age approximately 1 minute) and the integrated total release indicated by the stack monitor curve was 400 curies (age 10 minutes).

A carbon trap, sampling from the 80-foot level of the stack, was turned on at 2050, 28 minutes after the peak of the release, and sampled until 2340.

The carbon trap was taken to the radiochemistry laboratory at ITS where the first 4 inches of carbon was thoroughly mixed. A sample of the carbon was gross counted and a gross spectrum recorded. Chemical separations were made on other aliquots and the specific activity determined for  $I^{131}$ ,  $I^{133}$ ,  $I^{135}$  and  $Sr^{91}$ .

The activity of a particular isotope observed in the trap was extrapolated to the total released out the stack by applying corrections for fraction sampled, sample line loss, collection efficiency, and the fraction of the event sampled by the carbon trap (as indicated by the stack-monitor trace).

Flow-rate measurements taken where the trap sampled and total flow calculations established the fraction of total effluent sampled.

A sample-line-loss correction factor of 1.56 for this particular sampling point had been established during previous testing and was assumed to be applicable in this case.

From previous measurements of iodine distribution down the length of a carbon-trap sampling under similar flow conditions, it has been established that a least 90 percent of the iodine is retained in the first 5 inches of carbon. In the present case 80 percent was assumed to be retained in the portion analyzed (slightly less than 5 inches).

Since the trap was not sampling during the peak release period but was turned on 28 minutes later, a method was needed to extrapolate the actual collected activity to that which would have been collected if the trap had sampled during the entire release. The method used was to correct the indicated trap activity upward by the ratio of the total integrated area under the release curve (as indicated by the stack-monitor trace) to the integrated area under the portion of the curve during which the carbon trap was sampling. Although several assumptions that may be open to question are implicit in this extrapolation, it seemed to be the best available technique. The area ratio was calculated to be

$$\frac{A_{\text{total}}}{A_{\text{sampled}}} = 1.56 \times 10^3$$

These calculations indicate the release (as of 0 time) of 0.16 curie of  $I^{131}$ , 3.2 curies of  $I^{133}$ , 27 curies of  $I^{135}$ , and 0.6 curie of  $Sr^{91}$ .

UNCLASSIFIED

UNCLASSIFIED

76

SECRET

Site Survey

Area surveys were performed from the IET exclusion fence to a desert road approximately 5.4 miles downwind from the IET stack. Primary data were obtained with a gamma scintillation counter mounted on the bed of a panel truck. Vegetation samples were collected from the area in which the scintillator readings were obtained, and chemical separations for specific isotopes were performed on these samples. The activity detected by the scintillator could thus be related to the activity per unit mass of the vegetation for that isotope. These techniques were applied to obtain fallout (plateout) data on three iodine isotopes and one strontium isotope. Figure 46 is a plot of I<sup>135</sup> concentration as of 2000 on November 18; the ratio of the other iodine and the strontium activities to the I<sup>135</sup> activity are included on the same page for ready reference. The isopleths of concentration are in units of microcuries per square meter, obtained by converting activity per unit mass to activity per unit area. For the dry, sparse, desert vegetation of the NRTS, this conversion constant has been determined to be 50 grams of vegetation per square meter. The I<sup>131</sup> activity on the vegetation exceeded a working limit of 3 x 10<sup>-3</sup> curie per square meter by a factor of 4 at a distance of 3 to 5 miles. At a distance of 1.5 miles, the point of maximum axial concentration, the beta-gamma dose rate at ground level measured 6 hours after the event was 0.08 milliroentgen per hour. The gross activity decreased a factor of 10.5 in a 48-hour period from 2000 on November 19 to 2000 on November 21. This decrease is more rapid than would be expected but it seems to be approximately what would be expected of the iodine isotope ratios determined for the vegetation samples.

An integration over the area covered by the isopleths of I<sup>135</sup> activity indicates that there was a total deposition of about 8 curies on the ground out to a distance of 5.4 miles.

The fraction of the amount emitted that would be deposited can be calculated from the relation\*

$$F_D = 1 - e^{-\frac{-2V_D}{u\pi^{1/2}} \int_0^x \frac{\exp\left(\frac{-h^2}{C_z^2 X^2 - n}\right) dx}{C_z X^{\frac{2-n}{2}}}}$$

where:

F<sub>D</sub> is fraction of the amount emitted that would be deposited

V<sub>D</sub> is deposition velocity

u is wind speed

h is effective stack height

n is stability parameter

C<sub>z</sub> is vertical diffusion coefficient

X is distance downwind

The weather at the time of the event is described as a weak lapse condition. The temperature difference from the 180-foot level to the 5-foot level was 0.7°F. Wind speed at the top of the stack was 4 meters per second. Diffusion parameters supplied by the U. S. Weather Bureau were: n = 0.25 C<sub>z</sub> = C<sub>v</sub> = 0.135.

\*Healy, J. W., "Calculations on Environmental Consequences of Reactor Accidents," General Electric Hanford Atomic Products Operation, HW-54128, December 11, 1957.

UNCLASSIFIED

SECRET

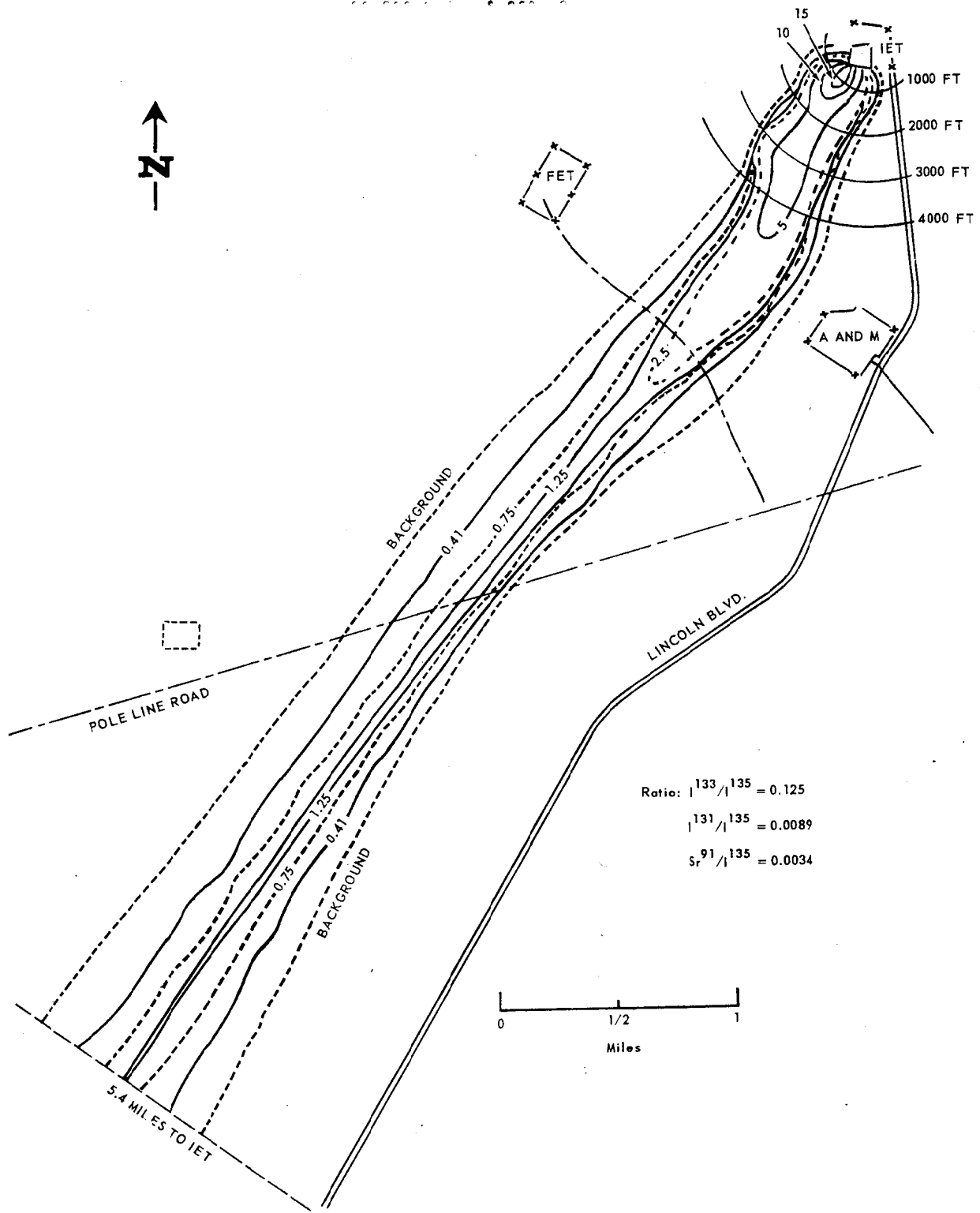


Fig. 46 - Isopleths of  $I^{135}$  activity at test site corrected to 2022



Using these data along with a value of 0.025 meter per second for  $V_D$  for halogens gives a value of  $F_D = 0.25$  for the iodine isotopes. The value of  $V_D$  for  $Sr^{91}$  was assumed to be less by a factor of 10 and the value of  $F_D$  would be about 0.025.

Core inventory calculations were made based on the following reactor history for November 18: from 1432 to 1512 (40 minutes), reactor power was 10 kilowatts; from 1535 to 1635 (60 minutes), 56.7 kilowatts; from 2021 to 2022 (1 minute), 10 megawatts.

A summary of the inventory and release data is given in Table 7.

TABLE 7  
EFFLUENT DATA

Core Inventory	Stack Release		Field	
	Curies	Fraction	Curies	Fraction
Gross (10 min) 4 x 10 <sup>5</sup> curies	400	0.001		
<sup>131</sup> I (0 minutes) 80	0.16	0.002	0.3	0.004
<sup>133</sup> I 480	3.2	0.0067	4	0.0083
<sup>135</sup> I 1100	27	0.025	30	0.027
<sup>91</sup> Sr 900	0.58	0.0006	0.1	0.001

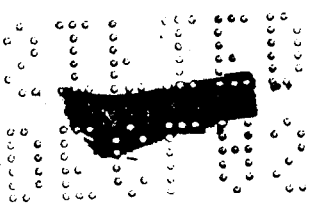
*from  
2022*

*122*

*042*

Cloud Gamma Dose Measurement

The remote area monitoring system mounted in the A and M area is the main source of information available on the dose rate experienced during the passage of the cloud. This ion chamber instrument was located 2960 feet from the centerline of the cloud and indicated a maximum dose rate of 0.04 milliroentgen per hour (net) during the passage of the cloud. A second instrument, located 3510 feet from the centerline of the cloud, indicated a maximum dose rate of 0.017 milliroentgen per hour (net). Working with infinite line source models and the knowledge that the dose rate falls off with distance at a rate approximately linear with distance (for very long sources based on measurements made on the exhaust duct at IET), an estimate can be made of what the cloud gamma dose would have been had an instrument been located at ground level beneath the cloud. The cloud gamma dose rate as estimated by this method was 12 milliroentgens per hour. The total integrated dose as measured by the Jordan chamber in the A and M area was 0.026 milliroentgen. The corresponding total integrated dose for the estimate made for the field would be 8 milliroentgens.



## 4. THEORETICAL ANALYSIS OF DATA

### 4.1 INTERPRETATION OF PERIOD AND FLUX RECORDS

The probable action of the control system is reconstructed here to give a plausible explanation for the traces from the linear-flux, log-flux, and period recorder. The account given by the operator is considered, along with the action and reaction of the control system components under conditions either postulated or known to have existed.

During the data run (run 15-4), the automatic control system was adjusted so that under normal conditions the reactor could be brought to 0.15 megawatt; thus 0.15 will be considered as full power (FP) in this discussion. Section 4.3 describes the channels that were operative and other conditions at the time of the event.

At the beginning of the test, the photoneutron level from the previous test run was sufficiently high to give an indication on the log-flux meters at the operator's console. Therefore, the source-range instrumentation was not used. The safety rods were withdrawn, and the reactor was put on automatic servo control in the intermediate range with the power-demand setting at the lowest level ( $10^{-6}$  FP). This occurrence is shown at about point (a) of the log-flux curve in Figure 47. At this time, the demanded flux was greater than the indicated flux and the error signal initiated dynamic-rod withdrawal. When the dynamic rods were withdrawn 5 inches from their midposition, shim-rod withdrawal was initiated. The shim frames withdraw in sequence, and as the actuating frame reached about halfway withdrawn it was bypassed by operator manual action and the next frame was withdrawn until it reached its midposition. This procedure was followed until the indicated flux equalled the demand as shown at point (b) in Figure 47. The flux then appeared to level and the period rose toward infinity. It is probable that the reactor was not yet critical. At point (c) the servo demand was advanced to  $10^{-1}$  or  $1.5 \times 10^{-1}$ . The servo demand rate had been previously set at a 25-second period and remained at that setting. This meant that under normal conditions the servo demand would be driven at a rate that would increase reactor power on a constant period of 25 seconds from  $10^{-6}$  to  $10^{-1}$  full power. Full withdrawal of the dynamic rods was initiated, and the shim rods again began to withdraw. At point (d) all shim frames were withdrawn about halfway and bypassed except frame A, which cannot be bypassed; it began to withdraw. The demand servo continued to drive at a constant rate and was demanding a 25-second period. At point (e') frame A was fully withdrawn and frame F was removed from bypass. The constant indicated period between points (d) and (e) is difficult to explain and may be associated with the fact that there were only two rods on frame A and that the reactor was not yet critical. The value of frame A may have been just sufficient to keep the flux on an exponential rise and thus a constant period. At point (e) the reactor passed through critical and frame A was able to begin to decrease the period. The length of time from (d) to (e') corresponds to the time required to withdraw one frame fully. The sharp change in the period between (e') and (f) is attributed to the shift from frame A to the more valuable frame E. A large error had built up in the servo

loop. This error allowed the shim rods to continue to withdraw, causing the period to become shorter with time until the period interlock and override safety responses actuated. This occurred at point (f).

In the D102A control system the override response causes the servo demand to be driven down and all shim rods to begin to be inserted. This condition exists until the safety response is cleared, at which time the power is held constant at the lower demand setting. During the event, the override existed for a second or two and cleared, as shown at point (g) in Figure 47. The reactor power and the servo demand were then equal and flux level was held at 0.13 percent FP. The period increased toward infinity. At point (h), Figure 47, the operator cleared the interlock and the demand servo began to drive again, demanding a 25-second period. The control system permitted the power to increase at the demanded rate. Sufficient shim worth was withdrawn to maintain the required period, and the dynamic rods returned to their midposition.

At 4 percent FP in the intermediate range, point (i) in Figures 47 and 48, the control was transferred to the power-range control, which demanded 10 percent FP. This put a step demand into the system from 4 to 10 percent FP. At the time of transfer the reactor was on a 20-second period with the dynamic rods in midposition. This step demand caused the dynamic rods to move out resulting in a sudden increase in reactor power, which produced an 8-second period indication.

The 8-second period caused an interlock and override safety response, point (j) in Figures 47 and 48, causing all shim rods to drive in simultaneously for about 1 second. The control system leveled power at 10 percent FP, and the period increased to 90 seconds.

The operator cleared the interlock and advanced the power-range-demand servo to 80 percent FP, point (k). The dynamic rods withdrew fully to satisfy the demand, and the power level began to increase. An interlock safety response was initiated, point (l). This stopped the demand potentiometer from driving and allowed the flux to approach the demand, which reduced the error and caused the dynamic rods to start in. Interlock is self-clearing when the affected parameter is satisfied; therefore, when the period increased sufficiently (above 10 seconds), the interlock cleared and the demand began to drive again.

At 20 percent FP and above, the log-flux-sensor circuitry becomes linear and later saturates, and therefore is not reliable at the higher powers. It was not designed to be operated above 10 percent FF. It is supposed that from points (m) to (n), Figure 47, the log-flux circuitry became linear. At point (m) it saturated and therefore did not respond to rate of change of flux. The period consequently increased. (An explanation of saturation of the log flux circuitry is given in Section 4.3.)

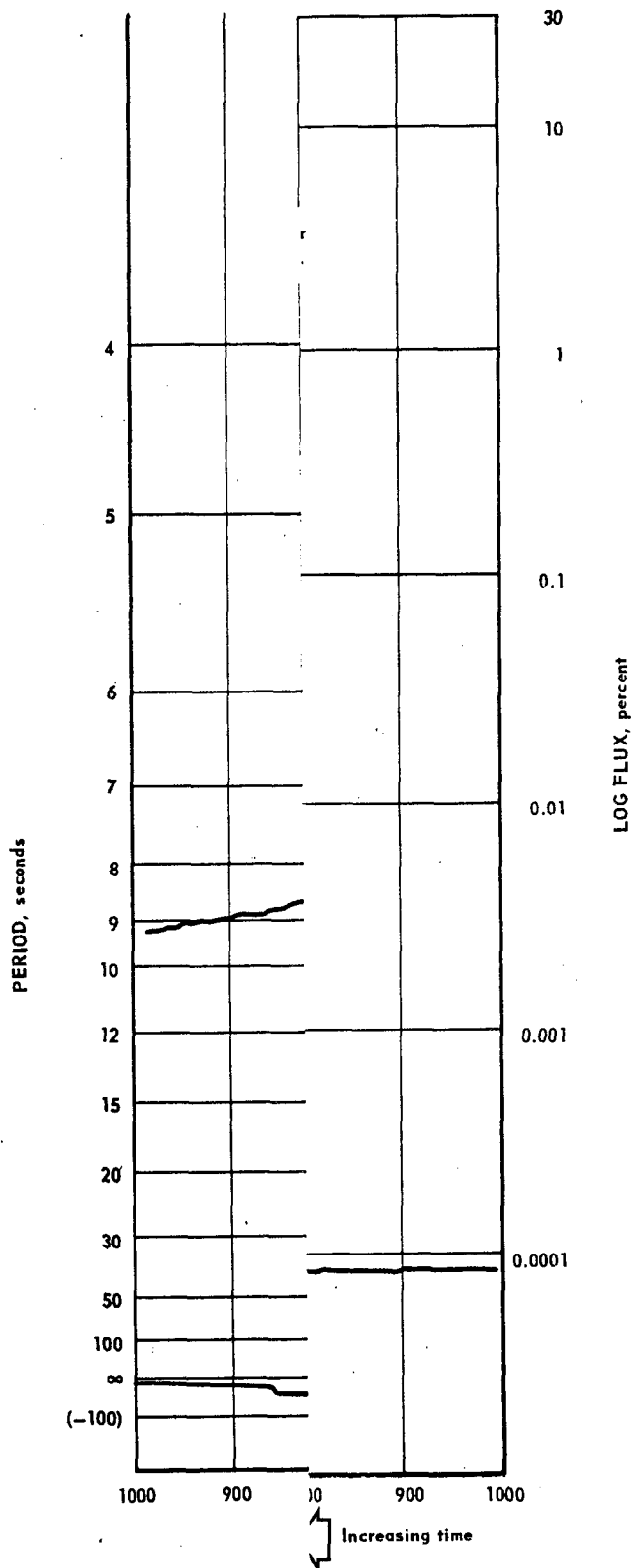
It appears that flux followed the demand from point (l) to about point (p) without deviation. The demand servo was calling for power increase on a ramp function, which would increase the reactor power at a linear rate from 10 to 100 percent in 40 seconds. This increase requires an average or equivalent period of 20 seconds, and the label on the control console is printed "20." At about point (p) the uncompensated chamber current became limited by the large filter resistor and the circuit no longer put out a current proportional to flux. An error began to build up in the servo loop, which called for an increased amount of rod withdrawal. Because of circuit limitation the demand could not be satisfied, and rods were withdrawn until another safety parameter caused a scram.

At point (q), Figure 48, the true reactor flux had gone so high that other phenomena occurred. Because of a high gamma flux, a shorting current began to flow between the

UNCLASSIFIED

24030  
00000

UNCLASSIFIED



00000  
00000

UNCLASSIFIED

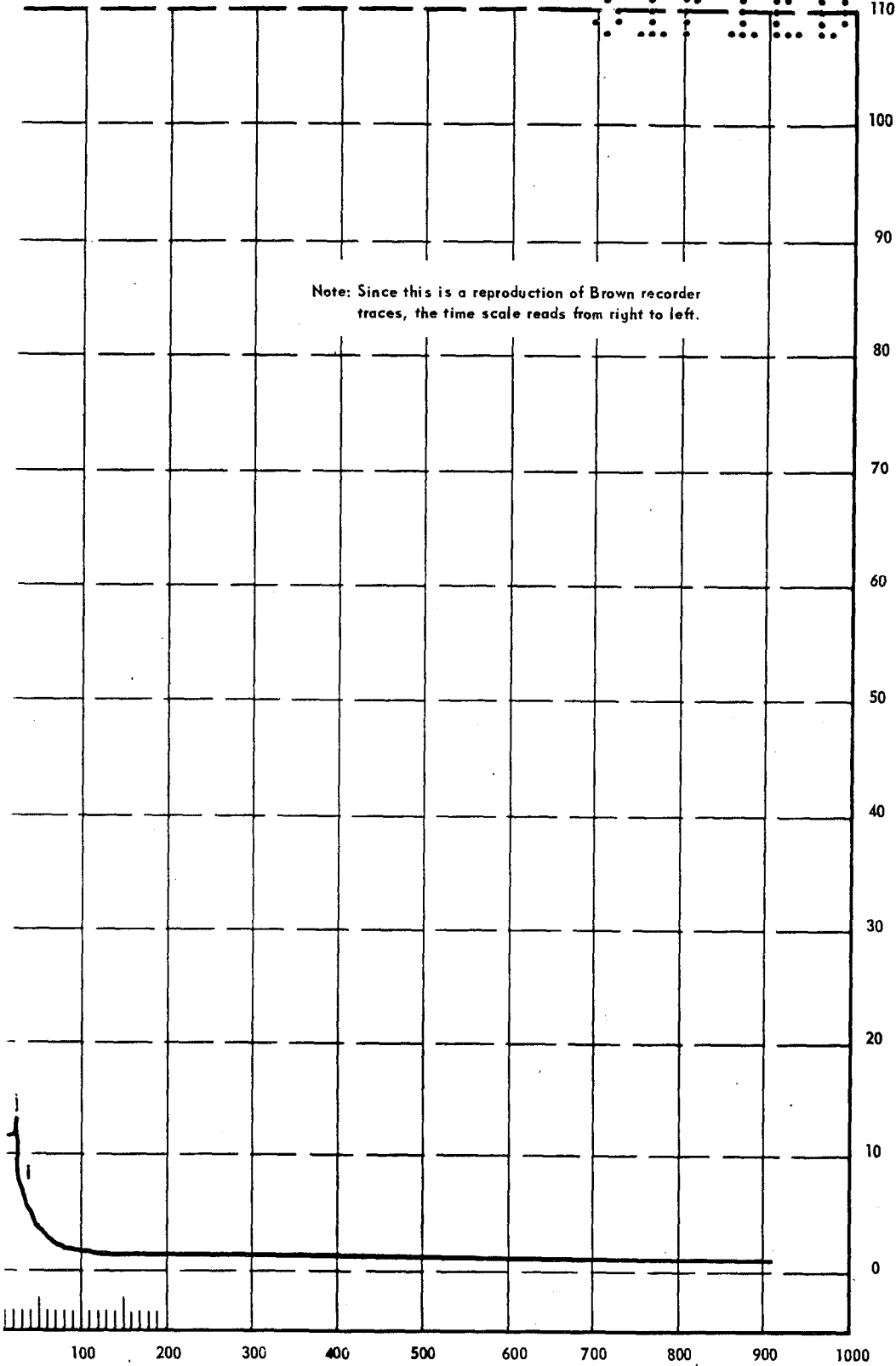


UNCLASSIFIED

020105

UNCLASSIFIED

020105



LINEAR FLUX, percent

conds

Increasing time

ar-flux trace

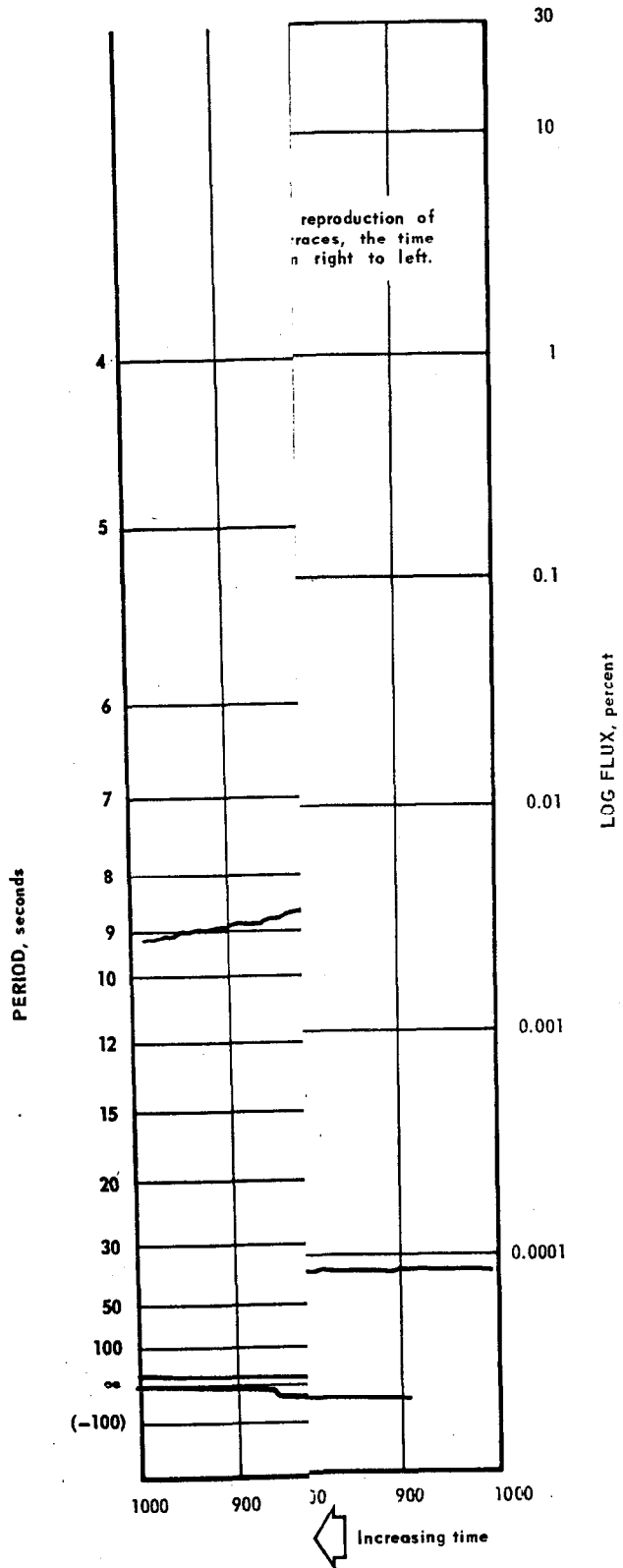
RET

UNCLASSIFIED

020105  
020105

UNCLASSIFIED

02101  
03102



02101  
03102

UNCLASSIFIED

UNCLASSIFIED

SECRET

high-voltage electrode and the case and caused a decrease in the signal current. Therefore only that amount of current remaining produced the chart record. (Points (q) to (r), Figure 48.)

At or near point (r), the reactor scrammed. This action reduced the gamma flux, and consequently the shorting current began to reduce. The result was more and more signal current. This current increase continued until point (s), at which it appears that the effect of any gamma current to ground is insignificant. The chamber may still have been saturated because of low voltage. At point (t), however, saturation probably terminated and the recorder traced true flux from then on.

Near point (r) the log-flux trace appears to start downward. This could have been caused by the compensated ion chamber circuits becoming saturated. At a particular point in the saturation process it is possible for the current in the compensated-ion-chamber circuit to drop to zero or even become negative. This type of action caused the rapid up and down traces along the log-flux chart and consequently the period chart, since they derive their signal from the same circuit. For ease of comparison, the log-flux, period, and linear-flux traces are presented compositely in Figure 49.

After the incident the automatic control system was given a static test and appeared to be functioning as designed. This test did not include the nuclear sensors, associated power supplies, filters, or other circuit components. The accuracy of the control system depends on correct signal information from the nuclear sensor circuits. Since the nuclear sensor signal saturated before the demanded power level was reached, the control system received a signal demanding power-level increase until safety action was initiated.

#### 4.2 ANALYTICAL VERIFICATION

Calculations have been performed to verify the measured total energy release and the postulated mechanism of the power excursion. Although independent, bracketing calculations can be easily made, much iteration would be required to produce an exactly self-consistent reconstruction of events. For example, it is possible to calculate ring by ring the temperatures to which the fuel elements would be raised for a given postulated power input if the assumption is made that no heat is removed by the small amount of cooling air present. Although not exact, the latter is a good engineering assumption. On the other hand an existing machine program can calculate the effect of the amount of air flowing through the reactor, using characteristics of an average fuel ring. These calculations show that although the effect of airflow is not of great significance during the excursion, it is needed to explain the appearance of the latter stages of the reactor. The calculations show that the stages were heated by continuing transfer of heat after the reactor power transient was over. Synthesizing these two calculations to produce a ring-by-ring peak temperature would be extremely complicated. Another example of the iterative nature of the calculations is seen in analysis of the mechanism of reactor shutdown. It is almost certain that the reactor shutdown was caused by a scram that was initiated by high fuel element temperature.

Analysis shows that the 19th stage reached temperatures corresponding to the scram settings at about the same time that melting started in the interior stages. However, there is reason to suspect some lag between the response of the thermocouple and the temperature of the fuel sheet caused by the unusual construction of these thermocouple junctions, which were not attached to the fuel sheet. Some anomalous behavior, such as melting of the thermocouple wires and the formation of new junctions in the molten mass, must be assumed to explain the high temperature indications reported by the witnesses. It is

UNCLASSIFIED

SECRET

impossible to state conclusively whether the scram was produced by the junction temperature or the formation of new thermocouples or both, and it is difficult to state whether and at what rate a loss of reactivity was introduced, prior to scram, by collapse of fuel rings. Therefore, although the time of scram can be placed within a period of 2 or 3 seconds, any finer analysis does not appear practical. Because the total energy release obtained from the transient calculation is somewhat sensitive to the time of scram, the reconstruction of all the parameters of the incident cannot be precise beyond a certain point.

A series of independent calculations has been performed on the basis of different assumptions to assure the investigators that these assumptions are reasonable rather than that they are exact. The resulting analyses are presented without attempts at synthesis beyond the point of engineering assurance of consistency. Enough work has been done to verify that the measured total energy release is probably accurate within 20 percent (on the high side) and that the power excursion curves represent a good estimate of true events.

#### THERMODYNAMIC CORRELATIONS

##### Energy Release During Excursion: Appearance of Fuel

Figures 76 through 95 in section 5 show the appearance of the cartridges in cells 510 and 273. These cartridges are representative of some of the least damaged and most damaged cells in the reactor. Critical experiment data indicate that all the cells in the reactor produce equal power within  $\pm 7$  percent. These two cartridges, representing maximum and minimum power regions, can be taken as typical of the extremes. The photographs, confirmed by close inspection of the cartridges, indicate that stage 3 did not get hot enough to melt any ring completely and that stage 4 melted at least partly from nuclear heat. It is possible that oxidation of the 80 Ni - 20 Cr furnished enough heat to complete the melting.

The total reactor energy release that would produce enough heat in ring 12 of stage 4 to raise its temperature to the melting point and then melt it was calculated to be 540 megawatt-seconds.

##### Energy Produced During Excursion: Moderator Heat Sensors

The total energy produced by the reactor during the power excursion may be obtained by comparing the temperature increases of the slugs inside the sensors during the power excursion to the temperature increases during some time interval of the previous run.

During the previous run (run 15-2) when reactor power was at about 0.060 megawatt, the hydrided zirconium slugs in the heat sensor in control rod hole 520 showed a temperature increase of about 0.030 degree per second during the first part of the run when heat losses from the slugs were small (see Figure 50). The sensor therefore measures reactor energy at the rate of 2.0 megawatt-seconds per  $^{\circ}\text{F}$  when losses are low. Extrapolation of data shows that during the power excursion, this same slug was heated from about  $130^{\circ}\text{F}$  to at least  $380^{\circ}\text{F}$ , a difference of  $250^{\circ}\text{F}$ . The energy released during the power excursion was, therefore, at least 2.0 megawatt-seconds per  $^{\circ}\text{F} \times 250^{\circ}$ , or 500 megawatt-seconds.

For this calculation the temperature of the slug before the excursion was assumed to be the same as the inlet air temperature, which was measured 6 minutes after shutdown and found to be about  $130^{\circ}\text{F}$ . However, the inlet air temperature during previous runs at the same flow rate was about  $80^{\circ}\text{F}$ . If this temperature were applied to the calculation, the energy release determined would be at least 600 megawatt-seconds. Therefore,

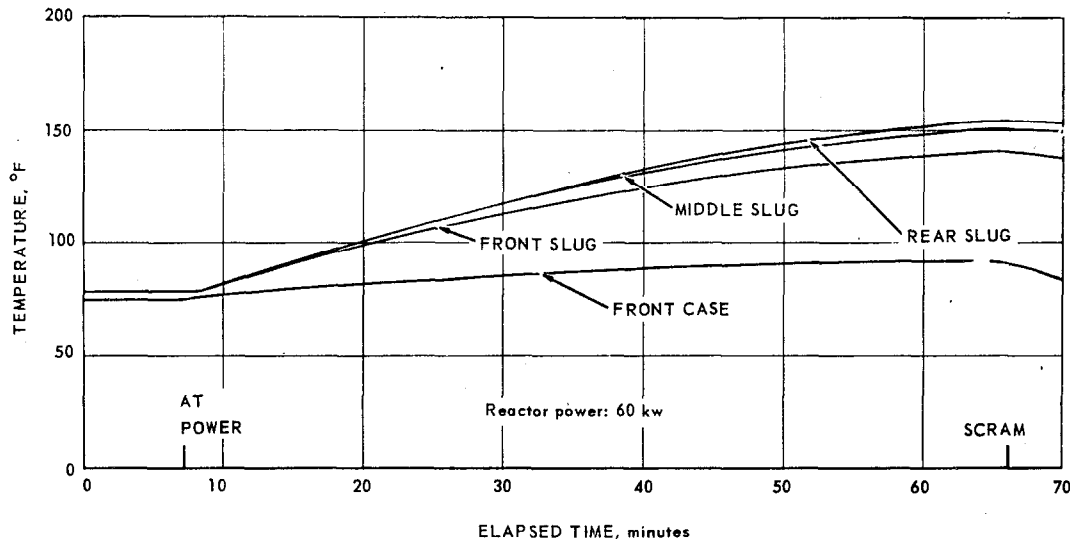


Fig. 50 - Hydrided zirconium heat sensor temperatures, control rod hole 520, run 15-2

this method showed reactor energy release to be at least 500 or 600 megawatt-seconds. This calculation agrees well with the 540 megawatt-seconds calculated from the appearance of the fuel, and also fairly well with the 765 megawatt-seconds obtained by indium foil exposure during the excursion.

The local moderator heating rates determined from the temperature increase of the heat sensor slugs in run 15-2 were higher than predicted by a factor of about 2. Such high values of moderator heating rates are found to be impossible if compared with predictions of total gamma radiation and neutrons available to heat the whole core. That is, the fission process produces a certain amount of gamma radiation energy, which is predicted to be absorbed in the fuel elements, moderator, reflector, control rods, shield, and structure, and also partly lost to the surroundings. If the moderator is assumed to absorb all of this energy, an unlikely situation, the heating rates produced in the moderator would still be less than those heating rates determined from the heat sensors. Since the heating rates determined are believed to be impossible, the value of reactor power used in the calculation was suspected of error. However, this reactor power was determined by two independent methods, exposure of an indium foil in the reactor and measurement of the temperature increase and flow rate of the core cooling air. The results of the two methods agree that the reactor power was about 60 kilowatts. The value of airflow used for the heat balance is questionable. To date an accurate determination of this airflow has not been made.

However, the discrepancy between the indicated moderator heating rate and the heating rate that seems plausible on the basis of energy available in the fission process remains an anomaly which to date has not been explained. It seems almost impossible that the power determinations could have been in error by a factor of 2. The strongest argument to support this statement is the close correlation of the appearance of stages 3 and 4 to the estimated energy release as mentioned in the first paragraph of this section.

### Core Temperatures

Temperatures of fuel elements and moderator at various times during and after the power excursion were computed using the Core Transient Temperature Program for the IBM 704 computer. This program allows for heat exchange between the fuel cartridge and the moderator due to convection and conduction. Since the program does not cover this kind of excursion, the following comments apply to the program as used in this special case. The loss of heat transfer surface suffered by the center stages of the fuel elements when they melted together into a mass was considered and corrected for. Values for heat generation of the rear end of the fuel tubes were increased 25 percent above critical experiment values to include the extrapolated effect on power distribution of the presence of the rear plug. The heat of fusion of fuel elements was applied where applicable. As a result the maximum temperatures of fuel elements are less than those actually computed by the Core Transient Temperature Program, which neglects the fact that heat is used in melting the 80 Ni - 20 Cr. Since the fuel elements are not as hot as the program computes, the transfer of heat through the insulation to the moderator would be less than computed. The moderator temperature was therefore corrected downward. Any heat added to the core from oxidation of the 80 Ni - 20 Cr was not included.

The results of this calculation are shown in Figure 51. The temperatures shown agree very well with reports of the physical damage and appearance of the core. They also agree with the temperatures observed during the event and those recorded 4 minutes after shutdown. The calculations show complete melting of fuel elements near the center of the core longitudinally, partial melting of fuel elements at the rear end of the core, and no melting at the front end. The longitudinal hottest portion of the inner moderator hexagons, about three-quarters of the distance from front to rear of the core, was calculated to reach 1200°F after 3 minutes and then to cool slowly. This calculation agrees qualita-

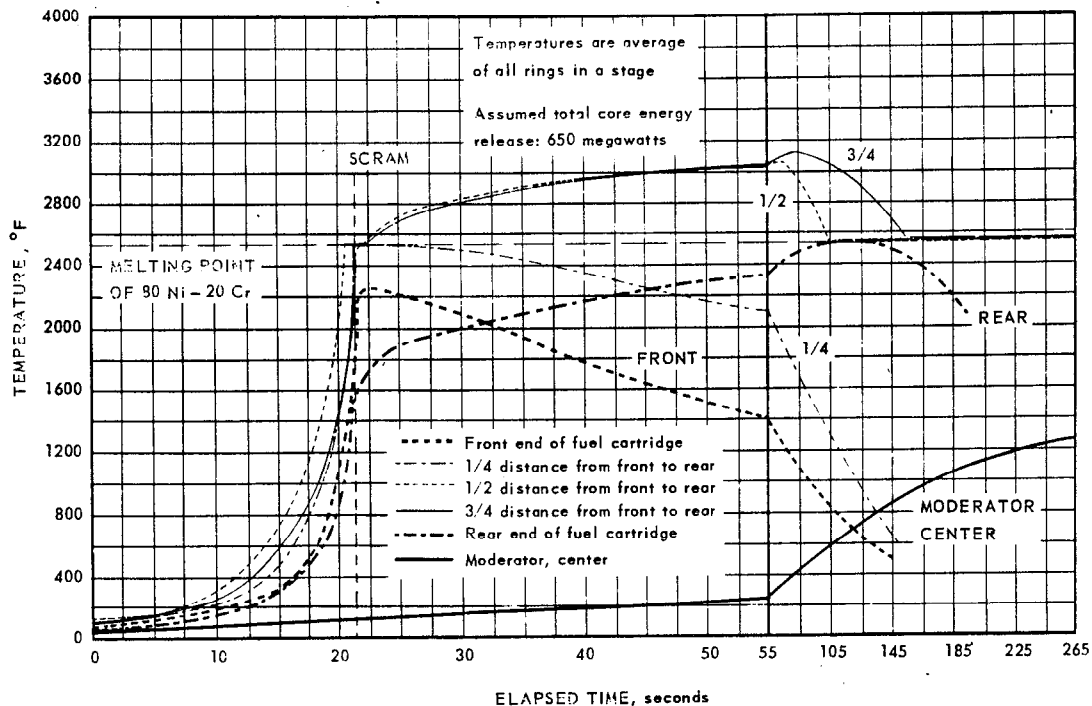


Fig. 51 - Calculated core temperatures caused by power excursion

tively with observed temperatures. The transient power generation function used is depicted in Figure 59. The total energy resulting from that calculation was 650 megawatt-seconds.

#### Heat Added By Combustion of 80 Ni - 20 Cr

Calculations indicate that 5 megawatts of additional power is available if all the oxygen in the cooling air is used in the oxidation of 80 Ni - 20 Cr. This maximum consumption rate of material corresponds to 1.3 stages per minute or 45 seconds per stage. Analysis of the slag recovered from a typical cartridge was made for nickel oxide and chromium oxide and is reported in section 5.3. The results of this analysis can be used to make an estimate bracketing the amount of heat produced due to oxidation of the fuel stages. Inspection of the photographs of the fuel cartridges shows that roughly eight stages downstream of stage 5 were melted or badly distorted. If it is assumed that the oxide from the samples taken from the mixed slag is typical of all eight stages and this amount is added to the values reported for stages 4 and 5 in section 5.3, the value obtained for the total energy release due to oxidation is about 470 megawatt-seconds. On the other hand, the decreasing amount of oxide between stages 4 and 5 and the remaining samples, as indicated in Table 8 and as confirmed by the visual appearance of the cartridges, indicates that the oxidation rate fell off rapidly beyond stage 5 consistent with the possibility that most of the oxygen in the air was consumed prior to that point. If, for instance, it is assumed that effectively only two stages contributed to oxidation beyond stage 5, the total energy released by oxidation is 230 megawatt-seconds. The estimate of 5 megawatts equivalent of oxygen available in the air shows that either of these two estimates is consistent; it is difficult to fix the total time available for oxidation, although it appears to have been of the order of 1 or 2 minutes.

#### Calculated Temperatures of Fuel Element Stages 3 and 4

For each fuel ring of stages 3 and 4 in an average tube, the calculated temperatures that would be produced by the HTRE No. 3 power excursion are given in Table 8 for total reactor energy releases of 650 and 750 megawatt-seconds. It is assumed that convection and radiation of heat are insignificant for the short time period involved.

TABLE 8  
CALCULATED RING TEMPERATURES AT STAGES 3 AND 4<sup>a</sup>

Ring No.	650 Megawatt-Seconds		750 Megawatt-Seconds	
	Stage 3	Stage 4	Stage 3	Stage 4
1	1560°F	1720°F	1790°F	1990°F
2	1810°F	2010°F	2080°F	2310°F
3	2120°F	2340°F	2430°F	18%
4	2340°F	5%	17%	50%
5	1%	33%	46%	84%
6	33%	69%	83%	2770°F
7	37%	73%	87%	2810°F
8	40%	77%	90%	2840°F
9	52%	87%	2570°F	2950°F
10	71%	2620°F	2760°F	3160°F
11	44%	80%	96%	2880°F
12	94%	2880°F	3020°F	2460°F

<sup>a</sup>Temperatures below 2550°F are for those rings that did not reach melting point. Percentages are those of total heat of fusion for partially melted rings. Temperatures above 2550°F are those reached by molten material assuming the same rate of heat addition as for whole rings. Vaporization temperature of 80 Ni - 20 Cr is 5000°F.

The temperatures and melting calculated for the 650 megawatt-second energy release appear to fit the observed condition of the fuel cartridges after the power excursion if it is assumed that no rings of stage 3 collapsed because none reached 100 percent melting and that the high temperatures reached by rings 10 and 12 contributed to and perhaps caused combustion to contribute to the collapse of the adjacent four or five rings in stage 4.

#### Shutdown Mechanism

Figure 51 summarizes most of the available information on which to base conclusions regarding the mechanism of shutdown of the excursion. It should be remembered that the calculation portrayed in this figure is based on the total power in a stage and the total heat capacity. It therefore represents the behavior of an average ring more nearly than that of a high-power ring. The average ring is ring 9, and the 12th ring, which is the highest power density ring, produces about 30 percent more heat per mass of ring than the average ring. At the assumed time of scram the average ring in the rear of the reactor had reached about 1600°F. This seems to be enough to assure that the outside ring, on which the scram thermocouples were mounted, had reached temperatures well above the scram settings. However, the unusual construction of this thermocouple, which is not attached directly to the fuel sheet, being shielded from the airstream with a small cap, makes it likely that the junction temperature can lag the plate temperature by several hundred degrees in a transient of this sort. Also, at the initiation of scram the central regions of the reactor had already started to melt. Figure 51 shows that the melting time for the average ring was about 2 seconds in the very center of the reactor. Since the witnesses reported that temperatures of 3000°F were indicated by the temperature instrumentation in the control room, it is possible that these temperatures were produced by melting of the thermocouple lead wires and the formation of new junctions in the central regions of the reactor, especially since the calculation shows that the rear of the reactor did not reach this temperature. Depending on the configuration of the melting it is possible that these junctions could have formed very near the time of scram. Therefore, it seems impossible to say whether the scram signal was produced by the actual thermocouple junction or by open circuit indications or by the formation of new thermocouples in the center of the reactor. In addition, the figure shows that at or very near the time of scram, collapse of the fuel elements had started. The total amount of reactivity reduction produced by this collapse was 2.13 percent. This is slightly greater than that carried in the scram rods. Therefore, it appears that collapse of fuel rings contributed substantially to the shutdown mechanism, although the 2.13 percent produced in this manner could not have been introduced instantaneously. The actual rate of introduction of this loss of reactivity is indeterminate, and the total energy released is sensitive to the rate of introduction of negative reactivity.

Regardless of the precision of the numbers it appears reasonable to conclude that the excursion proceeded about as indicated in Figure 51. The strongest evidence that supports the total energy release is the appearance of the fuel cartridges confirmed by the calculation reported in the first paragraph of this section and summarized in Table 8. The single discrepancy lies in the fact that the moderator heat sensor data, although consistent from run to run, indicates much too large a fraction of total energy deposited in the moderator. This indication remains an anomaly at the time of this writing, although it will be the subject of further investigation.

#### ANALYTICAL RECONSTRUCTION OF TRUE POWER

The reconstruction of the reactor power history from the time of loss of control to the time power decayed to essentially zero following the scram is given in two parts. The first is a discussion of analog computer results. The computer was programmed to sim-



ulate the rod-servo control system characteristics, which were determined from measurements made before the excursion. With this simulation rod positions were calculated as a function of time during the excursion using the well-known power-demand variations and the flux-sensor nonlinearities. The calculated rod position variation with time determined the excess reactivity time dependence. Rod motions calculated in this manner were supplied as input to a digital computer program for a more exact power calculation.

Performing the calculation in this way allows use of the best features of both computers: control response simulation on the analog, and wide power-range capability of the digital machine.

The accuracy of both of the calculations after the instant of scram is less than that of the data describing the rise in power. Both methods treat the core as a unit; neither method accounts for the variation in the normal modes associated with the delayed neutron groups after the scram. These variations can affect the response of a detector at a certain point by  $\pm 50$  percent, depending on the location. This may account in part for the mismatch between computed power and linear-flux trace after the scram. These two investigations considered together yield the following conclusions:

1. The analytical reconstruction gives a power history consistent with thermodynamic and integrated flux data obtained at the time of the excursion and with the flux sensor signals. Further precision was not attempted in view of the uncertainties of knowledge of flux, temperature, time, and rod motion.
2. The mechanism that initiated the safety rod insertion was a temperature trip caused either by air or plate temperature or by thermocouple failure (more probably the latter).
3. If the safety rods had not been tripped by temperature signals, the reactor would have shut down by fuel collapse or removal, but this would have resulted in a significantly higher energy release. One of the more difficult assumptions to evaluate is that of the rate of reactivity reduction by fuel element collapse. Rather than conduct detailed analyses of rate of collapse (which must then be iterated with instantaneous power level) various rates were assumed to evaluate the sensitivity of the excursion to this parameter.
4. Inability of the sensor channels to respond in a linear manner to the reactor power was the only control system malfunction contributing to the loss of control and resulting damage.

The calculations supporting these conclusions are detailed in the following paragraphs.

#### ANALOG COMPUTER SIMULATION OF HTRE NO. 3 POWER EXCURSION

##### Reactor Kinetics

The method used to simulate the reactor kinetics represented the six delayed neutron groups; it was arranged on the computer so that the simulation could be operated over several decades of reactor power. This method also included the moderator temperature coefficient of reactivity.

##### Power-Range Control

The reactor power-range control, shown in Figure 52, was represented by a complete nonlinear simulation including velocity and rod position limits, reactivity nonlinearities in the dynamic and shim rods, and the variable gain integrator in the forward loop.

The ion-chamber feedback was estimated to saturate in the manner shown in Figure 53. These data were obtained through extrapolation of previously derived curves in combination with ion-chamber power supply and sensing circuit load characteristics.

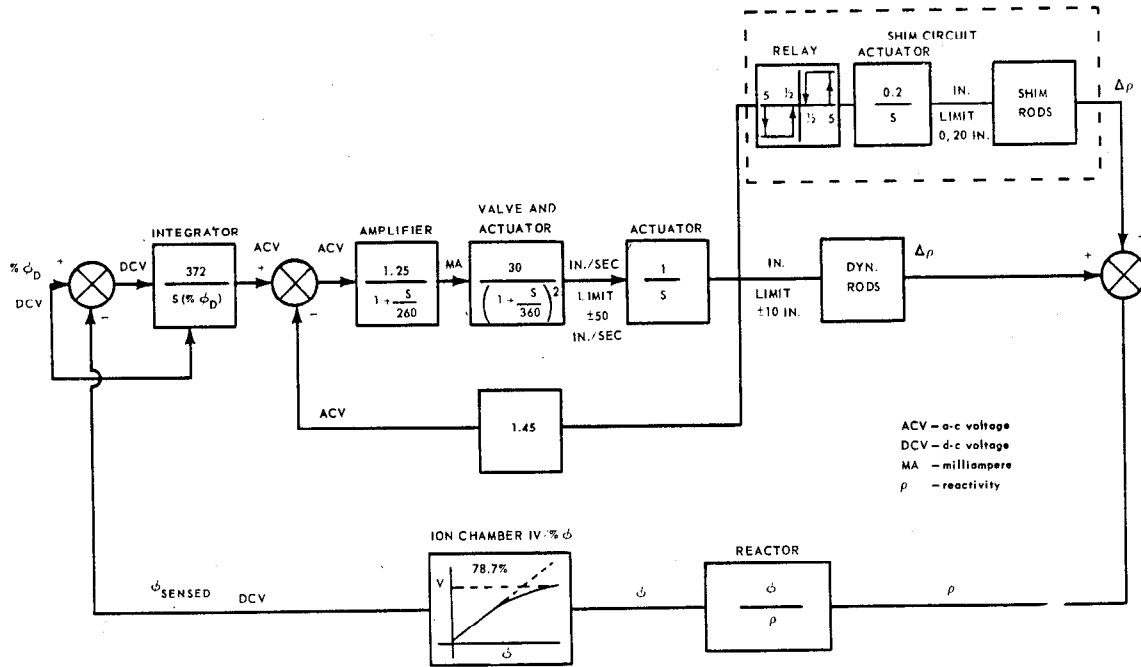


Fig. 52 - Reactor power-range control circuitry

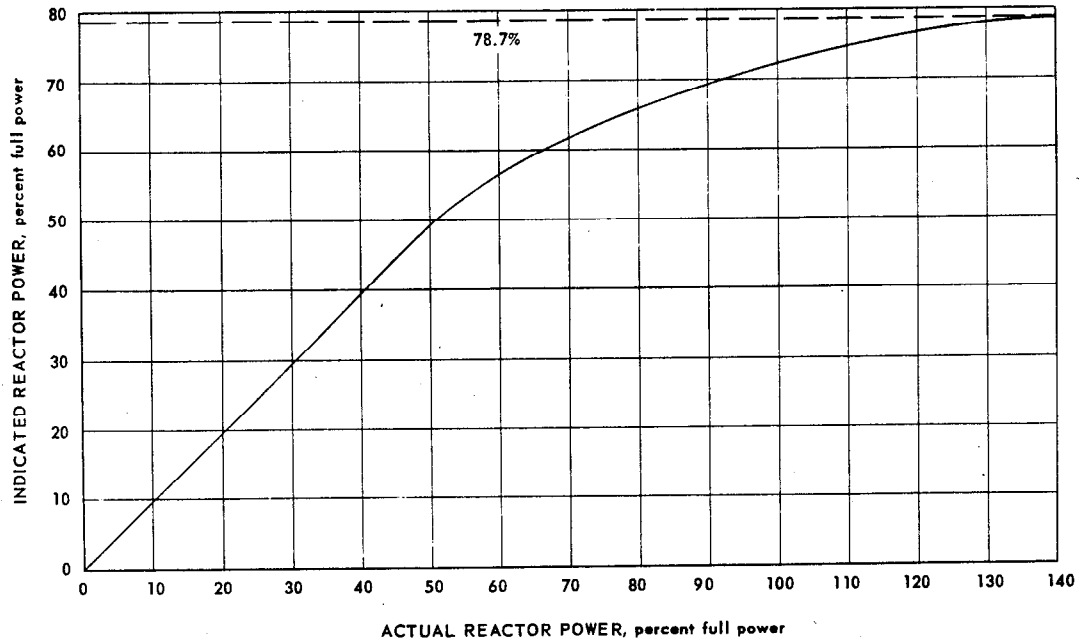


Fig. 53 - Calculated ion chamber saturation

UNCLASSIFIED

~~SECRET~~

### Basic Assumptions

The computer analysis started at the point at which the reactor was transferred from intermediate-range control to power-range control.

The following assumptions were made regarding the condition of the reactor and the control system at this point:

1. The reactor was on a 22.5-second period. This value was scaled from the log power trace.
2. The reactor had been on a 22.5-second period long enough that shim rod motion had caused the dynamic rods to be driven to the point at which the shim relay would drop out. The dynamic rods were either 9.5 inches inserted or 10.5 inches inserted.
3. All shim frames except A and F were half inserted; frame A was entirely withdrawn; frame F was located so that the net reactivity at transfer was 0.198 percent (22.5-second period). The total net positive reactivity available was 0.53 percent.
4. The movable reactivity in dynamic rods was 0.44 percent and that in frame F was 0.817 percent.

The total measured integrated power was 760 or 765 megawatt-seconds. In this study the integrated power was taken as 760 megawatt-seconds; the fuel element collapse was started at various integrated power levels to obtain a "right" total integrated power.

The shutdown mechanism was assumed to be as follows:

1. Fuel elements melted and collapsed, inserting 2 percent negative reactivity in 16-2/3 to 33-1/3 seconds at a rate linear with time.
2. Thermocouple leads were broken or melted by molten fuel a short while after fuel collapse started, but at such a time that the power had not yet started to decrease. This point occurs 0.4 to 3.0 seconds after the start of fuel collapse, depending on the collapse rate.
3. Melting of thermocouple leads caused a scram of 1.7 percent negative reactivity in 380 milliseconds, inserted at a linear rate.

### Procedure

The program of operation of the simulation was as follows:

1. Step the power demand from 6.6 kilowatts (4% full power) to 16.5 kilowatts (10% full power). Hold this demand constant for 21.7 seconds.
2. At 21.7 seconds increase the power demand at the rate of 2.25 percent per second (10% full power to 100% full power in 40 seconds).
3. At 24.9 percent demand power, hold demand constant for 5 seconds, then resume until 100 percent full power (165 kilowatts) is reached. This simulates the period interlock.
4. At an undetermined integrated power, start the fuel element collapse, inserting -2 percent reactivity in 16-2/3, 20, 25, 30, or 33-1/3 seconds.
5. When the power approaches its maximum value, scram with 1.7 percent reactivity in 380 milliseconds.
6. Measure the integrated power at 1 minute after scram.
7. Repeat 4, 5, and 6 until 760 megawatt-seconds is obtained for integrated power at 1 minute after scram for each of the fuel element collapse rates.

### Results

The results obtained are shown in Figures 54 through 56. Figure 54 shows peak reactor power, total time to scram, integrated power at start of collapse, and time from start of collapse to scram as a function of the estimated time for collapse of the fuel elements.

UNCLASSIFIED

~~SECRET~~

Explanation of Computer Traces  
(Figures 55 and 56):

1. First two decades (6.6 kw to 100 kw)

On the simulator it was not possible to obtain the transient overshoot that was indicated at transfer to power-range control on both the linear power trace and the log power trace. To obtain the desired power overshoot, it was necessary to place the dynamic rods inserted 15 inches at the time of transfer to power-range control. This condition conflicts with the second assumption concerning position of the dynamic rods.

In the attempt to duplicate the power overshoot it was noted that, regardless of the dynamic rod position at the time of transfer, the same time was required to reach 100 kilowatts. This indicates that the control system, although receiving the wrong feedback signal from the linear-flux channel, was still holding the reactor under some measure of control at 100 kilowatts (60.6% full power).

2. Third decade (100 kilowatts to 1 megawatt)

In this decade the difference in dynamic rod position at transfer begins to have its effect, since the amount of dynamic rod that was initially inserted determines the amount that may quickly be removed when the flux feedback saturates completely.

3. Fourth and fifth decade (1 megawatt to 100 megawatts)

In this double decade, power increases while frame F is continually being withdrawn; the moderator temperature coefficient of reactivity also begins to have some effect here.

4. Sixth decade (100 megawatts and up)

Scram occurs here. It was found that a slight difference in the integrated power level at which collapse was initiated made a very great difference in the total integrated power. Thus for a given assumed rate of fuel collapse the integrated power that initiates collapse may be determined closely.

The total time to scram was slightly (0.3 second) longer for the dynamic rod insertion of 9.5 inches at transfer than it was for the 10.5-inch insertion.

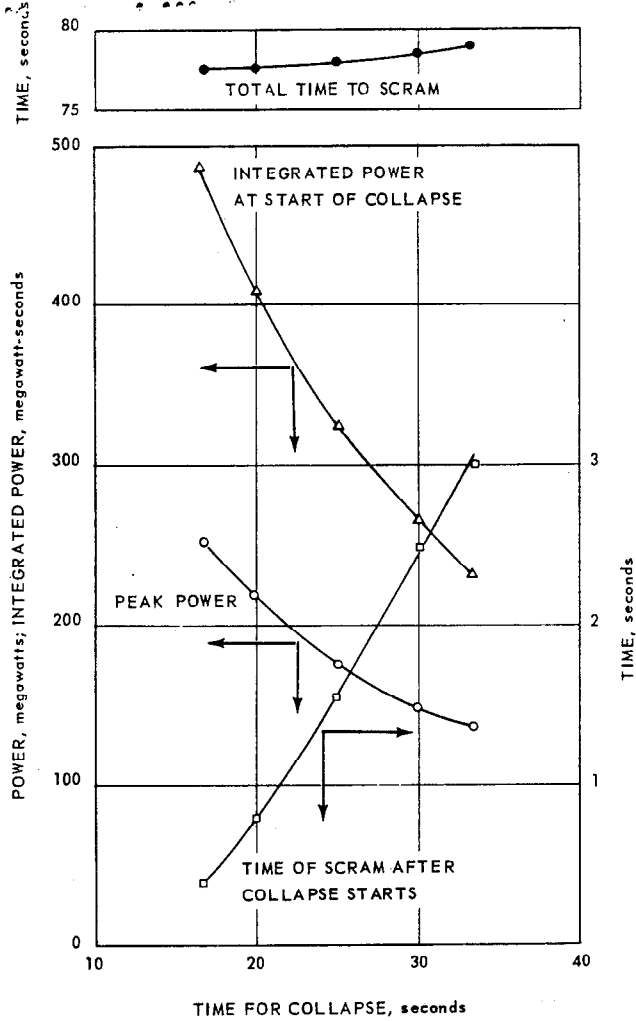


Fig. 54 - Power, total energy, and time to scram as a function of various assumptions, dynamic rods inserted 9.5 inches at transfer

UNCLASSIFIED

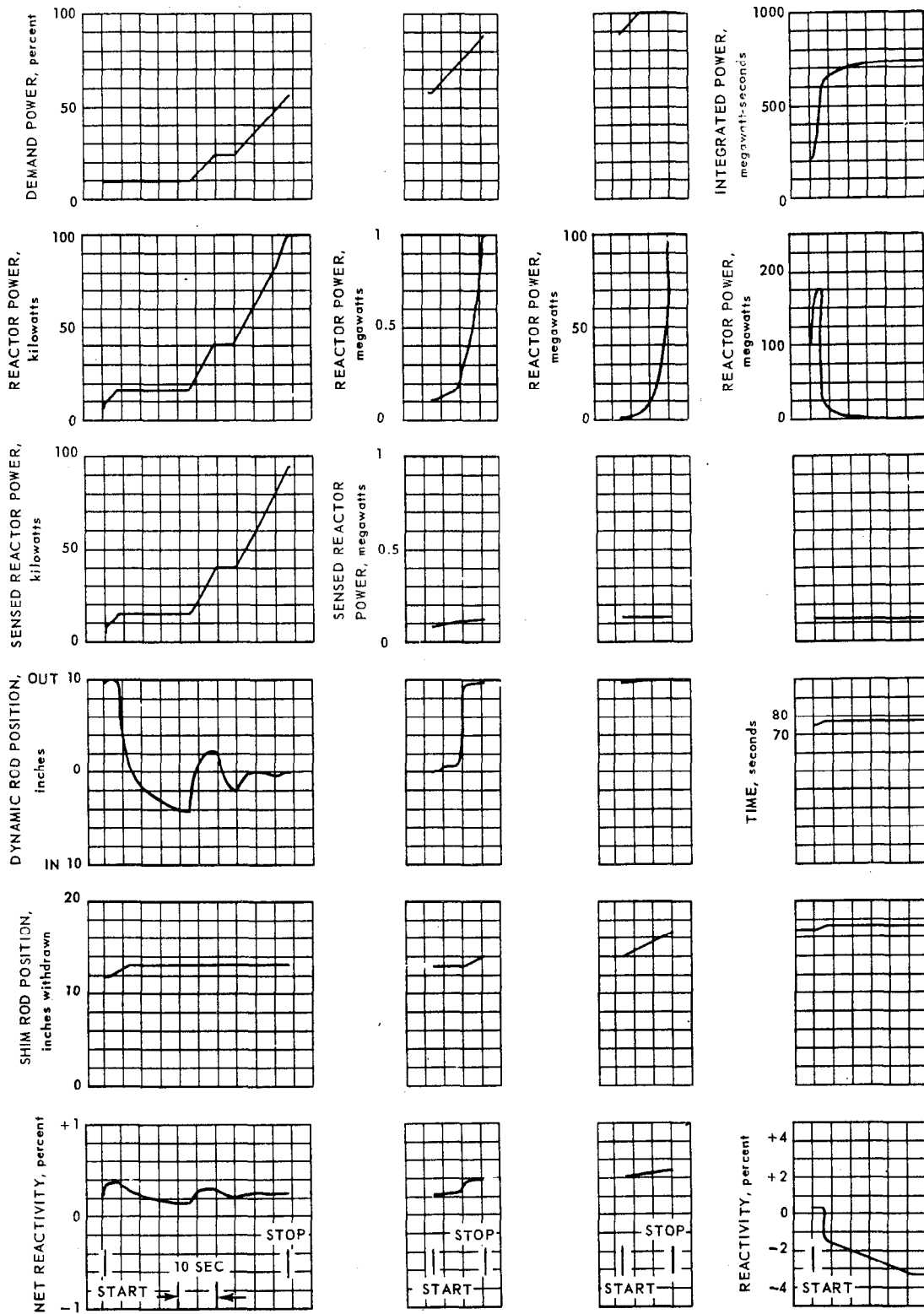


Fig. 55 - Computer traces of transient with dynamic rods 9.5 inches inserted

UNCLASSIFIED

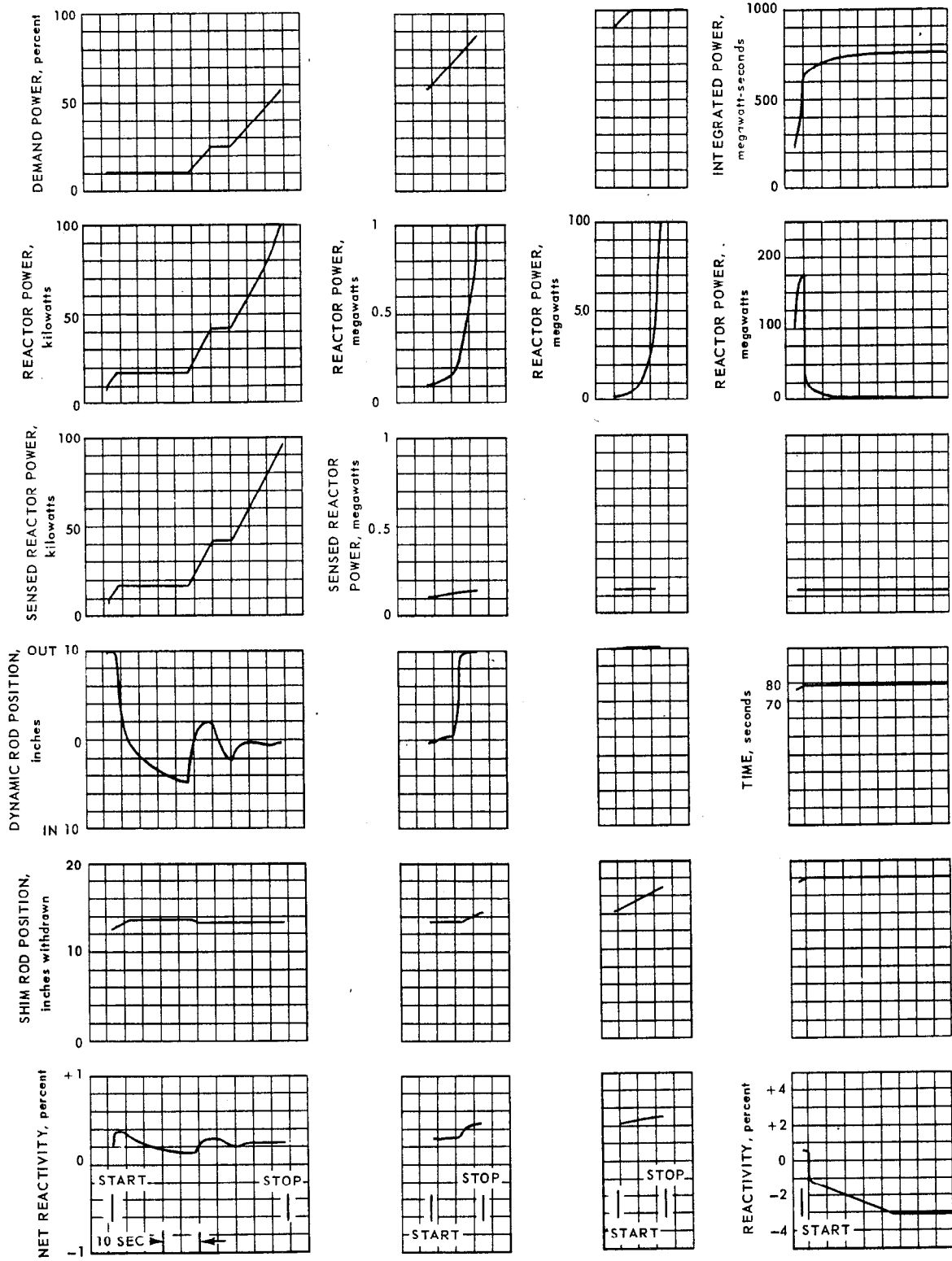


Fig. 56 - Computer traces of transient with dynamic rods 10.5 inches inserted

UNCLASSIFIED

DIGITAL COMPUTATION OF THE POWER HISTORY

An attempt was made to duplicate the excursion analytically using the information available from recorder traces, the report of the operator, the integrated energy measurements, and the reactivity measurements following the incident. To accomplish this objective a reasonable sequence of events was based on the control system response and a number of thermodynamic assumptions.

As a result of these studies the following have been established:

1. The positive temperature coefficient had little effect upon the excursion.
2. The amount of reactivity added during the excursion did not reach the prompt-critical value.
3. Had no scram occurred, the loss in reactivity due to fuel element collapse was sufficient to stop the excursion. A higher power level would have been reached and a higher integrated energy would have resulted.
4. The control system operated normally during the event.

A comparison of the analysis with the recorder traces is presented in succeeding paragraphs. This comparison can be summarized by pointing out the differences between the analytic reconstruction and the excursion as shown on the linear-flux trace.

1. The analytic peak power is reached approximately 2.7 seconds before the dip on the linear-flux trace. This difference is a minor one. Exact correspondence can be achieved by changing the initial power level and/or the rate at which the dynamic rods are removed.
2. An energy of 590 megawatt-seconds was calculated, as compared to a foil measurement of 760 megawatt-seconds.
3. A discrepancy exists in the calculated power and the linear-flux trace in the region in which the recorder should be proportional to power following the peak of the excursion.

These differences are affected by the assumptions as to energy level of fuel element collapse, the rate at which the collapse occurred, and the energy level at which the scram took place.

The degree of correlation that has been achieved indicates that the postulated sequence of events is reasonable. However, it cannot be assumed that these results describe the actual sequence of events, since the basic assumptions and the energy measurements are uncertain.

Analysis of the Reconstructed Excursion

Rod Motion - The rod motion throughout the excursion is based on the best estimate of rod positions in the period immediately before the transfer from the intermediate to the power range and on the analog computer analysis from the transfer point to a power level of approximately 113 kilowatts. These rod locations and the excess reactivity inserted were:

Frame	Before Transfer		At 113 Kilowatts	
	Length Inserted, in.	Reactivity Per Frame, % $\Delta k/k$	Length Inserted, in.	Reactivity Per Frame, % $\Delta k/k$
A	0	0	0	1.07
B, C, D, E	10	1.07	10	0.147
F	7.6	0.177	6.83	0.152
Dynamic rods	9.5	0.138	9.91	
Excess reactivity	0.215% $\Delta k/k$		0.228% $\Delta k/k$	

SECRET

UNCLASSIFIED

The analog studies show that as the linear-flux instrumentation saturates, the dynamic rods would be fully withdrawn in 2.5 seconds.

The bypass switches were set so that reactivity could be increased only by removal of frame F. The rod motion during the excursion therefore consisted of (1) removal of dynamic rods in 2.5 seconds, (2) withdrawal of frame F until scram occurs, (3) insertion of safety and dynamic rods at scram, and (4) insertion of all shim frames at normal rate of travel.

Figure 57 shows the rod positions throughout the excursion. The rod speeds used in the analysis were:

1. Safety and dynamic rods - full insertion in 0.38 second.
2. Shim rods - 12.39 inches per minute, normal rate of travel.

Thermodynamic Assumptions - Thermodynamic calculations indicate that the fuel element collapse could have started at an integrated energy of approximately 320 megawatt-seconds and that a fuel element temperature scram could have occurred at an integrated energy level of approximately 480 megawatt-seconds.

In the analysis the fuel element collapse time was arbitrarily varied from 2 to 50 seconds. The total reactivity loss due to the fuel element collapse was known approximately from a postincident reactivity measurement. A value of 2 percent  $\Delta k/k$  was used in the analysis.

#### Method of Analysis

A digital computer program was used to follow the excursion. Therefore it was necessary to establish a number of time regions characterized by a specific event whose effect was treated as either a step or ramp change in reactivity. The sequence of events that best fits the linear-flux trace and the manner in which these events were used in the program is outlined as follows:

1. At an initial power of 40 kilowatts, a step and a negative linear change of reactivity were inserted to establish the proper delayed-neutron characteristics at the start

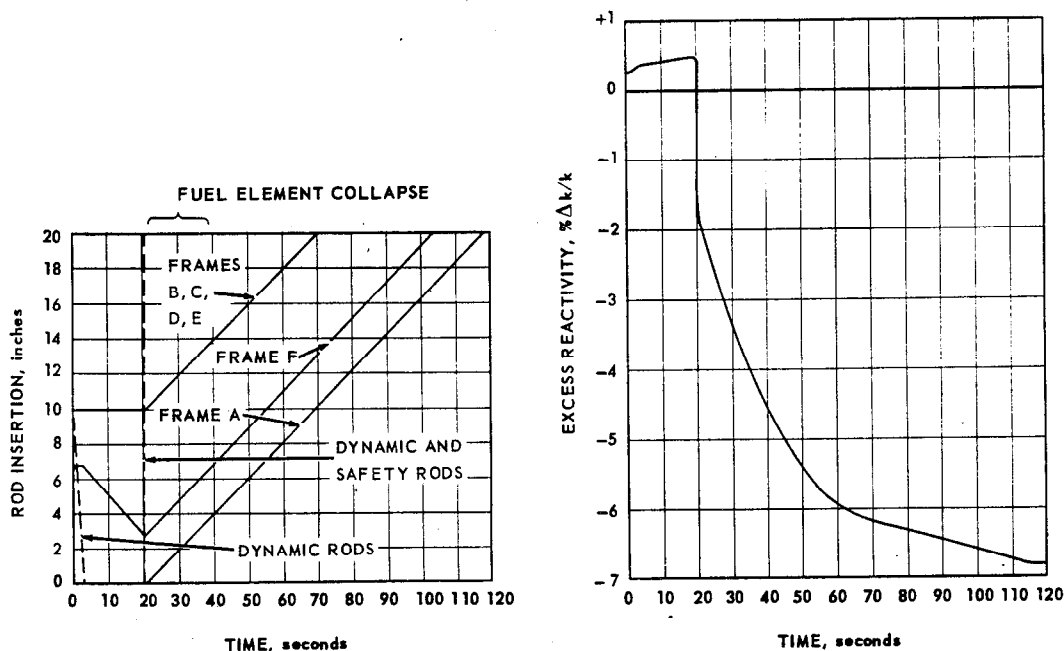


Fig. 57 - Rod motion and excess reactivity versus time



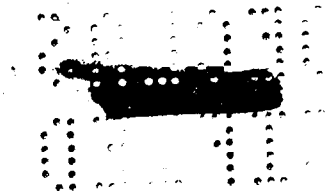
of the excursion. Near the end of this interval the power reached 113.3 kilowatts with 0.227 percent  $\Delta k/k$  inserted. This point is regarded as the reference time for the excursion.

2. In this time interval the dynamic rods were removed in 2.5 seconds corresponding to instrument saturation. A linear change of 0.15 percent  $\Delta k/k$  in 2.5 seconds was used in the program.
3. After complete removal of the dynamic rods, frame F was withdrawn starting from the 6.83-inch inserted position. The reactivity change associated with the removal of frame F was linearized over the time required to reach peak power.
4. At an energy level of 316.40 megawatt-seconds a negative linear change of 2 percent  $\Delta k/k$  in 20 seconds was used. This represents the effect of the fuel element collapse. Frame F continued to withdraw.
5. During this interval the fuel element collapse and frame F withdrawal were continued for 0.8 second, at which time the dynamic and safety rods were inserted. The peak power reached was 212.77 megawatts at approximately 20.3 seconds after the 113.3-kilowatt reference point. The integrated energy to peak power was 492.15 megawatt-seconds. Frame F was 2.7 inches inserted at this point.
6. In this interval a negative linear change in reactivity of 2.17 percent  $\Delta k/k$  in 0.38 second was used to represent the dynamic and safety rod insertion. The fuel element collapse continued.
7. After the scram action, all shim frames were inserted. The time used represents the time required to completely insert frames B, C, E, and D, which start at the 10-inch position. At the end of the interval, frame A is 10 inches and frame F is 12.7 inches inserted. The total reactivity change of 2.63 percent  $\Delta k/k$  was linearized over a 48.43-second interval. Fuel element collapse ended 18.82 seconds after the start of this interval.
8. This interval corresponds to the time required to insert frames A and F completely. (0.74 percent  $\Delta k/k$  in 48.43 seconds.)
9. During the last interval the only effect on the reactivity was the positive temperature coefficient that was used throughout the excursion.

## Results

Power Comparison - Figure 57 diagrams the rod motion and resulting reactivity outlined in the sequence; Figure 58 compares the calculated power with the linear-flux trace. The total integrated energy for the analytic excursion was 590 megawatt-seconds as compared to a foil-measured value of 760 megawatt-seconds.

Fuel Element Collapse Rate - Similar calculations were made for a change in the fuel element collapse rate to 2 percent  $\Delta k/k$  in 49.61 seconds. The effect of this change was to increase the peak power reached to 280.49 megawatts and the total energy release to approximately 650 megawatt-seconds. The results of this calculation, shown in Figure 59, were used as input to the temperature calculation depicted in Figure 51. Use of the shorter fuel element collapse time improves the correlation of the linear-flux trace and the calculated power near the end of the excursion. Reducing the fuel element collapse time to less than 20 seconds would probably improve this comparison, however, the total energy would be reduced still further. In addition, equal power points as shown on the linear-flux trace before and after the excursion do not necessarily correspond to equal power levels. The reason is that the delayed fission product gammas produce an increase in the gamma-to-neutron ratio following the excursion. Consequently the saturation characteristics of the linear-flux instrumentation are changed, in effect increasing the recovery time of the chamber.



UNCLASSIFIED 99

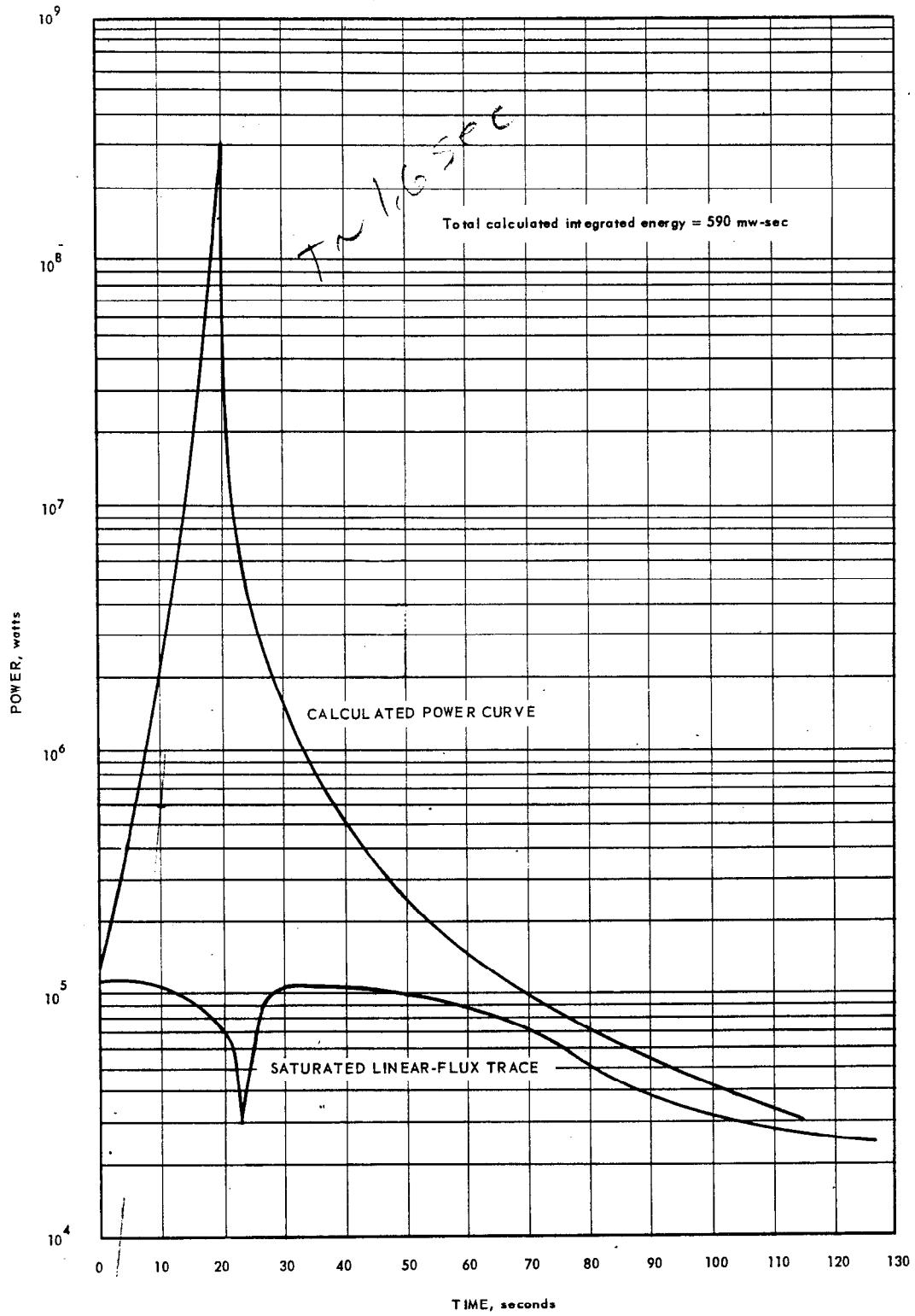
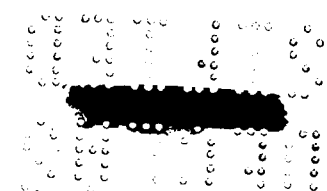


Fig 58 - Comparison of calculated power with observed linear-flux trace assuming a negative linear change of 2 percent  $\Delta k/k$  in 20 seconds



UNCLASSIFIED

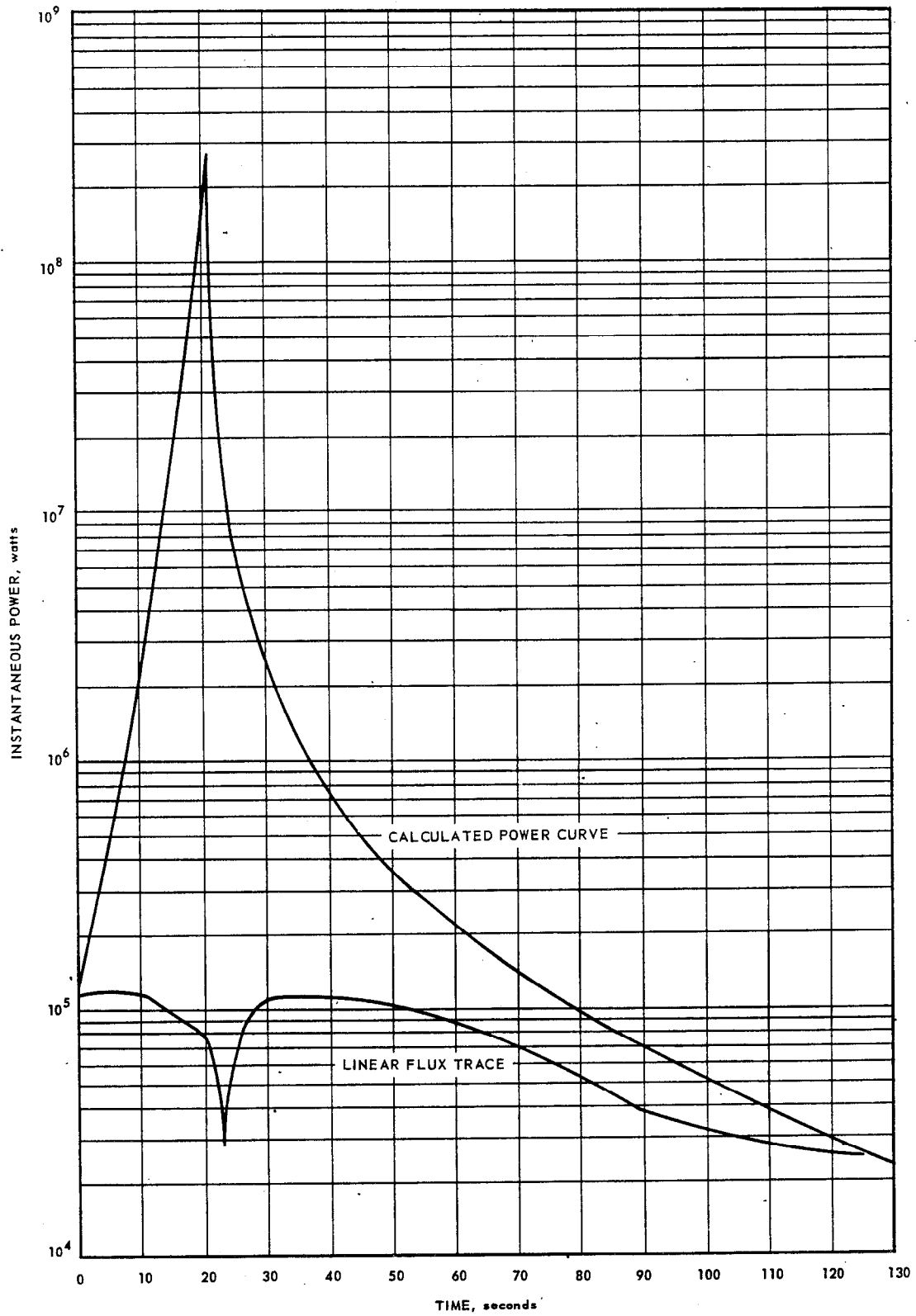


Fig. 59 - Comparison of calculated power with observed linear-flux trace assuming a negative linear change of 2 percent  $\mu\text{A}/\mu\text{s}$  in 49.61 seconds

Shutdown by Fuel Element Collapse -- Calculations were made in which the fuel element collapse was assumed to act alone for the thermodynamic conditions outlined in the previous sequence of events. A fuel element collapse rate of 2 percent  $\Delta k/k$  in 20 seconds results in a total energy of 1930 megawatt-seconds. This calculated energy shows that an increase in the collapse rate would have occurred before the assumed 20-second interval. To establish a more realistic basis for determining what would have happened had no scram occurred, calculations were made using an arbitrary energy of 600 megawatt-seconds as the point at which the shutdown mechanism started and increasing the fuel element collapse rate to 2 percent  $\Delta k/k$  in 2 seconds.

The total energies for the two cases studied were:

1. Fuel element collapse (2 percent  $\Delta k/k$  in 2 seconds),  $E = 903.87$  megawatts.
2. Safety action and fuel element collapse combined (safety = 1.73 percent  $\Delta k/k$  in 0.38 second; collapse = 2 percent  $\Delta k/k$  in 2 seconds),  $E = 718.69$  megawatt-seconds.

Temperature Coefficient - Duplicate calculations showed no effect due to a positive temperature coefficient.

### 4.3 ANALYSIS OF CIRCUIT PERFORMANCE

#### Conditions at the IET in the Control System During Run 15-4

1. Mode of control - automatic servo control.
2. Operating range - through intermediate range to power range.
3. Channel in use - channel 2 in control with channel 1 linear sensor and channel 2 log-flux sensor.
4. Operative channels - 2 and 3, power range.
5. Temperature channel selector set on channel 1.
6. Safety conditions - Interlock, override, and scram on channel 1 power range were initiated because the safety board was removed. Hydraulic pressure and minimum airflow were bypassed in the bypass panel. The  $10^{-1}$  intermediate-range interlock contact in the intermediate-to-power-range transfer circuit was jumpered.
7. Filters were used in the high-voltage supply to the uncompensated ion chambers.
8. The high voltages to the compensated and uncompensated chambers were inadvertently reversed. The uncompensated should have had 1500 volts d.c.; the compensated, 800 volts d.c.

#### Saturation of Log-Flux Circuitry

The log-flux amplifier is not normally used during power-range operation. The amplifier is so designed that the log diode characteristic becomes linear above 20 to 30 percent of full power, depending on the individual diode. A typical characteristic curve showing the upper portion of the log-flux amplifier response is shown in Figure 60. During the operation of this amplifier in this region of linear response, the period signal response indicates a shorter period than the actual period of the reactor. For this reason, the period-amplifier safety circuits are normally automatically bypassed during the power-range operation. Complete saturation of the log-flux amplifier occurs at an input current between 500 microamperes and 1 milliampere, depending upon the particular log-flux amplifier board checked. This represents a flux level of approximately 100 to 200 percent.

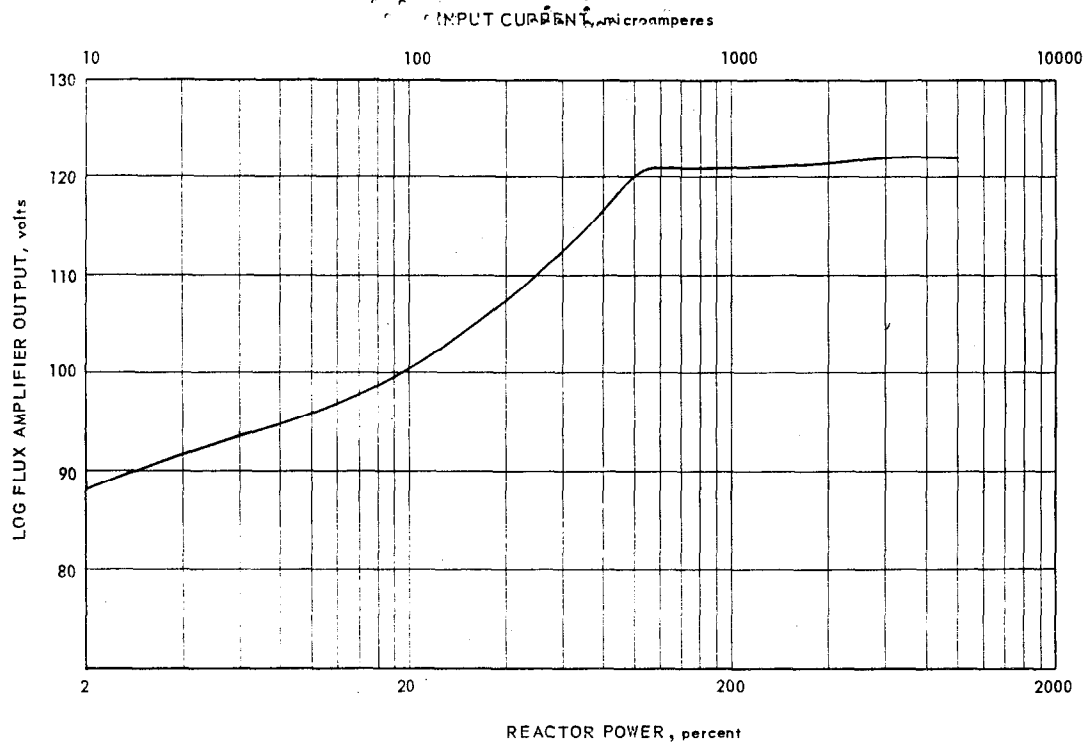


Fig. 60 - Typical log-flux response, upper portion

The amplifier saturation plus chamber saturation at a later time caused the intermediate-range safety circuits to be inoperative during the excursion, even though the operations personnel had removed the bypass action that usually exists around the intermediate-range safety contacts when operating in the power range. Saturation in the amplifier occurs in the plate circuit of the starved pentode amplifier, shown in Figure 61, because of the grid currents of the cathode-follower output tube through the plate load resistor of the pentode.

#### Behavior of the Linear Flux Circuit (Uncompensated Ion Chamber)

At the start of this reactor experiment the power level of the reactor was being increased under control of the servo system toward a power level setting of 80 percent of the full range of the power-demand control. This power level corresponded to about 72 percent of full scale on the recorder chart scale. The ionization chambers were located so that they were indicating power-range operation although the actual reactor power level was considerably lower. Subsequent measurements showed that a current of 0.64 milliampere was required to drive the recorder to 80 percent of its full-scale value. Since 80 volts is developed by this input current, the composite input circuit resistance for this signal level was 125,000 ohms. If all had gone well, the final current from the ionization chamber would have been approximately 0.65 milliampere after the reactor power had leveled off at 80 percent as indicated by the demand-servo potentiometer.

Figure 62 shows the portion of the linear-flux channel that is necessary to determine the direct cause of the accident and to explain the recorded linear-flux trace. An uncompensated ionization chamber consisting of three concentric cylinders, each insulated from the others, is the flux-sensing element. (The inner electrode is shown as a dashed line

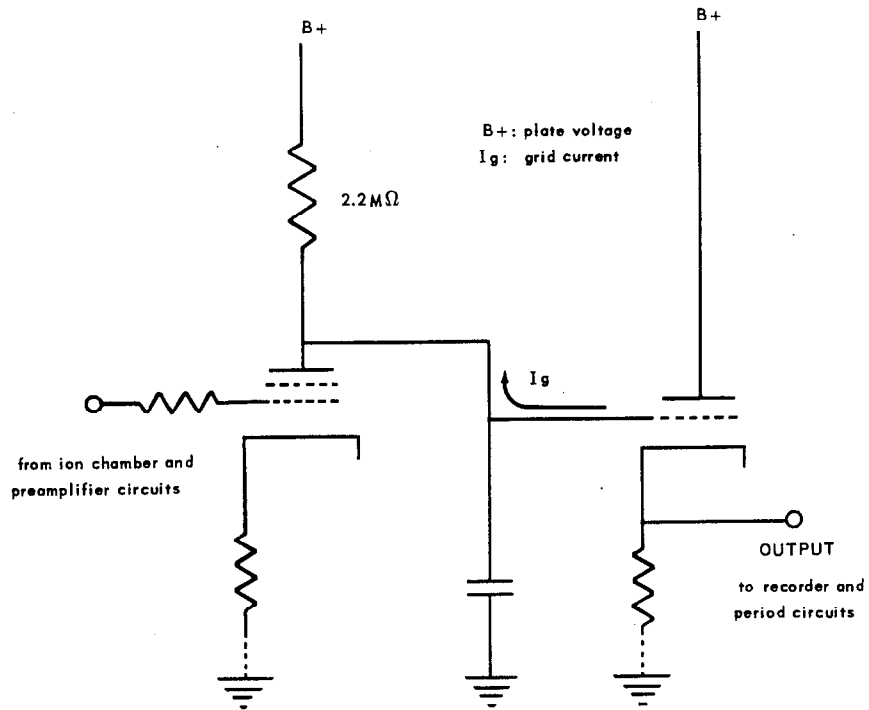


Fig. 61 - Pentode amplifier

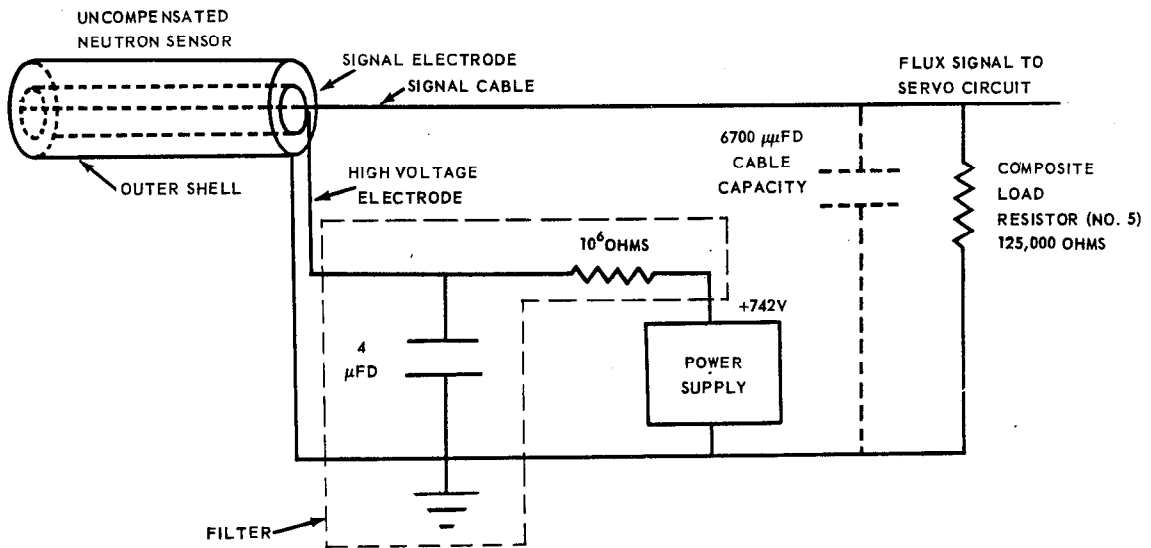
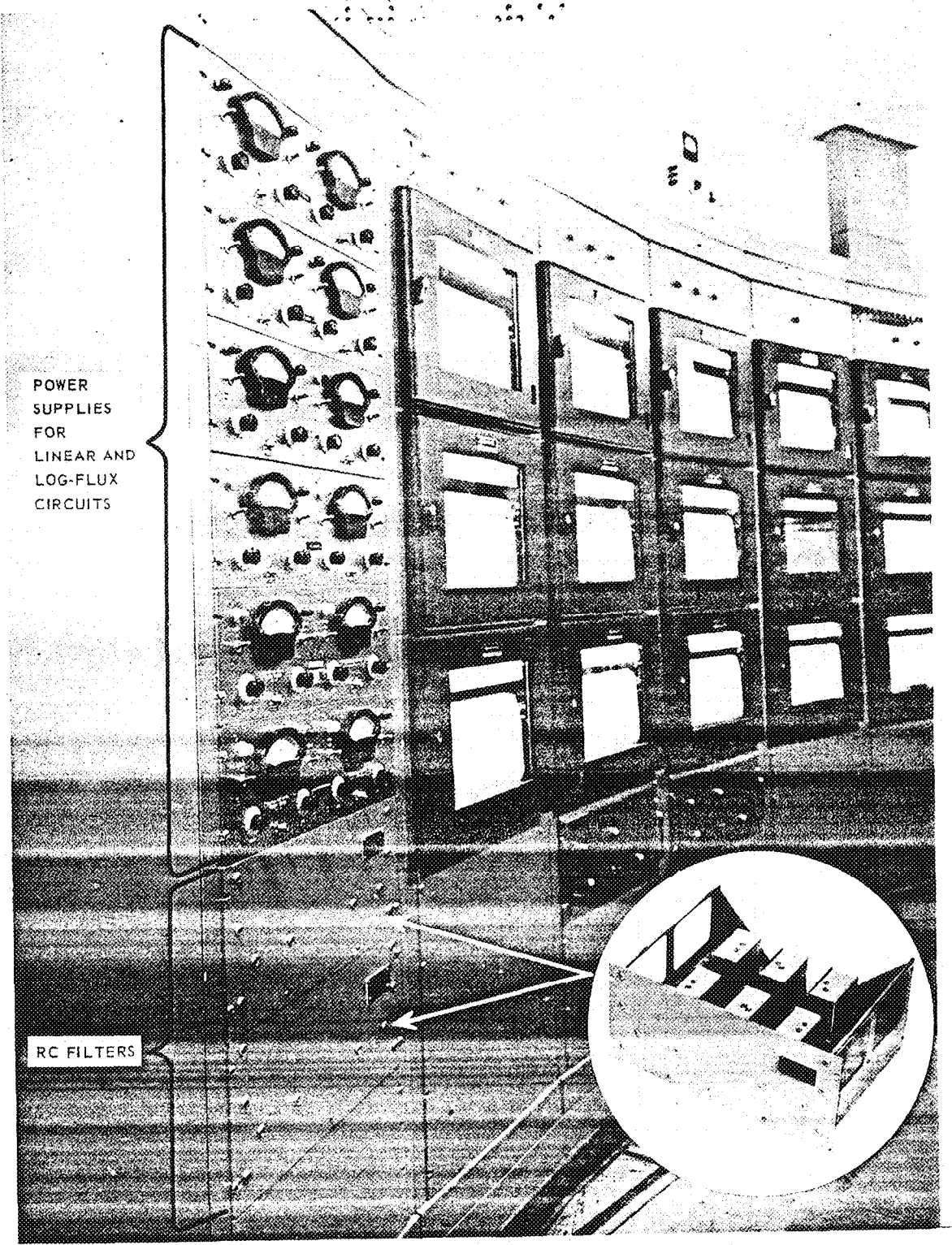


Fig. 62 - Neutron sensor and portion of linear-flux channel

on Figure 62.) The outer surface of the inner electrode and the inner surface of the middle electrode are coated with boron, thus making the chamber neutron sensitive. The signal current is normally derived from the inner electrode and the chamber collecting voltage is normally applied between the middle electrode and ground. The signal electrode is connected to ground through a 125,000-ohm signal voltage developing resistor. The outer electrode or housing is connected directly to ground and prevents an electrical shock hazard, facilitates chamber mounting within the reactor, and provides extrinsic electrostatic shielding of the signal electrode. There was approximately 0.0007 microfarad of cable capacity across the signal-developing resistor; the chamber collecting voltage was obtained through an RC filter from a variable voltage power supply that was set for an output voltage of 800 volts. (The design setting for the power supply was 1500 volts.) The actual voltage out of the power supply however, was 742 volts. The power-supply filter, which was not a part of the circuit as designed, consisted of a 1-megohm resistor electrically connected between the power supply and the high-voltage electrode in the ionization chamber and a 4-microfarad condenser, which is electrically connected across the chamber high-voltage electrode and ground. Figure 63 shows a photograph of the RC filter and its location with respect to the linear-flux and log-flux power supplies in the IET control console. This filter was originally used with the HTRE No. 1 (compensated ion chamber) linear flux circuits to eliminate difficulties due to power-supply noise being coupled from the high-voltage electrode to the signal electrode by means of the chamber interelectrode capacity. The filters were permanently mounted in a separate drawer in the IET secondary relay panels and were connected into the circuit by means of coaxial cables. Figure 64 shows the characteristic curves of a prototype ionization chamber.

By examination of Figures 64 and 65 it is possible to determine why the linear-flux-channel signal could not satisfy the signal demand of the servo system. The 80 percent demand setting required a signal current of 0.65 milliamperes. If the ionization chamber were operating in a voltage-saturated condition, that is, on the flat part of its characteristic curves, as it should, the thermal neutron flux level as seen by the chamber would be approximately  $5 \times 10^{10}$  nv. The curves show that to collect this amount of current properly a minimum of 300 volts must exist across the chamber electrodes. However, if 0.65 milliamperes flows through the 1-megohm filter resistor, it must cause a voltage drop of 650 volts. In addition, the voltage drop across the signal-developing resistor must be approximately 80 volts. Thus if this condition were possible, only 20 volts would remain to act as the ionization chamber collecting potential, considerably less than the 300 volts required for proper operation.

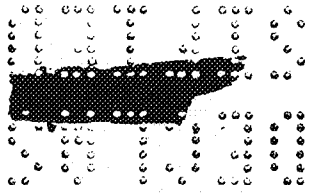
In actual operation the increasingly inadequate collecting voltage available to the ionization chamber results in increasingly inefficient ionization current collection as the flux goes up. As a limit the signal current would approach 0.74 milliamperes as the flux increases without limit if other effects did not further distort the operation. For example, if the current rises to 0.53 milliamperes, approximately 140 volts is left as a collecting potential. The curves show that this current and this voltage identify the magnitude of thermal neutron flux as approximately  $6 \times 10^{10}$  nv. However, if the available ionization chamber collecting potential was sufficient for proper operation, the ionization chamber signal current would have been about 0.8 milliamperes. Thus the actual signal is significantly in error at this point and very rapidly worsens. If this were the only mechanism involved, one would expect the signal current to approach and remain at a maximum value of 0.74 milliamperes until the flux level decreases sufficiently for the ionization chamber to again respond properly to the flux level. However, once the ionization chamber is voltage-starved and the reactor power continues to increase, another effect starts taking place, an effect induced by the increasing gamma radiation.



POWER SUPPLIES FOR LINEAR AND LOG-FLUX CIRCUITS

RC FILTERS

Fig. 63 - IET control console showing location of RC filter





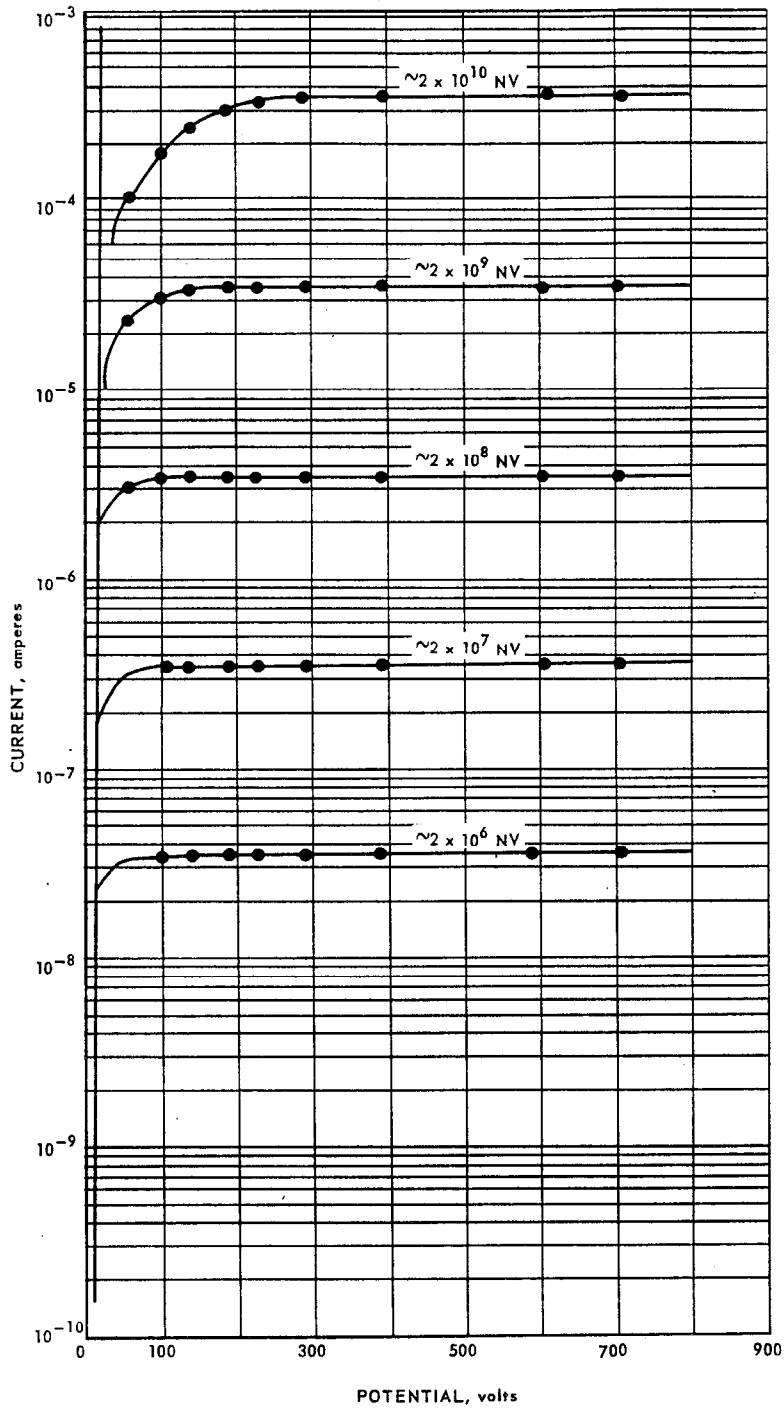
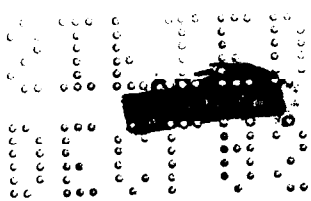
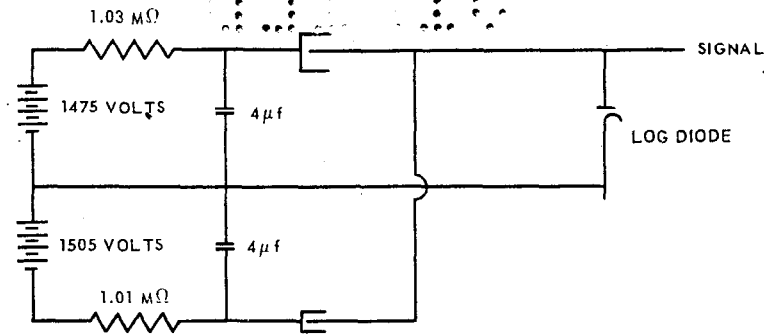


Fig. 64—Output current as a function of applied potential, prototype uncompensated ion chamber





LOG FLUX CIRCUIT

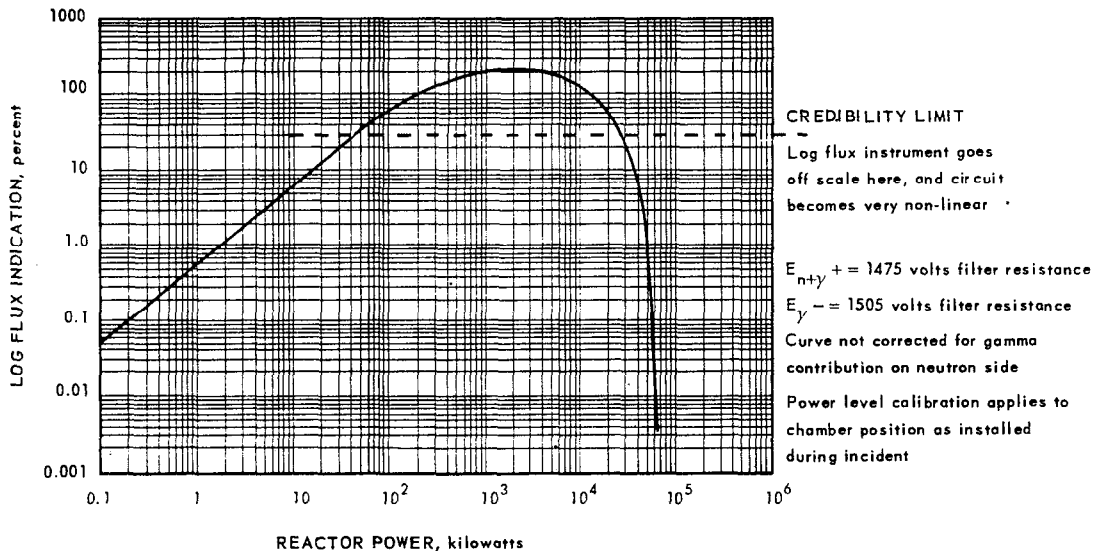


Fig. 65 - Saturation curve for log-flux current

Any ionization chamber is sensitive to gamma radiation to some extent. Under usual reactor operating conditions the neutron-induced ionization current is 100 to 200 times greater than the gamma-ray-induced ionization current in an uncompensated ionization chamber, and the gamma-induced currents are regarded as negligible. However, the abnormal operating conditions during the excursion allowed the effects of parasitic gamma current to become so pronounced that the signal current decreased as the reactor power increased. The result was a dip in the recorded trace of the linear-flux-channel signal level. The reason for this dip is indicated in Figure 62. If a very high gamma-induced ionization density exists, there are two possible paths of current flow within the ionization chamber. One is between the collecting voltage electrode to the signal electrode through a 125,000-ohm composite load to ground. The gamma-induced current in this section has no appreciable effect, since the gamma-induced ionization is negligible compared to the neutron-induced ionization. However, another path exists between the collecting voltage electrode and the housing case, which is at ground potential. Under normal conditions of adequate current and voltage available to the collecting electrode, this path would have no effect on the signal. However, the voltage and current starvation that existed has the effect of diverting current from the signal electrode to the parasitic path, thus resulting in an increasing loss of signal current through the signal electrode as the gamma flux increases.

One of the uncompensated ion chambers in use during the excursion was tested in the MTR to determine the amount of gamma leakage current and to reaffirm the chamber characteristics. The curves thus obtained are shown in Figure 66. The curve of current versus collection voltage shows that the chamber behavior was very close to that of the prototype, the characteristics of which were used to construct the hypothesis regarding behavior of the chamber. The gamma leakage current is about as expected and is such that the current bypass produced by the gamma leakage can be expected to begin driving the circuit downscale at fluxes or power levels roughly 100 times greater than those at which the circuit becomes current limited. Based on the characteristics of signal current

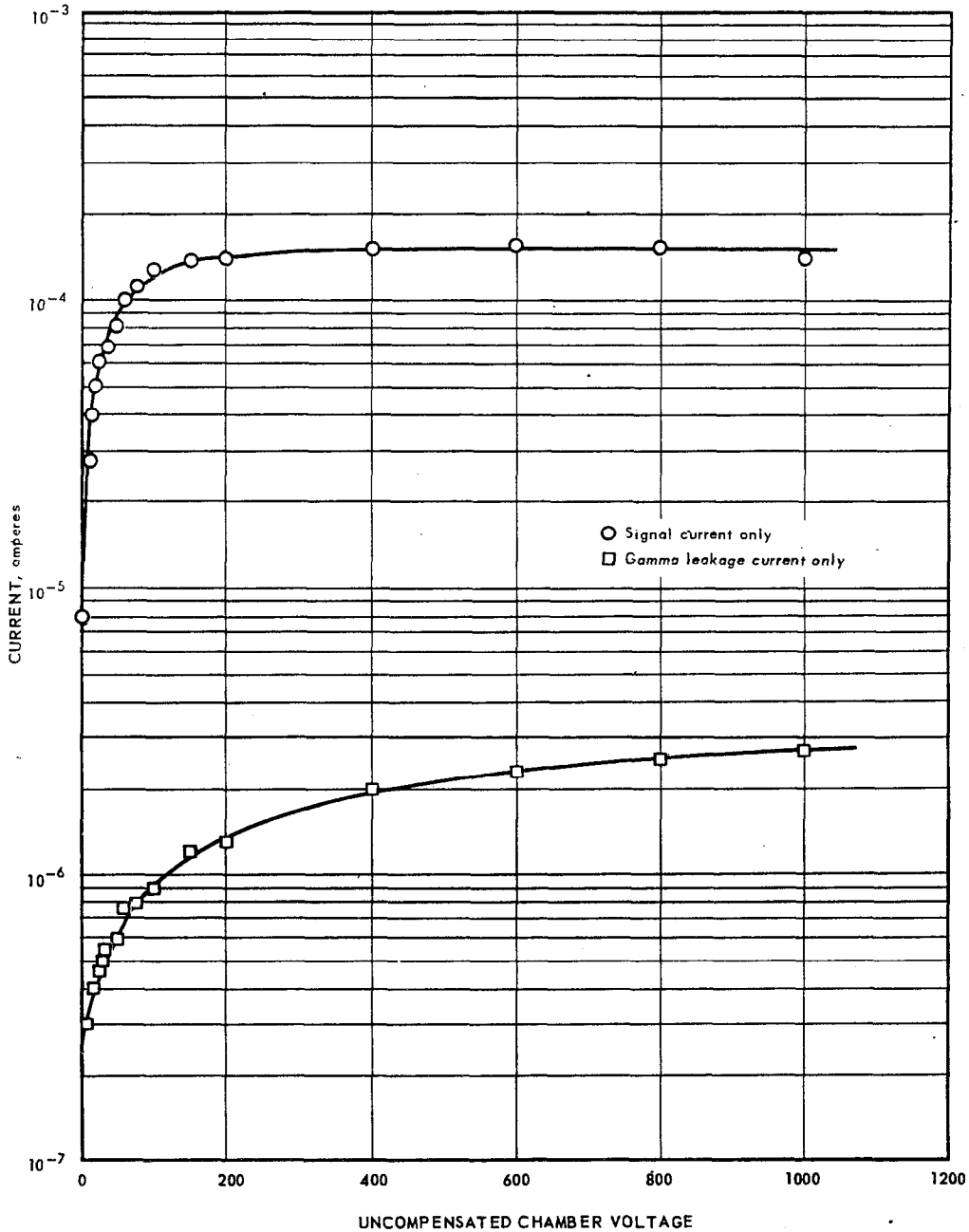


Fig. 66 - Uncompensated ion chamber characteristics derived from MTR test, reactor at 80 kilowatts ( $2.88 \times 10^{19}$  n/v)

and gamma current shown in Figure 66, a circuit characteristic curve has been derived and is shown in Figure 67. This curve is calculated from the characteristics obtained in the MTR test and shows the expected linear-flux-circuit indication as a function of relative flux level.

#### Compensated Ion Chamber

If each half of the chamber is regarded as being supplied by each high voltage alone (both positive and negative), the signal current supplied by each half will approach some value asymptotically as flux increases. This value will be determined by the circuit parameters -- power supply voltage and external resistances. The circuitry, as shown in Figure 65, is such that the signal current on the gamma-sensitive side of the chamber subtracts from the signal current of the neutron-sensitive side. The net signal current supplied to the log diode is the difference current. For a given neutron flux, the current supplied by the gamma side is 1 to 2 percent of the current supplied by the neutron side. Under ideal conditions, in which power-supplied balances and external resistances are equal, the current supplied to the logarithmic diode will increase with flux up to a maximum value and will then decrease to zero at the same rate with further flux increase. This effect will be due to the subtractive nature of the gamma-side signal current, the current being limited by the external resistance in the power supply circuits when fluxes are high enough to cause both sides of the chamber to conduct freely.

Figure 65 shows the circuit parameters as they were measured following the incident. With an imbalance in the power supplies and external resistances as measured for the compensated ion chamber circuitry, the current supplied to the log diode is not the same function of flux as it would be in the balanced theoretical case. The primary difference is in the rate of decrease of log-diode current with increasing flux. The measured imbalance would produce a very rapid decrease of log-diode current with increasing flux. Actually the signal current tries to reverse polarity. Figure 65 indicates that the instrument comes back on scale and then drives downward below the bottom of the scale when flux has increased by a factor of only 2.1 to 2.2. The actual flux and power levels probably differ slightly from those indicated in the illustration. One of the compensated ion chambers was also tested in the MTR to confirm the chamber characteristics. A typical chamber characteristic curve is shown in Figure 68. During the MTR test the chamber circuit was set up as indicated in Figure 65, in order to demonstrate that a downscale indication was possible. With the estimated flux level at the chamber at  $3.39 \times 10^{12}$  n/cm<sup>2</sup>-sec, zero current flow was indicated and the log-N instrument read below the bottom of the scale. This confirms the conclusion that the signal could actually try to drive negative. As indicated in the discussion of the uncompensated ion chamber, the flux at the chamber position during normal reactor operation should be around  $10^{10}$ .

#### Fuel Element Temperature Bridge Circuit

The fuel element temperature bridge was checked in Idaho after the excursion. Three upscale readings were found to be required for an interlock response, four for override, and five for scram. Potentiometers in series with each safety-level relay will change the number of thermocouples required to give a safety response by one or two thermocouples. The chart in Figure 69 shows the number of upscale readings (overtemperature) versus the number of thermocouples that are open (causing a downscale reading) required to give the various safety responses. The potentiometers of the bridge were adjusted to correspond to the number of upscale indications required at Idaho. This test was then carried out up to 10 open-couple responses in tests made at Evendale. Because of the settings of the recorders for normal power-range operation, the low airflow in the system, and the initial low-temperature operation, the fuel element temperature

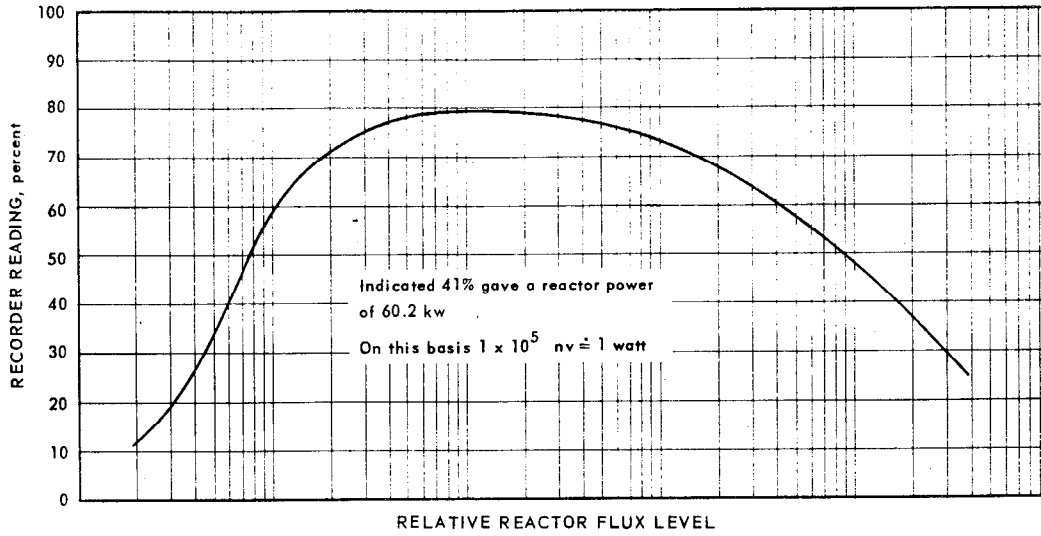


Fig. 67 - Calculated linear-flux circuit characteristics based on MTR test

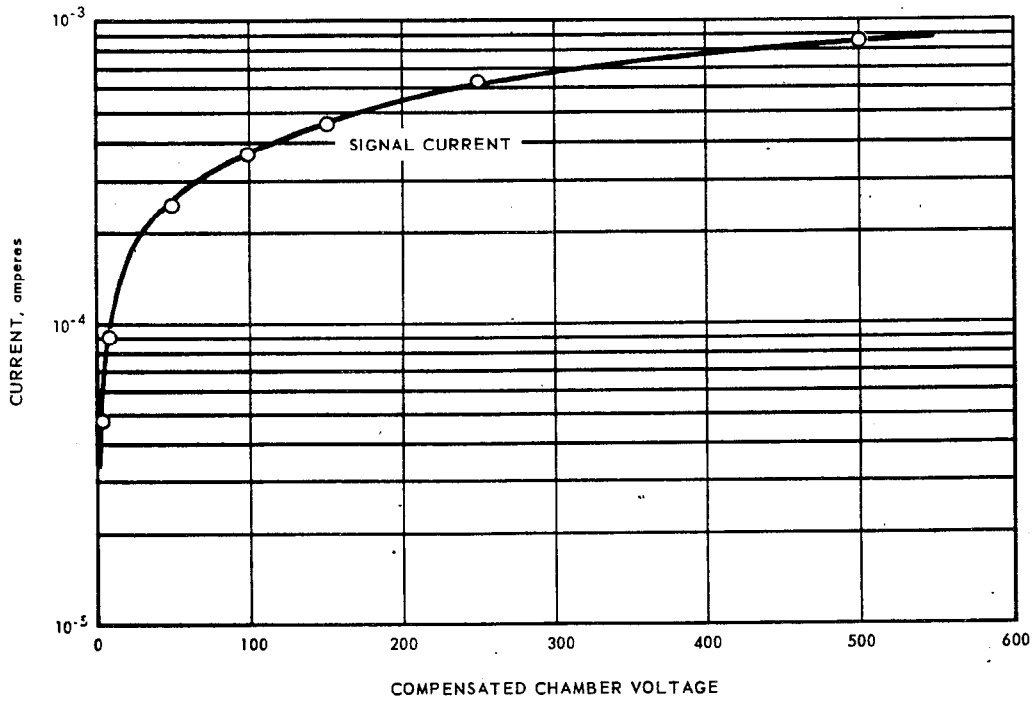


Fig. 68 - Compensated ion chamber characteristics derived from MTR test, reactor at 400 kilowatts ( $2.64 \times 10^{10} \text{ nv}$ )

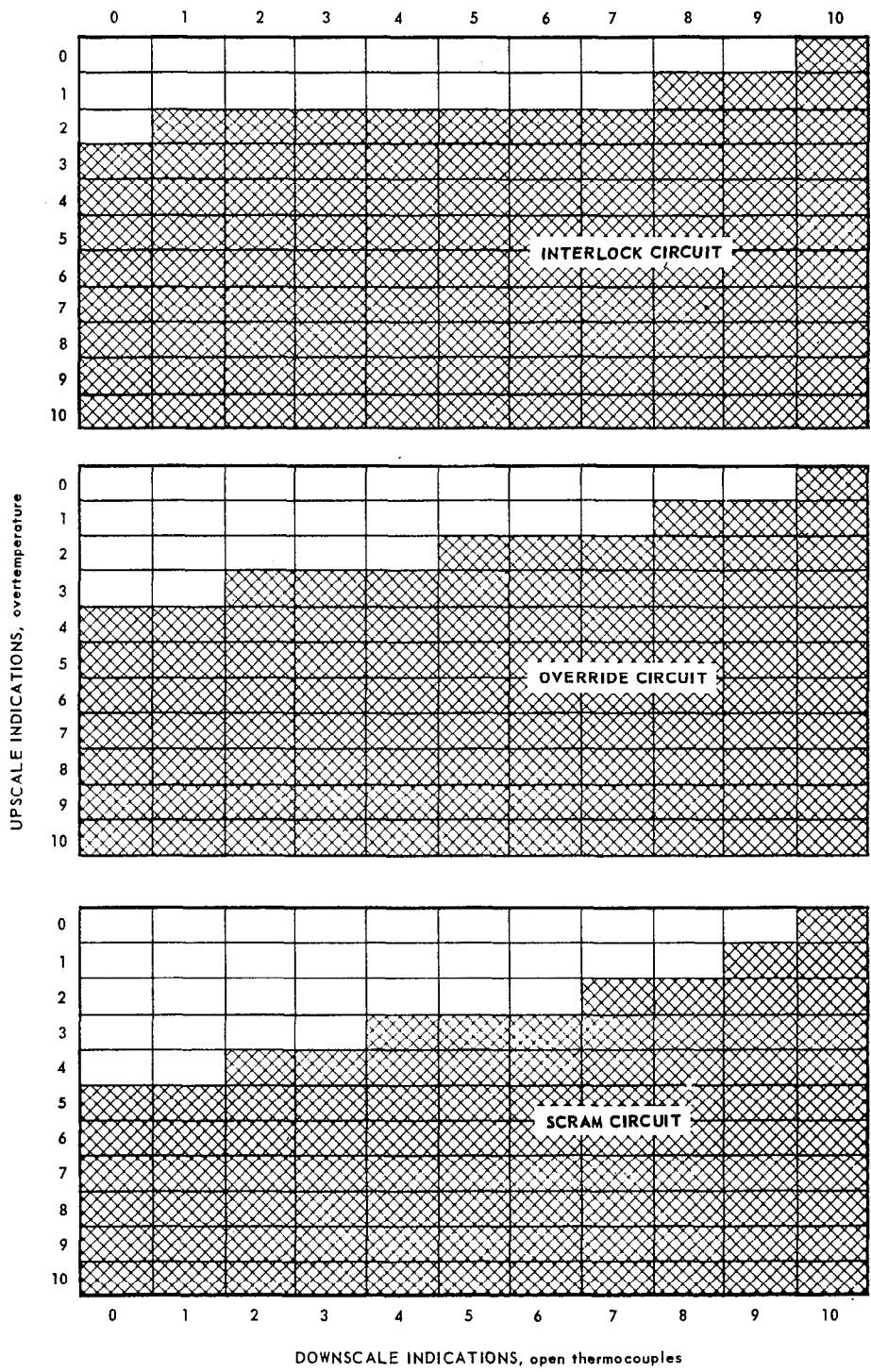


Fig. 69 - Fuel element temperature bridge

SECRET

circuit was slow to respond. The fuel element temperature circuit was credited with giving the initial scram action as observed by the operators. Ten thermocouple open circuits are required for a scram response in the absence of any upscale reading. Table 6 (page 70) shows the postexcursion condition of the ten thermocouples that were connected into the scram circuit.

As previously indicated, analysis based on the observed condition of the fuel cartridges and reconstruction of the power history based on possible rod motions indicate that the 19th-stage temperatures reached the scram settings at about the same time that the interior stages of the fuel cartridges began to melt. The persons present in the control room indicated that (1) the temperature scram light was the first one to appear, and (2) temperatures of 3000°F were observed. The 3000°F temperatures could have been produced by melt-through of leads and formation of new thermocouples in the interior stages of the reactor. Since several combinations of upscale readings and open circuits could scram the reactor, it is impossible to reconstruct a unique action that can be said to have produced the scram. It is possible that the scram was induced either by the thermocouple junctions reaching the scram settings, or by the formation of new thermocouples in the interior stages, or by some combination of both. Because the ten fuel element recorders were not operating during the initial approaches to power, there is no definite record of their temperature indications.

#### Loop Error Meter

The loop error meter was checked and found to be operating satisfactorily. The excessive-error lamp was adjusted to light when the difference between the demand signal and the flux feedback signal was greater than approximately 10 volts.

SECRET

~~SECRET~~

UNCLASSIFIED

## 5. POSTOPERATION STUDIES

### 5.1 DISASSEMBLY INSPECTION

#### Disassembly of the Power Plant

Following the criticality check performed on November 23, all control rods and actuators that could be pulled were replaced with transport rods and the power plant was then moved to the Hot Shop for disassembly. Three rods (231, 510, and 541) were held in place by molten material, possibly fuel or moderator.

In the Hot Shop the nuclear sensing instruments were removed from the core and three BF<sub>3</sub> counters were placed on the side of the primary shield for monitoring the core during disassembly, as shown in Figure 70. The instrumentation cabling, pressure tubing, aft header, hot ducting, and cold ducting were removed from the dolly; the primary shield, front plug, core, rear plug, and combustor were lifted as a unit and placed in the upending fixture still in the horizontal position. This unit is shown in Figure 71.

The combustor and rear plug were removed from the core and primary shield (while the unit was still in the horizontal position) in that order, exposing the rear tube sheet, shown in Figure 72. An attempt was then made to release all fuel cartridges by inserting a release rod through the center of each cartridge. It was impossible to insert the rod more than 3 or 4 stages into any of the cartridges because of the collapse of the fuel cartridge stages.

The upending fixture containing the front plug, primary shield, and core was then rotated to a vertical position, and the core-removal fixture was placed on top of the upending fixture as shown in Figure 73. After withdrawal of the front plug and core from the primary shield into the core removal fixture, this assembly was moved onto the tube-loading machine.

Fuel cartridges and liners were then removed. The cartridges were unlatched by manually pulling the release pins in the bellmouths. A maximum downward axial load of 1500 pounds was applied to each fuel cartridge and liner combination in the two outside circles of cartridges. Although attempts were made to remove 69 units, only 32 fuel cartridges and liners could be removed. At 400 pounds force the moderator latch fingers slipped from their catches and allowed the moderator cell and fuel to come to rest on the aft tube sheet. Because of the damage to these fuel cartridges and liners and the anticipation of greater damage on cartridges toward the center of the core, and because all 69 moderator cells were resting on the rear tube sheet, no further attempts were made to pull fuel cartridges and liners with the tube-loading machine.

The core and front plug were transferred to the core and plug alignment fixture, where the two units were separated. The three control rods that were stuck in the core were burned off between the front tube sheet and the front plug to allow the core

~~SECRET~~

UNCLASSIFIED



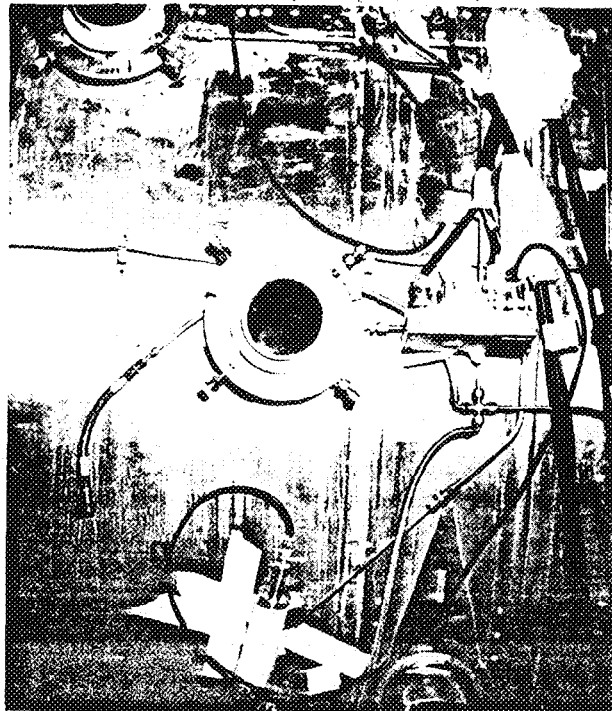


Fig. 70 - D102A primary shield showing placement of  $\text{BF}_3$  counters

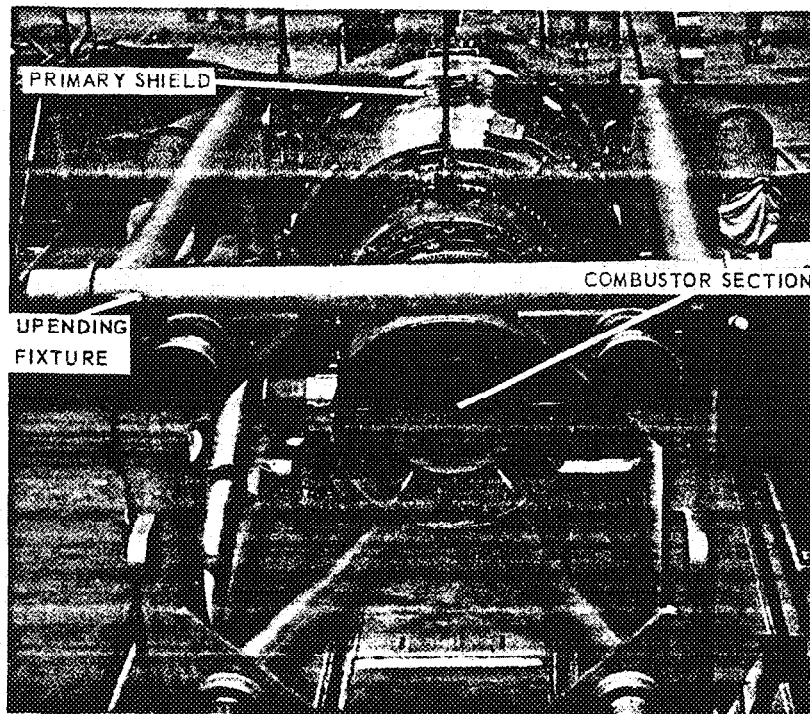
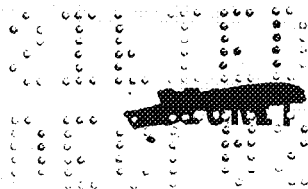


Fig. 71 - Reactor-shield assembly in upending fixture



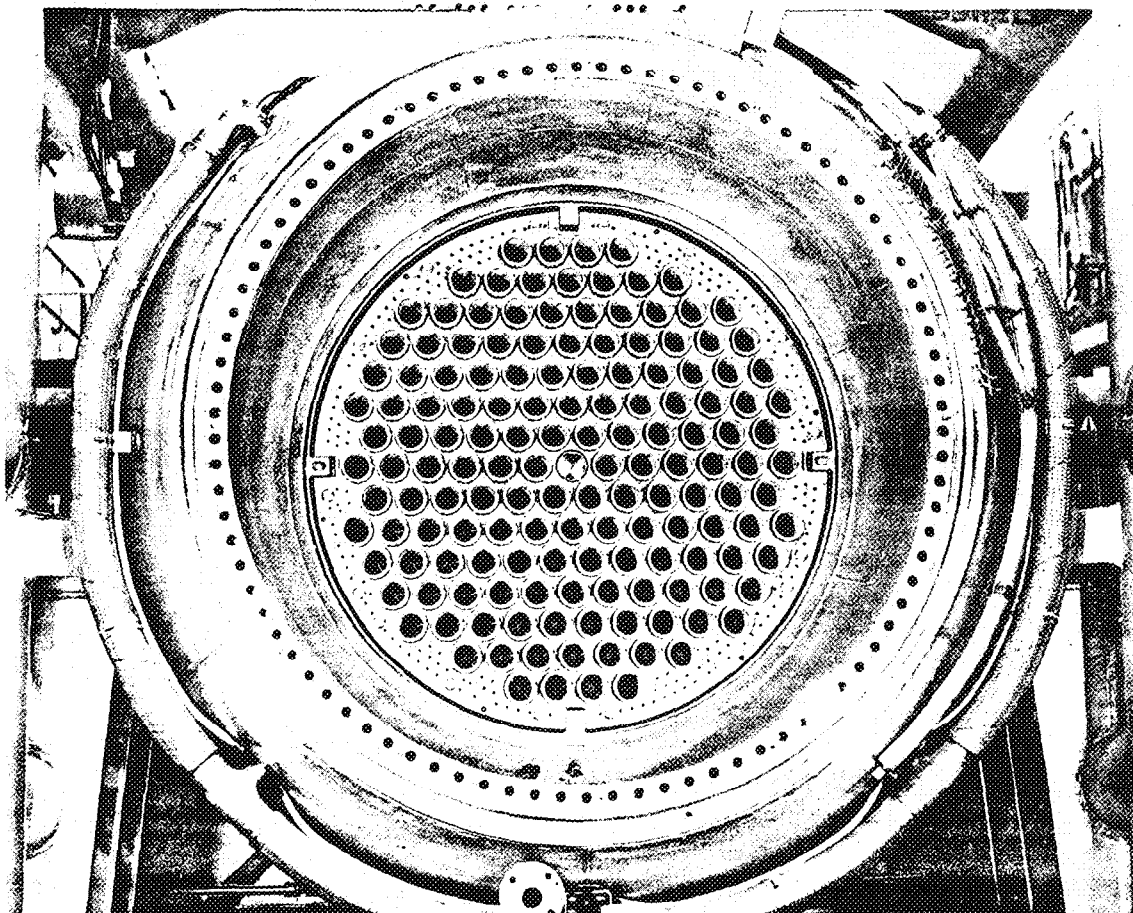


Fig. 72 - Rear tube sheet exposed after removal of cambuster and rear plug

to be parted from the front plug. The core was then placed in the Initial Criticality Experiment tank for further disassembly in the horizontal position.

The rear tube sheet was removed from the core to expose the moderators, shown in Figure 74. The unlatched moderator cells were then removed from the core. The latched moderator cells with fuel were released by manually moving the latch fingers together with a suitable tool placed through the bellmouth assemblies on the front tube sheet. All but five moderator cells with fuel could then be removed from the core. The remaining five moderator cells were fused to the control rod guide tubes. The control rod guide tubes that were fused to the moderator were then cut off just upstream of the fused section.

After removal of the moderator cells from the core, further attempts were made to remove the fuel. The first method used was to anchor the moderator to the Hot Shop floor and then apply a force of 2000 to 10,000 pounds to the fuel cartridge insulation liner flange. Twenty-nine fuel cartridges and liners were removed in this manner. An additional 30 fuel cartridges were tried with this method, but the insulation liner flange broke away at a force of 10,000 pounds. The next approach to removing fuel was to cut moderator aft casing off and then to pull the support tube with fuel through the forward end of the cell. This method proved unsuccessful because the moderator cells cracked. The cracking was caused by the decreasing diameter of the moderator toward the forward end of the

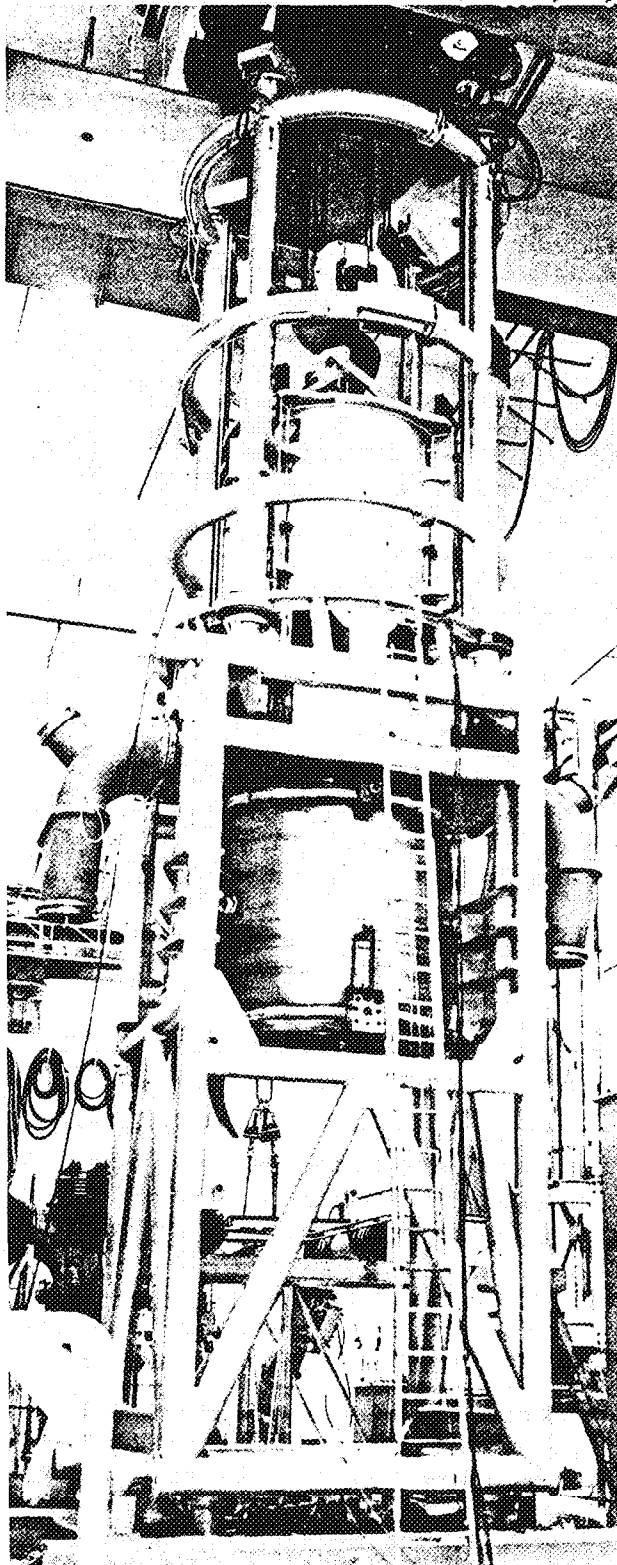


Fig. 73 - Upending fixture in vertical position with core-removal fixture on top

cell. The next method was to pull fuel cartridges and liners out the rear of the cell by first cutting off the front casing and removing the moderator support tube, insulation liner, and cartridges as a unit. This operation proved satisfactory for removal of the remaining fuel cartridges and insulation liners.

Figure 75 presents a core disassembly survey that summarizes the disassembly of the power plant.

#### Damage to the Power Plant

The damage sustained by the power plant is confined entirely to the reactor core and limited mainly to the fuel cartridges and insulation liners, moderator cells, control rods, and control rod guide tubes.

#### Fuel Cartridge and Liner Damage

Inspection of the fuel cartridges that were removed from the moderator cells shows that melting and collapsing of the fuel elements was confined to stages 4 through 16. Fuel cartridge SN 1060 was removed from cell 273, which is in the outside circle of moderator cells. These cells produce about 7 percent less than the average total tube power and are representative of the lowest-power cells. The radial orientation (in degrees) indicated on the photographs is clockwise rotation from the "0" point (vertical centerline), looking downstream through the cartridge. Figure 76 shows the over-all fuel cartridge damage. The meltdown and chemical oxidation damage to stages 4, 5, and 6 of the fuel cartridge is clearly shown in Figure 77. The almost complete meltdown and oxidation of stage 5 is shown in Figure 78. Meltdown damage to stages 7, 8, and 9 is shown in Figure 79. Damage to stages 10 through 16 is shown in Figures 80 and 81. The meltdown

UNCLASSIFIED

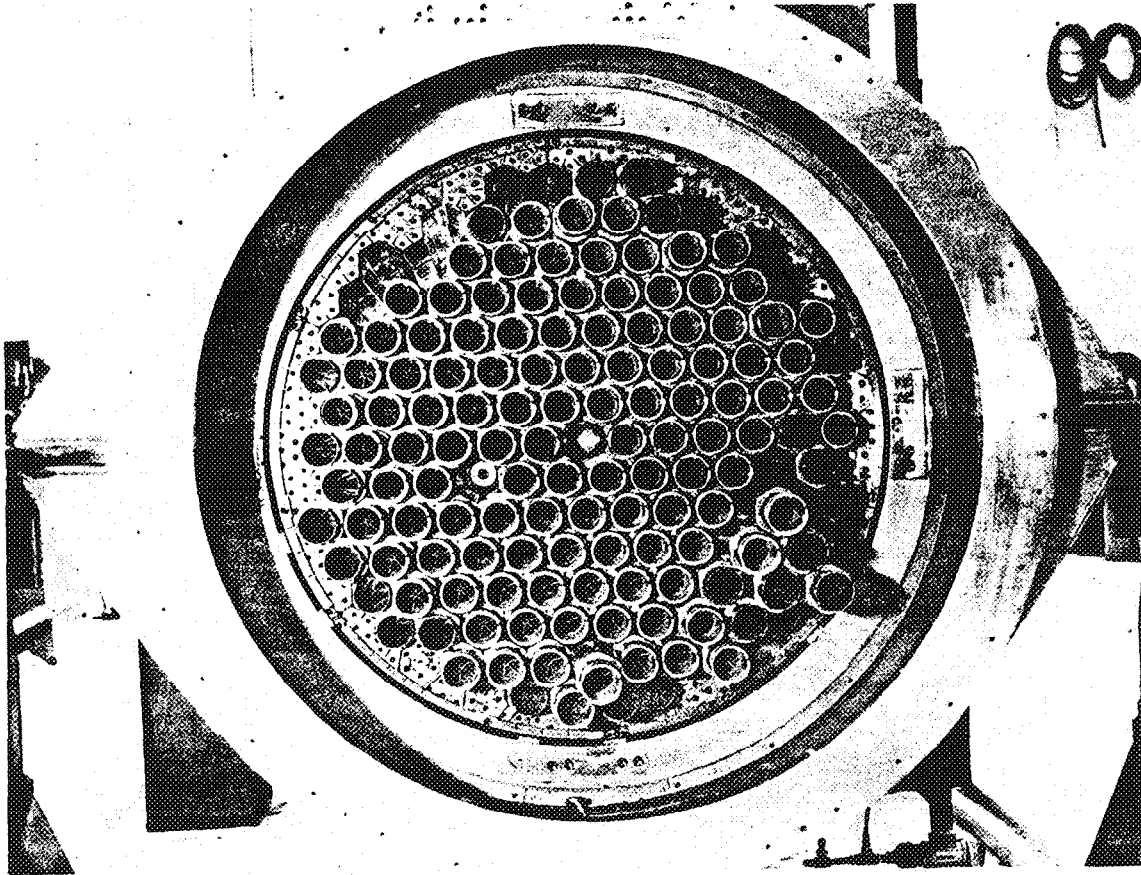


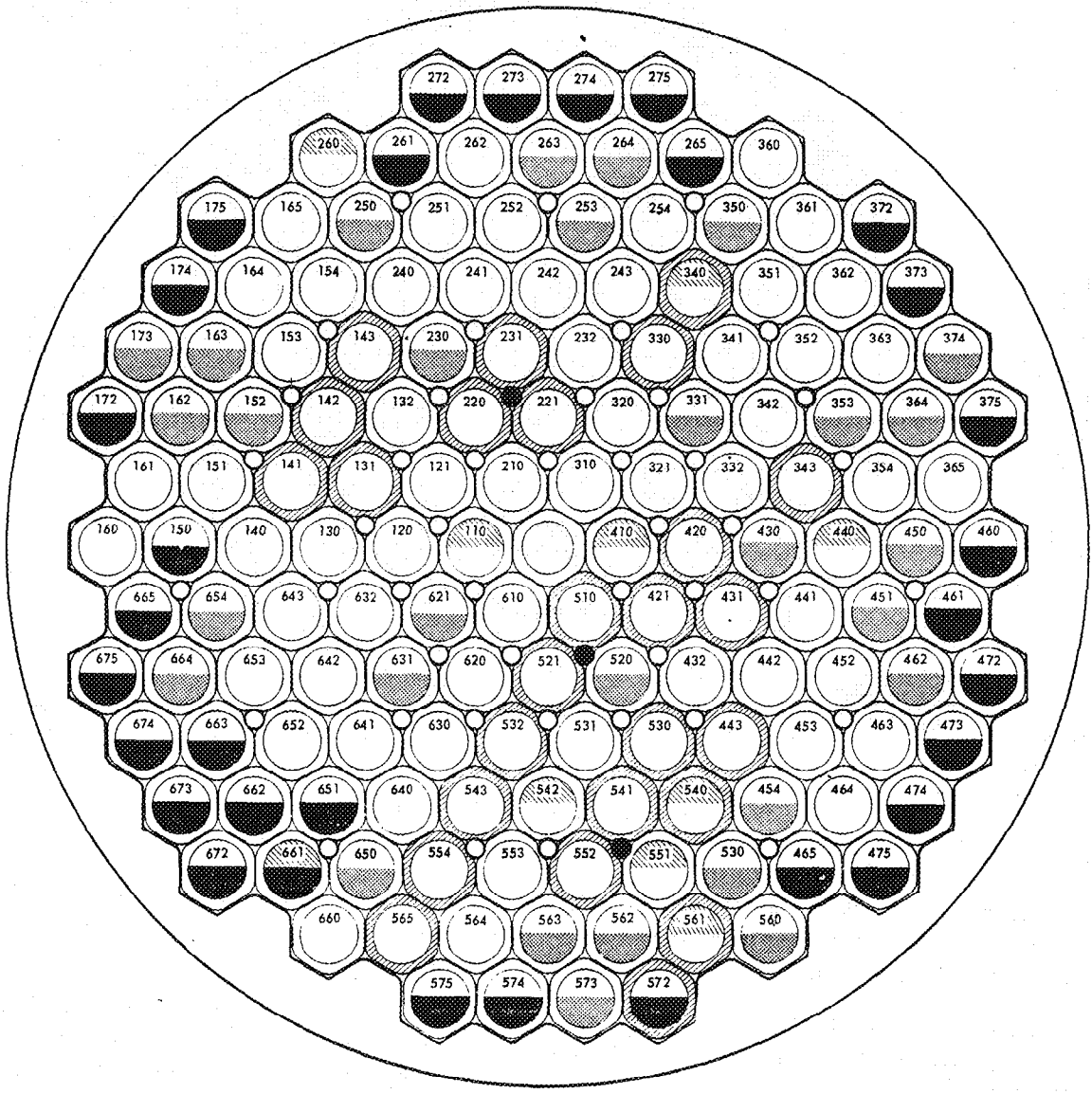
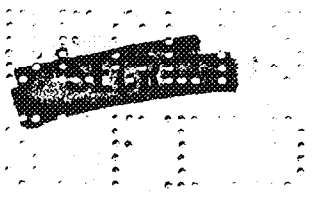
Fig. 74 -- Moderators exposed after removal of rear tube sheet

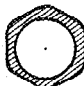
of stage 12 is shown in Figure 82. The 19th stage, which did not reach a temperature level as high as stages 4 through 16, is shown in Figures 83 and 84 to have sustained relatively little damage.


This series of photographs shows that the greatest damage is in stages 4, 5, and 6. An explanation for this is that more chemical oxidation occurred in these stages than in stages 7 through 16. Chemical analysis of the molten material obtained from stages 4 and 5 verifies that chemical oxidation did occur in these stages. Figure 85 shows the downstream face of stage 3 and indicates some damage to this stage. Stage 4, shown in Figure 86, shows the meltdown of the outer ring and the 180-degree position (the lower side of the fuel cartridge when installed in the core). Another view of stage 4 at the 0-degree position is shown in Figure 87.


Another example of cartridge damage was obtained from cell 510, which is located in the innermost circle of moderator cells. These cells produce 7 percent above average total tube power and are representative of the highest-power cells. The total damage to this fuel cartridge is shown in Figure 88. Stages 1, 2, and 3, shown in Figure 89, appear to have sustained little or no damage. Figure 90 shows the meltdown and chemical oxidation damage in stages 4, 5, and 6. Figures 91, 92, and 93 show the damage that occurred to stages 7 through 15. The meltdown and possible chemical oxidation damage appear to be greater than the damage to the same stages in Cell 273 (Figures 79, 80, and 81). The damage sustained in stages 16 through 19 is shown in Figures 94 and 95.


UNCLASSIFIED

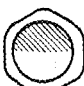



- 

Moderator blocks with surface burned spots
- 

Unable to extract fuel elements
- 

Fuel elements extracted with maximum load of 1500 lb
- 

Fuel elements extracted with minimum load of 1500 lb
- 

Scram circuit thermocouple on 19th stage of fuel element
- 

Control rods fused to guide tubes

Fig. 75 - Core damage survey

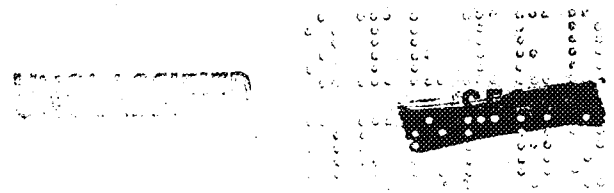
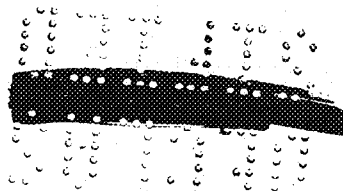




Fig. 76 - Over-all damage to fuel cartridge 1060, cell 273



Fig. 77 - Damage to stages 4, 5, and 6, cartridge 1060, cell 273



UNCLASSIFIED

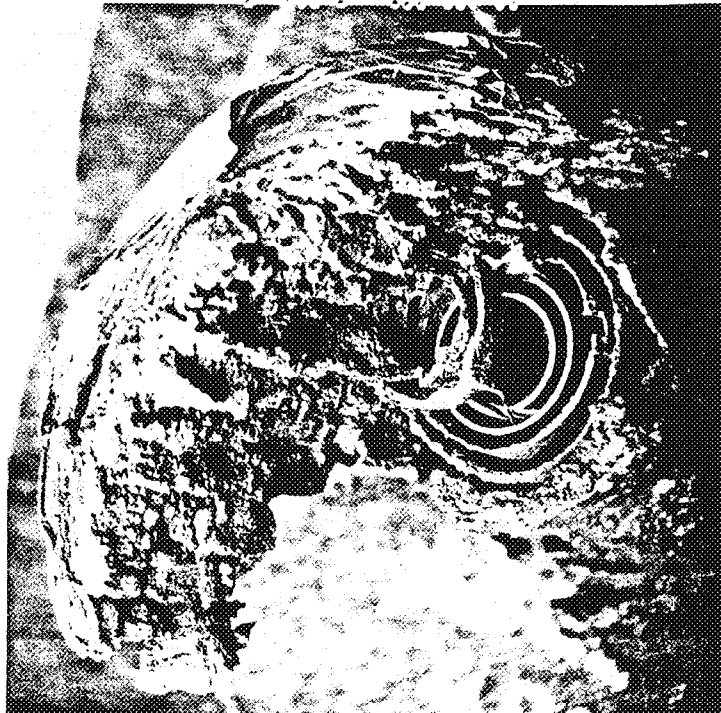
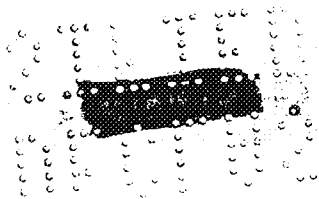


Fig. 78 - Meltdown and oxidation of stage 5, cartridge 1060, cell 273



Fig. 79 - Damage to stages 7, 8, and 9, cartridge 1060, cell 273

UNCLASSIFIED



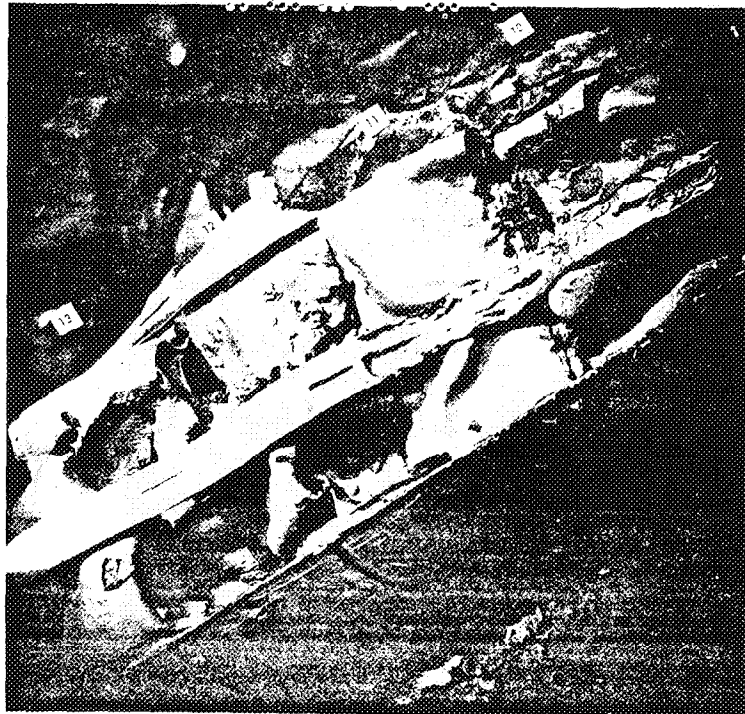


Fig. 80 - Damage to stages 10, 11, 12, and 13, cartridge 1060, cell 273

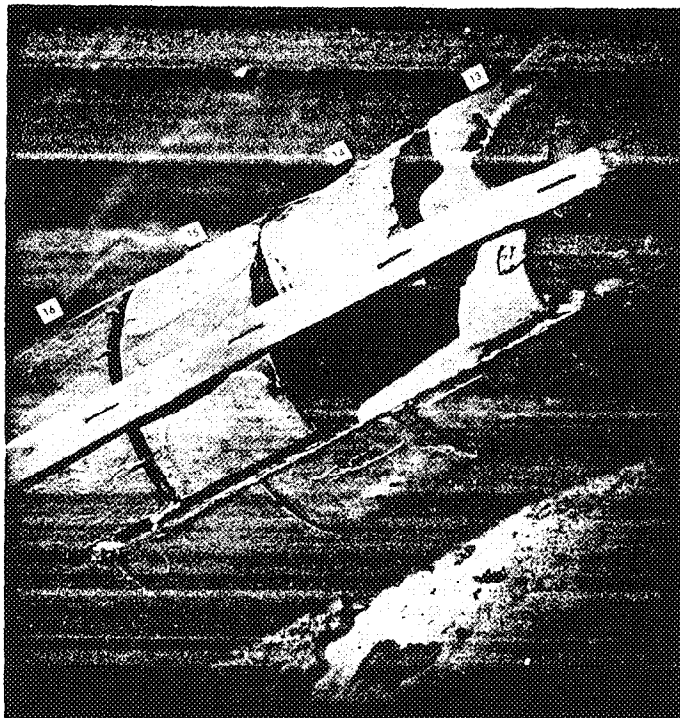


Fig. 81 - Damage to stages 13, 14, 15, and 16, cartridge 1060, cell 273

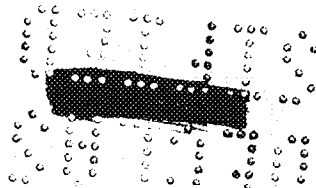






Fig. 82 - Upstream face of stage 12, cartridge 1060, cell 273

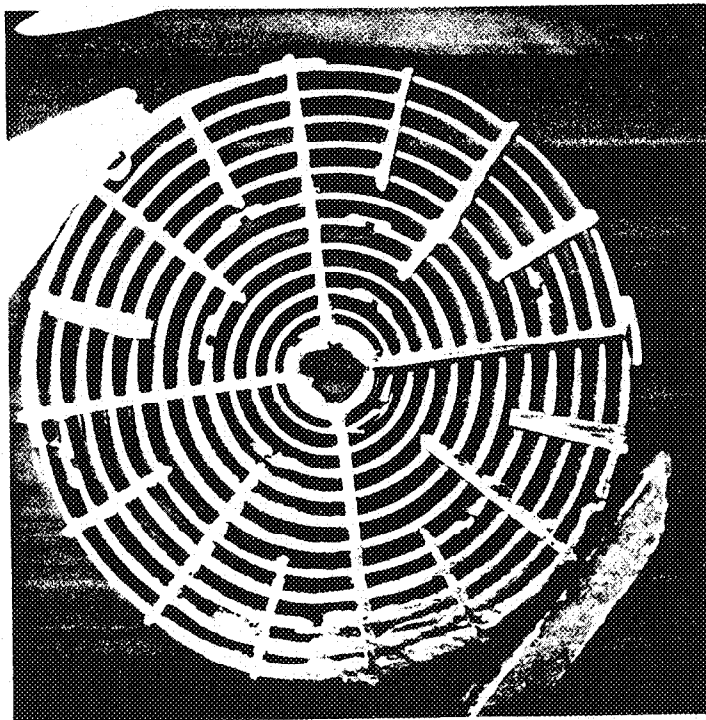
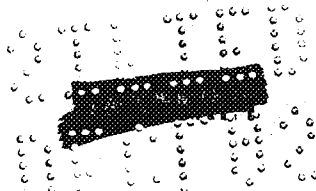


Fig. 83 - Upstream face of stage 19, cartridge 1060, cell 273



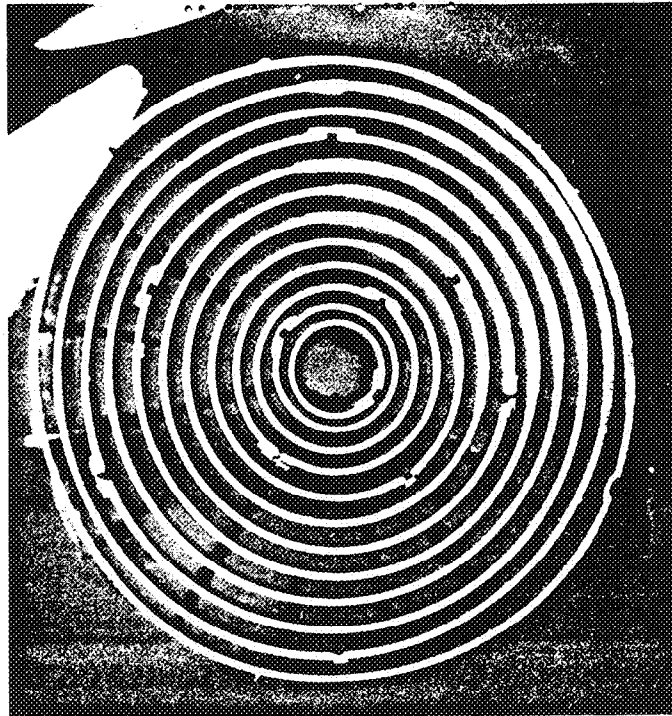
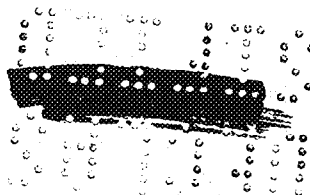


Fig. 84-- Downstream face of stage 19, cartridge 1060, cell 273



Fig. 85-- Downstream face of stage 3, cartridge 1060, cell 273



UNCLASSIFIED



Fig. 86 - Upstream face of stage 4, cartridge 1060, cell 273

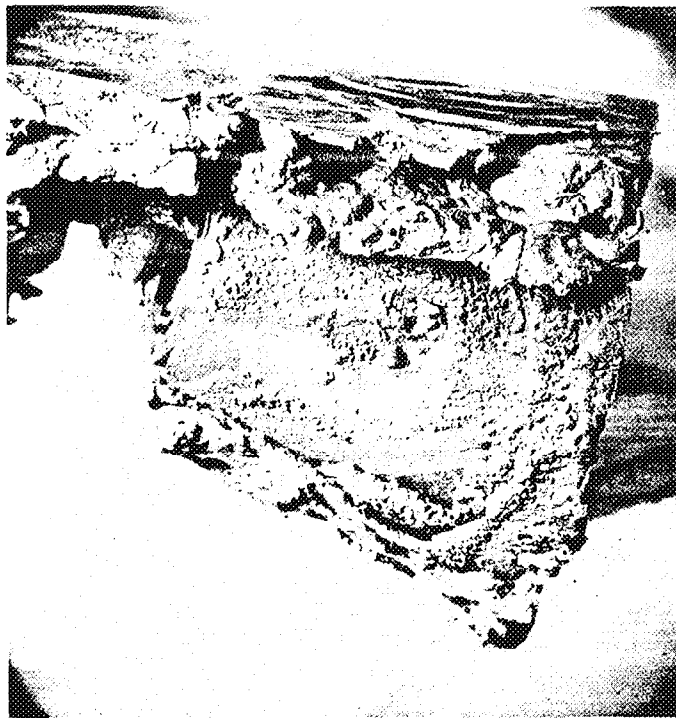


Fig. 87 - Stage 4 at 0-degree position

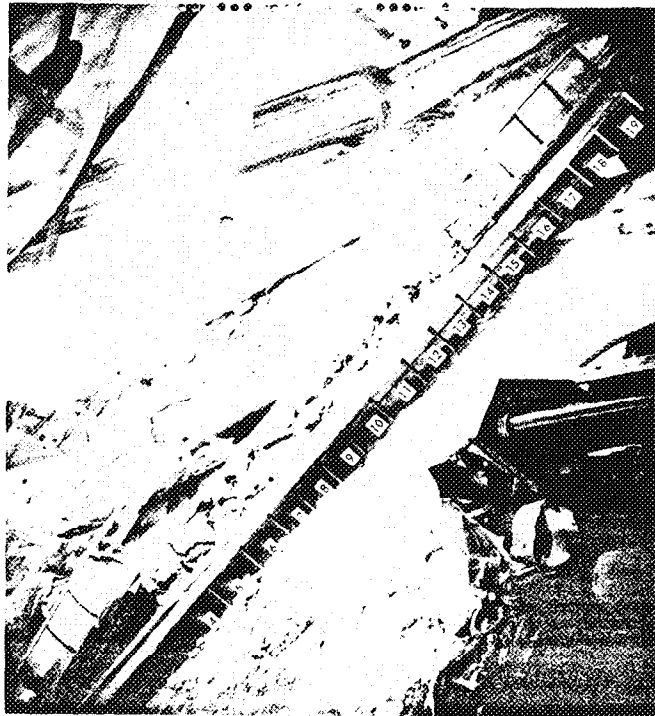


Fig. 88 - Overall damage to fuel cartridge 1129, cell 510

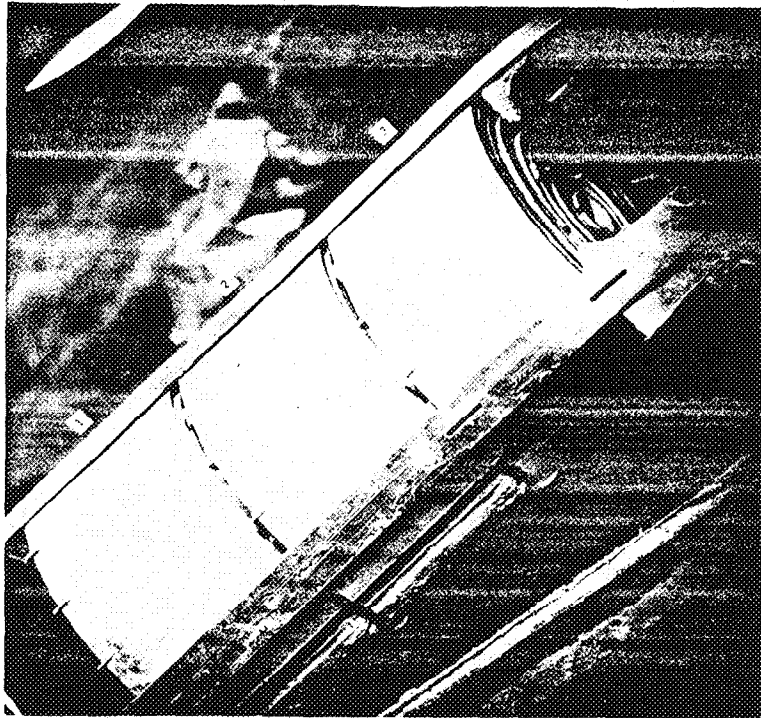


Fig. 89 - Stages 1, 2, and 3, cartridge 1129, cell 510



Fig. 90 - Stages 4, 5, and 6, cartridge 1129, cell 510



Fig. 91 - Stages 7, 8, and 9, cartridge 1129, cell 510



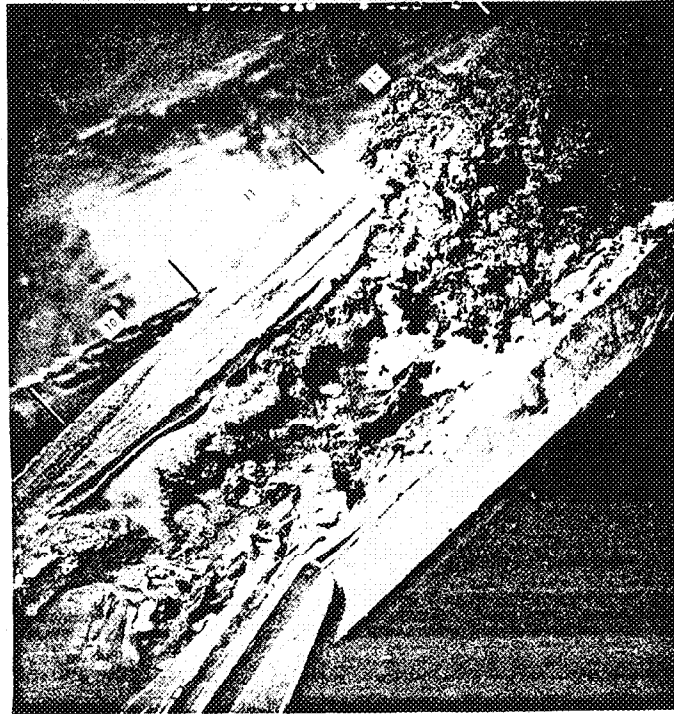


Fig. 92 - Stages 10, 11, and 12, cartridge 1129, cell 510



Fig. 93 - Stages 13, 14, and 15, cartridge 1129, cell 510

UNCLASSIFIED

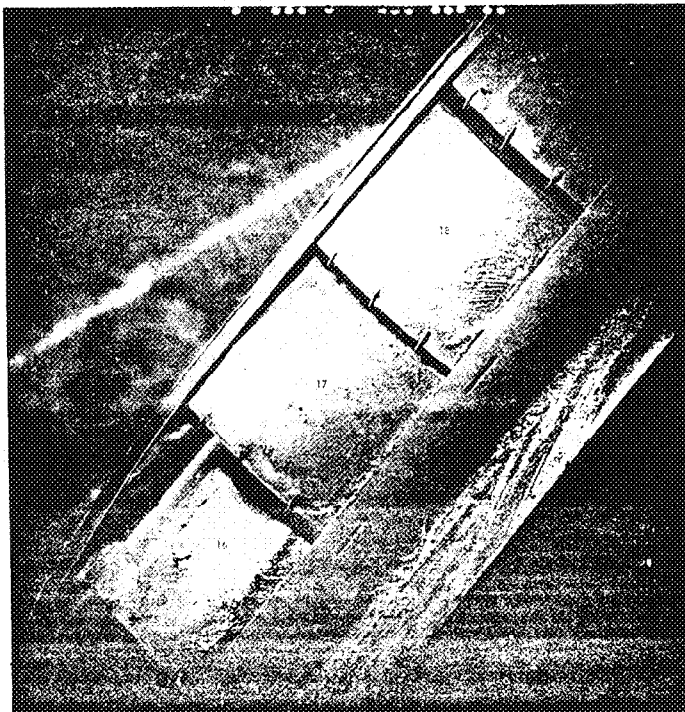
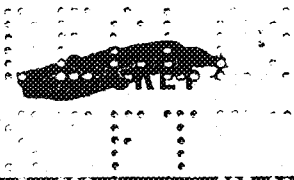


Fig. 94 - Stages 16, 17, and 18, cartridge 1127, cell 510

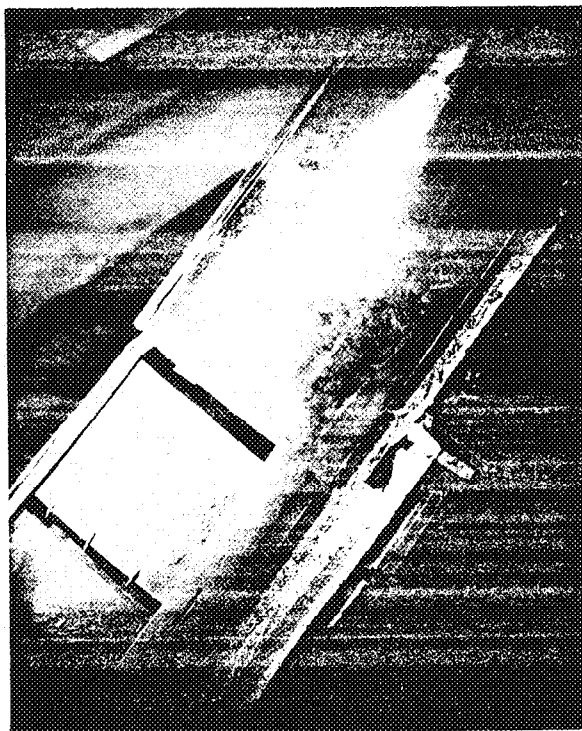
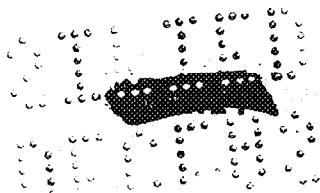


Fig. 95 - Stage 19 and tail cone, cartridge 1129, cell 510

UNCLASSIFIED



An example of ring deformation in the 19th stage is evident in Figure 96. This deformation is typical for approximately 35 fuel cartridges.

All fuel cartridges and liners removed from the core were burned, wrinkled, and bowed, as exemplified in Figure 97.

To date only a few liners have been removed from their fuel cartridges in the Radioactive Materials Laboratory (RML). A summary of the data obtained on these fuel cartridges is given in Table 9.

Examination of fuel cartridges 273 and 510, one from the outside and one from the center of the core, shows that fuel cartridge damage was extensive and was distributed generally throughout the reactor.

TABLE 9  
DAMAGE TO FUEL CARTRIDGES AND LINERS  
DETERMINED IN RADIOACTIVE MATERIALS LABORATORY

Tube No.	Cell No.	Stages Good	Stages Deformed or Melted	Comments
1060 A	273	1, 2, 3, 17, 18, 19	4 through 16	Stages 4 and 5 show greatest damage
1046 B	575		4 through 16	Stages 4 and 5 show greatest damage
1115 A	231	Similar to 1060 A	4 through 16	Control rod guide tube welded on at stages 10 and 11
1019 B	541	Similar to 1060 A	4 through 16	Control rod guide tube welded on at stages 10 and 11
1129 A	510	Sagging center rings - Stage 19	4 through 16	Control rod guide tube welded on at stage 11
1093 AS	420	Similar to 1129 A	4 through 16	Control rod guide tube welded on at stages 10 and 11
1043 AS	421	Similar to 1129 A	4 through 16	Holes burned in top of block from adjacent cell

#### Scram Circuit Thermocouple Investigation

At the time of the event, 10 thermocouples that were attached to fuel element plates were being monitored on the 10 high-temperature control room Brown recorders. These thermocouples made up the fuel element high-temperature scram circuit. The thermocouples and their scram temperature settings are listed in Table 6.

To date seven of these fuel element scram circuit thermocouples have been inspected. Because of the method used in disassembly of these moderator cells containing fuel elements (Cell No. 110, 410, 440, 542, 551, 260, and 661), the exact cause of what happened to these scram circuit thermocouples was not determined. The thermocouple lead wire on cell 661 was cut in two during the removal of the fuel cartridge from the moderator cell; consequently, a valid resistance reading was not obtained. However, visual inspection of this cartridge revealed that one of the lead wires was fused to a fuel element plate at stage 10. Figure 98 shows photographic information on fuel element thermocouples in cells 661 and 410. The fused thermocouple lead was noted where the leads pass beneath



UNCLASSIFIED

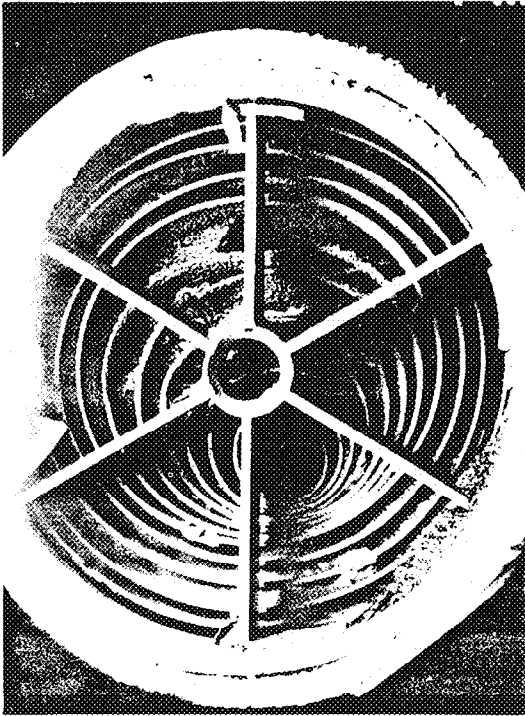


Fig. 96 - Typical ring deformation at 19th stage, downstream face

some fuel element material at stage 10. The lead wire sheath for this 19th-stage thermocouple was also noted to be badly charred at the sixth, seventh, and eighth stages. The thermocouple lead bead and shield appeared to be in satisfactory condition (see cell 661-19th stage photograph in Figure 98).

The fuel cartridge in cell 410 sustained extreme melting at stages 9, 10, 11, and 19. This melting can be noted in Figure 98. The 19th-stage leading edge where the thermocouple lead wires entered the stage as well as the entire stage sustained a high degree of meltdown. Because of the meltdown damage the lead wire could not be traced along the entire length of the cartridge.

The scram circuit thermocouple in cells 110, 542, and 551 all read infinite resistance, indicating that the leads are broken but not grounded at the time of writing this report.

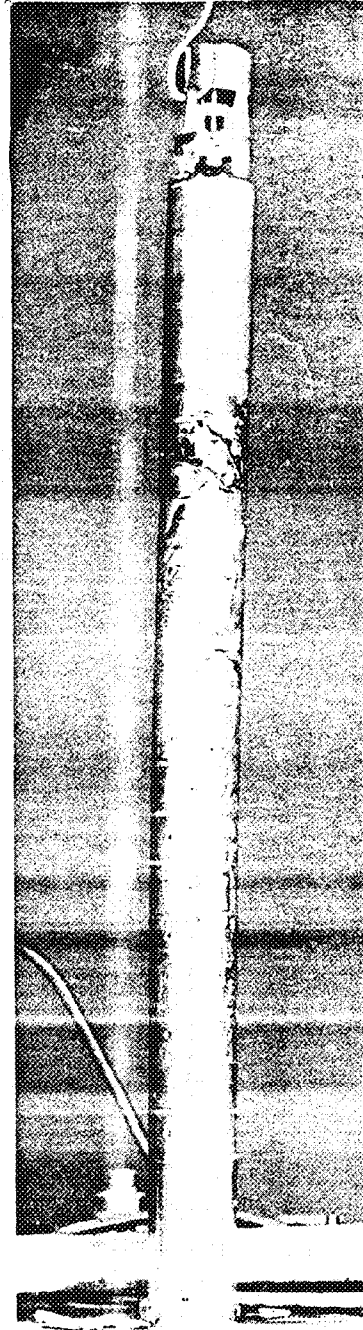
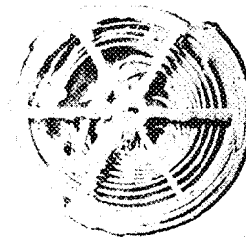
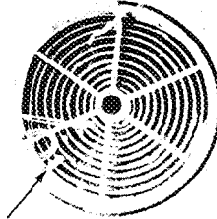


Fig. 97 - Example of burning, wrinkling, and bowing of fuel cartridges and liners

UNCLASSIFIED

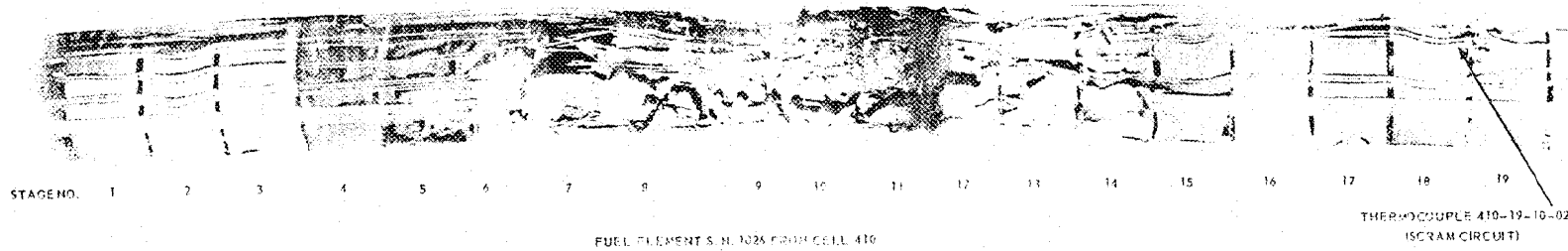


FUEL ELEMENT 1026 CELL 410 STAGE 19  
LOOKING THROUGH TAIL PIECE



FUEL ELEMENT 1999 CELL 661 STAGE 19  
LOOKING THROUGH TAIL PIECE

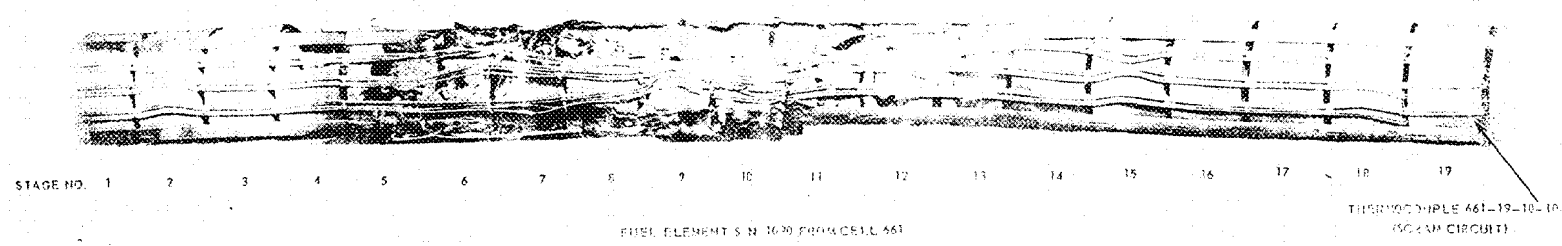
661-19-10-10  
THERMOCOUPLE



STAGE NO. 1 2 3 4 5 6 7 8 9 10 11 12 13 14 15 16 17 18 19

FUEL ELEMENT S. N. 1026 FROM CELL 410

THERMOCOUPLE 410-19-10-02  
(SCRAM CIRCUIT)



STAGE NO. 1 2 3 4 5 6 7 8 9 10 11 12 13 14 15 16 17 18 19

FUEL ELEMENT S. N. 1670 FROM CELL 661

THERMOCOUPLE 661-19-10-10  
(SCRAM CIRCUIT)

Fig. 98 - Fuel cartridges from cells 410 and 661 showing fuel element thermocouples

UNCLASSIFIED

UNCLASSIFIED

The photographs of these cells as well as the photographs of cells 440 and 260 have not been analyzed. It should be pointed out that it is impossible to determine whether these thermocouples were damaged during disassembly.

Of the 10 thermocouples to be examined, three have not been inspected. The fuel cartridges to which these thermocouples are attached are still contained in their respective moderator cells (cells 340, 540, and 561). Resistance readings have been obtained on these thermocouples. All three of these read zero resistance, indicating possible fusing of the leads to a common ground.

#### Damage to Moderator Cells

Inspection of the moderator cells revealed that:

1. 74 moderator cells will be re-usable.
2. 16 moderator cells have minor defects, such as hairline cracks.
3. 60 moderator cells have cracks, were broken during handling, or were split open to remove the fuel cartridges.

Examination of the moderator cells upon removal from the core revealed visible external damage to 28 cells. The moderator damage is in the form of burn spots, as shown in Figures 99 and 100. A cross section of the burn spots appearing on moderator cell 421 is shown in Figure 101. These slices of the moderator cell were cut to obtain hydrogen migration samples.

During the event several control rod guide tubes were fused to moderator cells. Figures 102, 103, and 104 show typical examples of this damage. An example of the fused control rod, moderator, liner, and fuel cartridges is shown in Figure 105. These examples were all obtained from moderator cell 510.

Detailed inspection of 22 moderator cells after the removal of the fuel elements revealed misshapen support tubes and some blisters in the bottom inside surface of the support tube. These blisters may have been caused by the melting and collapsing of the fuel element. Of intact moderator cells inspected to date, all show upward bowing at the longitudinal center of the cell of from 0.008 to 0.051 inch, with an average bowing of 0.012 inch.

#### Damage to Control Rod Guide Tubes

Before removal of the power plant from the IET, a boroscope inspection was made on 44 control rod guide tubes. Three control rods were fused to their guide tubes, and the source rods were not inspected. The examination revealed extensive damage to guide tube 420, which had a break in the wall of the tube through which a small quantity of molten material had flowed. All other control rod guide tubes showed varying degrees of scoring from rod motion and heat discoloration. A dimensional inspection indicated that all salvaged tubes were within tolerance except for one that showed a bow of 0.050 inch. Thirty-three tubes were salvageable.

#### Damage to Front Tube Sheet, Rear Tube Sheet, and Reflector

No visible damage that can be attributed to the incident was noted on the front and rear tube sheets or reflector. Only normal heat discoloration on the inside walls of the reflector and on the rear tube sheet was evident (see Figure 106). Some damage occurred to the instrumentation on the front tube sheet during disassembly and will require shop rework.

#### Front and Rear Plug Shield, Primary Shield, Combustor, and Aft Header

No visible damage was sustained during the event by the front and rear plug shields, primary shield, combustor, and aft header. Figure 107 shows the aft face of the front

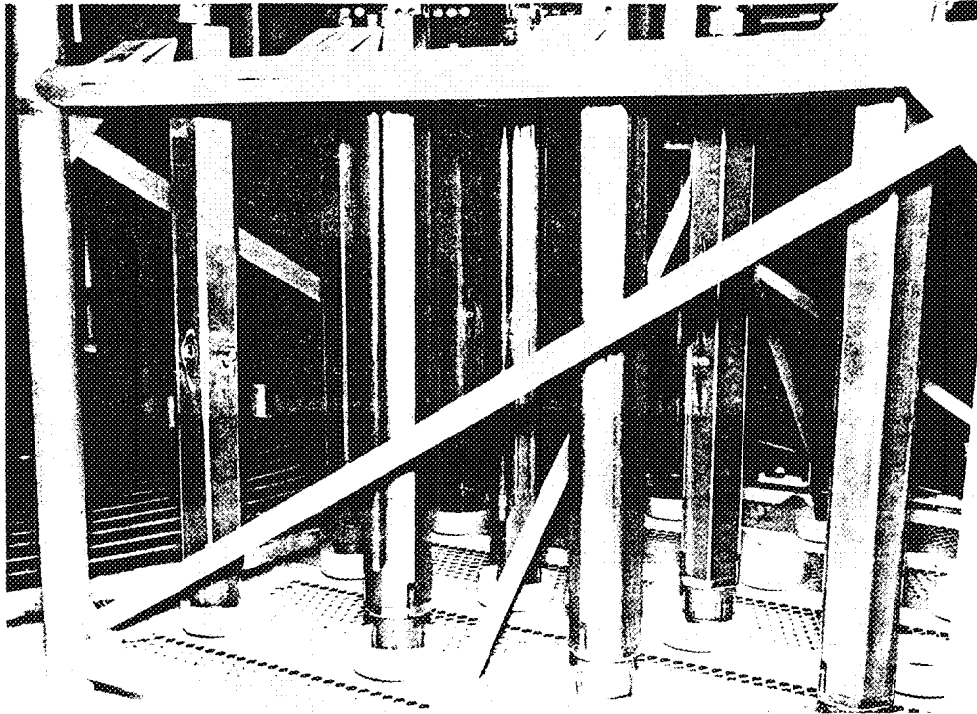
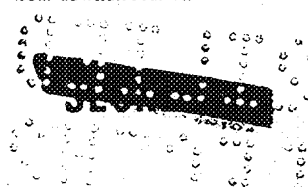


Fig. 99 - Moderators in storage rack showing burn spots



Fig. 100 - Moderator from cell 421 showing burn hole approximately 14 inches from downstream end



UNCLASSIFIED

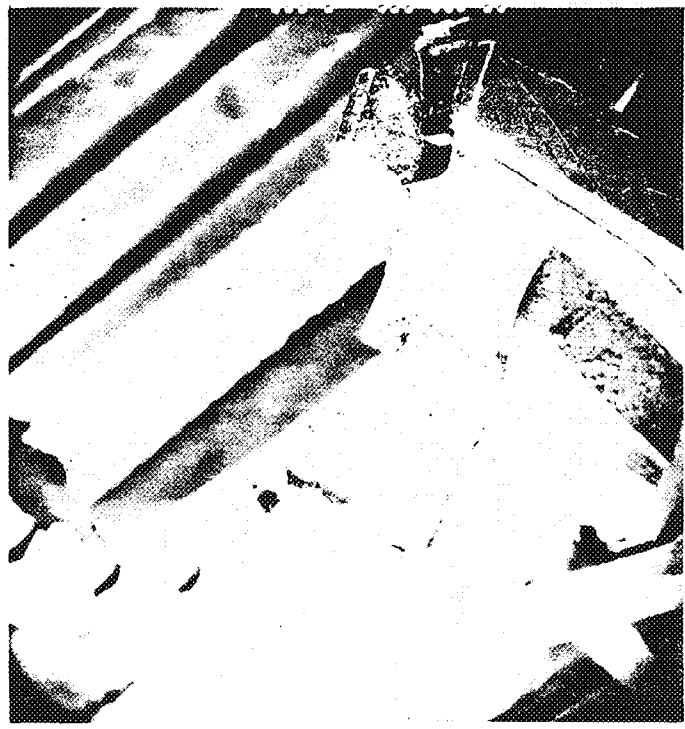


Fig. 101 - Cross section of moderator showing melting and burning damage

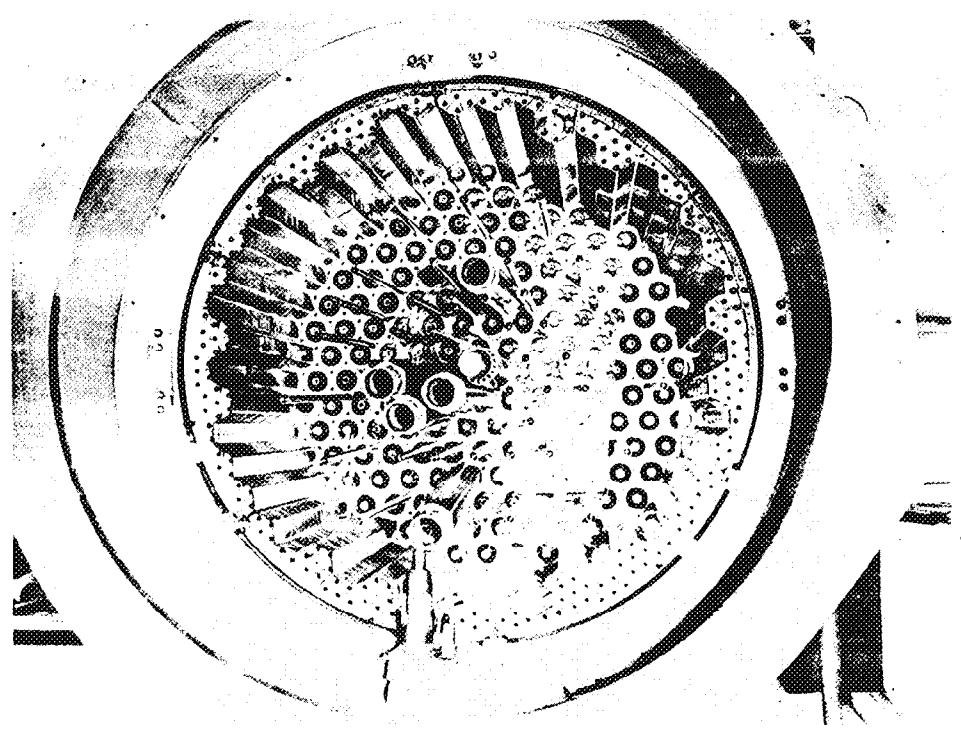
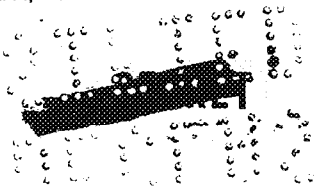


Fig. 102 - Reactor core showing five moderator blocks welded to control rod guide tubes, View A



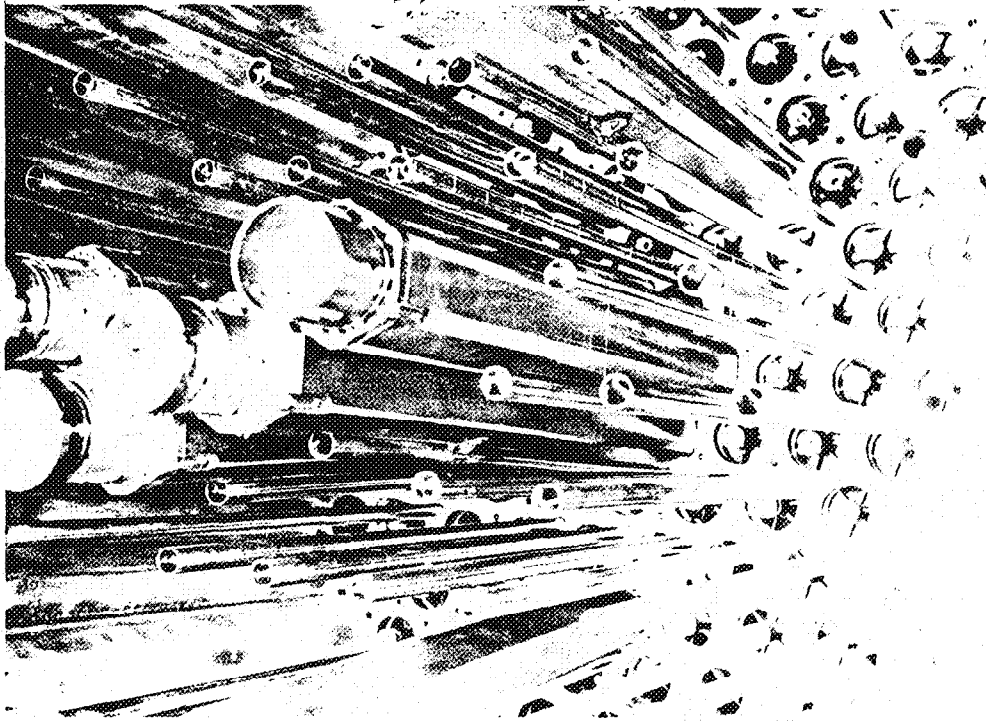


Fig. 103 - Reactor core showing five moderator blocks welded to control rod guide tubes, View B

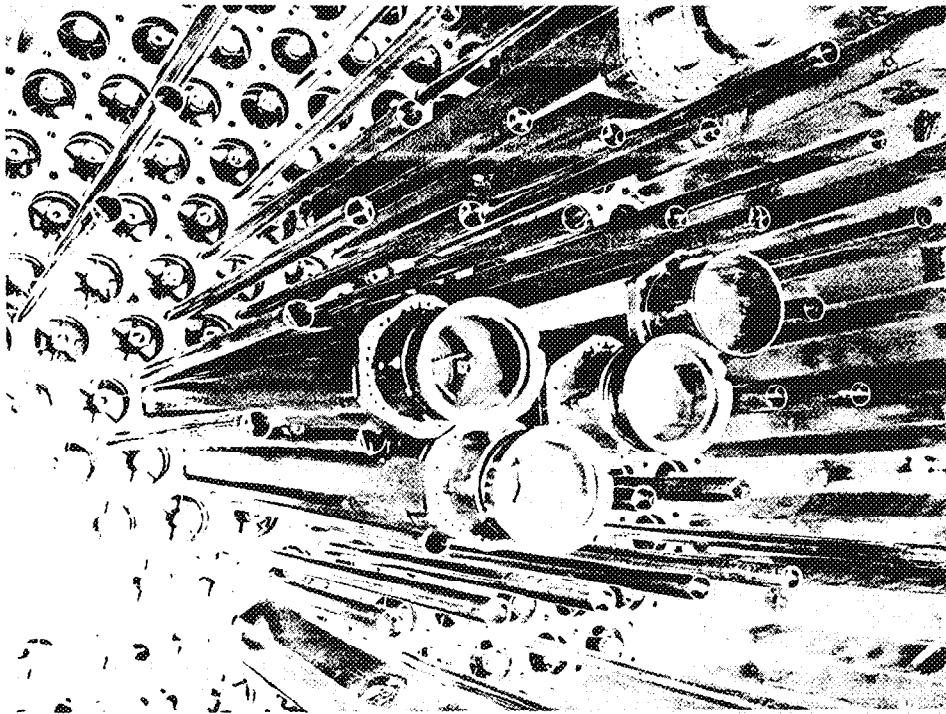


Fig. 104 - Reactor core showing five moderator blocks welded to control rod guide tubes, View C

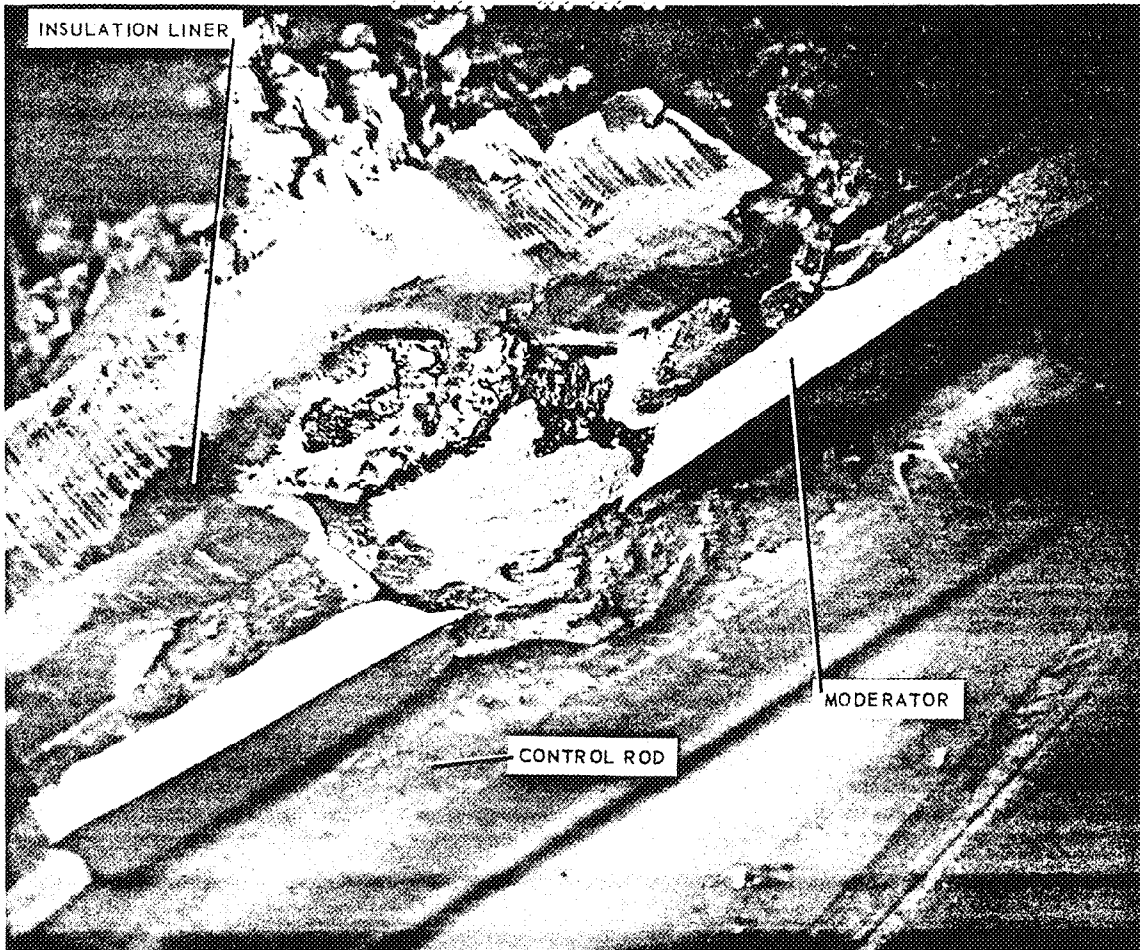


Fig. 105-- Fused control rod and fuel cartridge, cell 510, with moderator removed

plug shield. Figure 108 shows the rear plug shield. Some foreign material was noted in the plenum aft of the core and can be noted in Figure 109. Figure 110 shows a view of the combustor. Figure 111 shows the aft header. The foreign material noted in the combustor and aft header was determined to be the remains of the aft-plug shielding measurement devices; that is, copper foils, aluminum and cadmium cover, and sulfur pills. One section of insulation material in the rear-plug shield will be replaced because of damage caused by the melted aft-plug measurement devices.

## 5.2 HYDROGEN MIGRATION

Metallographic examination of one moderator block showed a uniform microstructure with no indication of mechanical failure.

Hydrogen migration samples have been obtained on cell 421. The moderator cell was sectioned into seven equally spaced transverse slices, each 0.5 inch thick. Figure 112 shows the sectioning of moderator cells. A slice (0.5 inch) was taken from each end,

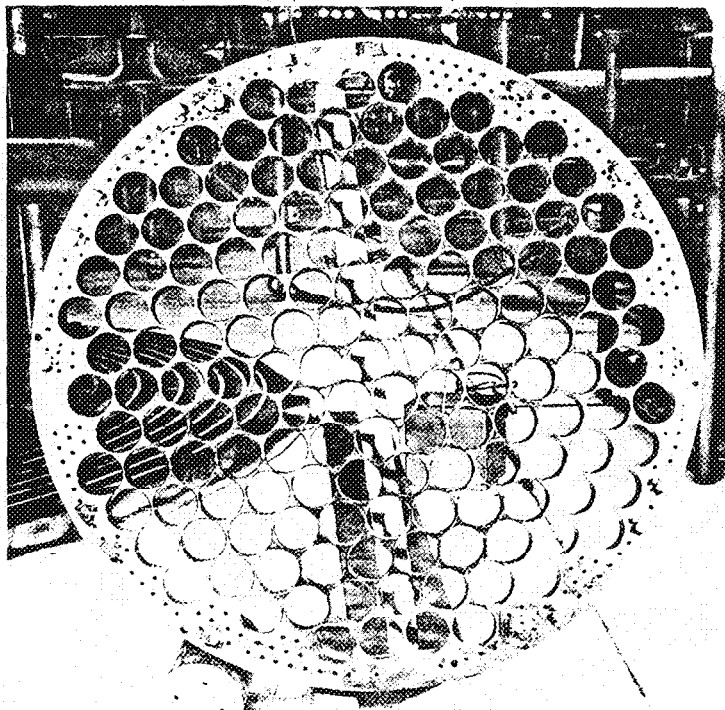
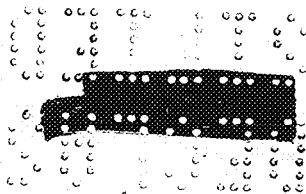


Fig. 106 - Rear tube sheet, upstream face



Fig. 107 - Aft face of front plug shield





UNCLASSIFIED

~~SECRET~~

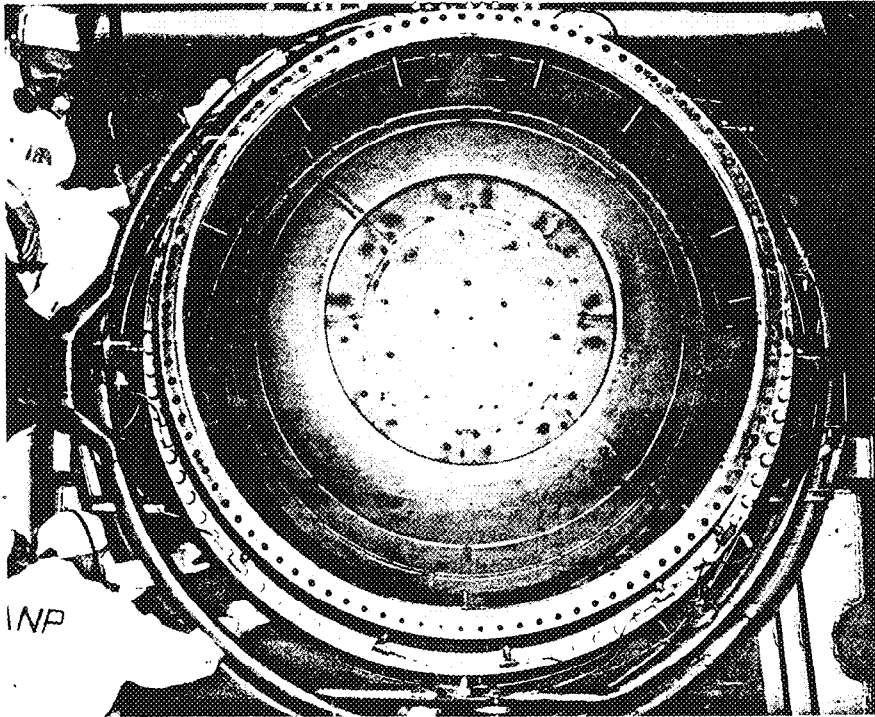


Fig. 108 - View of rear plug looking upstream

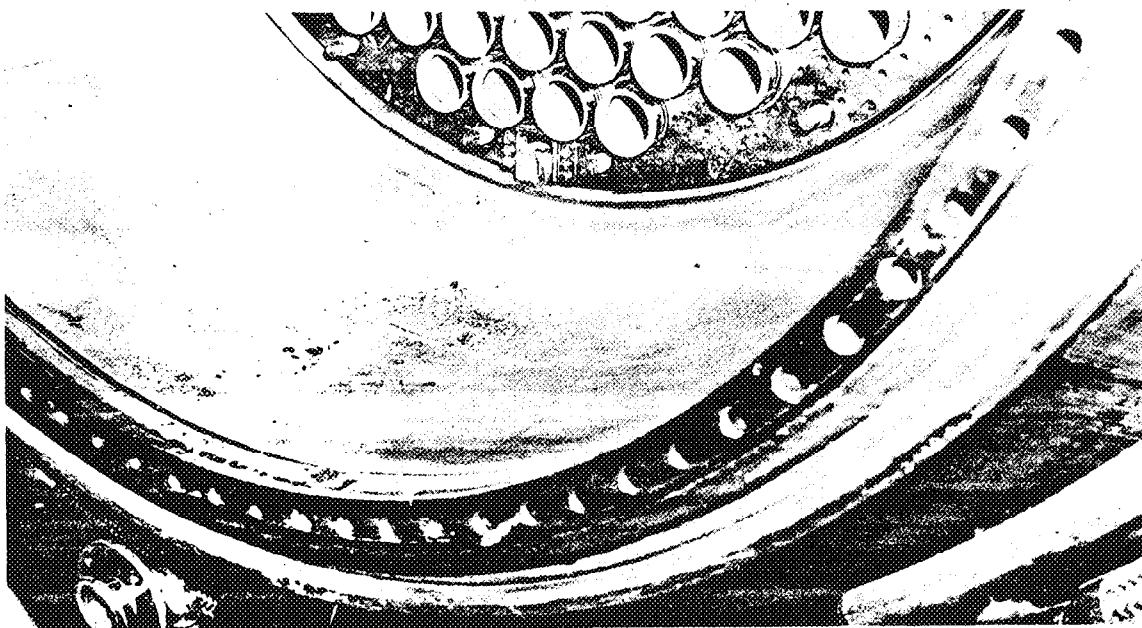


Fig. 109 - Deposits at bottom of primary shield

~~SECRET~~

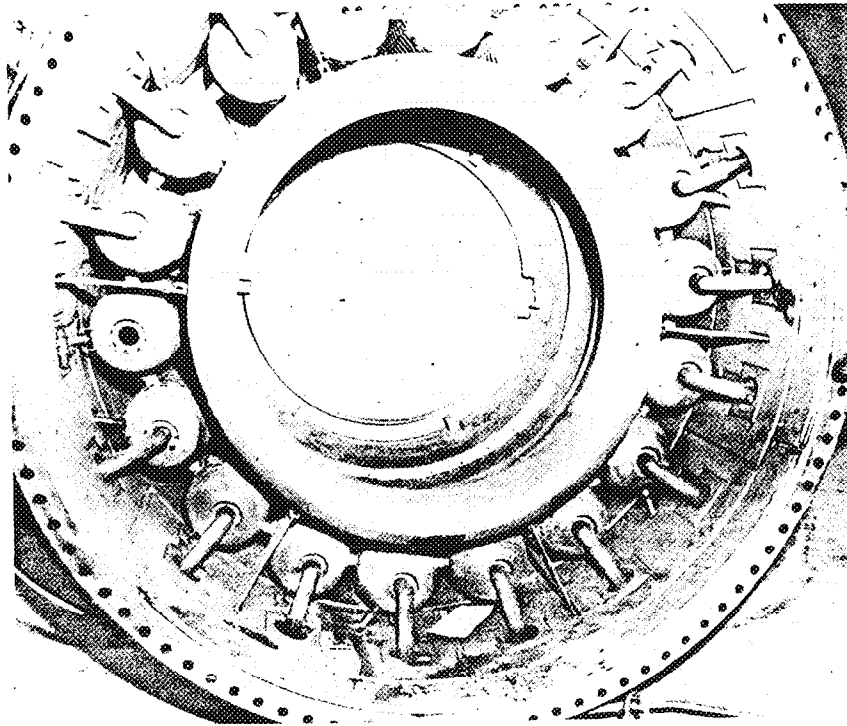


Fig. 110 - Unit combustor

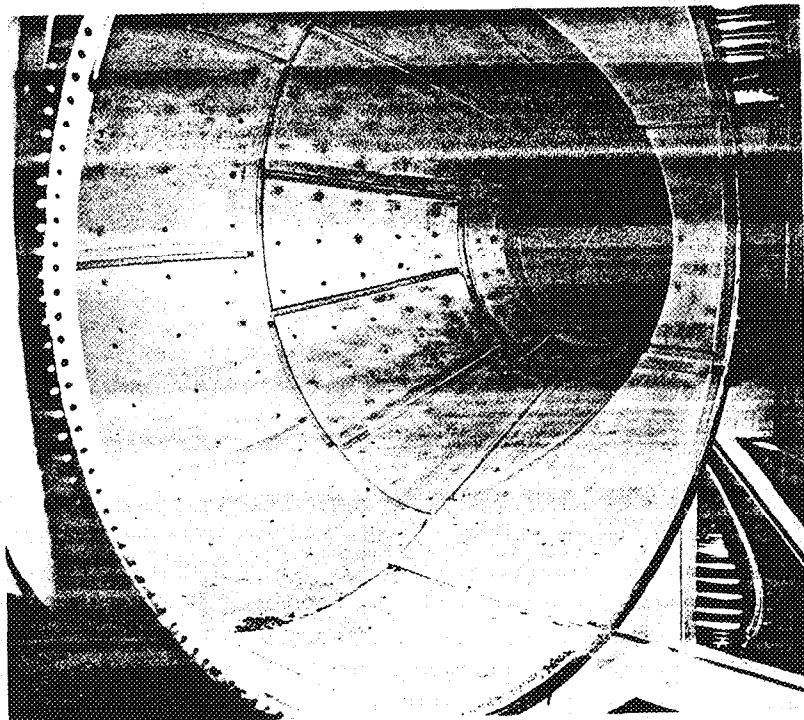
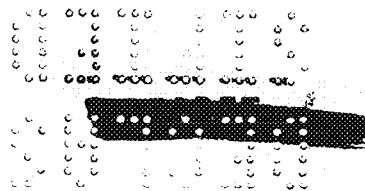


Fig. 111 - Aft header



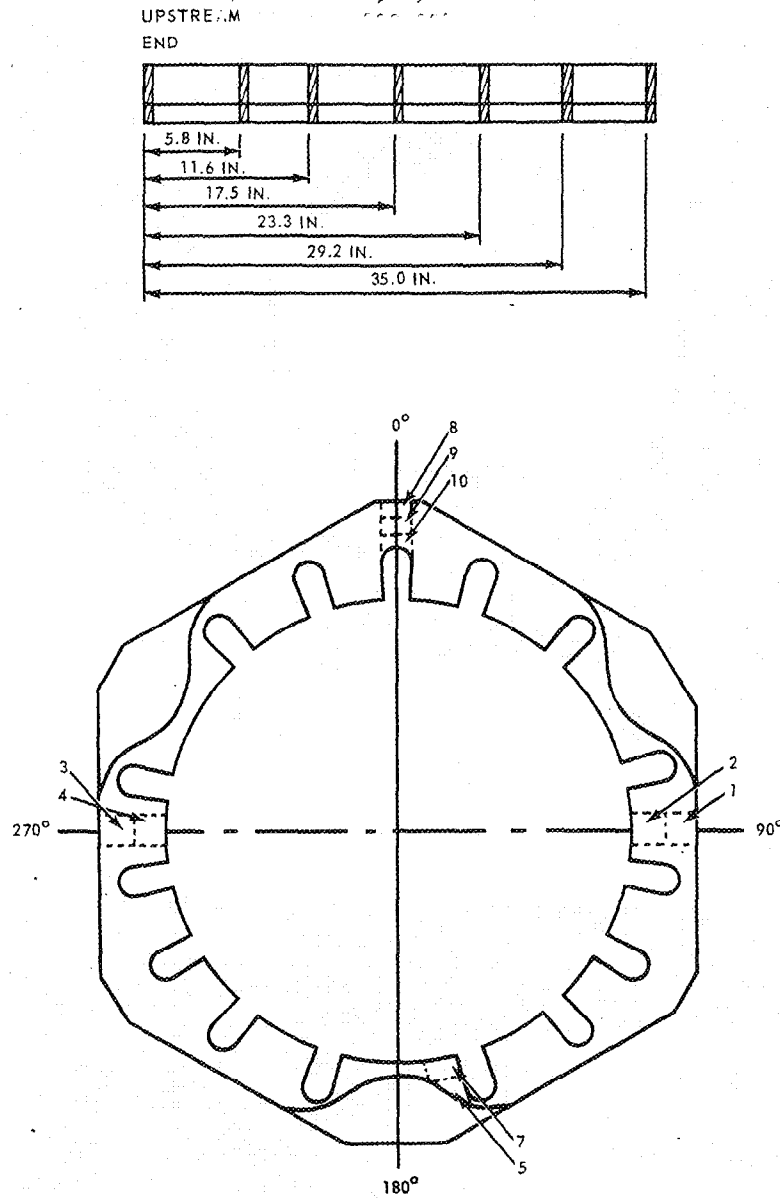


Fig. 112 -- Sectioning of moderator block for hydrogen migration sampling

and the remaining five slices were equally spaced. Nine representative samples were obtained from each of the seven slices and analyzed for hydrogen content. As a close check on the hydrogen migration sampling technique, every fifth sample was an Evendale standard sample of known hydrogen content. The accuracy of these measurements was  $\pm 4.5$  percent of the percentage value for the hydrogen content in the moderator cell. Figures 113 and 114 show the results obtained. On Figure 113, for comparison, data are included from analysis performed on the Insert 1c (D101-C3) moderator. This moderator cell had an  $N_H$  value of 3.00 or 0.82 percent by weight. The present analysis indicates deviation from the nominal initial values that only slightly exceeded experimental uncertainty.

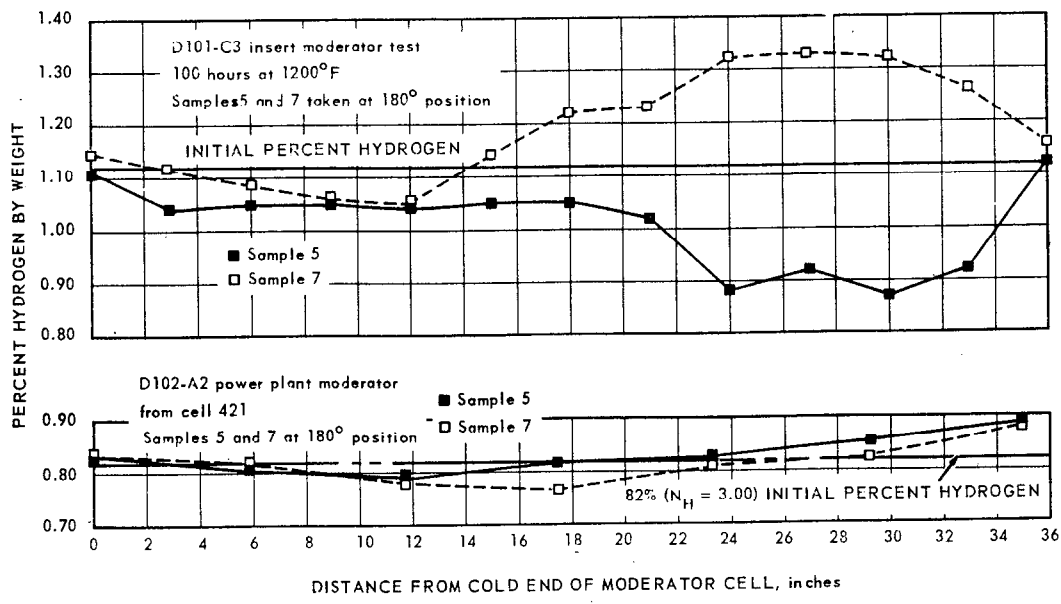


Fig. 113 - Comparison of hydrogen migration in D102A core with D101C-3 insert samples

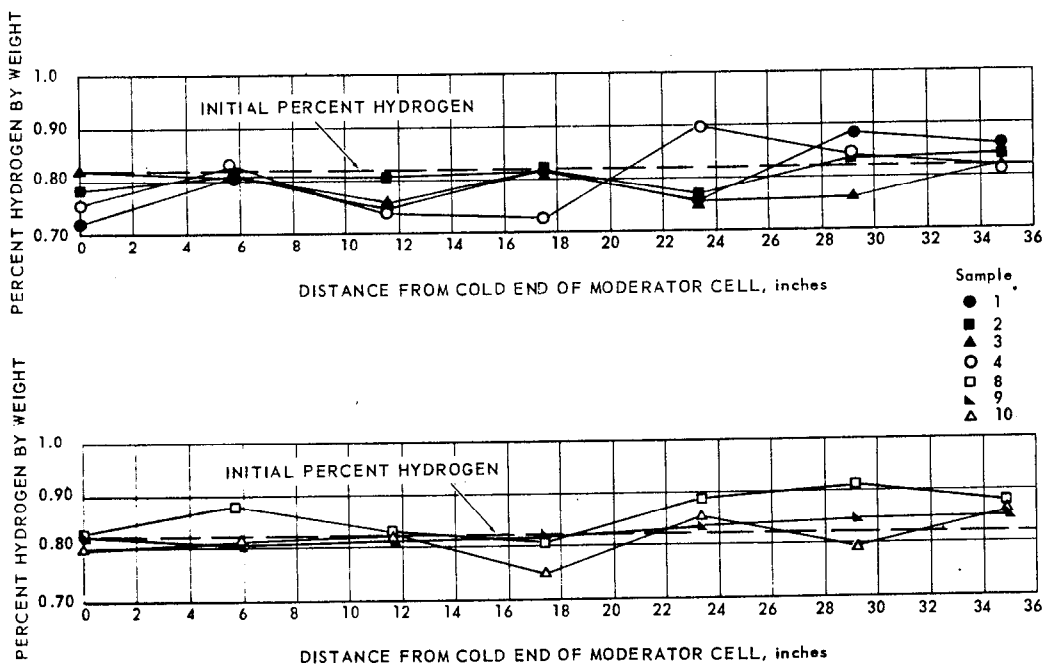


Fig. 114 - Hydrogen migration samples from cell 421, D102A

There is no general redistribution of hydrogen. Since the moderator reached peak temperatures at 10 minutes after the event and was at temperatures above 1000°F for only a matter of minutes, the data appear consistent, as 100 hours at 1200°F does not produce more than 5 percent loss. Therefore, it is believed that no general loss or redistribution of hydrogen occurred because of the event.

The radiation level of each moderator cell containing a fuel element was 3 roentgens per hour at 1 inch, 150 milliroentgens at 1 inch after removing the fuel element and liner, and approximately 75 milliroentgens per hour after decontamination of the empty moderator cell.

### 5.3 OXIDATION ANALYSIS AND FUEL LOSS

Samples of slag from stages 4 and 5 and from the general melted areas of the fuel cartridge in cell 575 were chemically analyzed for evidence of oxidation products, NiO and Cr<sub>2</sub>O<sub>3</sub>. Table 10 indicates the degree of oxidation of the nickel and chromium present in these stages.

The degree of oxidation of the fuel cartridges was greatest in stage 4 followed by stage 5 and then by the general area of the burned-out portion. This was apparently caused by the fact that stage 4 was on the upstream end of the fuel cartridge and possessed more available oxygen in its immediate environment for the oxidation process. The results also show that the chromium was oxidized to a much greater extent than the nickel, and some separation of the nickel from the oxidized chromium occurred. X-ray diffraction analyses also indicate that extensive oxidation occurred.

TABLE 10  
DEGREE OF OXIDATION IN NICKEL-CHROMIUM  
IN SLAG SAMPLES

Sample No. <sup>a</sup>	% Ni Oxidized	% Cr Oxidized
120-1	3.5	34.3
120-2	4.5	18.2
121-1	19.3	92.3
121-2	18.6	94.9
123-1	14.8	85.1
123-2	0.3	26.9
126-1	13.1	54.5
126-2	14.4	53.6

<sup>a</sup>Sample locations are as follows:

Sample No. 120 - general area of melted portion  
121 - 4th stage  
123 - general area of melted portion  
126 - 5th stage

A study was performed to determine approximately how much evolved heat was due to the rapid oxidation. The results of these calculations are shown in Table 11. These calculations are based on the composition of a stage (Ni = 206.2 g, Cr = 21.5 g, UO<sub>2</sub> = 62.0 g), the heat of formation (Ni to NiO = -58 kcal/mole Ni, Cr to Cr<sub>2</sub>O<sub>3</sub> = -135 kcal/mole Cr, UO<sub>2</sub> to U<sub>3</sub>O<sub>8</sub> = -25 cal/mole UO<sub>2</sub>), and the heat of fusion (Ni = 4.2 kcal/mole Ni, Cr = 3.9 kcal/mole Cr). A specific heat of 0.13 calorie/gram-°C was assumed. It was also assumed that the conversion of UO<sub>2</sub> to U<sub>3</sub>O<sub>8</sub> was complete and that the reaction started near the melting point of the nickel and chromium (about 1500°C). Taking the values

TABLE 11

## CALCULATED HEAT EVOLVED DURING OXIDATION OF SLAG SAMPLES

Sample No. <sup>a</sup>	Ni Oxidized per Stage		NiO Heat of Formation per Stage (moles Ni x 58)		Cr Oxidized per Stage		Cr <sub>2</sub> O <sub>3</sub> Heat of Formation per Stage (moles Cr x 135)		UO <sub>2</sub> Oxidized per Stage (assumed complete oxidation)		U <sub>3</sub> O <sub>8</sub> Heat of Formation per Stage (moles UO <sub>2</sub> x 25)		Total Heat of Formation per Stage	
	grams	moles	grams	kcal	grams	moles	grams	kcal	grams	moles	grams	kcal	kcal	mw-sec
120-1	6.59	0.112	6.50	16.2	0.311	42.0	62	0.23	5.8	54.3	0.217			
120-2	8.47	0.144	8.35	8.57	0.165	22.3	62	0.23	5.8	36.5	0.146			
121-1	36.3	0.618	35.8	43.5	0.836	113	62	0.23	5.8	155	0.620			
121-2	35.0	0.595	34.5	44.7	0.860	116	62	0.23	5.8	156	0.624			
123-1	27.9	0.474	27.5	40.1	0.769	104	62	0.23	5.8	137	0.548			
123-2	0.56	0.010	0.58	12.7	0.244	32.9	62	0.23	5.8	39.3	0.157			
126-1	24.7	0.419	24.3	25.7	0.494	66.7	62	0.23	5.8	96.8	0.387			
126-2	27.1	0.461	26.7	25.2	0.485	65.5	62	0.23	5.8	98.0	0.392			

<sup>a</sup>Sample locations given in Table 10

given for stages 4 and 5 and assuming that the slag samples yield average values for eight other stages, the total energy released by combustion in the reactor is extrapolated to be 470 megawatt-seconds. For comparison, the nuclear-energy release was measured between 600 and 800 megawatt-seconds.

Airflow calculations were performed to determine whether a sufficient amount of oxygen was present to support the observed oxidation. The results of these calculations indicate that a sufficient supply of oxygen was available for the observed oxidation if the reaction occurred over a period of 30 seconds or longer.

All stages of the fuel cartridge from cell 620 were gamma-scanned to determine the relative concentration of Zr<sup>95</sup> in each segment. A gamma spectrum of each stage was obtained on the 256-channel gamma ray spectrometer connected to a scintillation head, and the Zr<sup>95</sup> peak height was determined from the gamma spectrum. The data are presented in Figure 115. From these data an approximation to the longitudinal power profile of the fuel cartridge can be obtained. The data scatter noted on this graph can be attributed to the following:

1. Variation of the stage orientation front of the scintillation head.
2. The fact that only stages 1, 2, 3, 4, and 19 were intact or had a relatively small amount of damage. The remaining stages were melted down and had considerable oxidation. Thus a geometrically different source was given for the scintillation crystal.
3. Use of a short-time count in obtaining gamma scan readings.

The data appear to be reasonable in that the peak in the longitudinal power profile should occur around the ninth stage.

#### Smear Data Analysis

During the disassembly of the D102A power plant a series of smears was obtained from surfaces that were exposed to the airflow through the reactor during the event. The smear survey was accomplished to evaluate the amount and location of any uranium that might have left the reactor and deposited on components aft of the core.

The smears were counted in a 2π alpha counter to determine the alpha activity. All smears were counted in the same geometry and the results reduced to counts per minute per square centimeter as shown in Table 12, column 2. The location of each smear is shown in Figure 116.

In order to relate the amount of uranium removed by the smearing technique to the total amount deposited on an area, one of the smeared areas was masked off and decontaminated

TABLE 12  
SMEAR DATA RESULTS

Location	$\alpha$ $\frac{\text{cpm} \times 10}{\text{cm}^2}$	$\beta$ $\frac{\text{cpm} \times 10^3}{\text{cm}^2}$	$\gamma$ $\frac{\text{cpm} \times 10^3}{\text{cm}^2}$	Normalized Value $\gamma$ Activity	U Content $\frac{\text{mg}}{\text{cm}^2} \times 10^{-3}$
1	0.016			0.000367	0.076
2	5.47			0.125	26.0
3	5.93			0.136	28.0
4	34.9			0.800	166.0
5	16.5	4.50		0.378	78.5
6	11.9	9.02		0.273	56.4
7	12.5	2.70		0.287	59.3
8	5.39	1.48		0.124	25.7
9	34.1	5.70		0.782	162.0
10	3.78	1.17		0.087	18.0
11	42.0	5.04		0.963	200.0
12	3.17	0.31		0.073	15.0
13	22.3	7.80	2.70	0.511	105.0
14	20.2	7.85	2.71	0.463	96.0
15	11.5	2.20	0.712	0.264	54.7
16	13.6	6.10	1.30	0.312	64.6
17	10.7	1.05	0.362	0.245	50.9
18	14.8	6.50	2.37	0.339	70.3
19	36.2	13.4	4.90	0.830	172.0
20	42.8	15.0	5.74	0.982	203.0
21	8.25	6.52		0.189	39.0
22	23.0	20.0		0.528	109.0
23	11.4	11.2		0.261	54.2
24	1.6	0.73		0.036	7.6
25	43.6	20.0		1.000	207.0

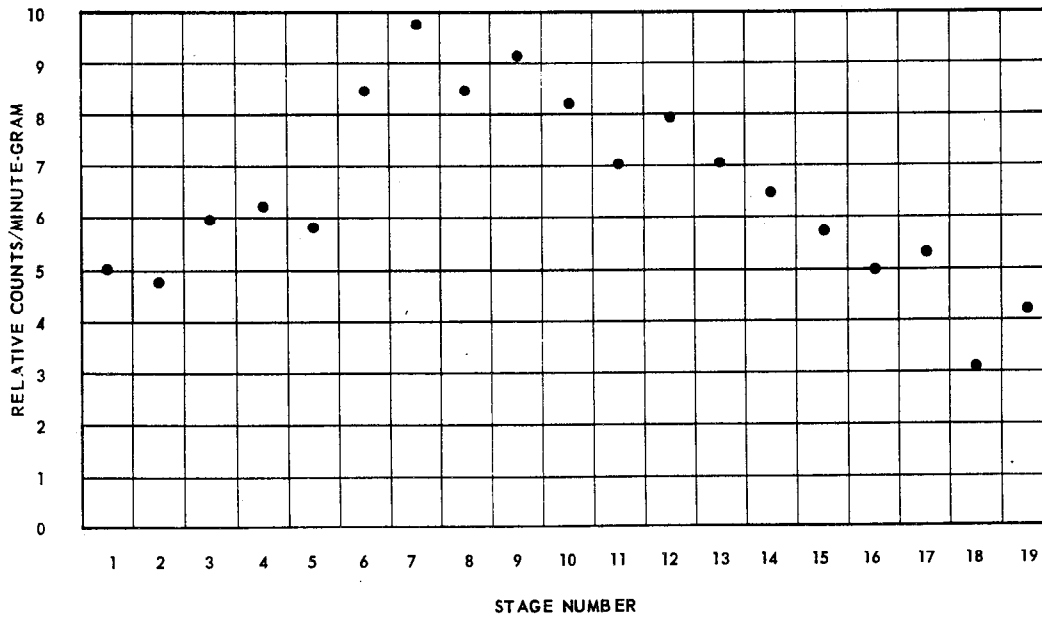


Fig. 115 - Gamma-scan data from cell 620

UNCLASSIFIED

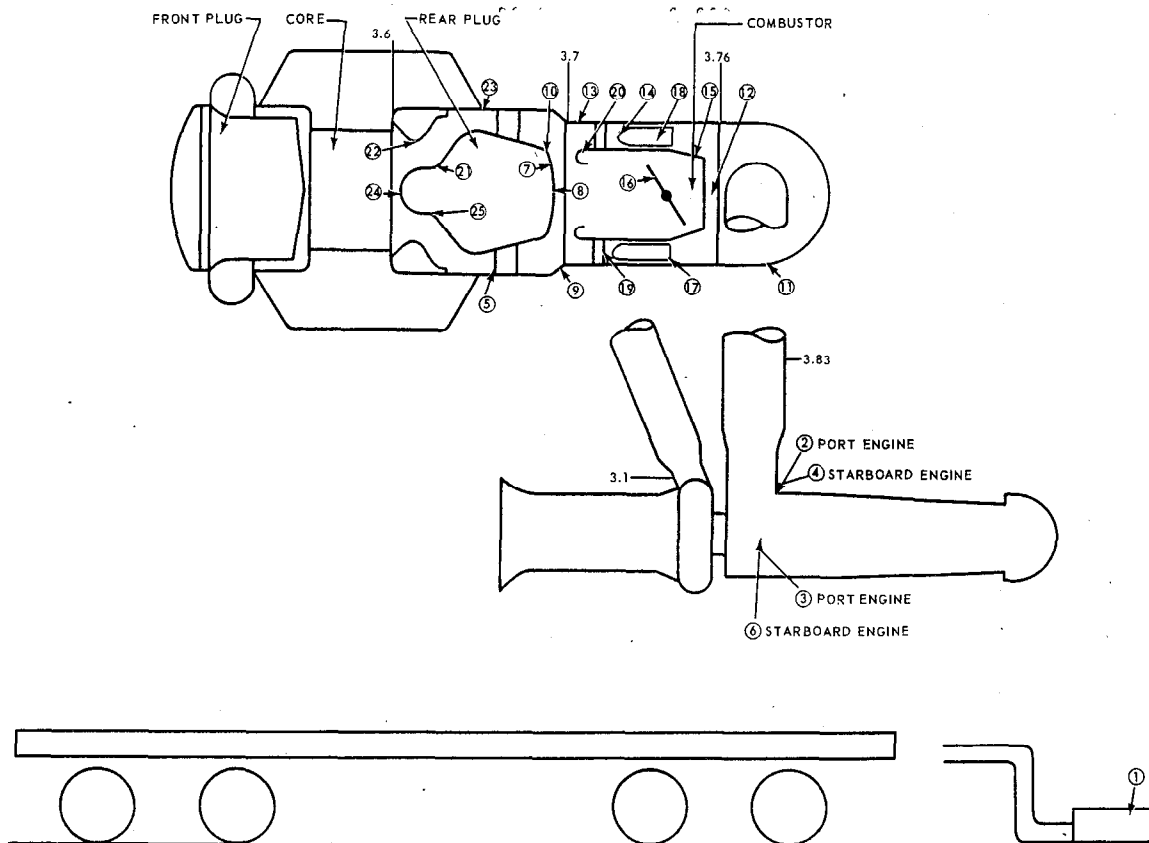


Fig. 116 - Smear locations on D102A power plant

with an acid solution. A portion of the decontamination solution was evaporated and counted for alpha activity in the same geometry used to count the smears. The results indicated that the total uranium removed by the smear and the decontamination process was a factor of 19 greater than the amount removed by the smear.

To relate the observed alpha activity on the smear to an absolute value of uranium, several standard uranium samples prepared by the National Bureau of Standards were counted in the same geometry as that in which the smears were counted. The standard sampler had approximately the same percent composition of  $U^{234}$  as the D102A fuel elements. The indicated calibration number from counting four different samples was  $4 \times 10^4$  alpha cpm/mg of uranium.

The amount of uranium deposited on the smeared surfaces was calculated from the alpha activities of the smears by means of the calibration number obtained from NBS samples and the above-described smear-to-total ratio of 19. The results are shown in column 6, Table 12.

The lack of precision in this type of analysis is obvious. Smears obtained side by side at several points indicated agreement within a factor of 2 or 3. The method of arriving at a calibration number is also less than ideal but is probably good within a factor of 2 or 3. The over-all results should be interpreted with these things in mind.

UNCLASSIFIED

UNCLASSIFIED



## 5.4 RADIATION SURVEY

The following paragraphs present radiation, contamination, smear, and air activity level survey data obtained during the disassembly of the D102A power plant.

Radiation levels, except as noted, were obtained with a Cutie Pie instrument at contact. Contamination levels are listed as counts per minute. The smear samples covered an area of approximately 100 square centimeters and were counted in an end window proportional counter with efficiencies of 9.4 percent for beta activity and 13 percent for alpha activity using a Ra D and E NBS source. Air samples were obtained with a Staplex Hi-Volume air sampler with MSA all-dust filters, BM 2133 dusts.

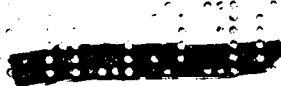
Contamination levels are to be regarded as orders of magnitude only; the other data presented are subject to the usual uncertainties involved in radiation survey measurements with portable equipment.

11/25/58 - Prior to disassembly of the power plant in the hot shop a radiation survey was obtained on the D102A dolly at 1130 hours.

Around primary shield	less than 5 mr/hr
Aft ducting	125 mr/hr
Combustor: Aft end	100 mr/hr
Middle	215 mr/hr
Fore end	150 mr/hr
Bottom	480 mr/hr
Aft header: Center	90 mr/hr
Bottom	340 mr/hr
No. 2 engine: Scroll	100 mr/hr
Turbine	200 mr/hr
Tail pipe	360 mr/hr
No. 1 engine: Scroll	10 mr/hr
Turbine	20 mr/hr
Tail pipe	20 mr/hr
Rods	less than 5 mr/hr
Hot ducting between scroll and aft header on No. 2 side; vertical part	60 mr/hr
Smears: Insert plug	769 cpm
Top core	6700 cpm
Engine No. 1	2760 cpm
Engine No. 2	2590 cpm
Aft header	584 cpm

11/26/58 - A radiation survey was obtained during and after removal of the aft header from the power plant at 1510 hours.

Material in aft header	5 rad/hr at approximately 1 foot
Approximately 1/4 cup of material removed	5 rad/hr beta at contact 250 mr/hr gamma at contact
Air activity: on the aft platform of the dolly during removal of aft header	Approximately $5 \times 10^{-9}$ $\mu\text{c}/\text{cc}$ beta activity



The following smears indicated that no appreciable spread of contamination to the dolly or the hot shop was caused by this operation.

Dolly: Aft platform	2300 cpm
Constant support hangers	1150 cpm
No. 1 engine ducting outside surface	3470 cpm
No. 2 engine ducting outside surface	2980 cpm
Reactor face (by rods)	1607 cpm
Instrument panel (horizontal surface)	3000 cpm
Coupling plug	
Hot Shop: West of dolly	100 cpm
North of dolly	130 cpm
East of dolly	470 cpm
Floor west of tube-loading machine	110 cpm
Floor north of tube-loading machine	130 cpm
Tube-loading machine: First landing -	less than 20 cpm
Plastic apron -	less than 20 cpm
Cily section -	4,000 cpm

11/26/58 - A survey was obtained during removal of combustor at 0830 hours.

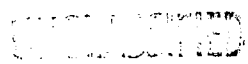
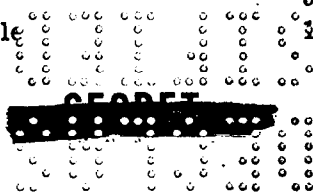
Tail plug	2 rad/hr at contact
Between plug and outside shell	3.5 rad/hr open window, 350 mr/hr closed window
Approximately 3 feet from plug	350 mrad/hr
Approximately 9 feet from plug	25 mr/hr
Air activity: on aft platform of dolly during this operation	2 x 10 <sup>-10</sup> $\mu$ c/cc
No smears were taken after this operation	

11/26/58 - A survey was obtained during removal of rear plug from the power plant at 1340 hours.

Upstream face of plug	4 rad/hr at contact
Center of rear tube sheet	10 rad/hr at approximately 3 inches with Jordan chamber
Approximately 1 foot from tube sheet (even with edge of primary shield)	5 rad/hr open window, 3 r/hr closed window
At edge of upending fixture	110 mr/hr
Approximately 1 cup of material located at bottom edge of tube sheet	10 rad/hr at approximately 5 inches with Jordan (not much higher than background here)
Air activity: during this operation with the air sampler located 3 feet above floor approximately 5 feet from plug	3.2 x 10 <sup>-10</sup> $\mu$ c/cc

12/2/58 - Survey data were obtained during the preparation for removal of core from primary shield.

On top by control rods	less than 5 mr/hr
Middle of core	5 mr/hr
Beam from fission chamber hole	100 mr/hr



UNCLASSIFIED

~~SECRET~~

Directly under core 8-10 feet off floor	300 mr/hr
Outside edge of upending fixture 5 feet off floor	170 mr/hr
Four feet from edge of upending fixture	30 mr/hr

12/2/58 - A radiation survey was obtained with the core removed from the power plant and mounted in the tube-loading machine at 1530 hours. Results of this survey are shown in Figure 117.

Note: These are dose rates encountered during fuel element removal from core. Parts of the core removal fixture shielded out considerable amounts of the dose rates, which probably will cause exposure estimates to be high. This could be caused by the fact that personal dosimeters were generally worn where the shielding effect of the core removal fixture was most pronounced.

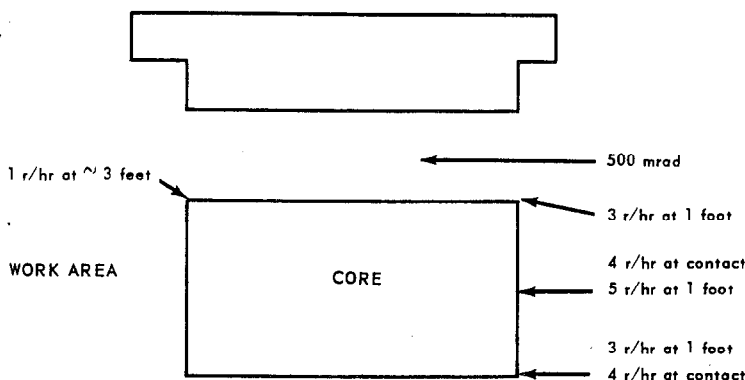


Fig. 117 - Radiation survey of core, December 2, 1958

12/5/58 - The general smear survey results on the D102A power plant listed below indicate no significant increase in surface contamination as a result of disassembly.

D102A Power Plant

Bottom level	1189 cpm
Bottom level	638 cpm
Chrysler motor	2372 cpm
Fuel tank	941 cpm
Fuel tank	1238 cpm
Piping	1964 cpm
Core cradle	1199 cpm
No. 1 engine turbine	4126 cpm
No. 2 engine turbine	567 cpm
Instrument panel	1231 cpm

12/6/58 - A survey was obtained after the removal of the outer ring of fuel elements from the core while the core was still on the tube-loading machine.

Four feet from edge of core midway between tube sheets	350 mr/hr
--	-----------

Note: This compared with 1 r/hr on 12/4/58 before a removal of any fuel elements.

~~SECRET~~

UNCLASSIFIED

UNCLASSIFIED

~~SECRET~~

12/8/58 - A smear survey was obtained in the hot shop after partial power plant disassembly.

Average approximately 5000 cpm beta; minimum 1000 cpm beta; maximum 50,000 cpm beta.

Average approximately 100 cpm alpha; minimum 15 cpm alpha; maximum 4,000 cpm alpha.

In addition visible amounts of contamination reading up to 5 rad/hr accumulated on the turntable and the floor where the reactor core was placed.

The following survey was obtained after the removal of front plug from core:

Top of reactor	1 r/hr, detector in contact with bellmouths
Through side of ICE tank	800 mr/hr maximum
At top of ICE tank	200 mr/hr

12/9/59 - A survey was obtained after the removal of the rear tube sheet from the power plant at 1900 hours.

Bare moderators lying close together	200 mr/hr
Fueled moderators vary from	3 r/hr to 5 r/hr
Bottom face of reactor	3 rad/hr at edge of ICE tank
Forward face of reactor	5 rad/hr at contact 220 mrad/hr at edge of ICE tank (approximately 3 feet from tube sheet) 60 mrad/hr at 10 feet

12/10/58 - The following survey was obtained during manual removal of fuel element moderator block assemblies from core.

Body exposure to persons removing fuel	1.5 r/hr maximum
Single unfueled moderator block	100 mr/hr
Group of unfueled moderator blocks	200 mr/hr
Smear of block: Outside	712 cpm
Outside	270 cpm
Inside	7100 cpm
Smear of rear tube sheet	52,000 cpm beta
Air activity approximately 5 feet from bottom face of reactor 3 feet above floor	$2.9 \times 10^{-9}$ $\mu\text{c/cc}$ beta; $1.5 \times 10^{-12}$ $\mu\text{c/cc}$ alpha

12/10/58 - The following survey of D102A core was obtained after removal of all fuel and moderator blocks and with the reactor mounted horizontally in the ICE tank.

Along horizontal centerline of reactor:

Upstream, at end of guide tubes	200 mr/hr
Geometric center of reactor	1.5 r/hr
Downstream at bottom edge of reactor (even with bottom tube sheet before removal)	500 mr/hr
At contact with inside surface of reactor shell midway between tube sheets	1 r/hr

The floor between the core and fuel element racks was contaminated to 100,000 cpm.

~~SECRET~~

UNCLASSIFIED

UNCLASSIFIED

~~SECRET~~

12/11/58 - A survey was obtained during the removal of the fuel element from moderator cells.

Body exposure rate	1-1/2 r/hr maximum
Fueled moderator block	4 r/hr at contact
Unfueled moderator block	100 mr/hr at contact
Bare fuel	5 r/hr at approximately 5 inches
Material reading up to 3 rad/hr accumulated on the plug (part of removal tool) during removal of fuel.	
Air activity during this operation at edge of dummy plug	
At floor level:	$3.6 \times 10^{-9}$ $\mu$ c/cc beta; $2.8 \times 10^{-10}$ $\mu$ c/cc alpha
At edge of dummy plug 5 feet above plug: (breathing zone)	$2.8 \times 10^{-10}$ $\mu$ c/cc beta; $5.6 \times 10^{-11}$ $\mu$ c/cc alpha

1/13/59 - The following is a radiation survey of D102A dolly and combustor.

Aft plug each side	9 mrad/hr
At contact downstream	650 mrad/hr
Three feet from plug, downstream	50 mrad/hr
Top of primary shield (by fission chamber)	less than 1 m/hr
Unit combustor: maximum at burners	700 mrad/hr
maximum elsewhere	300 mrad/hr

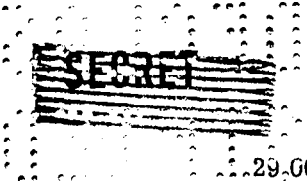
#### Smear Surveys

A smear survey was obtained on the inside surfaces of aft plug, combustor, scroll, and aft header. Efficiencies are approximately 2.5 percent of beta activity and 13.4 percent for alpha activity with Ra D and E source.

<u>Combustor</u>	<u>Beta cpm</u>	<u>Alpha cpm</u>
12/1/58 Upstream	780,000	5,658
	785,000	6,806
	220,000	4,000
	610,000	5,300
	105,000	3,600
	650,000	5,369
11/25/58 Downstream	1,337,000	10,000
	450,000	6,900
	270,000	5,176
	148,000	2,148
	570,000	15,700
	117,000	1,201
12/1/58 Aft plug upstream	1,500,000	11,000
	652,000	8,250
	2,000,000	23,000
	1,120,000	11,400
	730,000	1,650
12/1/58 Aft Header	4,000,000	43,600
	504,000	13,000

UNCLASSIFIED

~~SECRET~~



11/25/58 Scroll southside	29,600	1,650
southside	31,000	2,535
northside	370,000	11,147
northside	902,000	8,745
<u>1/14/59</u> Combustor - upstream	248,000	13,000
downstream	60,400	18,900

UNCLASSIFIED

Decontamination Studies

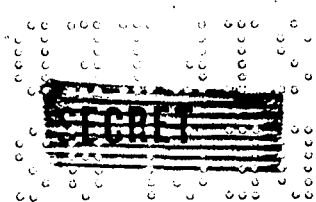
Two areas on the inside diameter of the D102A aft plug were selected for decontamination to assist in determining plate-out and decontamination factors. One area selected was to be decontaminated by use of a nitric acid solution and the other area to be dry wiped.

The aft plug was in a horizontal position at the time of test and attached to the reactor shell on the D102A dolly. The two areas selected were approximately 16 inches apart and located on the lower circumferential arc of the plug. The plug has a perforated, stainless steel - clad insulation liner and it was necessary to limit the area between the perforations. This surface was measured to be approximately 3 by 4 inches.

The following results were obtained from the two methods of decontamination:

	<u>Wet Method</u>	<u>Dry Method</u>
Surface area	80 cm <sup>2</sup>	80 cm <sup>2</sup>
Pre-decontamination Smear		
Alpha	8.4 x 10 <sup>4</sup> d/m	
Beta and Gamma	1.8 x 10 <sup>6</sup> d/m	
Contamination removed by smears		
Alpha	-----	1.45 x 10 <sup>5</sup> d/m
Beta and Gamma	-----	1.6 x 10 <sup>6</sup> d/m
Contamination removed by acid leach and water rinse		
Alpha	1.5 x 10 <sup>6</sup> d/m	
Beta	3.12 x 10 <sup>6</sup> d/m	
Gamma	4.5 x 10 <sup>4</sup> d/m	
Smear count after decontamination		
(First smear)		
Alpha	60 d/m	
Beta and gamma	690 d/m	
(Second smear)		
Alpha	0 d/m	
Beta and gamma	70 d/m	
Gross spectrum		
Ba-140, Ce-141, Ru-103, Ru-106, La-140, CePr-144		

No attempt was made to compare the effectiveness of decontamination by use of the wet or dry method. However, the wet method did remove most of the contamination.



UNCLASSIFIED

2019  
0310

0319  
2019

~~SECRET~~

UNCLASSIFIED

CONFIDENTIAL

# GENERAL ELECTRIC

*General Electric*

~~CONFIDENTIAL~~  
~~SEP 24 1959~~

RECEIVED  
SEP 23 1959  
Los Alamos  
Scientific Laboratory  
P. O. Box 1663  
Mail & Records

~~SECRET~~

UNCLASSIFIED